5. SEISMIC EFFECTS AND ABSTRACTIONS

This section describes the calculations and abstractions for the postclosure structural response of EBS components to the seismic hazards of vibratory ground motion and fault displacement. Figure 5-1 illustrates the EBS components in a typical emplacement drift. This section includes discussion of:

- Criteria for determining the failed areas of waste packages and drip shields under vibratory ground motion
- Rockfall calculations in the lithophysal and nonlithophysal zones under vibratory ground motion, and the response of the drip shield to rockfall
- Structural response calculations and their abstractions for damage to the waste package, the drip shield, and the cladding under vibratory ground motion
- Abstraction of damage to the waste package, drip shield, and cladding from fault displacement
- Postseismic event changes in the hydrologic environment.

Table 5-1 identifies the major references for the rockfall calculations, for the structural response calculations, and for the hazard curves and seismic abstractions for TSPA.

Table 5-1. Major References for Calculations and Seismic Abstractions

Damage Process	Reference
Uncertainty in input parameters for rockfall and structural response calculations	*Sampling of Stochastic Input Parameters for Rockfall and Structural Response Calculations Under Vibratory Ground Motions* (BSC 2003d)
Damage to the waste package from vibratory ground motion	*Structural Calculations of Waste Package Exposed to Vibratory Ground Motion* (BSC 2003e)
Damage to the drip shield from vibratory ground motion	*Structural Calculations of Drip Shield Exposed to Vibratory Ground Motion* (BSC 2003f)
Damage to the drip shield from rockfall	*Drift Degradation Analysis* (BSC 2003b) and *Drip Shield Structural Response to Rock Fall* (BSC 2003g)
Acceleration of the fuel assemblies and cladding due to end-to-end waste package impacts	*Maximum Accelerations on the Fuel Assemblies of a 21-PWR Waste Package During End Impacts* (BSC 2003h) and *Structural Calculations of Waste Package Exposed to Vibratory Ground Motion* (BSC 2003e)
Fault displacement and ground motion hazard curves for determining the amplitude of seismic events	*Probabilistic Seismic Hazard Analyses for Fault Displacement and Vibratory Ground Motion at Yucca Mountain, Nevada* (CRWMS M&O 1998)
Damage abstractions and computational algorithm for seismic scenario class	*Seismic Consequence Abstraction* (BSC 2003i)

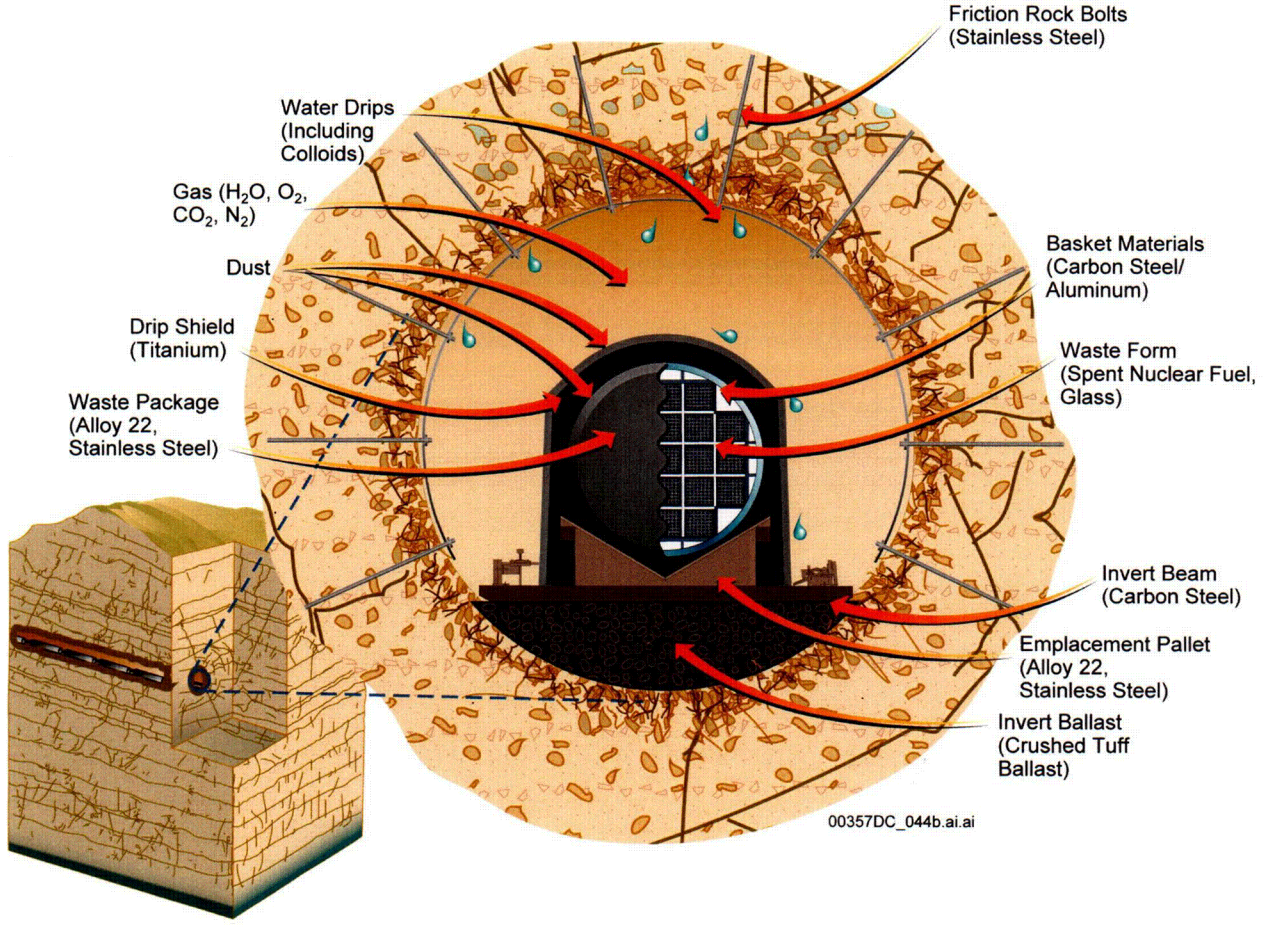

NOTE: CAM = corrosion allowance material; CRM = corrosion-resistant material.

Figure 5-1. Engineered Barrier System Components in a Typical Emplacement Drift

The damage abstractions for EBS components are defined in a different manner than the typical response surface for a seismic fragility analysis. A typical response surface represents the mean or median damage (or the mean or median probability of failure) and its standard deviation, often as normal or lognormal distributions whose parameters are functions of the amplitude of the ground motion or fault displacement. The damage abstractions for the seismic scenario class are often uniform distributions that provide a conditional distribution of the range of damage as a function of the amplitude of the seismic hazard. While the use of a uniform distribution is not typical for fragility analyses, this approach does provide a simple and transparent approach for representing the variability and uncertainty in seismically induced damage in the Monte Carlo sampling scheme for TSPA.

C29

5.1 SEISMIC FAILURE CRITERIA AND FAILURE MORPHOLOGY

5.1.1 Failure Mechanism from Seismically Induced Deformation

Mechanical processes that occur during a seismic event can result in permanent structural deformation and residual tensile stress in EBS components. These mechanical processes include impacts between adjacent waste packages and impacts between the waste package and its emplacement pallet, the surrounding drip shield, and the invert. Impacts will also occur between the drip shield and the emplacement pallet, the invert, and the drift wall. These mechanical processes may also include other loads, such as static load from rockfall or thermal load, in addition to the seismic load; however, these static and thermal loads are small relative to seismic loads for the large, low-probability ground motion that may occur during the 10,000-year regulatory period.

Permanent structural deformation during these mechanical processes has the potential to result in immediate tensile failures from puncture or tearing. However, the robustness of the waste package and drip shield makes this immediate failure mode extremely unlikely. On the other hand, the presence of residual tensile stress may result in enhanced local degradation from general corrosion, stress corrosion cracking, or localized corrosion (pitting or crevice corrosion). This combined mechanical-chemical failure mechanism is expected to be the most likely cause of the failure of waste package and drip shield as barriers to flow and transport for the seismic scenario class.

Application of a residual tensile stress threshold for seismic failures is nonmechanistic in the sense that detailed calculations with accelerated corrosion rates or crack propagation are not used to determine the actual failure time after a seismic event. Rather, a barrier is assumed to fail immediately once the residual tensile stress threshold is exceeded, providing potential pathways for flow and transport through the areas exceeding the residual stress threshold. The residual tensile stress threshold is often referred to as the residual stress threshold or more simply the stress threshold in this section; the principal residual stress must always be tensile to initiate an accelerated corrosion process.

The areas that exceed the residual tensile stress threshold are referred to as the "failed area" throughout this document. No damage is equivalent to 0% failed area on the surface of the waste package, so there is no flow or transport through the barrier. Note that the effective area for flow and transport through a barrier will be substantially less than the failed area because the cross-sectional area of the stress corrosion cracks is much less than the surface area that exceeds the residual stress threshold.

Figure 5-2 is a simplified illustration of how residual stress is generated by permanent (plastic) deformation in a simple uniaxial strain model. Figure 5-2 also shows that plastic deformation does not always generate a failed area because the final residual stress state may be compressive or, if tensile, may be below the tensile threshold to initiate accelerated localized corrosion or stress corrosion cracking.

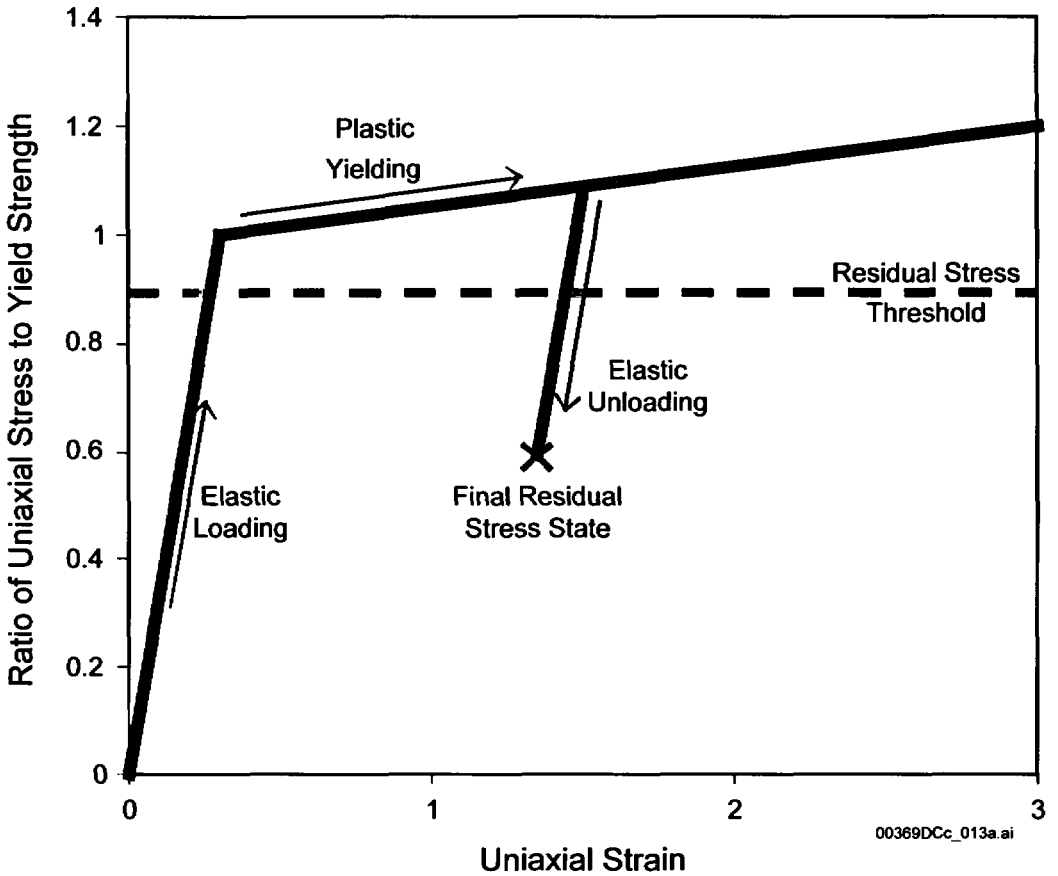

Figure 5-2. Permanent Deformation from Plastic Yielding Generates Residual Stress

The residual stress thresholds for seismic response are similar to the criteria for initiation of stress corrosion cracking on smooth surfaces of Alloy 22 and Titanium Grade 7 (UNS R52400) (BSC 2003j, Section 6.2.1). The use of a stress corrosion cracking initiation criterion is appropriate for seismic analysis because regions where the residual stress from mechanical damage exceeds the tensile failure criterion are expected to be severely cold-worked and, hence, potentially subject to enhanced stress corrosion cracking

A residual stress threshold is a conservative failure criterion because detailed corrosion models will have a delay time until failure. This approach is appropriate because it is consistent with other tensile failure criteria (BSC 2003j, Section 6.2.1), because the residual stress failure criterion is transparent, and because it is easily applied to the output from structural response calculations.

Permanent deformation could also result in immediate puncture or tearing of an EBS component if the localized strain exceeds the ultimate tensile strain. The constitutive model for the structural response calculations includes the potential for immediate breach of EBS components through tensile and shear failure, although the computational meshes are generally too coarse to realistically simulate a localized puncture. Supporting calculations for waste package drops on the emplacement pallet indicate that the maximum stress intensity for the impact velocities observed in the vibratory ground motion calculations is significantly below the ultimate tensile

strength (BSC 2003k). In this situation, a localized puncture or tearing of the waste package will not occur and the seismic damage abstractions for the waste package and drip shield are based on a residual tensile stress threshold as a failure criterion. In a similar fashion, the drip shield will not buckle from the static load of a large rockfall, as discussed in Section 5.3.2.

5.1.2 Residual Stress Damage Threshold for the Waste Package

The residual stress threshold for failure of the waste package is represented by a uniform distribution with a lower bound of 80% of the yield strength of Alloy 22 and an upper bound of 90% of the yield strength of Alloy 22. The upper bound is based on experimental data and conservatively incorporates a safety factor of 2.2 (BSC 2003j, Section 6.2.1, third paragraph). The lower bound is introduced to evaluate the sensitivity of failed area to residual stress threshold for the seismic scenario class.

5.1.3 Residual Stress Damage Threshold for the Drip Shield

For the drip shield barrier, the residual stress threshold for failure is represented by a fixed lower bound of 50% of the yield strength of the drip shield plate material (Titanium Grade 7) (BSC 2003j, Section 6.2.1, third paragraph).

There is a significant experimental database for Titanium Grade 7 that justifies the use of 50% of yield strength as a stress corrosion cracking initiation criterion (BSC 2003j). These data include long-term constant load tests in a concentrated groundwater environment at 105°C with specimens loaded to stresses of 110% to 140% of the yield strength. A second source of information comes from U-bend tests. Initiation of stress corrosion cracking is not observed in fixed deflection U-bend tests on Titanium Grade 7 exposed for 1 year and Titanium Grade 16 (UNS R52402) (an analogous titanium/palladium alloy) exposed for 5 years to a range of relevant aqueous environments at 60°C and 90°C. These U-bend tests are more representative of secondary residual stress loading that might result from deformation following seismic loadings. A very conservative value of 50% of yield strength is selected as a threshold criterion for Titanium Grade 7, even though the initiation of stress corrosion cracking is not observed in U-bend test specimens for residual stresses greater than yield strength. A conservative failure criterion is used here because it is consistent with other failure criteria for initiation of stress corrosion cracking on smooth surfaces of Titanium Grade 7. More detailed discussion of the experimental data for both Titanium Grade 7 and Alloy 22 can be found in *Stress Corrosion Cracking of the Drip Shield, the Waste Package Outer Barrier, and the Stainless Steel Structural Material* (BSC 2003j).

5.1.4 Morphology of Damage on the Waste Package

The material for the waste package outer corrosion barrier, Alloy 22, has been shown to be potentially susceptible to stress corrosion cracking under environmental conditions that are relevant to the repository. The stress corrosion cracking mode (morphology) is transgranular stress corrosion cracking rather than the intergranular stress corrosion cracking which is commonly observed in pressurized systems, such as pipelines or light water reactor components (Andresen et al. 2001). The primary issue for the seismic scenario class is to define the effective area and transport mode (advective or diffusive) resulting from seismically induced deformation

and the associated transgranular stress corrosion cracking through the outer corrosion barrier of the waste package. To this end, the conditions leading to transgranular stress corrosion cracking and the potential geometry of the crack system have been investigated (Herrera 2004).

Seismically induced deformation can lead to crack initiation and crack propagation on the waste package. A range of aqueous brine type environments may form on the waste package outer corrosion barrier, producing the requisite concurrent conditions for accelerated stress corrosion cracking of (1) high residual tensile stress; (2) an environment that supports corrosion; and (3) a material that has been cold-worked during the seismic event. Once initiated, the strain fields (residual stresses) produced by the seismically induced impacts can drive crack growth. Depending on the stress distribution, cracking may propagate through-wall if the stress intensity factor remains positive. If multiple cracks are initiated in the same general area, it is possible, but very unlikely, that multiple cracks will intersect or coalesce, creating a continuous crack around the deformed region.

It is very unlikely that a residual stress profile would be created that would allow an initiated stress corrosion crack to propagate both through-wall and circumscribe a dent or deformed area. Any through-wall residual stress fields resulting from seismic impact loads would be a secondary type stress (displacement controlled). There is no significant stress from other sources, such as stress induced by internal pressure. In addition, stresses and strains are generally of higher magnitude at the outer surface and tend to decrease through the thickness for the deformation-induced damage from a seismic event. In this situation, any crack that initiates and propagates may arrest before penetrating the full thickness of the outer barrier and is highly unlikely to have a sufficiently positive stress intensity factor to result in both through-wall and 360° cracking around the entire dent.

Even postulating that a through-wall crack occurs and circumscribes the dented area, the nature of stress corrosion cracking will preclude the dented area from falling out. Cracks in Alloy 22 are transgranular, but whether transgranular or intergranular, the crack path has complex local branches with a roughness and tortuosity, as illustrated in Figure 5-3 (Herrera 2004, Figure 2-1), that make it essentially impossible for an inner "plug" to disengage from the vessel in the absence of a superimposed primary load (i.e. significant internal pressure). Any internal pressure that develops from heat up to about 150°C or corrosion-generated gas or both with the small amount of internal water vapor that is available would not be sufficient to force the dented area from the wall.

Source: Herrera 2004, Figure 2-1.

Figure 5-3. Typical Example of Transgranular Stress Corrosion Cracking in Stainless Steel

This analysis is consistent with many years of experience with stress corrosion cracks in light water reactor components and other internally pressurized systems. A number of incidents of stress corrosion cracking have been observed in light water reactors involving both austenitic stainless steels and nickel-based alloys (Herrera 2004, Appendix A). The observed stress corrosion cracking has been extensive in many of these incidents, sometimes becoming fully circumferential in response to weld-induced residual tensile stress and pressure-induced primary

stresses. But even under these conditions, which are more severe than in the postseismic environment, there has never been a documented case where any section of material dropped out as a result of the observed cracking (Herrera 2004, Appendix A).

5.1.5 Effective Area for Flow and Transport through the Waste Package

Since the most likely failure mechanism from a seismic event is accelerated stress corrosion cracking and since the deformed or failed areas that exceed the residual stress failure for Alloy 22 are expected to remain physically intact, it is reasonable to represent these areas as a dense network of stress corrosion cracks, rather than as a plug of material that separates from the outer barrier. The effective area for transport through the crack network has been estimated with the following procedure.

The range of crack densities and crack widths has been estimated for four closely spaced networks of cracks, based on cracks that are oriented in random or parallel directions and that have two different spacings between crack centers (Herrera 2004, Section 6.2; DTN: MO0403SPASCRKD.000). Figure 5-4 presents one of these hexagonal arrays, with parallel rows of randomly oriented cracks. In this approach, centers of through-wall cracks are located in a densely packed hexagonal array and are separated by at least a wall thickness. The wall thickness is anticipated to be the minimum possible separation because stress relief from propagation of adjacent cracks relieves the local stress intensity factor, preventing tighter spacing between through-wall cracks. The width of each crack is estimated by assuming an elliptical opening with constant through-wall stress given by the elastic yield strength. This is a conservative approach because the crack tips tend to narrow at the inner surface (see Figure 5-3) and because stress relief from adjacent cracks will again tend to reduce the local stress levels at a crack.

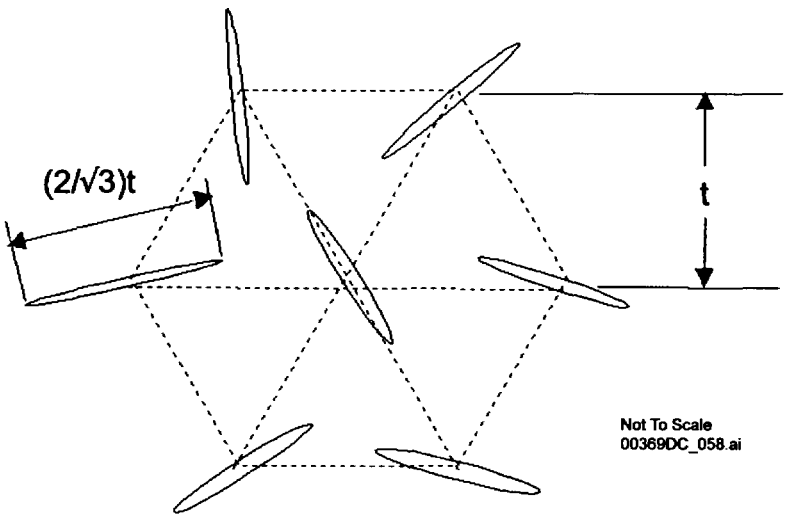

Source: Herrera 2004, Figure 6-2.

Figure 5-4. Parallel Rows of Randomly Oriented Flaws, with Row Spacing Equal to Wall Thickness

The hexagonal network of closely spaced cracks is a convenient conceptual model for estimating a range of crack densities and crack opening areas for TSPA; however, this crack geometry is not

commonly observed in industrial systems. Rather, an axisymmetric dent will often produce cracks that are oriented circumferentially around the center of the dent because the circumferential direction is normal to the main stress gradients in the radial direction. An analysis for circumferential cracks (Herrera 2004, Section 6.3) indicates that the effective area of a typical circumferential crack network is within the range of uncertainty for the hexagonal model.

The ratio of the effective area for transport through the waste package to the failed area that exceeds the residual stress threshold is given by the product of the crack density per unit surface area and the gap area per crack. This product ranges from 0.00328 to 0.0131 (Herrera 2004, Table 6-1) for the four crack networks. As a numerical example, if a surface area of 1 m^2 exceeds the residual stress threshold on the surface of the waste package, then the effective area for flow and transport will be 0.00328 to 0.0131 m^2, equivalent to a factor of 76 to 305 times less than the original failed area. The product has been evaluated using material properties for room temperature because this is slightly more conservative than material properties at 150°C.

The network of stress corrosion cracks on the waste package has high tortuosity and surface roughness and narrow to very small apertures at the crack tip (see Figure 5-3). It is likely that this physical morphology will eliminate advective flux through the cracks because of infilling of small apertures with corrosion products because of high surface tension when a narrow aperture is bridged by a single droplet and because there is minimal head gradient or pressure gradient driving flow through the narrow apertures. Evaporation-induced precipitation of calcite and other minerals in the groundwater may also occur within the cracks on the waste package over the timescale of a few hundred years, similar to the predictions for the drip shield (BSC 2001a). In this situation, the physical morphology of the crack network on the waste package will not permit significant advective flow of liquid but does provide a pathway for diffusive transport of radionuclides out of the waste package in TSPA.

5.1.6 Effective Area for Flow through the Drip Shield

The Titanium Grade 7 plates of the drip shield are also subject to stress corrosion cracking induced by residual stresses from seismic ground motion and from rockfall induced by seismic ground motion. However, the presence of a crack network in the drip shield is not represented in the seismic scenario class for TSPA because the drip shield cracks are predicted to plug within a few hundred years after a seismic event, preventing a significant flux of liquid seepage from falling on the waste package. The cracks will plug from mineral precipitation resulting from evaporation of seepage and from in-filling of the crack gap with corrosion products. Once the cracks are plugged, the quantity of liquid that can pass through the drip shield and impinge on the waste package will be reduced to an insignificant level. The presence of the crack network in the drip shield is therefore not included in TSPA.

As with Alloy 22, the most likely failure mechanism for Titanium Grade 7 after a seismic event is accelerated stress corrosion cracking, rather than immediate puncture or tearing of the drip shield. The deformed or dented region is expected to remain physically intact because individual cracks are complex branching structures with high surface roughness and tortuosity. In this situation, it is reasonable to represent the areas that exceed the residual stress failure criterion for

Titanium Grade 7 as a network of stress corrosion cracks, rather than as a plug of material that separates from the outer barrier.

Damaged areas on the drip shield and waste package result in a dense network of tight stress corrosion cracks. These cracks have high tortuosity and surface roughness, narrowing to very small apertures at the crack tip. It is likely that this physical morphology will eliminate advective flux through the cracks because of infilling of narrow apertures with corrosion products, because of high surface tension when a narrow aperture is bridged by a single droplet, and because there will be minimal head gradient or pressure gradient driving flow through the narrow apertures with high tortuosity and surface roughness.

The small heat flux across the drip shield will also result in evaporation of slowly flowing seepage, causing a scale deposit to form around the mouth of the crack and within the crack. A detailed calculation of the expected rate of crack plugging due to evaporation-induced precipitation of calcite has been performed for a pore water of typical composition dripping onto a drip shield (BSC 2001a). Cracks are sealed within a few hundred years when water is allowed to flow through the cracks at the expected (very low) rate for thin film flow (BSC 2001a, Section 6.3). Once a crack is plugged with precipitates, the magnitude of the liquid flux through the crack will become insignificant because of the expected high density of calcite deposits (BSC 2001a), the lack of a significant pressure head or gradient to drive liquid through the crack, and the observed high tortuosity and roughness of the crack geometry (Herrera 2004, Section 2 and Figures 2-1 and 2-2).

The formation of scale deposits, primarily calcium carbonate (calcite), is well documented in flow systems in seawater environments and in heat exchangers with natural brines, such as in desalination plants (carrying about 6% NaCl solutions) and in potash plants (carrying greater than 12% mixtures of NaCl/KCl. Mineral deposits form rapidly at elevated temperatures and must be regularly removed to avoid loss of heat exchanger efficiency. In the case of seepage based on the J-13 groundwater from Yucca Mountain, calcite precipitation is the first stage of the concentration process (BSC 2001b, Section 6.7.1). Other minerals such as amorphous silica will also precipitate from J-13 groundwater.

The sealing process may take thousands of years when a liquid droplet bridges a crack. However, the associated capillary forces when a liquid droplet is present prevent any advective flux from passing through the crack in this situation.

This analysis has not been extended to stress corrosion cracks in the waste package for the seismic scenario class. Rapid plugging of cracks requires evaporation of groundwater and precipitation of minerals. The initial precipitation of minerals will occur on the drip shield, which is directly exposed to the seepage of groundwater into the emplacement drifts. Secondary precipitation may occur on the waste package. However, the mineral concentrations on the waste package would be reduced by the initial precipitation on the drip shield and diluted by the presence of any condensate that falls onto the waste package from the underside of the drip shield. The potential for stress corrosion cracks in the waste package to prevent a significant advective flux onto the waste package internals is a subject of ongoing study.

5.2 ROCKFALL CALCULATIONS

Although stress corrosion cracks on the drip shield are predicted to plug from evaporation-induced precipitation of mineral deposits, the drip shield may fail as a flow barrier due to buckling and collapse under loads from rockfall induced by ground motion. The rockfall calculations that define the potential loads from individual rock blocks in the lithophysal zones or from a collapsed drift in the lithophysal zones are described in this section.

5.2.1 Rockfall in the Nonlithophysal Zone

Geologic structure and rock strength defines the failure mode in the nonlithophysal rock. The failure mode in these rocks results from stress-induced yield in the intact rock or along joint surfaces, followed by gravity-induced drop of discrete rock blocks. The analysis of the failure mechanism is complicated by the fact that the jointing in the nonlithophysal zones is usually of short continuous trace length and inherently discontinuous, thus forming few kinematically removable blocks. This type of discontinuous jointing results in an inherently stronger rock mass compared to typical jointed rock where the block structure is well defined by multiple, continuous joint sets (BSC 2003b, Executive Summary).

Analysis of rockfall in the nonlithophysal zone requires ground motion time histories, fracture geometries, and fracture properties as input parameters or boundary conditions for the calculations. To ensure adequate representation of uncertainty and variability, the inputs for individual rockfall calculations are sampled from 15 ground motion results[2] at (horizontal) peak ground velocity levels of 2.44 m/s and 5.35 m/s (corresponding to the 10^{-6} and 10^{-7} per year ground motion levels) and from 105 synthetic fracture patterns. These synthetic fracture patterns are statistically and geologically consistent with mapped sections of the tunnel in the ESF. The synthetic fracture patterns (BSC 2003b, Section 6.1.6) for the rockfall analysis are drawn from a random sampling of 105 centroid locations within a cube of rock that is 100 m on a side. A Monte Carlo sampling scheme provides the appropriate combinations of ground motion and synthetic fracture pattern for the rockfall analyses (BSC 2003d, Sections 6.1 and 6.2).

A total of 76 simulations with the 3DEC computer code were performed for the 2.44 m/s peak ground velocity time histories (BSC 2003b, Section 6.3.1.2.3 and Attachment XI). A similar series of 3DEC calculations were also performed for the 5.35 m/s peak ground velocity time histories (BSC 2003b, Section 6.3.1.2.4). This latter series of analyses is not described in detail here because the overall results are similar to those for the 2.44 m/s peak ground velocity.

Figure 5-5 illustrates the rock-block impacts on the drip shield for a specific simulation. As shown in Figure 5-5, the drip shield is represented as a simple rectangular region for the purpose of defining the impact location and impact velocity of individual rock blocks on the drip shield. Approximately 33% of the simulations predict no rockfall for the 2.44 m/s peak ground velocity. The simulations without rockfall correspond to synthetic fracture patterns that do not allow discrete blocks to be shaken loose from the walls. A total of 281 rock blocks, with a total

[2] A total of 17 sets of three component ground motions are generated for the emplacement drifts. Rockfall calculations are performed with 15 sets of ground motions numbered 1, 2, 3, ..., 14, and 16. The 15th ground motion is not used because it has an anomalous response spectrum.

volume of 101.8 m^3, are shaken loose from the walls of the drift. The associated impact parameters for these rock blocks include:

- Rock block volume falling on the drip shield
- Relative impact velocity of rock block to the drip shield
- Impact location.

Summary statistics for these parameters are provided in Table 5-2. Figure 5-6 is a histogram of the block masses from the 76 simulations. The maximum rock block mass is 21.42 metric tons, while the median block mass is 0.23 metric tons. Figure 5-7 is a histogram of the block impact velocities from the 76 simulations. The rockfall results generally show large variance and high skewness with the exception of impact velocity.

Table 5-2. Summary of Rock-Block Statistics for the Horizontal Peak Ground Velocity of 2.44 m/s

	Block Mass (MT)	Relative Impact Velocity (m/s)	Impact Angle (degree)	Impact Momentum (kg x m/s)	Impact Energy (Joules)
Mean	0.87	3.39	132	2747[a]	5,267
Median	0.23	3.49	120	663	902
Standard Deviation	1.97	1.61	81	6,209	1,2941
Skewness	6.04	0.04	1.12	6.23	7.52
Range	21.39	7.54	355	68,836	163,083
Minimum	0.02	0.02	5	4	0
Maximum	21.42	7.56	360	68,840	163,083
Sum	245.55	NA	NA	771,861	1479,888

Source: BSC 2003b, Table 14.

NOTE: MT = metric ton = 1,000 kg; NA = not applicable.
[a]The mean impact momentum is not equal to the product of the mean values of the block mass and impact velocity because of the skewness of the block mass distribution.

5.2.2 Rockfall in the Lithophysal Zone

The lithophysal rock mass is characterized by about 20% lithophysal cavities by volume. This rock type has numerous small-scale fractures between lithophysae that result in a relatively weak rock mass relative to the nonlithophysal rock. Lithophysal failure is controlled by the transient ground–motion induced stress concentrations that occur around the excavation. The mode of failure is primarily from tension generated by the impinging seismic waves.

A lithophysal rockfall model was developed using the two-dimensional discontinuum code UDEC. In this model, the rock mass is represented as an assembly of polygonal, elastic blocks in which the bond strength of the blocks is calibrated such that the overall mechanical behavior of the mass is consistent with the material model developed for the lithophysal rock. The lithophysal rockfall model allows for the formation of fractures between blocks (i.e., the formation of internal fracturing), separation, and instability (under action of gravity) of the rock mass around the drift. The UDEC model is based on unsupported drift openings (BSC 2003b, Section 6.4).

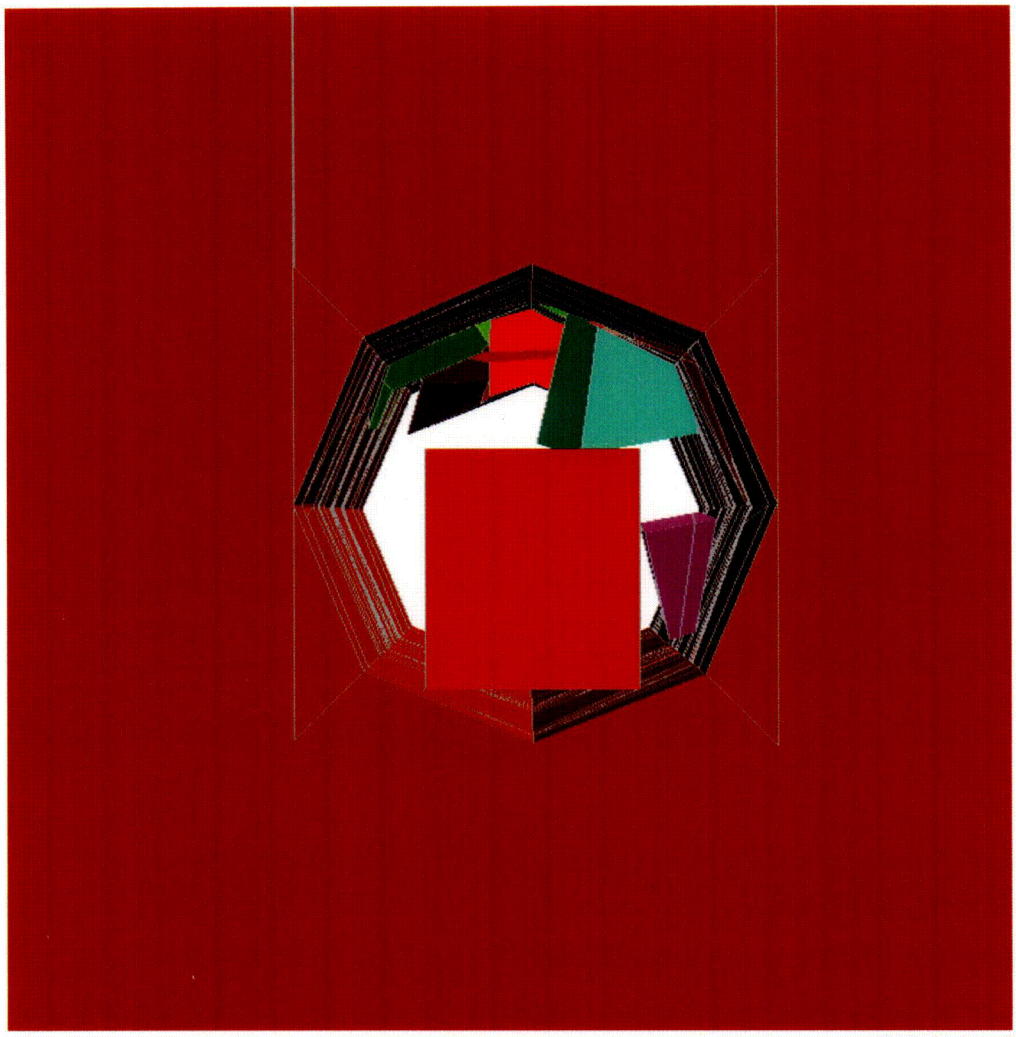

00369DCc_014a.ai

Source: BSC 2003b, Figure 44.

NOTE: Simulation is for rockfall in nonlithophysal rock.

Figure 5-5. Illustration of Rockfall Impacts on the Drip Shield for 3DEC Simulation 55, 10^{-6} Ground Motion 12 with Peak Ground Velocity of 2.44 m/s and Time of 6.6 s

C30

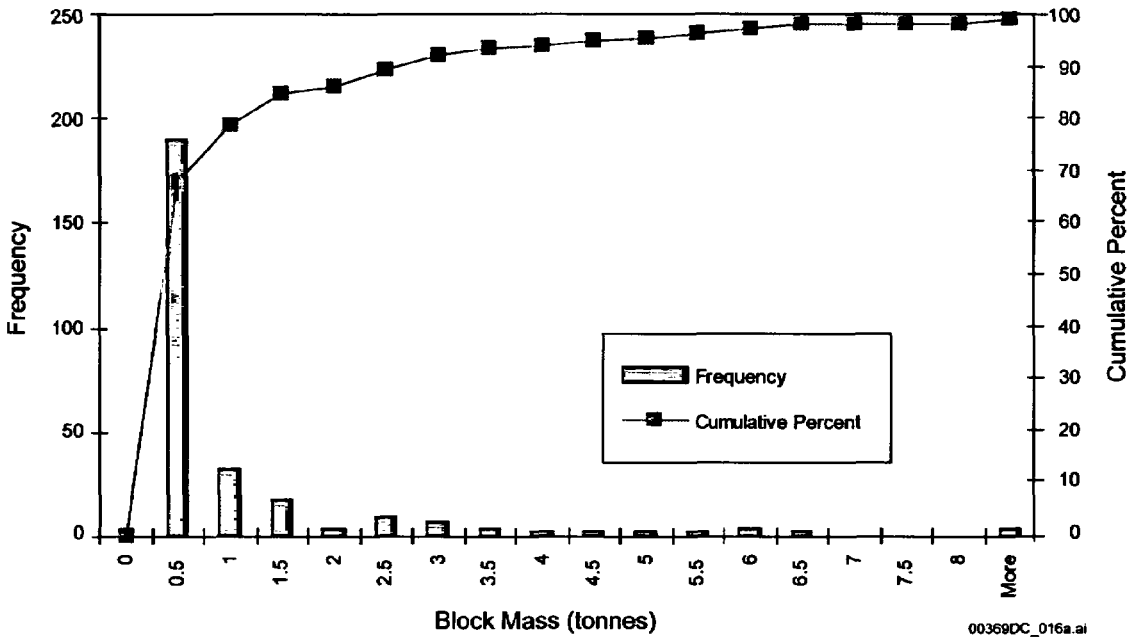

Source: BSC 2003b, Figure 48.

NOTE: Results are for rockfall in nonlithophysal rock.

Figure 5-6. Histogram for Block Mass for a Peak Ground Velocity of 2.44 m/s (10^{-6} Exceedance Hazard)

To ensure adequate representation of uncertainty and variability, the inputs for individual rockfall calculations are sampled from 15 ground motion results at (horizontal) peak ground velocity levels of 2.44 m/s (corresponding to the 10^{-6} per year ground motion level) and from 5 rock mass categories. Rock mass category 1 represents a weak rock with a lithophysal porosity of 25% to 30%. Rock mass category 5 represents strong lithophysal rock with a lithophysal porosity of less than 10%. Rock mass categories 2, 3, and 4 represent intermediate cases with lithophysal porosities of 20% to 25%, of 15% to 20%, and of 10% to 15%, respectively. The effective mechanical properties corresponding to these rock mass categories vary with the porosity of the lithophysae (BSC 2003b, Tables 34 and 45). A Monte Carlo sampling scheme provides 15 combinations of ground motion number and rock mass category for the lithophysal analyses (BSC 2003d, Section 6.3). The rock mass categories are assumed to be equally likely for the sampling calculation.

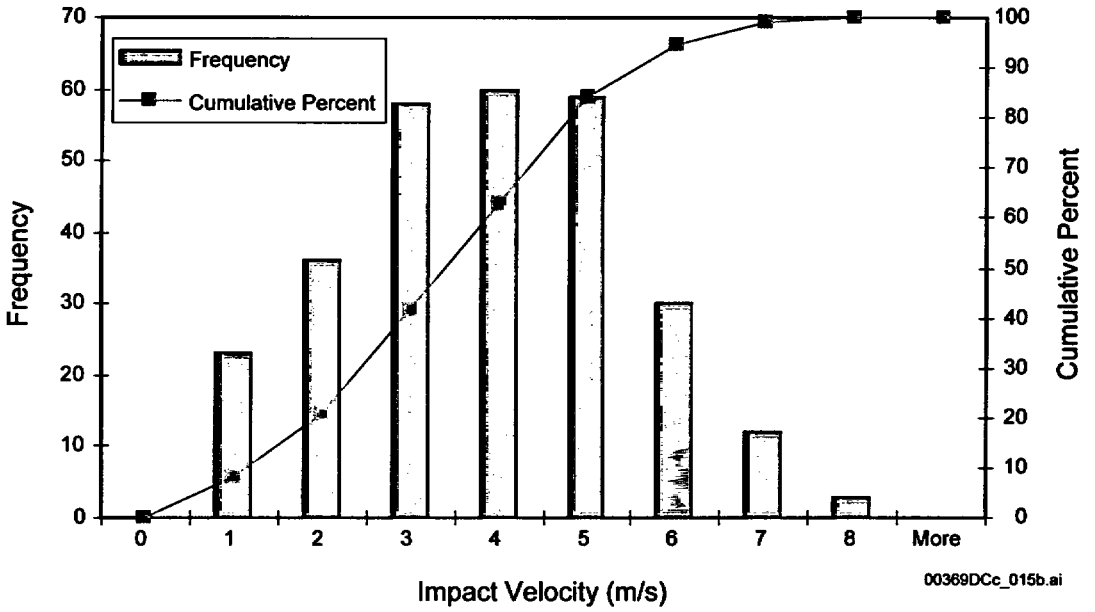

Source: BSC 2003b, Figure 49.

NOTE: Results are for rockfall in nonlithophysal rock.

Figure 5-7. Histogram for Relative Impact Velocity for a Peak Ground Velocity of 2.44 m/s (10^{-6} Exceedance Hazard)

All the calculations for a peak ground velocity of 2.44 m/s, corresponding to an exceedance frequency of 10^{-6} per year, cause complete drift collapse in the lithophysal zone, irrespective of rock mass category (BSC 2003b, Section 6.4.1.1). Figure 5-8 presents the final drift geometry after the ground motion for the first six realizations. It is evident from Figure 5-8 that the drifts experience complete collapse, in the sense that they are completely filled with rubble and the boundary with the intact rock is well beyond the initial excavation. Postclosure ground motion for all peak ground velocities greater than 2.44 m/s are also expected to collapse the drifts.

A computational investigation evaluated the potential for large key blocks to be shaken loose from lithophysal rock during the collapse process (BSC 2003b, Section 6.4.3). Only two blocks are shaken loose in almost 2 km of drift, with a total block volume of 0.15 m^3. The conclusion from this investigation is that the probability of large rock blocks in the lithophysal zone is very low and that drift collapse from postclosure ground motion will produce fragmented rock particle sizes on the order of centimeters to decimeters (tens of centimeters) (BSC 2003b, Section 8.1).

A series of six UDEC calculations was also performed for a single ground motion time history at the 5×10^{-4} annual exceedance frequency for each of the five rock mass categories, plus a sixth category with very poor rock quality as an extreme lower bound. The 5×10^{-4} annual exceedance frequency corresponds to a peak ground velocity of 0.38 m/s at the emplacement drifts. These analyses indicate that this ground motion will not induce any rockfall for rock mass categories 2 through 5. A relatively small amount of rockfall from the drift walls occurred for rock mass categories 1 and 6. The observed rockfall is a consequence of regions that are above the yield limit, after excavation of the drift, and are being shaken down by the vibratory ground motion (BSC 2003b, Section 6.4.1.1).

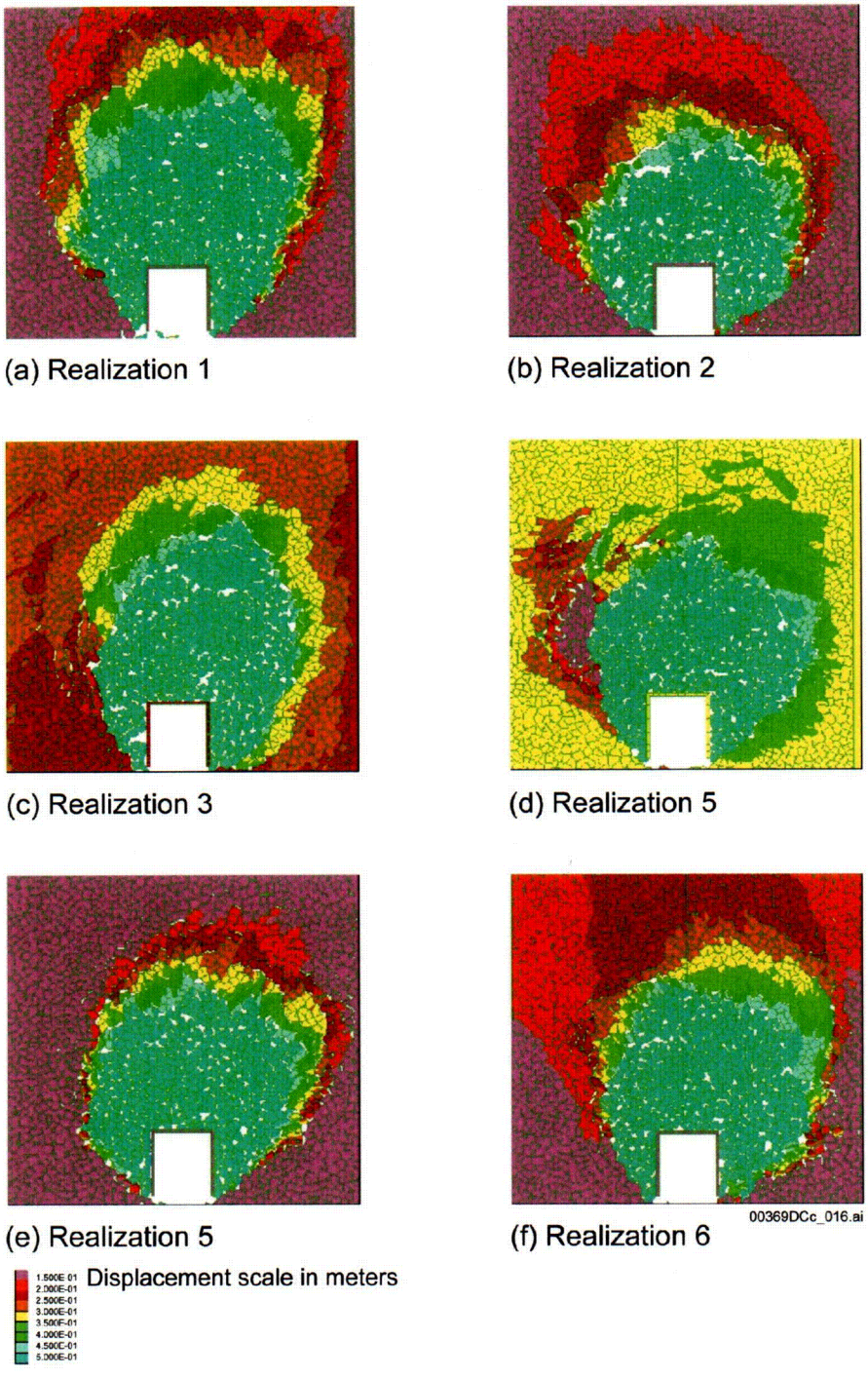

Source: BSC 2003b, Figure 115.

NOTE: Blocks are colored by magnitude of displacement. On the legend, numbers correspond to the boundaries between colors. Thus, the color of the top block represents a displacement of less than 0.15 m, the color of the second block from the top represents a displacement of between 0.15 and 0.20 m, and so on. For all realizations, the drifts are completely filled with rubble well beyond the initial excavation boundary.

Figure 5-8. Drift Geometry in the Lithophysal Zone after the 2.44 m/s Peak Ground Velocity Ground Motion

C31

5.3 STRUCTURAL RESPONSE TO ROCKFALL

5.3.1 Damage to the Drip Shield from Rockfall in the Nonlithophysal Zone

A set of six representative blocks and three representative impact locations was selected to span the range of blocks from the UDEC analyses. The idea behind this approach is to perform a limited set of calculations that span the range of rock sizes, rock velocities, rock impact angles, and rock impact points on the drip shield. This limited set of calculations then provides the basis for determining the response of the drip shield (1) to the maximum rock blocks in the nonlithophysal zone and (2) to the smaller blocks that can be ejected during drift collapse in the lithophysal zone.

The selection of representative rocks is based on their kinetic energy because the impact energy of a rock block should provide a reasonable correlation with failed area (see Table 5-3). The impact energies associated with the selected rocks correspond to the minimum, the 5th percentile, the median (50th percentile), the 95th percentile, and the maximum of the sorted impact energies for the 2.44 m/s peak ground velocity time histories (BSC 2003b, Attachment XI). A sixth block has been added to capture the maximum rock block energy observed for the 5.35 m/s peak ground velocity ground motion results.

Table 5-3. Characteristics of Selected Rock Blocks for the Single Block Impact Analyses

Rock Block Mass (MT)	Kinetic Energy (J)	Vertical Velocity (m/s)	Lateral Velocity (m/s)
0.25	~0	0.0137	0.0103
0.11	42	0.202	0.383
0.15	902	3.09	0.955
3.3	24,712	3.75	0.0824
14.5	163,083	4.69	0.656
11.5	348,174	7.7	0.295

Source: BSC 2003b, Attachment XI.

Damage to the drip shield from impact of individual rock blocks is determined by structural response calculations using a commercially available version of the finite-element program LS-DYNA V960 (LSTC 2001). The objective of these calculations is to determine the areas on the drip shield where the residual first principal stress in the drip shield plates exceeds the failure criterion for Titanium Grade 7 and to determine the potential for buckling and collapse during impact from rock blocks with the greatest kinetic energy. The rationale for using the first principal stress as a measure of susceptibility to accelerated corrosion is documented in the response to RDTME 3.18, Appendix F of *Technical Basis Document No. 6: Waste Package and Drip Shield Corrosion.*

These calculations incorporate the potential for corrosion to degrade the drip shield over the first 20,000 years after repository closure by reducing the thickness of the drip shield plates by 2 mm. The 20,000-year period is selected to demonstrate that repository performance remains robust well after the 10,000-year regulatory period. These calculations also evaluate mechanical properties at 150°C to represent the potential degradation in mechanical strength if a seismic

hazard occurs during the initial thermal pulse after repository closure. The adequacy of the finite-element mesh was determined by systematically reducing the mesh size to obtain convergence of the stress intensity and first principal stress. This process is described in the licensing letter report supporting the resolution of PRE 7.02 (Williams 2003).

A total of 18 calculations have been performed with LS-DYNA for each of the six representative rock sizes at three representative locations: top, corner, and side (BSC 2003g). Figure 5-9 is a schematic of the initial configuration for the top-impact calculation. The block impacts the drip shield edge-on to maximize damage.

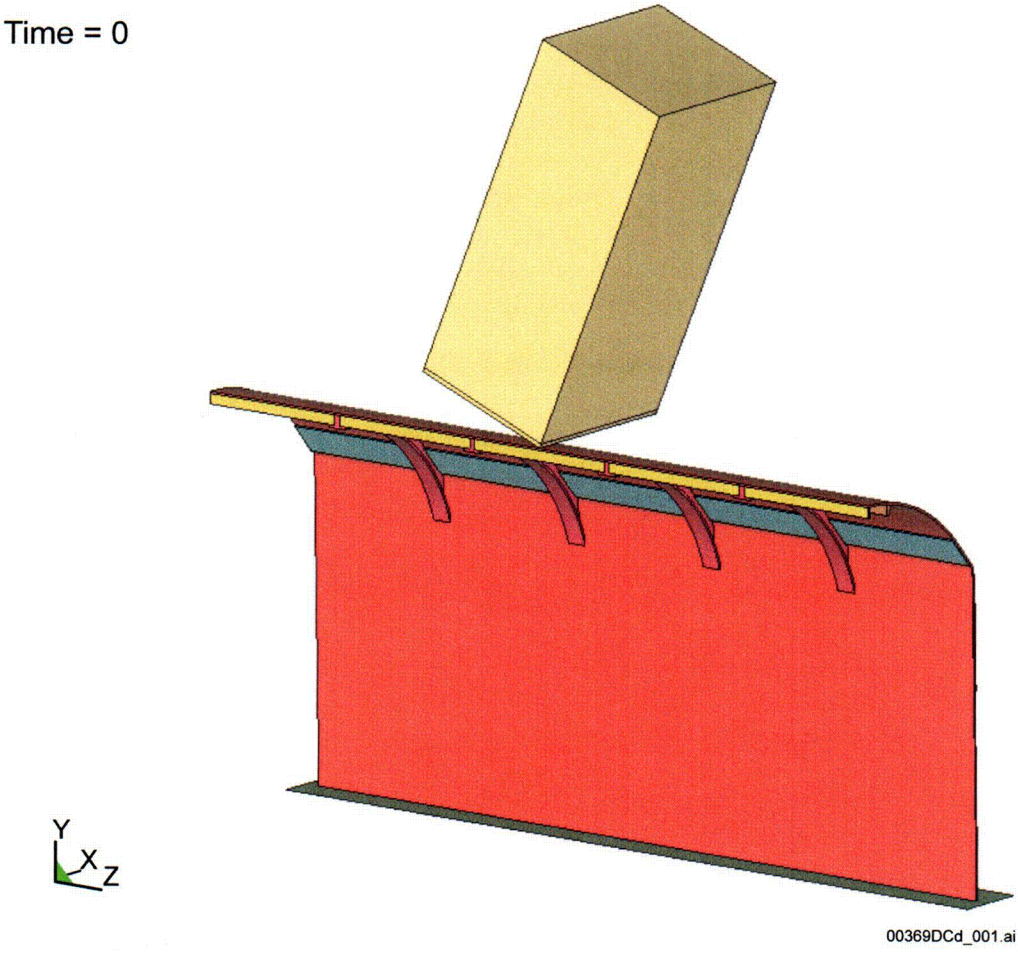

Source: Anderson 2003, Slide 18.

Figure 5-9. LS-DYNA Analysis Configuration for Rock-Block Impact Calculations

A key result from this suite of calculations is that the maximum vertical displacement in the drip shield components takes place in the longitudinal stiffener during the vertical impact of the 11.5 metric ton rock block, which has the highest kinetic energy (BSC 2003g, Section 6). The maximum displacement is 25.4 cm (BSC 2003g, Figure II-5). The drip shield does not buckle or collapse from this impact. In addition, this maximum displacement is less than the minimum clearance, 361.1 mm, between the inside height of the drip shield and the top of any waste package (BSC 2004e, Figure 1). It follows that the drip shield does not contact the waste

package by an impact of the largest rock block, thereby providing a mechanical barrier against rockfall for the waste package and cladding.

The results from each structural response calculation are postprocessed to determine the elements in the drip shield plates where residual stress exceeds 50% of the yield strength of Titanium Grade 7. The failed elements are then converted into a failed surface area. This conversion conservatively assumes that if a single element on the surface of the drip shield fails, then all elements beneath this element also fail. This is conservative because the elements inside the thickness of the drip shield may be in a compressive state that will arrest crack propagation from a stress corrosion crack. Table 5-4 shows the results for the structural response calculations (BSC 2003g, Section 5.5.1).

The information in Table 5-4 provides insights into the potential for smaller rocks generated by collapse of drifts in the lithophysal zones to damage the drip shield. The failed areas in Table 5-4 could also be used to estimate damage to the drip shield from rockfalls with multiple blocks in the nonlithophysal zone. However, the failed area from multiple rock blocks has not been abstracted for TSPA because the resulting network of stress corrosion cracks on the drip shield is expected plug from evaporation-induced mineral precipitation within a few hundred years, preventing significant advective flow through the crack network (see Section 5.1.6).

Table 5-4. Failed Areas from Individual Rock Blocks Impacting the Drip Shield

Rock Mass and Kinetic Energy	Failed Area (m^2) and Failed Area as a % of Total Drip Shield Surface Area		
	Vertical Rockfall (90° from horizontal)	Rockfall onto Drip Shield Corner (60° from horizontal)	Rockfall onto Drip Shield Side-Wall (40° from horizontal)
11.5 MT Rock (348174 J)	4.304 (11.25%)	2.835 (7.41%)	1.126 (2.94%)
14.5 MT Rock (163083 J)	3.508 (9.17%)	0.612 (1.60%)	0.079 (0.21%)
3.3 MT Rock (24712 J)	0.548 (1.43%)	0.416 (1.09%)	0.0 (0.00%)
0.15 MT Rock (902 J)	0.0015 (0.00%)	0.0091 (0.02%)	0.0 (0.00%)
0.11 MT Rock (42 J)	0.0 (0.00%)	0.0 (0.00%)	0.0 (0.00%)
0.25 MT Rock (~0 J)	0.0 (0.00%)	0.0 (0.00%)	0.0 (0.00%)

Source: BSC 2003g, Section 5.5.1.

NOTE: MT = metric tons, J = Joules.

5.3.2 Drip Shield Damage from Rockfall in the Lithophysal Zone

Two potential sources of damage to the drip shield have been considered in the lithophysal zone: damage from the individual rock fragments that fall onto the drip shield (Table 5-4) and the static load on the drip shield from drift collapse. The individual rock fragments are too small to do significant damage to the drip shield and the mean static loads from a collapsed drift are not

predicted to collapse the drip shield. Damage to the drip shield from rockfall in the lithophysal zone is not included in the drip shield damage abstraction for TSPA on this basis.

In the lithophysal zones, the rock mass is permeated with void spaces of varying size. Average joint spacing is less than 1 m, and at certain locations this spacing is much smaller, on the order of 0.1 m (BSC 2003b, Section 6.1.4.1). Drifts in the lithophysal zones are predicted to collapse into small fragments with particle sizes of centimeters to decimeters (BSC 2003b, Section 8.1) under the loads imposed by vibratory ground motion with a peak ground velocity of 2.44 m/s or greater.

The small fragments from drift collapse in the lithophysal zones will not damage the drip shield because the small mass and energy of the individual fragments cannot cause significant permanent deformation of the drip shield, as shown in the top rows of Table 5-4. The probability of large coherent (key) blocks being generated by the collapse process in the lithophysal zones is very low (BSC 2003b, Section 6.4.3). Rockfall in the lithophysal zones also does not damage the waste package and cladding because the drip shield remains intact until a seismic event occurs, deflecting any rockfall away from the waste package.

Drift collapse in the lithophysal zones can impose a static load on the drip shield from the weight of the natural backfill that fills the drifts as a result of the collapse. The structural response of the drip shield to this "dead" load from debris on the drip shield has been evaluated with structural response calculations (BSC 2003l) using the LS-DYNA software. The static load for these calculations is represented as the equivalent pressure from a layer of sand backfill that is about 1 m thick and a layer of fragmented rock backfill that is 5.5 m thick. The calculations are performed using material properties at room temperature and at 150°C. The calculations also consider a general thinning of the drip shield plates by 1 mm on all sides and by 1.5 mm on all sides.

The maximum stress in all components of the drip shield is always less than the yield strength for this combined load (BSC 2003l, Section 6 and Table 6.2). In addition, the average stress in the large support beams (the peripheral bulkheads) of the drip shield is far enough below the yield strength of Titanium Grade 24 (UNS R56405) to alleviate any concern of buckling. (The drip shield plates are fabricated from Titanium Grade 7, while the supporting framework is fabricated from Titanium Grade 24.)

The equivalent pressure approach for these static load calculations does not consider stress risers due to the presence of angular rock fragments with sharp edges. Local deformation of the drip shield plates should redistribute these stress risers into a more uniform external load on the drip shield.

It is important to differentiate between dynamic and static failure criteria for the drip shield. For dynamic loading of the drip shield due to rockfall, an area fails as a flow barrier when the residual stress exceeds 50% of the yield strength of Titanium Grade 7. This failure is a combined chemical-mechanical response of a cold-worked material to dynamic impacts. For static loading, the failure of the drip shield is determined by mechanical rupture or buckling of the drip shield. In the static situation, a local stress below 100% of the yield strength of Titanium Grade 7 does not imply structural failure.

5.3.3 Damage to the Waste Package and Cladding from Rockfall

Damage to the waste package and cladding from rockfall has been screened out from TSPA. The waste package and cladding are not damaged because the drip shield remains structurally intact for seismic hazards with a peak ground velocity up to 2.44 m/s, deflecting any rockfall away from the waste package. Seismic hazards with peak ground velocity of 5.35 m/s or greater result in separation of the drip shields, potentially exposing the waste package and cladding to rockfall. However, drip shield separation will not damage waste packages in the lithophysal zones of the repository because the lithophysal rock is predicted to shatter into small fragments (see Section 5.3.2) that have little potential to damage the waste package. It is reasonable to screen out damage to the waste package and cladding from rockfall because (1) the drip shields remain intact up to a ground motion amplitude of 2.44 m/s; (2) 85% of the emplacement drifts are in lithophysal zones, where the small fragments have little capacity to damage the waste package; and (3) separated drip shields continue to provide partial protection for at least 50% of the waste packages in the repository. (The maximum drip shield separation is 50%, equivalent to assuming that each drip shield completely covers or is completely covered by its adjacent neighbor; lower values for drip shield separation provide more coverage for the waste packages.)

5.4 STRUCTURAL RESPONSE TO VIBRATORY GROUND MOTION

5.4.1 Structural Response of the Waste Package

Structural response calculations have been performed to determine the damage from impacts between the waste package and emplacement pallet and from impacts between adjacent waste packages under vibratory ground motion (BSC 2003e). The potential for damage from impacts between the waste package and drip shield is included in the analysis, but produces negligible damage because the drip shield is unrestrained.

Damage to the waste package from vibratory ground motion is determined by structural response calculations using a commercially available version of the finite element program LS-DYNA V960 (LSTC 2001). A set of 15 calculations for the dynamic waste package response was performed for a set of 15 ground motion results[3] with a peak ground velocity of 2.44 m/s. A similar set of calculations was also performed for a peak ground velocity of 5.35 m/s (BSC 2003e). Figure 5-10 shows the cutaway view of the analysis configuration for the waste package simulations. The adjacent waste package is conservatively represented in Figure 5-10 as an essentially rigid wall anchored to the invert. The rigid wall is used for computational feasibility but results in an overestimate of the damage from end-to-end impacts. Figure 5-11 shows the finite-element mesh on the outer shell of the waste package. This mesh is very fine in regions labeled "C" and "F" because most impacts occur in these regions for the 2.44 m/s peak ground velocity ground motion.

[3] Structural response calculations are performed with 15 sets of ground motions. They are selected from the 17 sets that were developed. Two extra sets were developed to serve as replacements if any of the original 15 sets were found to be inappropriate. The damage abstractions are often based on results from less than 15 calculations because of input errors or numerical difficulties (see note to Table 5-5).

The stochastic (uncertain) input parameters for the 15 simulations are the 15 sets of three-component ground motion time histories, the metal-to-metal friction coefficient, and the metal-to-rock friction coefficient. A Monte Carlo sampling scheme defines the appropriate combinations of ground motion time histories and friction coefficients (BSC 2003d, Section 6.4) for each peak ground velocity level. The set of 15 ground motion time histories for these analyses is identical with that for the analyses of rockfall induced by vibratory ground motion.

These calculations incorporate the potential for corrosion to degrade the waste package over the first 20,000 years after repository closure by reducing the thickness of the Alloy 22 outer barrier on the waste package by 2 mm. These calculations evaluate mechanical properties at 150°C to represent the potential degradation in mechanical strength if a seismic hazard occurs during the initial thermal pulse after repository closure. The adequacy of the finite-element mesh and the effect of the use of rigid elements to reduce run times were considered through detailed studies that support the primary calculations (BSC 2003e, Attachments IX and VI).

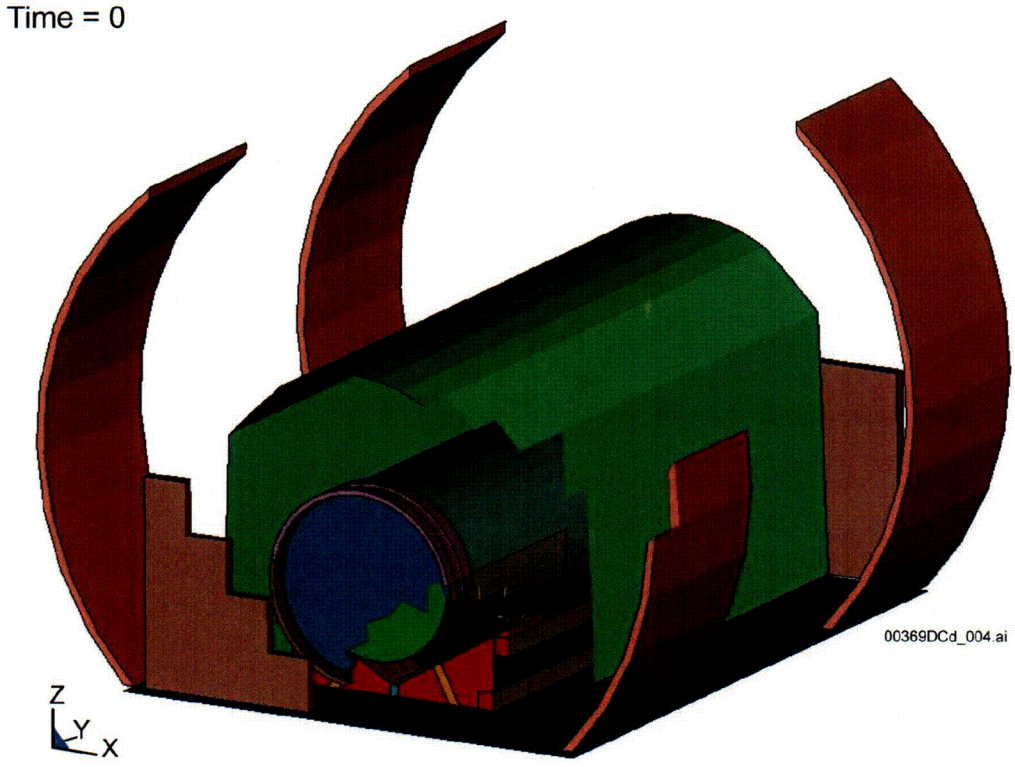

Source: BSC 2003e, Figure 2.

Figure 5-10. Cutaway View of Analysis Configuration for Waste Package Vibratory Simulations

C33

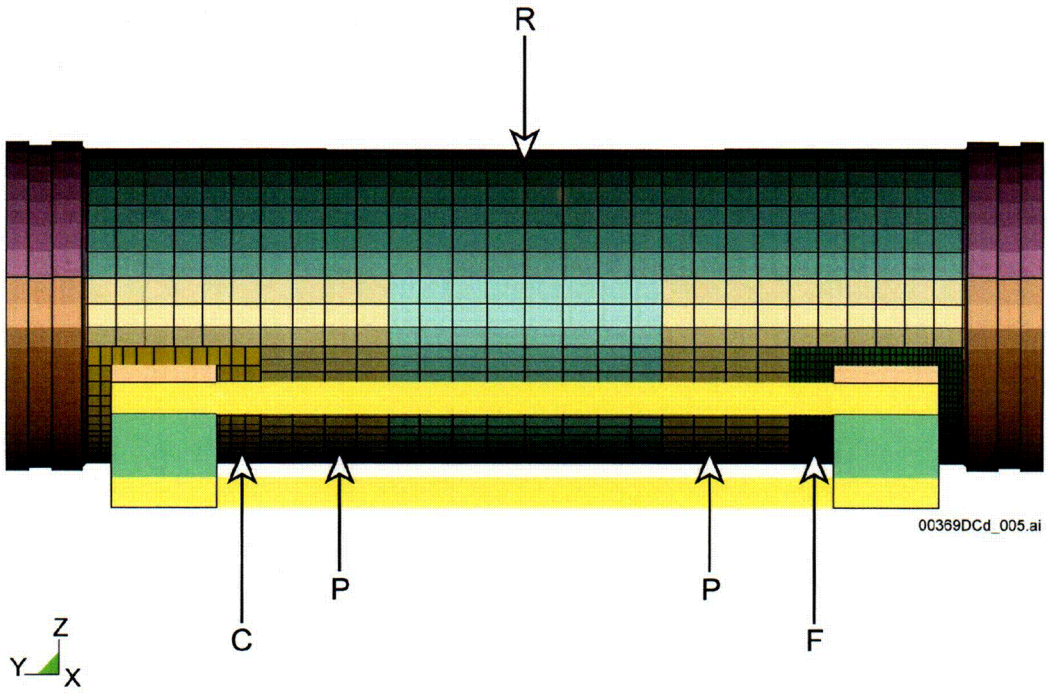

Source: BSC 2003e, Figure 4.

Figure 5-11. Finite-Element Mesh for the Outer Shell of the Waste Package

The structural response calculations do not represent the dynamic response of the invert to the ground motion. The invert is represented as an elastic body whose surface responds instantaneously and uniformly with the three-component ground motion time history. This is a reasonable approach for small-amplitude ground motion because the invert is compacted under the weight of the waste package and drip shield and because any remaining steel framework in the invert will provide some integrity to the rock mass. For high-amplitude ground motion, the invert ballast is likely to be violently redistributed, allowing the heavy EBS components to settle on the bottom of the drift, directly in contact with the rock floor. Applying the ground motion in the rock directly to the surface of the invert is again a reasonable approach for this case.

The damage to the waste package is determined by comparing the residual first principal stress on the waste package outer shell to the failure criterion for Alloy 22. Two residual stress thresholds are used to define the failed area on the outer shell of the waste package. The two stress thresholds are 80% and 90% of the yield strength of Alloy 22. These values correspond to the lower and upper bounds of the uniform distribution for the residual stress threshold (see Section 5.1).

The results from each structural response calculation are postprocessed to determine the elements in the outer shell of the waste package whose residual stress exceeds 80% or 90% of the yield strength of Alloy 22. The failed elements are then converted into a failed surface area. This conversion conservatively assumes that if a single element on the surface of the waste package fails, then all elements beneath this element also fail. This is a conservative approach because the elements inside the thickness of the drip shield may be in a compressive state that will arrest crack propagation from a stress corrosion crack. Note that the effective area for flow and

C34

transport through the waste package for TSPA will be a factor of 76 to 305 less than the failed area because the cross-sectional area of the resulting network of tight stress corrosion cracks is much less than the surface area that exceeds the residual stress threshold (see Section 5.1.5). As a numerical example, if a surface area of 1 m^2 exceeds the residual stress threshold on the surface of the waste package, then the effective area for flow and transport will be 0.00328 to 0.0131 m^2.

5.4.1.1 Waste Package Damage

The failed areas for 14 realizations at a peak ground velocity of 2.44 m/s are summarized in Table 5-5 (BSC 2003e, Table 6.1.4-2). The mean damage for the 80% residual stress threshold is approximately twice as large as the mean damage for the 90% residual stress threshold. The variability in damage (i.e., the ratio of the maximum damage to the minimum damage for a given peak ground velocity value ground motion level), is approximately a factor of 10 for each residual stress threshold. The uncertainty in ground motion rather than the uncertainty in the residual stress threshold dominate the uncertainty in damage. These observations are also true for the 14 calculations for a peak ground velocity of 5.35 m/s, corresponding to an exceedance frequency of 10^{-7} per year (BSC 2003i, Section 6.5.1).

The results in Table 5-5 also demonstrate that the total failed area is dominated by the contribution from end-to-end impacts of adjacent waste packages. The failed area from waste package-to-pallet impacts is much smaller than the damage due to the end-to-end impacts of adjacent waste packages, with the exception of realization number 14. The damage from end-to-end impacts is the dominant contribution because the adjacent waste package is conservatively represented as an essentially rigid wall anchored to the invert. The rigid wall is used for computational simplicity, but results in overestimating the damage from end-to-end impacts. This same observation is true for the failed areas from the 5.35 m/s peak ground velocity level.

The results for peak ground velocities of 2.44 m/s and 5.35 m/s have been supplemented with three additional simulations for a peak ground velocity value of 1.067 m/s, corresponding to the 10^{-5} per year annual exceedance frequency. Exact ground motion is not available for a peak ground velocity of 1.067 m/s, so approximate ground motion was created by scaling the three acceleration components for selected ground motion with a peak ground velocity of 2.44 m/s by the ratio of the peak ground velocity values, or by (1.067/2.44 =) 0.4066. This procedure is not exact, but it provides a reasonable approach to extend the peak ground velocity range of this damage abstraction. The three selected ground motion results have the highest intensity (energy) among the set of 15 ground motion results with 2.44 m/s peak ground velocity. The damage results for these three scaled ground motion results are documented in *Structural Calculations of Waste Package Exposed to Vibratory Ground Motion* (BSC 2003e, Table XI-2).

Table 5-5. Failed Area from Vibratory Ground Motion at a Peak Ground Velocity of 2.44 m/s

Realization Number[a]	Ground Motion Number	Failed Area on the Waste Package					
		Waste Package to Pallet Interaction (m^2; % of total OS area)		Waste Package to Waste Package Interaction (m^2; % of total OS area)		Total (m^2; % of total OS area)	
		80% Yield Strength	90% Yield Strength	80% Yield Strength	90% Yield Strength	80% Yield Strength	90% Yield Strength
1	7	0.0029; 0.010	0.0014; 0.0050	0.023; 0.082	0.012; 0.043	0.026; 0.092	0.013; 0.046
2	16[b]	0; 0	0; 0	0.017; 0.060	0.0089; 0.032	0.017; 0.060	0.0089; 0.032
3	4	0.0050; 0.018	0; 0	0.19; 0.67	0.083; 0.29	0.20; 0.71	0.083; 0.29
4	8	0.030; 0.11	0.0064; 0.023	0.12; 0.43	0.061; 0.22	0.15; 0.53	0.067; 0.24
5	11	0.0015; 0.0053	0; 0	0.15; 0.53	0.066; 0.23	0.15; 0.53	0.066; 0.23
6	1	0.025; 0.089	0.0028; 0.0099	0.15; 0.53	0.063; 0.22	0.18; 0.64	0.066; 0.23
7	2	0.017; 0.060	0; 0	0.11; 0.39	0.057; 0.20	0.13; 0.46	0.057; 0.20
9	10	0.0035; 0.012	0; 0	0.12; 0.43	0.062; 0.22	0.12; 0.43	0.062; 0.22
10	9	0; 0	0; 0	0.014; 0.050	0.0071; 0.025	0.014; 0.050	0.0071; 0.025
11	5	0.012; 0.043	0.0037; 0.013	0.074; 0.26	0.032; 0.11	0.086; 0.30	0.036; 0.13
12	6	0.0039; 0.014	0; 0	0.073; 0.26	0.036; 0.13	0.077; 0.27	0.036; 0.13
13	12	0; 0	0; 0	0.032; 0.11	0.016; 0.057	0.032; 0.11	0.016; 0.057
14	14	0.010; 0.035	0.0043; 0.015	0.0056; 0.020	0.0029; 0.010	0.016; 0.057	0.0072; 0.026
15	3	0.0078; 0.028	0.0015; 0.0053	0.020; 0.071	0.010; 0.035	0.028; 0.099	0.012; 0.043
				Mean Value[c]		0.310%	0.136%
				Standard Deviation[c]		0.237%	0.097%
				Minimum Value[c]		0.050%	0.025%
				Maximum Value[c]		0.710%	0.290%

Source: BSC 2003e, Table 6.1.4-2.

NOTE: [a] Only 14 realizations are presented in this table. Results for realization 8 are not presented because of an error in the input file for this calculation.

[b] Calculations are performed with 15 ground motion sets numbered 1, 2, 3, ..., 14, and 16. Time history 15 is not used because it has an anomalous response spectrum.

[c] Mean, standard deviation, minimum and maximum failed areas are calculated in *Seismic Consequence Abstraction* (BSC 2003i, Attachment II).

OS = outer surface of waste package.

5.4.1.2 Abstraction for Waste Package Damage

The uncertainty in failed area is dominated by ground motion rather than the residual stress threshold, as discussed above. In this situation, it is reasonable to simplify the damage abstraction for the waste package by averaging the failed areas at the two extremes (80% and 90%). In effect, this corresponds to a failure criterion for the average (85%) value of the residual stress thresholds. The use of the average or mean value is consistent with the release limits for the repository at Yucca Mountain, which are expressed in terms of the mean of the distribution of projected dose to the reasonably maximally exposed individual, per 10 CFR 63.303 and 63.311.

A uniform distribution provides a reasonable description of the failed area data and is simple and transparent. Figure 5-12 compares the damage results for the 2.44 m/s peak ground velocity ground motion results to the cumulative distribution function for a uniform distribution, which is simply a straight line. The fact that a straight line provides an excellent fit to the results confirms that a uniform distribution is a reasonable representation for the damage abstraction. A uniform distribution also provides a very good description of the damage results for the 5.35 m/s peak ground velocity ground motion level (BSC 2003i, Section 6.5.1).

Figure 5-13 presents the abstraction for waste package damage as a function of peak ground velocity. This damage abstraction is a uniform distribution with upper and lower bounds that are functions of peak ground velocity. The function for the upper bound is a linear fit to the maximum failed areas for 2.44 m/s and 5.35 m/s peak ground velocity ground motion. The maximum failed area is estimated with a Bayesian procedure that determines the 95th percentile confidence limit for data with a uniform distribution (Rossman et al. 1998). The function for the lower bound is constant at 0%. (See also Section 5.4.1.3 for discussion of an alternate analysis.)

The data in Figure 5-13 have been supplemented with the failed areas from the three additional simulations for a peak ground velocity of 1.067 m/s. While there are only three data points at a peak ground velocity of 1.067 m/s, these points do provide additional confidence in the extrapolation of the abstraction for waste package damage to values of peak ground velocity of 1 m/s and below.

The damage to the waste package is applied to all waste packages in the repository. There is no spatial variability for damage to the waste package because including this variability would have little impact on the mean or expected dose from the repository.

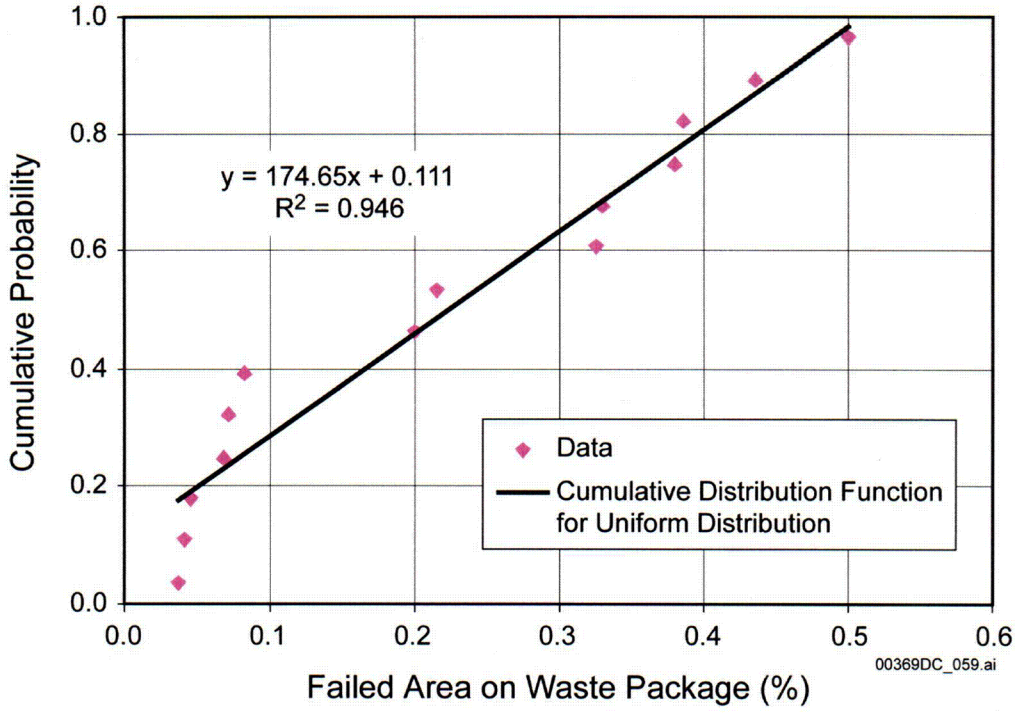

Source: BSC 2003i, Figure 5.

Figure 5-12. Comparison of Failed Area Data for the 2.44 m/s Peak Ground Velocity Ground Motion Results to a Cumulative Distribution Function for a Uniform Distribution

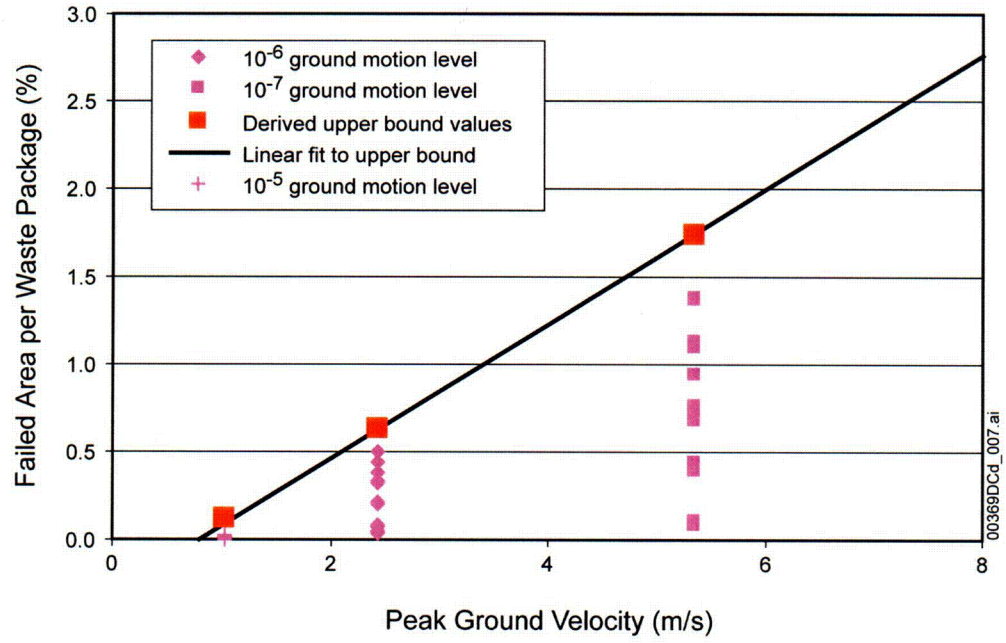

Source: BSC 2003i, Figure 7.

Figure 5-13. Comparison of Linear Fit to Bayesian Upper Bound of Damage Distribution for Peak Ground Velocity Values of 2.44, 5.35, and 1.067 m/s

C35

5.4.1.3 Fragility Analysis of Waste Package Damage

An independent technical review of the damage abstraction for the waste package has been performed (BSC 2003i, Attachment III). An alternate analysis of the damage information for the waste package was developed based on a fragility approach. In a fragility approach, the structural response data are analyzed to determine the probability that damage will exceed a given percent of surface area for a given value of peak ground velocity. A lognormal distribution is often found to provide a good fit for the fragility curves for nuclear power plant components. Following this methodology, a lognormally distributed approximation to the waste package data is fit by trial and error (BSC 2003i, Equation III-9 in Attachment III).

A comparison of the lognormal distribution at peak ground velocity of 2.44 m/s and 5.35 m/s with the uniform distribution identifies regions where the uniform distribution is nonconservative with respect to the lognormal distribution. For a peak ground velocity of 5.35 m/s, the uniform damage surface provides a good approximation for lower levels of damage but significantly underestimates exceedance probability for higher levels of damage in comparison to a lognormal distribution.

The nonconservatism at higher damage values can be easily corrected by changing the linear fit for the upper bound of the damage abstraction. Figure 5-14 compares the modified upper bound for the lognormal fit to the original upper bound for the uniform distribution. The upper bound from the lognormal distribution is the basis for the waste package damage abstraction for TSPA. With this upper bound, the failed areas for the waste package damage abstraction at the lower and upper ends of the damage range are:

- At a peak ground velocity of 1.067 m/s, corresponding to the 10^{-5} per year exceedance hazard (BSC 2003i, Table 5), the maximum failed area on the waste package is 0.16% of the surface area (BSC 2003i, Equation (4)). The minimum failed area is 0%.

- At a peak ground velocity of 10.73 m/s, corresponding to the 10^{-8} per year exceedance hazard (BSC 2003i, Table 5), the maximum failed area on the waste package is 4.4% of the surface area (BSC 2003i, Equation (4)). The minimum failed area is 0%.

The failed area on the waste package goes to zero at 0.70 m/s, which corresponds to the 3×10^{-5} per year exceedance hazard (BSC 2003i, interpolation of data in Table 5).

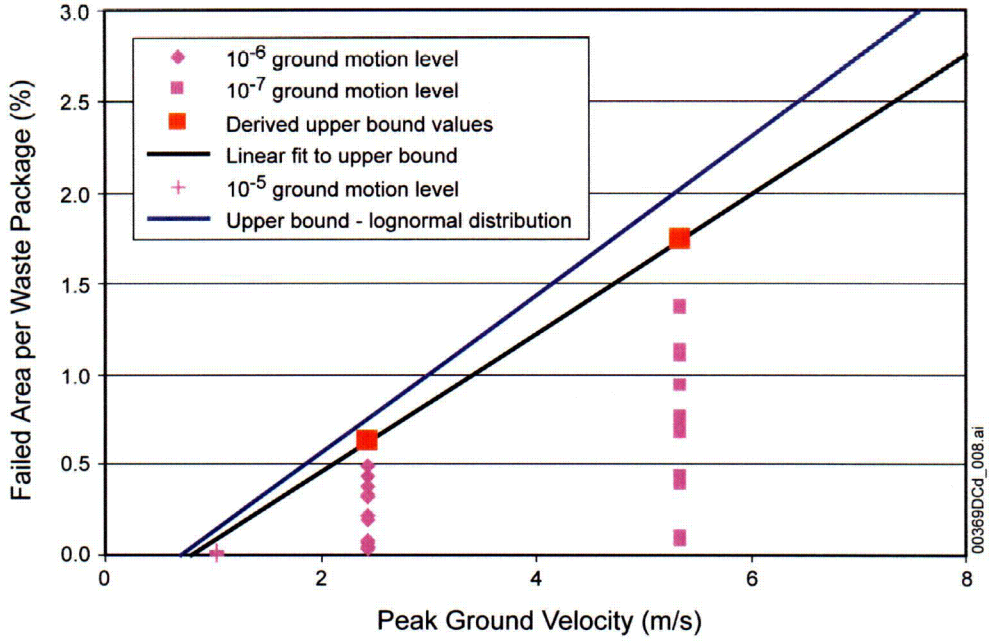

Source: BSC 2003i, Figure 8.

Figure 5-14. Upper Bound for a Lognormal Distribution (Blue Curve) in the Abstraction for Total System Performance Assessment for the License Application

5.4.2 Structural Response of the Drip Shield

Structural response calculations have been performed with the LS-DYNA code to determine if adjacent drip shields separate during high-amplitude ground motion (BSC 2003f). Separation is an important consideration because it neutralizes the drip shield as a flow barrier and rockfall barrier. These calculations also determine the failed areas on the drip shield from impacts between the drip shield and the waste package, emplacement pallet, invert, and drift wall. However, the presence of failed areas and the associated network of stress corrosion cracks is not abstracted into TSPA because the cracks are predicted to plug from evaporation-induced precipitation of calcite and other minerals in the seepage, preventing any advective flux through the drip shields.

Damage to the drip shield from vibratory ground motion is determined by structural response calculations using a commercially available version of the finite element program LS-DYNA V960 (LSTC 2001). A set of 15 calculations for the dynamic drip shield response was performed for a set of 15 ground motion results with a peak ground velocity of 2.44 m/s. A similar set of calculations was also performed for a peak ground velocity of 5.35 m/s (BSC 2003f). Figure 5-15 presents a cutaway view of the structural configuration for these calculations. The waste package and emplacement pallet is represented as a rigid, lumped mass for computational efficiency. The drip shields and package/pallets are indicated with different color schemes to distinguish the various structures in this figure.

The stochastic (uncertain) input parameters for the 15 calculations are the 15 sets of three-component ground motion time histories, the metal-to-metal friction coefficient, and the metal-to-rock friction coefficient. A Monte Carlo sampling scheme defines the appropriate

C36

combinations of ground motion time histories and friction coefficients (BSC 2003d, Section 6.4). The set of 15 ground motion time histories for these analyses is identical with that for the analyses of rockfall induced by vibratory ground motion and for waste package structural response.

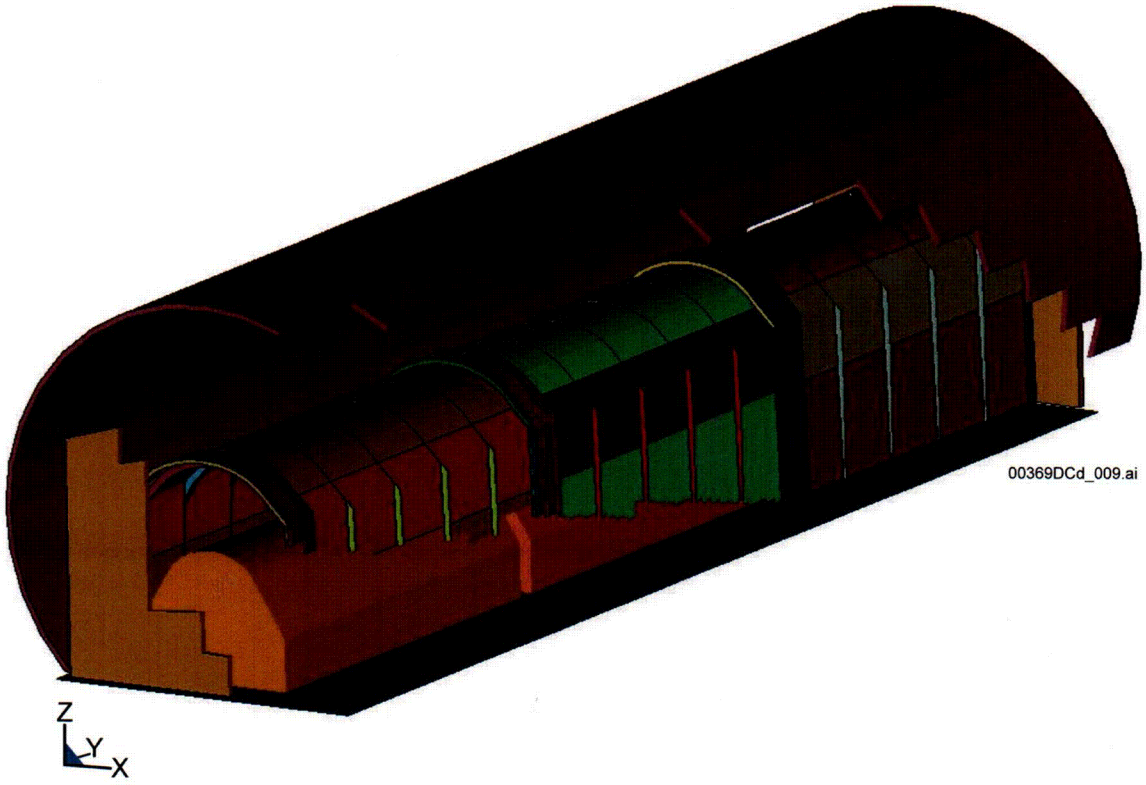

Source: BSC 2003f, Figure 2.

Figure 5-15. Cutaway View of Setup for Drip Shield Ground Motion Simulations

The damage to the drip shield from impacts is determined by comparing the residual first principal stress on the drip shield plates to the failure criterion for Titanium Grade 7. The results from each structural response calculation are postprocessed to determine the elements in the plates whose residual stress exceeds 50% of the yield strength of Titanium Grade 7; the failed elements are then converted into a failed surface area. This conversion conservatively assumes that if a single element on the surface of the drip shield fails, then all elements beneath this element also fail.

These calculations incorporate the potential for corrosion to degrade the drip shield over the first 20,000 years after repository closure by reducing the thickness of the drip shield plates by 2 mm. These calculations evaluate mechanical properties at 150°C to represent the potential degradation in mechanical strength if a seismic hazard occurs during the initial thermal pulse after repository closure. The objectivity of the finite-element mesh was also demonstrated (BSC 2003f, Attachment III).

5.4.2.1 Drip Shield Damage

The results of the structural response calculations for ground motion at the 0.18, 2.44, and 5.35 m/s peak ground velocity levels, corresponding to 5×10^{-4} per year, 10^{-6} per year, and 10^{-7} per year ground motion levels, are summarized as follows (BSC 2003f):

- One simulation performed at the 5×10^{-4} per year ground motion level indicates that there is no damage to the drip shield. More specifically, the drip shields do not separate and no area of the drip shield exceeds the residual stress threshold for Titanium Grade 7.

- Fourteen simulations are performed at the 2.44 m/s peak ground velocity ground motion level (BSC 2003f, Section 6.2 and Table 4). There is no indication of separation of drip shields in the calculations for the 2.44 m/s ground motion level. The mean percent surface area failed is 0.70% and the maximum percent failed area is 2.13%. This latter value is an outlier, in the sense that the second greatest failed area is 1.25%, or more than 40% below the maximum value.

- Five simulations performed at the 5.35 m/s ground motion level indicate separation of adjacent drip shields (BSC 2003f, Section 6.3). The ground motion becomes very intense at 5.35 m/s, resulting in large displacements and high-speed impacts for the unanchored repository components. Of the 15 simulations at this level, only one ran to completion. The other 14 simulations experienced numerical instability during some portion of the ground motion because of the large relative displacements and velocities of the EBS components.

  Separation occurs between adjacent drip shields because of plastic deformation of the drip shield and because of the large magnitude of the ground motion. In fact, each of the five simulations demonstrates that a drip shield rides over its adjacent neighbor, implying that a separation must occur somewhere in the emplacement drift. The degree to which the drip shield rides over its neighbor is substantial, on the order of 10% to 25% of the length of the drip shield (BSC 2003f, Figures IV-3 through IV-7). These separations represent a lower bound because four of the five numerical simulations terminated before the end of the ground motion time history.

A uniform distribution has been selected to represent the separation of the drip shield from vibratory ground motion. The motivation for selection of a uniform distribution is that there are only five realizations for the 5.35 m/s ground motion level, and a uniform distribution is a reasonable representation of the range defined by a small number of data points. The upper bound of the uniform distribution at the 5.35 m/s peak ground velocity or greater is 50%. The rationale for this value is that a drip shield can cover or overlap its neighbor by a substantial amount. In an extreme case, each pair of drip shields in the emplacement drifts could be reduced to one-half their original length if one member of the pair completely covers the other member of the pair. In this situation, the total length of drip shield in a drift would be reduced by 50%, and the corresponding value for the failed area is 50%.

The lower bound of the uniform distribution was initially defined as 0% at 5.35 m/s but has been modified to a positive value based on a fragility analysis of the computational results at 5.35 m/s, as described in Section 5.4.2.2.

As noted in Section 5.3.1, damage to the waste package and cladding from rockfall has been screened out from TSPA. The waste package and cladding are not damaged because the drip shield remains structurally intact for seismic hazards with a peak ground velocity up to 2.44 m/s, deflecting any rockfall away from the waste package. Seismic hazards with peak ground velocity of 5.35 m/s or greater result in separation of the drip shields, potentially exposing the waste package and cladding to rockfall. However, drip shield separation will not damage waste packages in the lithophysal zones of the repository because the lithophysal rock is predicted to shatter into small fragments (see Section 5.2.2) that have little potential to damage the waste package and its internals. Since 85% of the emplacement drifts are in lithophysal zones and since the drip shields provide partial protection in the nonlithophysal zones even for large amplitude ground motion, it is reasonable to screen out damage to the waste package and cladding from rockfall in TSPA.

5.4.2.2 Fragility Analysis of Drip Shield Damage

An independent technical review of this model abstraction has been performed (BSC 2003i, Attachment VI). The analysis is based on a fragility approach with a lognormal distribution. A comparison of the lognormal distribution to the uniform distribution shows that the uniform distribution is very conservative for percent failed areas of 0.50% and greater. This could lead to a significant overestimation of the annual probability of exceeding the percent damage when the damage is greater than 0.50% with a normal distribution.

There are only five data points for the damage at a 5.35 m/s peak ground velocity level. Given limited data, it was concluded that the drip shield is likely to be severely damaged at a peak ground velocity of 5.35 m/s or greater. The upper bound of 50% for damage is reasonable for a peak ground velocity of 5.35 m/s; however, the lower bound should probably be in excess of 10% at this level.

5.4.2.3 Final Abstraction for Drip Shield Damage

The final abstraction for drip shield damage from vibratory ground motion is based on a uniform distribution with an upper bound defined in Section 5.4.2.1 and a lower bound based on the fragility analysis in Section 5.4.2.2. The upper bound of the uniform distribution is 0% at 2.44 m/s because the structural response calculations show no indication of separation at the 2.44 m/s ground motion level and rises to 50% at the 5.35 m/s ground motion level and for all greater peak ground velocities. The value of 50% represents an upper bound when each pair of drip shields in the emplacement drifts is reduced to one-half their original length. The lower bound is a linear fit to two points: 0% damage at a peak ground velocity of 2.44 m/s and 10% damage at a peak ground velocity of 5.35 m/s. The recommendation of "in excess" of 10% does not seem appropriate because one realization already has approximately 10% damage. The minimum presumably lies below this value (BSC 2003i). The upper and lower bounds of the uniform distribution are illustrated in Figure 5-16.

These levels of damage are applied to all drip shields in the repository. There is no spatial variability to the separation of drip shields and there is no correction for effective area for flow because the damage is a physical separation, rather than a corrosion process in response to residual stress.

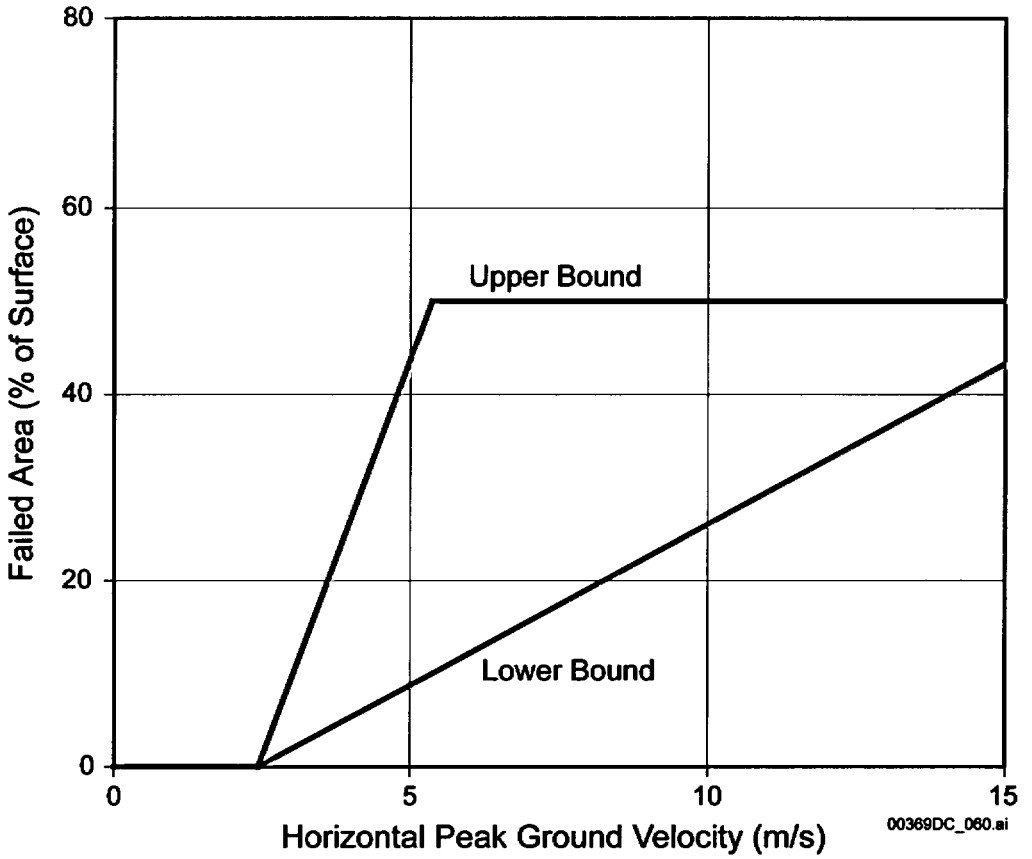

Figure 5-16. Upper and Lower Bounds of Drip Shield Damage Abstraction for Separation under Vibratory Ground Motion

5.4.3 Structural Response of the Cladding

The mechanical response of the waste package to vibratory ground motion can produce dynamic impacts between adjacent waste packages, between the waste package and its emplacement pallet, and between the waste package and the drip shield. During each of these impacts, the waste package and its internals may experience very high accelerations. These accelerations can be transmitted to the waste package internals and hence to the waste forms, and may result in failure of the cladding. The discussion in this section applies to cladding failure for commercial spent nuclear fuel. Failure of naval fuel rod cladding is not considered here. The Naval Nuclear Propulsion Program technical support document for the license application will provide the seismic analysis for naval cladding and naval spent nuclear fuel.

As noted in Section 5.4.1.1, the total failed area on the waste package is primarily generated by the end-on impact between two adjacent waste packages. In this situation, end-on impacts are expected to produce the dominant accelerations on the waste package internals. The accelerations on the fuel rod assemblies that result from end-on impact have therefore been

analyzed with the LS-DYNA finite-element program (LSTC 2001) for a range of end-on impact velocities and impact angles.

The results from each structural response calculation are postprocessed to determine the maximum peak acceleration within each fuel rod assembly and the average peak acceleration of the fuel rod assemblies. The finite-element calculations for the fuel assembly accelerations do not include any damping. Impact calculations with no damping often produce highly transient time histories with peak accelerations that are influenced by the spatial and temporal discretization of the calculations. In this situation, the output is typically filtered through a low-pass, Butterworth filter to determine a more realistic acceleration time history. The cutoff frequency for the filter is a compromise between damping the extraneous numerical noise while leaving the fundamental modes of the structure intact. A cutoff frequency of 450 Hz dampens the numerical noise but has minimal impact on the fundamental modes of fuel assembly and waste package (BSC 2003h, Attachment VIII).

The maximum peak acceleration and the average peak acceleration for all assemblies in a waste package with the 450 Hz cutoff frequency are reported in Table 5-6.

Table 5-6. Fuel Assembly Accelerations from Waste Package–to–Waste Package Impacts

	Initial Impact Velocity (m/s)				
Parameter	0.5	1	2	4	6
Maximum Peak Acceleration (g's)	75	144	263	323	506
Average Peak Acceleration (g's)	35	72	115	155	194

Source: BSC 2003h, Tables 4 and 5.

Table 5-6 provides a catalog that can be used to determine the fuel assembly accelerations at the minimum impact velocity through interpolation. The end-on impact velocities are already available through the structural response calculations for the waste package reported in Section 5.4.1. All realizations for the 2.44 m/s peak ground velocity level have an end-on impact velocity of 1.4 m/s to 4.5 m/s (BSC 2003e, Tables 6.1.2-1 through 6.1.2-15). Similarly, all realizations for the 5.35 m/s peak ground velocity level have an impact velocity of 1.3 to 6.5 m/s (BSC 2003e, Tables 6.2.2-1 through 6.2.2-15). The minimum value for the 5.35 m/s peak ground velocity level is less than that for the 2.44 m/s peak ground velocity level because of the stochastic variability in the 15 ground motion sets.

The minimum impact velocity for both sets of ground motion is 1.3 m/s. Interpolating on the data in Table 5-6 for impact velocities of 1 m/s and 2 m/s, the maximum peak acceleration for this minimum impact velocity is 180 g and the average peak acceleration for this minimum impact velocity is 85 g at 1.3 m/s.

The effect of this level of acceleration can be estimated from studies of the integrity of Zircaloy-clad light water reactor spent nuclear fuel assemblies during cask drop or tipover incidents (Chun et al. 1987; Sanders et al. 1992). Simple fuel rod failure criteria indicate that clad failure occurs between 82 and 252 g, depending on the type of fuel rod (Chun et al. 1987, Table 4). End-on impacts of adjacent waste packages result in average fuel assembly

accelerations of at least 85 g, and often much greater values for higher impact velocities. In this situation, 100% perforation of the cladding is reasonable when a ground motion event with a peak ground velocity of 2.44 m/s or greater occurs. It is also conservatively assumed that the cladding damage for the 1.067 m/s peak ground velocity level is 100%.

The cladding damage is assumed to go to zero at the 0.55 m/s peak ground velocity level. This approach is consistent with the other seismic damage abstractions (e.g., see Section 5.3.1.2). The response at this peak ground velocity level is consistent with the structural response calculation for the waste package at 0.38 m/s peak ground velocity, where there is no appreciable motion of the waste package, no impact between adjacent waste packages, and hence negligible impact forces on the fuel rods and cladding (BSC 2003e, Section 6.3). The response at this peak ground velocity level is also consistent with the assumption that damage to EBS components becomes nonzero between the 10^{-4} and 10^{-5} annual exceedance frequencies (BSC 2003i, Assumption 5.1).

The abstraction for damage to the cladding for commercial spent nuclear fuel is a simple lookup table with a linear interpolation between the four points in Table 5-7. The cladding is assumed to be 100% perforated after the seismic event for a peak ground velocity of 1.067 m/s, corresponding to the 10^{-5} per year exceedance hazard, and for a peak ground velocity of 10.73 m/s, corresponding to the 10^{-8} per year exceedance hazard. There is no uncertainty in this abstraction because the abstraction represents a conservative, bounding estimate for cladding response at all values of peak ground velocity.

Table 5-7. Abstraction for Damage to Commercial Spent Nuclear Fuel Cladding from Vibratory Ground Motion

Peak Ground Velocity Value (m/s)	Damage to Cladding (%)
0.0	0
0.55	0
1.067	100
20	100

5.5 STRUCTURAL RESPONSE TO FAULT DISPLACEMENT

Seismic events can also result in fault displacements within the emplacement drifts. Fault displacement could impact key EBS components in two ways:

- Separation between adjacent drip shields could allow a pathway for seepage to contact the waste packages, thereby potentially accelerating corrosion-induced waste package failure.
- Mechanical damage to the waste packages caused directly by the fault displacement.

For a fault displacement that occurs along an emplacement drift, a sudden discontinuity in the floor and roof of the tunnel may occur. This would result in one portion of the tunnel being displaced relative to the adjacent section. Such a discontinuity in the tunnel axis could cause

separation of adjacent drip shields and, if severe enough, could cause shearing of a waste package at that location. The discussion in this section identifies the conditions under which these damage mechanisms could occur.

5.5.1 Clearance between Engineered Barrier System Components and the Drift

The actual response of the EBS components to a fault displacement scenario is complicated. As a conservative simplification, the fault displacement is analyzed considering:

- The fault is perpendicular to the tunnel axis with the displacement being purely vertical.
- The fault displacement occurs at a discrete point, creating a "knife edge" discontinuity.

Vertical faulting is consistent with the faults investigated in the Cross-Drift tunnel that was excavated as part of the ECRB investigation. By treating the faults as perpendicular to the tunnel axis, no credit is taken for sideways movement of the waste packages that could lessen the degree to which fault displacement could cause damage.

A sudden discontinuity in the tunnel floor would tend to raise one end of a drip shield and waste package. However, the other EBS components, specifically the invert and emplacement pallet, would also be affected. A significant amount of the invert (ballast) from the elevated portion of the tunnel is expected to fall into the lower tunnel segment. In addition, the steel supports in the invert and the emplacement pallet are likely to collapse at the plane of displacement, further degrading the integrity of the invert.

The exact details of these events are difficult to predict. As a simplification, the approximation is simply made that the emplacement pallet collapses into the invert on the elevated side of the fault. No credit is taken for any further shifting of the ballast in the invert. Using this approximation, the clearance around the waste package ranges from 606 to 1,398 mm, based on the drip shield internal height and the diameter of the waste package type (BSC 2003i, Table 20).

Failure of the drip shields could also occur without direct waste package damage. One mechanism for this is lifting of one drip shield relative to its neighbor, thereby creating a pathway for ingress of seepage water onto the waste package. However, drip shield failure without waste package damage will have low consequence for performance assessment, so it will be screened out from TSPA based on low consequence and is not considered further.

5.5.2 Faults Intersecting Emplacement Drifts

Based on *Probabilistic Seismic Hazard Analyses for Fault Displacement and Vibratory Ground Motion at Yucca Mountain, Nevada* (CRWMS M&O 1998, Section 8), fault displacement can occur on five known faults that intersect the repository emplacement drifts: the western splay off the main Ghost Dance Fault, the Sundance Fault, the Pagany Wash Fault, the Sever Wash Fault, and the Drill Hole Wash Fault. During a major seismic event, faulting could also occur elsewhere in the repository. In evaluating the potential for this latter type of faulting, four generic rock conditions have been considered, ranging from intact rock to the presence of existing small faults with approximately 2 m of cumulative offset. Large displacement on any of these geologic features is inherently a very low probability event. For example, the exceedance

frequency on the known secondary faults must be less than 2×10^{-7} per year to equal or exceed the minimum clearance between any waste package and the drip shield.

The exact location and number of small faults with 2 m offset is not known, so it is necessary to estimate the density of these features throughout the repository. Based on data from the characterization of the ECRB Cross-Drift (Mongano et al. 1999, pp. 51 to 59), it can be estimated that there are 138 locations where small faults intersect the emplacement drifts in the repository.

5.5.3 Fault Displacement Hazards

The *Probabilistic Seismic Hazard Analyses for Fault Displacement and Vibratory Ground Motion at Yucca Mountain, Nevada* (CRWMS M&O 1998, Section 8) provides fault displacement hazard curves for the Drill Hole Wash Fault and the Sundance Fault; displacements on the Pagany Wash Fault and the Sever Wash Fault are assumed to be identical to those on the Drill Hole Wash Fault. The generic small faults with a 2-m offset are designated Site 7(a) and Site 8(a) in the PSHA. The fault displacement hazard curves are essentially identical at 7(a) and 8(a).

Table 5-8 provides the displacement values from the mean hazard curves for the relevant faults as a function of the mean annual exceedance frequency. Locations 7 and 8 have essentially the same estimated displacements, so the distinction between 7a and 8a for the 138 small fault intersections described in Section 5.5.2 is not relevant.

Table 5-8. Fault Displacements within the Repository from Mean Hazard Curves

Site Number and Fault Name	Vertical Displacement (cm)	Mean Annual Exceedance Frequency (1/yr)
3 – Drill Hole Wash[a]	< 0.1	10^{-4}
	< 0.1	10^{-5}
	17	10^{-6}
	80	10^{-7}
	240	10^{-8}
5 – Sundance	< 0.1	10^{-4}
	< 0.1	10^{-5}
	6	10^{-6}
	42	10^{-7}
	~145	10^{-8}
7a – Small fault with 2-m offset, and 8a – Small fault with 2-m offset	< 0.1	10^{-4}
	< 0.1	10^{-5}
	2	10^{-6}
	20	10^{-7}
	~75	10^{-8}

Source: DTN: MO0401MWDRPSHA.000.

NOTE: [a]Also representative of Pagany Wash Fault and Sever Wash Fault.

The potential tunnel intersections with the western splay off the main Ghost Dance Fault are not included in Table 5-8 and are not included in the fault displacement model for TSPA. The West Ghost Dance Fault intersects drifts 2-17 through 2-27, which lie within a contingency area for repository development. Given the uncertainties in the use of the contingency area at this time, it is reasonable to exclude consideration of displacement along the western splay off the main Ghost Dance Fault in TSPA.

5.5.4 Consequence for the Waste Package Groups

The information in Table 5-8 shows that the fault displacements on the Drill Hole Wash Fault and the Sundance Fault are greater than the minimum available clearance (606-mm) near the 10^{-8} per year level. In other words, fault displacement can crimp or partly shear the waste package at this probability level, resulting in failure. In addition, the largest diameter waste packages containing high-level radioactive waste can potentially fail when placed over the small generic fault with a 2 m offset (designated 7a and 8a). The likelihood of waste package failure at a given fault location is a function of the clearance for the specific type of waste package.

Waste package numbers by type are available in the design basis inventory. To simplify the analysis, the inventory of waste packages is split into four groups. The four groupings and the percentage of total inventory are shown in Table 5-9. The percentage of inventory for each waste package group is based on total length of the group versus the total length of all emplaced waste packages. Length is the appropriate parameter here because it more accurately represents the probability that a waste package will lie on a fault.

A determination of waste package failure is made by comparing the available clearance in Table 5-9 with the fault displacement hazard in Table 5-8. At mean annual exceedance frequencies between 10^{-7} per year and 10^{-8} per year, waste package failure may occur for any of the waste packages placed directly over the four known secondary faults intersecting the emplacement drifts because the fault displacement values in Table 5-8 exceed the available clearances in Table 5-9. A similar situation exists for any high-level radioactive waste packages placed over faults characterized by small generic fractures, sites 7a and 8a.

Table 5-9. Parameters for Simplified Groups of Waste Packages

Waste Package Group	Description	Clearance (cm)	Fraction of Waste Package (% of Total Length)
PWR	21-PWR with absorber plates, 21-PWR with control rods, and 12-PWR long with absorber plates	107.2	41.9
BWR	44-BWR with absorber plates and 24-BWR with absorber plates	104.2	26.7
Naval	Naval –SNF Long and Naval SNF Short	76.7	3.1
High-Level Radioactive Waste	5 defense high-level radioactive waste /1 DOE spent nuclear fuel–short, 5 defense high-level radioactive waste/1 DOE spent nuclear fuel–long, all other high-level radioactive waste designs	60.6	28.3

5.5.5 Damage Abstraction for Fault Displacement

Combining information on the known fault intersections with the probability of finding a particular waste package group at a given point in the repository (see Table 5-9), the expected number of each type of waste package found at the four secondary faults and at the generic fracture with a 2-m offset can be calculated. With this information, the expected number of waste package failures can be calculated as a function of annual exceedance frequency. A waste package is assumed to fail by vertical shearing when the (vertical) fault displacement (see Table 5-8) is greater than the clearance between the waste package and the drip shield (see Table 5-9). The number of failed packages is a function of annual exceedance frequency because the fault displacement varies with annual exceedance frequency. The number of failures is also a function of waste package type because clearance between waste package and drip shield varies with the waste package design. These results are summarized in Table 5-10 (BSC 2003i, Attachment VII). The maximum number of failed waste packages from fault displacement, 52.18, is a very small percentage (less than 0.5%) of the total number of waste packages in the repository.

Table 5-10. Expected Waste Package Failures versus Annual Exceedance Frequency

Annual Exceedance Frequency (1/yr)	Expected Number of Waste Package Failures				
	PWR	BWR	Naval	High-Level Radioactive Waste	Total
$> 2 \times 10^{-7}$	0	0	0	0	0
10^{-7} to 2×10^{-7}	0	0	0	4.53	4.53
6×10^{-8} to 10^{-7}	0	0	0.49	4.53	5.02
5×10^{-8} to 6×10^{-8}	6.71	4.28	0.49	4.53	16.00
4×10^{-8} to 5×10^{-8}	6.71	4.28	0.49	5.37	16.85
3×10^{-8} to 4×10^{-8}	6.71	4.28	0.58	5.37	16.94
2×10^{-8} to 3×10^{-8}	7.97	5.08	0.58	5.37	19.00
10^{-8} to 2×10^{-8}	7.97	5.08	0.58	38.56	52.18

When a waste package fails by fault displacement, there are two consequences for TSPA: (1) the failed area on the waste package is determined by sampling a uniform distribution with a lower bound of zero and an upper bound equal to the area of the waste package lid and (2) the drip shield and most cladding associated with this waste package are also assumed to fail as barriers to flow and transport. Failure of naval fuel rod cladding is not considered.

The failed area on the waste package represents the extremes of response. The failed area can be 0% for a package that experiences very minor crimping without failure. The failed area can also be as large as the waste package lid, if the lid welds are broken from severe crimping of the package due to fault displacement. The potential for minor crimping to result in accelerated crack growth and a network of stress corrosion cracks is ignored in determining releases for fault displacement in TSPA. In other words, the cross-sectional areas for flow and transport are simply the failed areas.

A sheared drip shield will allow all seepage to pass through it so there is no diversion of seepage by the drip shield. Similarly, the nonnaval fuel rod cladding becomes 100% perforated in response to a fault displacement that can shear a waste package. The consequences for the drip shield and cladding represent conservative, bounding approximations.

These consequence models are admittedly simplistic and almost certainly conservative. This approach is reasonable because there is significant uncertainty in the expected magnitude of fault displacements at very low probabilities and because the detailed response of EBS components directly above a fault is difficult to predict. Given this lack of precision, a highly detailed calculation of drip shield and waste package response to fault displacement is not warranted.

5.5.6 Alternate Conceptual Model for Damage from Fault Displacement

An alternate conceptual model for damage from fault displacement is based on historical earthquake activity in the western United States (Waiting et al. 2003). Surface rupture data from four representative historic earthquakes were analyzed to determine fault rupture density (length of faulting per unit area of surface). Median values ranged from 5 to 30 km/km^2 (Waiting et al. 2003, p. 383). Using representative values for fault rupture density (20 km/km^2), tunnel orientation (50°), and drift spacing (80 m), Waiting et al. (2003, p. 385) determined that there would be 191 waste package locations where a fault would intersect an emplacement drift. This result is comparable to the 168 fault intersections determined in *Seismic Consequence Abstraction* (BSC 2003i, Section 6.8.2) using site-specific data for Yucca Mountain.

To compute the probability-weighted number of waste package failures, Waiting et al. (2003) considered the 1983 Borah Peak, Idaho, earthquake as an analog for a fault displacement event at Yucca Mountain. Prior analysis of this event had shown that the maximum displacement was 2.7 m, with an average displacement of approximately 1 m. Based on the PSHA for Yucca Mountain, a fault displacement of 1 m has an annual probability of being exceeded ranging from 10^{-6} for the Solitario Canyon Fault to 10^{-8} for the Sundance Fault. Assuming that all waste package intersections lead to waste package failure, Waiting et al. (2003, p. 385) calculate an annual probability-weighted number of waste package failures ranging from 1.91×10^{-4} to 1.91×10^{-6}. In *Seismic Consequence Abstraction* (BSC 2003i, Section 6.8.6), the annual probability-weighted number of waste package failures is determined to be 2.38×10^{-6}, which lies within the range calculated using the alternate conceptual model.

5.6 POSTSEISMIC CHANGES IN THE LOCAL ENVIRONMENT

A large seismic event, involving both vibratory ground motion and fault displacement, can change the local environment around the emplacement drifts. The most obvious physical change is that the emplacement drifts in the lithophysal zone are predicted to collapse as a result of the 2.44 m/s peak ground velocity ground motion level and, by inference at greater peak ground velocity levels. Drift collapse can alter the shape of the drift and fill it with a natural backfill, resulting in the following potential process-level changes in and around the EBS:

- Seepage into a collapsed drift may increase because of the irregular drift shape and because of loosening of the fractures around the drift. A change in the seepage flux into the emplacement drifts in the lithophysal zones is being incorporated into the seismic

abstractions for TSPA. The effects of drift degradation on seepage are summarized in Section 4.7 of *Technical Basis Document No. 3: Water Seeping into Drifts*. There is no change in the seepage flux into the emplacement drifts in the nonlithophysal zones.

- Temperature of the drip shield and waste package may increase relative to an unfilled drift because the backfill provides an insulating blanket on top of the drip shield. The presence of rubble around the drip shield will also cause changes in relative humidity on the EBS components. The magnitude of these changes has been estimated with thermal-hydraulic calculations using the multiscale model (BSC 2004c). These calculations predict changes in temperature and relative humidity for eight different waste package emplacement configurations, using bounding (high or low) values for the thermal conductivity of the rubble surrounding the drip shield. The results from these calculations (DTN: LL040310323122.044) are included in the model for localized corrosion in TSPA.

A second seepage-related change can occur for seismic events during the rewetting period. If a damaging seismic event occurs at a time when the conditions for the existence of accelerated localized corrosion of Alloy 22 are satisfied, then all seepage that enters the drip shield will flow into the waste package without any flux splitting. This is a reasonable change because enhanced localized corrosion on the waste package will generate corroded areas directly beneath the seeps through the drip shield.

INTENTIONALLY LEFT BLANK

6. SEISMIC SYSTEM PERFORMANCE

6.1 SEISMIC SCENARIO CLASS

The seismic scenario class is based on a single modeling case, with a focus on seismic events with frequencies less than 10^{-4} per year because the associated ground motion and fault displacements have the potential to cause damage to the EBS components. The response of the drip shield, waste package, and cladding is represented through damage abstractions for the EBS components under vibratory ground motion and fault displacement. The failed areas on the EBS components define pathways for flow and transport through the engineered barriers. Once radionuclides are released from the EBS, flow and transport in the unsaturated zone and the saturated zone are based on the same models and algorithms as for the nominal scenario class, with the exceptions of the seepage abstraction in the lithophysal zones of the repository and of the flux-splitting for the waste package if accelerated localized corrosion can occur. Biosphere calculations and parameters for the seismic scenario class are also unchanged from those for the nominal scenario class.

The impact of seismic hazards on repository performance is being represented in TSPA by a scenario, called the seismic scenario class, which is separate from the nominal scenario class. The rationale for defining a separate scenario is based on several key observations:

- Seismic events with annual frequencies down to 10^{-8} per year must be considered by TSPA.

  10 CFR 63.114, Requirements for Performance Assessment, states that:

  > Any performance assessment used to demonstrate compliance with §63.113 must ... (d) Consider only events that have at least one chance in 10,000 of occurring over 10,000 years.

  Therefore, very large seismic hazards (i.e., ground motion or fault displacements or both) with annual probability of occurrence down to 10^{-8} per year must be considered by TSPA, even though their probability is very low during the 10,000-year regulatory period.

- The nominal scenario class cannot determine the impact of low-probability seismic events in a computationally efficient manner. A separate scenario class for seismic hazards is desirable.

  Events with very small annual probabilities of occurrence cannot be represented in the nominal scenario class in a computationally efficient fashion. Accurate representation of events with annual probability of occurrence down to 10^{-8} per year would require millions of realizations in the nominal scenario class, which is not computationally feasible. The alternative is to define a separate scenario for seismic hazards that determines dose in a probability-weighted manner, as explained below.

- The mean dose time history is the main parameter for compliance determinations.

  Radionuclide release limits for the repository are expressed in terms of the mean of the distribution of projected doses to the reasonably maximally exposed individual, per 10 CFR 63.303 and 63.311. Calculation of releases from the seismic scenario class must generate mean dose for consistency with the nominal scenario class.

- Damage from seismic events is expressed as a failed area or as an effective cross-sectional area for flow and transport through the surfaces of the drip shield, the waste package, and the cladding.

  The damage from seismic events is based on the separation area for advective flow through the drip shield, on the effective cross-sectional area of a network of stress corrosion cracks for flow and transport through the waste package, and on the perforation of the cladding. These areas are a function of the amplitude of the seismic event, such as horizontal peak ground velocity. The individual damage abstractions for the waste package, the drip shield, and the cladding are based on the results from structural response calculations and rockfall calculations, as discussed in Section 5.

6.2 COMPUTATIONAL APPROACH

The mean dose for the seismic scenario class is calculated using a two-step approach: (1) TSPA generates a set of R realizations that have robust sampling of all levels of seismic hazards with the potential to generate releases from the EBS, and (2) the mean or expected dose time history is calculated using a weighted sum and average of the dose time histories from the R realizations evaluated during the first step. Additional postprocessing can present results as cumulative distribution functions, as complementary cumulative distribution functions, or can evaluate the variability of the dose time histories, if necessary.

6.2.1 Description of the First Step

The first step generates R realizations of future performance with the TSPA model for the seismic scenario class for both fault displacement and ground motion hazards. This suite of R realizations represents the knowledge uncertainty and randomness uncertainty in the TSPA model for the seismic scenario class. Knowledge uncertainty, also called epistemic uncertainty, is represented by all those stochastic parameters that represent the "lack of knowledge" for geologic material properties, for engineered material properties, and for the models of long-term processes in the repository. Randomness uncertainty, also called aleatory uncertainty, is represented by the stochastic parameters that capture the randomness of events and their associated features, such as the uncertainty in the timing and amplitude of seismic hazards. Epistemic uncertainty can usually be reduced by performing additional experimental studies; aleatory uncertainty is inherent in the seismic hazards and cannot be eliminated.

The TSPA model for the seismic scenario class is very similar to the TSPA model for the nominal scenario class, with two major exceptions: (1) failed areas on the drip shield, waste package, or cladding are determined by sampling stochastic parameters in damage abstractions for EBS components, rather than by the waste package degradation (WAPDEG) model for

corrosion processes; and (2) a single seismic event occurs at a random time during each realization. The output from each of these R realizations is a time history of dose to the reasonably maximally exposed individual.

Each realization has a single seismic event that occurs at a randomly selected time during the duration of the calculation. For each realization, the time of occurrence of the seismic hazard, T_i, and the amplitude of the seismic hazard, PGV_i, are determined by Monte Carlo sampling of the mean peak ground velocity hazard curve. Once the value for PGV_i is known, the abstractions for the failed areas on the waste package, drip shield, and cladding are sampled. This approach explicitly includes the variability from the ground motion and structural response calculations in the TSPA model by sampling these distributions.

Damage from fault displacement occurs simultaneously with damage from vibratory ground motion. The value of the exceedance frequency determines the number of damaged waste packages by type, based on the abstraction in Table 5-10. The failed area on the waste package from fault displacement is determined by sampling a distribution with a lower bound of zero and an upper bound based on the lid area for each type of waste package. The associated drip shields and cladding are assumed to fail completely.

6.2.2 Description of the Second Step

Each of the R realizations generates a time history of dose to the reasonably maximally exposed individual, conditional upon the occurrence of a single seismic event. These dose time histories do not represent the mean dose, as called for in 10 CFR 63.303, because a damaging seismic event always occurs in each realization. A mean dose time history is calculated using a probability-weighted sum and average of all the realizations for the seismic scenario class. The mathematical basis for calculating the mean dose as a weighted sum and average of the individual dose time histories is presented in *Seismic Consequence Abstraction* (BSC 2003i, Attachment VIII). The weighting factors correct for the number of expected seismic events in each realization and for the distributions for the time of occurrence and amplitude of the seismic hazard.

6.3 TREATMENT OF UNCERTAINTY

Uncertainty has been directly represented in the seismic scenario for TSPA. The following discussion highlights the sources of uncertainty in the structural response calculations for the waste package and drip shield, the rockfall calculations, and the damage abstractions for TSPA.

The structural response calculations for the waste package and drip shield response under vibratory ground motion include three major sources of uncertainty: the ground motion time histories, the metal-to-metal friction coefficient, and the metal-to-rock friction coefficient.

- Fifteen sets of three-component ground motion time histories were used to represent the uncertainty in the seismic hazard at a given peak ground velocity frequency (i.e., 2.44 m/s for the 10^{-6} per year exceedance frequency or 5.35 m/s at the 10^{-7} per year exceedance frequency). Although each set of 15 ground motion results are scaled to have the same horizontal peak ground velocity, the peak ground acceleration and the

duration of the time histories span a wide range of response. For example, the peak ground acceleration for the first horizontal ground motion component at the 10^{-6} per year hazard level ranges from about 1.5 g to 7 g.

- The metal-to-metal friction coefficient between the waste package and emplacement pallet varies from 0.2 to 0.8. The friction coefficient affects the onset of sliding and dissipation of energy for the EBS components as a function of the amplitude of the ground motion. However, the importance of friction is expected to diminish with increasing ground motion level because the EBS components begin to slide almost immediately for high-amplitude ground motion.

- The metal-to-rock friction coefficient between the emplacement pallet and the invert or between the drip shield and the invert varies from 0.2 to 0.8. Again, the friction coefficient affects the onset of sliding and dissipation of energy for the unanchored EBS components as a function of the amplitude of the ground motion. However, the importance of friction is anticipated to diminish with increasing amplitude of the ground motion.

The variations of these uncertain input parameters are simultaneously included in the structural response calculations at each seismic hazard level. This is accomplished by a Monte Carlo procedure that ensures robust sampling of the uncertain parameters over their full ranges. The Monte Carlo procedure and the sampled values of the three uncertain input parameters are described and documented in *Sampling of Stochastic Input Parameters for Rockfall and Structural Response Calculations Under Vibratory Ground Motions* (BSC 2003d).

All rockfall calculations include 15 ground motion sets to again represent the uncertainty in the seismic hazard at each value peak ground velocity. In the lithophysal units, the rock mass category is an uncertain input parameter that is represented as five discrete levels of rock lithophysal porosity and associated mechanical properties. A sixth rock mass category with very poor rock quality is also defined as an extreme lower bound for some calculations. In the nonlithophysal units, the synthetic fracture pattern is an uncertain input parameter. The synthetic fracture pattern is a representation of the fracture system geometry in three dimensions. Approximately 70 synthetic fracture patterns are used in the rockfall calculations for the nonlithophysal units. The variations in these uncertain parameters are simultaneously included in the rockfall analyses at each seismic hazard level (BSC 2003d).

The calculations of failed areas on the waste package and drip shield due to vibratory ground motion and rockfall induced by vibratory ground motion exhibit substantial variability due to the uncertainties in seismic ground motion and other input parameters. This variability has been directly represented in TSPA by defining stochastic parameters that are sampled during each realization of the seismic scenario class. For example,

- For a given value of peak ground velocity, failed area on the waste package from vibratory ground motion is represented as a uniform distribution that is sampled for each realization of the seismic scenario class. The sampled value of the failed area is further reduced to define the effective cross-sectional area of a network of stress corrosion

cracks for flow and transport. This reduction is based on a uniform distribution that captures the uncertainty in the crack density and crack length for the network.

- Drip shield separation from vibratory ground motion is represented as a uniform distribution that is sampled for each realization of the seismic scenario class.

INTENTIONALLY LEFT BLANK

7. CONCLUSIONS

This technical basis document documents the case for the following six key conclusions about low-probability seismic events:

Much is known about seismic hazards at Yucca Mountain. The geology and seismology of the site have been studied intensively for more than 20 years. Site characterization activities have generated much data regarding the vibratory ground motion and fault displacement hazards at Yucca Mountain. These data sets include:

- Compilation of a historical catalog of earthquakes to support analyses of earthquake recurrence rate and magnitude distribution. A 47-station network of primarily vertical component seismometers was installed in 1978 and 1979 specifically to characterize the seismicity of the Yucca Mountain region. This network is still in place and has been reconfigured and upgraded with three-component seismograph systems and modern digital recording and telemetry technology.

- Establishment of a network of 27 three-component strong-motion stations to record ground motion from moderate and large earthquakes in the vicinity of Yucca Mountain. Seventeen of the strong motion stations are located at the surface, one is sited in Alcove 5 of the ESF, and nine are installed in three boreholes (surface, mid-depth, and bottom locations) in the surface facilities area near the North Portal of the ESF.

- Reconnaissance geologic surveys of known and suspected Quaternary faults within 100 km of the site to characterize their extent and rates of activity. These studies have shown that Yucca Mountain lies in the Walker Lane, a transitional zone of deformation between the Basin and Range domain to the northeast and the Inyo-Mono domain to the southwest. In this transitional domain, geologic faults accommodate a combination of extensional and strike-slip crustal deformation.

- Geophysical surveys conducted to assist with the interpretation of the geometry of structures in the subsurface and ongoing geodetic monitoring to determine the rates of regional tectonic deformation.

- Detailed geologic mapping and paleoseismic studies of known and possible Quaternary faults near Yucca Mountain to provide information on past earthquakes, including their number, size, extent, and timing. Detailed geologic mapping and data from 52 trenches that were excavated across possible Quaternary faults have identified those faults with evidence of Quaternary movement. Slip rates (time-averaged rates of displacement) on faults at Yucca Mountain are low relative to the range for faults in the Basin and Range Province.

- Analysis of ground motion data from local earthquakes to evaluate ground motion numerical models. Six different ground motion models were developed for Yucca Mountain by different experts. These models were calibrated against data from the nearby Little Skull Mountain earthquake of 1992.

- Analysis of ground motion data from extensional tectonic regimes to provide information on the regional rate of seismic-wave attenuation. The results of this analysis, the site-specific ground motion models described above and published attenuation relations based on western United States and global data sets, were carefully considered by a panel of ground motion experts in developing attenuation relations for Yucca Mountain.

The data sets that have been developed as a result of these site characterization activities over the past 20 years provide a strong basis for the PSHA interpretations.

Potentially significant seismic effects on repository performance have been considered and addressed as appropriate. A comprehensive list of seismic-related FEPs was considered and each FEP "screened" in or out of TSPA, based on assessments of the probability and consequence of each FEP. The FEPs considered and their screening status are summarized in Table 7-1.

Table 7-1. Seismic-Related Features, Events, and Processes and Screening Status

Seismic-Related Features, Events, and Processes	Screening Status
Tectonic activity—large scale	Out: low consequence
Fault displacement damages EBS components	In
Seismic ground motion damages EBS components	In
Seismic-induced rockfall damages EBS components	In
Seismic-induced drift collapse damages EBS components	Out: low consequence
Seismic-induced drift collapse alters in-drift thermal-hydrology	In
Seismicity associated with igneous activity	In
Hydrologic response to seismic activity	Out: low consequence
Seismic activity changes porosity and permeability of rock	Out: low consequence
Seismic activity changes porosity and permeability of faults	Out: low consequence
Seismic activity changes porosity and permeability of fractures	Out: low consequence
Seismic activity alters perched water zones	Out: low consequence

The technical bases for excluding the FEPs that relate to seismic effects on the natural systems at Yucca Mountain are summarized in Section 1.3. The effects of the screened-in FEPs were systematically analyzed. Seismicity associated with igneous activity is reflected in the PSHA seismic hazard curves that form the basis of the seismic consequences evaluation. Seismically induced stresses in the walls of the emplacement drifts can cause blocks of rock to be shaken loose and lead to accelerated drift degradation and rockfall. The mechanical impact of rockfall on the drip shields is not expected to cause immediate mechanical rupture but, rather, to leave residual stresses in the titanium plates of the drip shields. Similarly, vibratory ground motion is not expected to lead to immediate tensile failure but could, at very low probability levels, cause significant separation between adjacent drip shields. Severe, low-probability ground motion also could cause impacts between adjacent waste packages, between the waste package and its

emplacement pallet, and between the waste package and the drip shield. These impacts are not calculated to cause an immediate puncture or tear in the barrier but would impose residual stresses in the Alloy 22 outer shell of the waste package. Given the calculated residual stress levels in the drip shields and waste packages and a set of failure criteria that specify the residual tensile stress levels at which accelerated corrosion is expected to occur, the percent of the surface areas of the drip shields and waste packages that fail due to accelerated corrosion was calculated. In TSPA, immediate drip shield and waste package failure is assumed once the residual stress thresholds for Alloy 22 is exceeded, resulting a network of through-wall stress corrosion cracks. Similarly, the drip shield fails immediately once separation occurs from vibratory ground motion and the cladding fails immediately upon perforation. Analogous to the consequence analysis for seismic loading from vibratory ground motion, the EBS seismic effects analysis also calculates failed waste package surface areas from extremely low probability fault-displacement events. Seismically induced drift collapse would change the profile of emplacement drifts and result in rock rubble throughout part or all of an emplacement drift. The rock rubble would affect temperatures inside the drift, but not significantly. The change in drift profile would reduce the effectiveness of the drift as a capillary barrier and lead to increased water seepage into the emplacement drift. Seismic effects that have potentially significant consequences for repository performance are incorporated into TSPA.

The seismic hazard analysis that has been carried out for Yucca Mountain accounts for both the variability in vibratory ground motion and fault displacement due to the inherent randomness of earthquake processes and uncertainty due to limitations in scientific knowledge.

In the Yucca Mountain PSHA, seven seismologists and earthquake engineers who are experts in ground motion estimation evaluated available worldwide and regional strong ground motion recordings and other relevant data about seismic wave propagation in the Yucca Mountain region. As part of a formal, documented expert-elicitation process, each expert then separately identified alternative ground motion interpretations to express his or her uncertainty, due to data limitations, about the true nature of seismic-wave propagation at Yucca Mountain. Each expert also provided weights to be applied to each interpretation that reflect his or her evaluation of the relative likelihood that a particular interpretation is closer to physical reality than the other alternative interpretations. Variability in earthquake ground motion due to the inherent randomness in earthquake processes is expressed by random variables that are specified in each interpretation.

A similar process was followed in the PSHA study for the identification and characterization of seismic sources. In this case, six expert teams, rather than individual experts, provided the interpretations. Each expert team consisted of three earth scientists who collectively had sufficient expertise in seismology, geology, geophysics, and tectonics to be able to identify and characterize seismic sources based on the available information. Following a formal, documented process of expert elicitation, each team developed alternative seismic-source interpretations and weights for those interpretations. The range of interpretations and the assigned weights express uncertainty in current scientific understanding of seismic sources. Variability in earthquake location, recurrence rate, and magnitude due to the random nature of earthquake occurrences is expressed by random variables that are specified in each interpretation.

The Yucca Mountain PSHA was conducted in general accordance with current guidance published by the NRC (Kotra et al. 1996; Budnitz et al. 1997) regarding probabilistic seismic hazard analysis, uncertainty, and the elicitation of expert judgment.

Large ground motion predicted by the probabilistic seismic hazard analysis at annual exceedance probabilities of 1.0×10^{-6} and below may be physically unrealizable and may substantially overestimate the severity of low-probability ground motion at Yucca Mountain. This potential overestimation of ground motion is addressed through consideration of constraints on maximum ground motion imposed by the stress-release characteristics of seismic sources and by limits on strain that can be propagated by seismic waves through rocks similar to those at Yucca Mountain.

In the PSHA, random variability in ground motion was characterized by unbounded probability distributions. At lower annual probabilities of exceedance, tails of these unbounded distributions control the predicted ground motion. The predicted ground motion values are very high and may be physically unrealizable. The rocks at Yucca Mountain may not be able to sustain the strains that would be produced by such high ground motion without physical damage that would tend to limit the amplitude of the motion. In addition, the combinations of seismic source parameters needed to generate such high ground motion may not be reasonable.

Studies to examine limits to the upper range of ground motion at Yucca Mountain are underway. Three approaches are being explored to determine at what level the amplitude of ground motion may saturate. One approach looks at what level of ground motion would be required to physically damage the rock at Yucca Mountain. The strength of the rock will be compared to the levels of strain that would be induced in the rock by very high ground motion. Preservation of crystalline material lining some lithophysae and lack of observed shattered rock in underground excavations suggest that ground motion high enough to damage the rock has not occurred at Yucca Mountain since the rocks were deposited (i.e., in about the last 10 million years). A second approach examines how nonlinear effects below the PSHA reference rock outcrop might limit ground motion as the motion reaches very high levels. The third approach employs numerical modeling to assess what combinations of seismic source parameters are required to produce very high ground motion at Yucca Mountain. The parameter combinations will be assessed to determine if they are realistic and reasonable.

While these studies of ground motion saturation have been initiated, results are not yet complete. Consequently, there remains considerable uncertainty about upper-bound ground motion at Yucca Mountain. In the seismic consequences abstraction for the TSPA seismic scenario, this uncertainty is expressed by a broad probability distribution on upper-bound peak ground velocity. In each realization or run of the TSPA, a peak ground velocity is sampled from the appropriate PSHA hazard curve, and a value is sampled from the upper-bound distribution. If the sampled peak ground velocity is greater than the sampled upper bound, its value is reset to that of the sampled upper bound. The resulting value is then used in that TSPA realization.

Seismic and tectonic effects on the natural systems at Yucca Mountain will not significantly affect repository performance. Yucca Mountain lies in a region of ongoing tectonic deformation, but the deformation rates are too slow to significantly affect the mountain during the 10,000-year regulatory compliance period. Rises in the water table caused by seismic

activity would be, at most, a few tens of meters and would not reach the repository. The fractured and faulted volcanic tuff that comprises Yucca Mountain reflects the occurrence of many earthquake-faulting and strong ground motion events during the last several million years, and the hydrologic characteristics of the rock would not be changed significantly by seismic events that may occur in the next 10,000 years.

The engineered barrier system components are robust under seismic loads and will provide substantial protection of the waste form from seepage water, even under severe seismic loading. Damaging rockfall in the nonlithophysal zone is not expected for peak ground velocities of 0.55 m/s or less, corresponding to an annual probability of exceedance of 5×10^{-5}. For a peak ground velocity of 2.44 m/s, corresponding to an annual exceedance probability of 10^{-6}, approximately 33% of the simulations performed predict no rockfall. For the simulations that do predict rockfall, the resulting mode for failed surface area of drip shields is 0.197%, and the resulting mean is 1.698%. The failed-area estimate is based on the assumption that residual tensile stresses in excess of 50% of the yield strength of Titanium Grade 7 will lead to accelerated corrosion. For a peak ground velocity of 5.35 m/s, corresponding to an annual exceedance probability of 1.0×10^{-7}, approximately 21% of the simulations predict no rockfall. For the simulations that do predict rockfall, the resulting modal drip shield failed area is 5.83% and the mean failed area is 3.405%.

Any cracks that result from rockfall on the drip shield are expected to plug from evaporation-induced precipitation of minerals in the groundwater. The small heat flux across the drip shield will result in evaporation of slowly flowing seepage, causing a scale deposit to form around the mouth of the crack and within the crack. A detailed calculation of the expected rate of crack plugging due to evaporation-induced precipitation of calcite demonstrates that cracks will be sealed within a few hundred years when water is allowed to flow through the cracks at the expected rate for thin film flow. Once a crack is plugged with precipitates the magnitude of the liquid flux through the crack will become insignificant because of the expected high density of calcite deposits, the lack of a significant pressure head or gradient to drive liquid through the crack, and the observed high tortuosity and roughness of the crack geometry. Damage to the drip shield from rockfall has been excluded from TSPA on this basis.

A small amount of rockfall is predicted in the lithophysal zone for a peak ground velocity of 0.18 m/s (annual probability of exceedance of 5×10^{-4}). Total drift collapse is predicted for a peak ground velocity of 2.44 m/s (10^{-6} annual exceedance probability) and, hence, also for higher velocities and lower probability levels. However, because of the small joint spacing in the lithophysal zone, the drifts there are predicted to disintegrate into small fragments that would not have enough mass and energy to cause significant permanent deformation of the drip shield. Drift collapse in the lithophysal zone would impose a static load on the drip shields from the weight of the natural backfill that would form as a result of the collapse. However, the calculated average stress in the large support beams of the drip shields is far below their yield strength. Thus, rockfall and drift collapse in the lithophysal zone is not expected to damage drip shields and, because of the protection afforded by the drip shields, is not expected to damage waste packages or cladding.

Residual stress levels in the drip shields from impacts between EBS components caused by severe vibratory ground motion have been analyzed. The results indicate no failure due to

accelerated corrosion for ground motion with an annual exceedance probability of 5×10^{-4}. At a probability level of 10^{-6}, the mean failed surface area is 0.70%, and the maximum failed surface area is 2.13%. However, this failure is not represented in TSPA because the resulting cracks on the drip shield are expected to be plugged with mineral precipitates, preventing a significant advective flux through the drip shields. For ground motion at the 10^{-7} level, a limited number of simulations indicate that drip shields separate and ride over each other by a substantial amount. In the abstraction of drip shield damage for the TSPA, it is assumed that a drip shield can override an adjacent drip shield, for annual probability levels of 10^{-7} and below. Complete override of each pair of drip shields results in the maximum failed surface area on the drip shield of up to 50%.

The mechanical response of the waste package to severe vibratory ground motion can produce dynamic impacts between adjacent waste packages, between the waste package and its emplacement pallet, and between the waste package and the drip shield. During each of these impacts, the waste package internals may experience accelerations high enough to fail the cladding. In the TSPA abstraction for cladding damage, it is conservatively assumed that 100% of the cladding is damaged for ground motion levels with an annual probability of exceedance of 10^{-5} and below.

Structural response calculations for the waste package indicate, for vibratory ground motion with annual exceedance probabilities of 10^{-5}, 10^{-6}, and 10^{-7}, the maximum calculated failed surface areas are less than 0.2%, 0.8%, and 2%, respectively. The waste package damage abstraction predicts that the maximum failed surface area is less than 5% for an annual exceedance probability of 10^{-8}.

The most likely failure mechanism from a seismic event is accelerated stress corrosion cracking in the failed areas that exceed the residual stress threshold for Alloy 22. Previous industrial experience with pressurized systems, such as pipelines and light water reactors, indicated that these deformed areas are expected to remain physically intact, so it is reasonable to base the effective area for flow and transport through the waste package as a dense network of stress corrosion cracks, rather than as a plug of material that separates from the outer barrier. The effective area of the crack network has been conservatively estimated, based on the density of a hexagonal array of cracks with minimum separation given by the through-wall thickness and with variable length. The effective area of the crack network is a factor of 76 to 305 times less than the corresponding failed surface area for the waste package. This effective area is the cross-sectional area of the crack network for flow and transport calculations for TSPA.

Mean fault displacements from the PSHA fault-displacement hazard curves are less than the clearance between waste packages and drift walls for all annual exceedance probabilities greater than 2×10^{-7} and, hence, no fault-displacement damage is predicted at this probability level. Below this probability level, the expected number of waste package failures due to fault displacement ranges from about five waste packages (out of about 11,000) for annual exceedance probabilities between 10^{-7} and 2×10^{-7}, to about 50 waste packages, for annual exceedance probabilities between 10^{-8} and 2×10^{-8}. In the TSPA abstraction for damage due to fault displacement, it is conservatively assumed that the drip shield and cladding fail whenever the waste package fails.

In summary, no EBS damage is expected for vibratory ground motion with an annual exceedance probability of 5×10^{-5} (20,000-year recurrence). Cladding failure is assumed to occur with an annual probability of 10^{-5} (100,000-year recurrence). However, at this probability level no damage to the drip shields is expected from rockfall or vibratory ground motion because any resulting cracks plug from mineral precipitates, and the maximum waste package failed area due to vibratory ground motion and the corresponding maximum effective area are less than 0.2% and 0.003%, respectively. At an annual probability of 10^{-6} (million-year recurrence), the drip shield does not fail as a flow barrier due to rockfall or vibratory ground motion and the maximum waste package failed area and the maximum effective transport area due to vibratory ground motion are less than 1% and 0.013%, respectively. At an annual probability level of 10^{-7} (10-million year recurrence), adjacent drip shields can separate and ride over each other, reducing their effective surface area by up to 50%. However, at this probability level, substantial protection of the waste form from advective flow and transport is still provided by the waste package, with a maximum failed surface area of less than 2% and a maximum effective surface area for flow and transport through stress corrosion cracks of less than 0.03%. Fault displacement hazard is not a significant contributor to the risk of seismically induced EBS damage, with no damage predicted for mean fault displacements with annual exceedance probabilities greater than 2×10^{-7} (5-million year recurrence) and only a small fraction of the inventory of waste packages predicted to be damaged by fault displacement for probabilities down to 10^{-8} (100-million year recurrence). These results indicate that the EBS components are robust under seismic loads and will provide substantial protection of the waste form from seepage water even under severe seismic loading.

INTENTIONALLY LEFT BLANK

8. REFERENCES

8.1 DOCUMENTS CITED

Abrahamson, N.A. and Becker, A.M. 1996. "Estimation of Vibratory Ground Motion at Yucca Mountain." Chapter 10 of *Seismotectonic Framework and Characterization of Faulting at Yucca Mountain, Nevada.* Whitney, J.W., ed. Milestone 3GSH100M. Denver, Colorado: U.S. Geological Survey. TIC: 237980. ACC: MOL.19970129.0041.

Anderson, M.J. 2003. *Waste Package Design Technical Exchange, Waste Package Seismic Response.* Presented to U.S. Nuclear Regulatory Commission, June 5, 2003, Las Vegas, Nevada. Las Vegas, Nevada: Yucca Mountain Site Characterization Office. ACC: MOL.20030715.0011.

Andresen, P.L.; Emigh, P.W.; Young, L.M.; and Gordon, G.M. 2001. "Stress Corrosion Cracking of Annealed and Cold Worked Titanium Grade 7 and Alloy 22 in 110°C Concentrated Salt Environments." *Corrosion/2001, 56th Annual Conference & Exposition, March 11-16, 2001, Houston, Texas, USA.* Paper No. 01130. Houston, Texas: NACE International. TIC: 255671.

Anooshehpoor, A. and Brune, J.N. 2000. *Annual Report, Precarious Rock Methodology for Seismic Hazard.* Reno, Nevada: University of Nevada, Reno. ACC: MOL.20000824.0562.

Atkinson, G.M. 1995. "Attenuation and Source Parameters of Earthquakes in the Cascadia Region." *Bulletin of the Seismological Society of America, 85,* (5), 1327–1342. El Cerrito, California: Seismological Society of America. TIC: 247913.

Bennett, R.A.; Davis, J.L.; and Wernicke, B.P. 1999. "Present-Day Pattern of Cordilleran Deformation in the Western United States." *Geology, 27,* (4), 371–374. Boulder, Colorado: Geological Society of America. TIC: 246484.

Bennett, R.A.; Wernicke, B.P.; and Davis, J.L. 1998. "Continuous GPS Measurements of Contemporary Deformation Across the Northern Basin and Range Province." *Geophysical Research Letters, 25,* (4), 563–566. Washington, D.C.: American Geophysical Union. TIC: 248140.

Boore, D.M.; Joyner, W.B.; and Fumal, T.E. 1994. *Estimation of Response Spectra and Peak Accelerations from Western North American Earthquakes: An Interim Report, Part 2.* Open-File Report 94-127. Menlo Park, California: U.S. Geological Survey. TIC: 246666.

Brocher, T.M.; Hunter, W.C.; and Langenheim, V.E. 1998. "Implications of Seismic Reflection and Potential Field Geophysical Data on the Structural Framework of the Yucca Mountain-Crater Flat Region, Nevada." *Geological Society of America Bulletin, 110,* (8), 947–971. Boulder, Colorado: Geological Society of America. TIC: 238643.

Brune, J.N. 1996. "Precariously Balanced Rocks and Ground-Motion Maps for Southern California." *Bulletin of the Seismological Society of America, 86,* (1A), 43–54. El Cerrito, California: Seismological Society of America. TIC: 249711.

Brune, J.N. 2000. "Precarious Rock Evidence for Low Ground Shaking on the Footwall of Major Normal Faults." *Bulletin of the Seismological Society of America, 90,* (4), 1107–1112. El Cerrito, California: Seismological Society of America. TIC: 249712.

Brune, J.N. and Anooshehpoor, A. 1999. "Dynamic Geometrical Effects on Strong Ground Motion in a Normal Fault Model." *Journal of Geophysical Research, 104,* (B1), 809–815. Washington, D.C.: American Geophysical Union. TIC: 249707.

Brune, J.N.; Nicks, W.; and Aburto, A. 1992. "Microearthquakes at Yucca Mountain, Nevada." *Bulletin of the Seismological Society of America, 82,* (1), 164–174. El Cerrito, California: Seismological Society of America. TIC: 212563.

Brune, J.N. and Whitney, J.W. 2000. "Precarious Rocks and Seismic Shaking at Yucca Mountain, Nevada." Chapter M of *Geologic and Geophysical Characterization Studies of Yucca Mountain, Nevada, a Potential High-Level Radioactive-Waste Repository.* Version 1.0. DDS-058. Denver, Colorado: U.S. Geological Survey. TIC: 249438.

BSC (Bechtel SAIC Company) 2001a. *Plugging of Stress Corrosion Cracks by Precipitates.* CAL-EBS-MD-000017 REV 00. Las Vegas, Nevada: Bechtel SAIC Company. ACC: MOL.20011010.0168.

BSC 2001b. *Environment on the Surfaces of the Drip Shield and Waste Package Outer Barrier.* ANL-EBS-MD-000001 REV 00 ICN 02. Las Vegas, Nevada: Bechtel SAIC Company. ACC: MOL.20010724.0082.

BSC 2002. *Geotechnical Data for a Potential Waste Handling Building and for Ground Motion Analyses for the Yucca Mountain Site Characterization Project.* ANL-MGR-GE-000003 REV 00. Las Vegas, Nevada: Bechtel SAIC Company. ACC: MOL.20021004.0078.

BSC 2003a. *Preliminary Seismic Analysis for Preclosure Safety Analysis.* CAL-MGR-MD-000012 REV 00A. Las Vegas, Nevada: Bechtel SAIC Company. ACC: DOC.20030930.0001.

BSC 2003b. *Drift Degradation Analysis.* ANL-EBS-MD-000027 REV 02. Las Vegas, Nevada: Bechtel SAIC Company. ACC: DOC.20030709.0003.

BSC 2003c. *Development of Earthquake Ground Motion Input for Preclosure Seismic Design and Postclosure Performance Assessment of a Geologic Repository at Yucca Mountain, NV.* MDL-MGR-GS-000003 REV 00. Las Vegas, Nevada: Bechtel SAIC Company. ACC: DOC.20031201.0001.

BSC 2003d. *Sampling of Stochastic Input Parameters for Rockfall and Structural Response Calculations Under Vibratory Ground Motions.* ANL-EBS-PA-000009 REV 00. Las Vegas, Nevada: Bechtel SAIC Company. ACC: DOC.20030707.0003.

BSC 2003e. *Structural Calculations of Waste Package Exposed to Vibratory Ground Motion.* 000-00C-EBS0-00300-000-00B. Las Vegas, Nevada: Bechtel SAIC Company. ACC: ENG.20030520.0003.

BSC 2003f. *Structural Calculations of Drip Shield Exposed to Vibratory Ground Motion.* 000-00C-PEC0-00100-000-00A. Las Vegas, Nevada: Bechtel SAIC Company. ACC: ENG.20030618.0009.

BSC 2003g. *Drip Shield Structural Response to Rock Fall.* 000-00C-TED0-00500-000-00A. Las Vegas, Nevada: Bechtel SAIC Company. ACC: ENG.20030327.0001.

BSC 2003h. *Maximum Accelerations on the Fuel Assemblies of a 21-PWR Waste Package During End Impacts.* 000-00C-DSU0-01100-000-00A. Las Vegas, Nevada: Bechtel SAIC Company. ACC: ENG.20030327.0002.

BSC 2003i. *Seismic Consequence Abstraction.* MDL-WIS-PA-000003 REV 00. Las Vegas, Nevada: Bechtel SAIC Company. ACC: DOC.20030818.0006.

BSC 2003j. *Stress Corrosion Cracking of the Drip Shield, the Waste Package Outer Barrier, and the Stainless Steel Structural Material.* ANL-EBS-MD-000005 REV 01. Las Vegas, Nevada: Bechtel SAIC Company. ACC: DOC.20030717.0001.

BSC 2003k. *Drop of a Waste Package on Emplacement Pallet—A Mesh Study.* 000-00C-DSU0-02200-000-00A. Las Vegas, Nevada: Bechtel SAIC Company. ACC: ENG.20030915.001.

BSC 2003l. *Drip Shield Statically Loaded by Backfill and Loose Rock Mass.* 000-00C-TED0-00300-000-00A. Las Vegas, Nevada: Bechtel SAIC Company. ACC: ENG.20030224.0004.

BSC 2004a. *Preclosure Seismic Design Methodology for a Geological Repository at Yucca Mountain.* TDR-WHS-MD-000004 REV 00. Las Vegas, Nevada: Bechtel SAIC Company. ACC: DOC.20040121.0008.

BSC 2004b. *Features, Events, and Processes: Disruptive Events.* ANL-WIS-MD-000005 REV 001. Las Vegas, Nevada: Bechtel SAIC Company. ACC: DOC.20031212.0005; DOC.20040209.0001; DOC.20040401.0006.

BSC 2004c. *Multiscale Thermohydrologic Model.* ANL-EBS-MD-000049 REV 01. Las Vegas, Nevada: Bechtel SAIC Company. ACC: DOC.20040301.0004.

BSC 2004d. *Development of Earthquake Ground Motion Input for Preclosure Seismic Design and Postclosure Performance Assessment of a Geologic Repository at Yucca Mountain, NV.* MDL-MGR-GS-000003 REV 00, with errata. Las Vegas, Nevada: Bechtel SAIC Company. ACC: DOC.20031201.0001, DOC20040401.0004.

BSC 2004e. *D&E / PA/C IED Emplacement Drift Configuration and Environment.* 800-IED-MGR0-00201-000-00B. Las Vegas, Nevada: Bechtel SAIC Company. ACC: ENG.20040326.0001.

Budnitz, R.J.; Apostolakis, G.; Boore, D.M.; Cluff, L.S.; Coppersmith, K.J.; Cornell, C.A.; and Morris, P.A. 1997. *Recommendations for Probabilistic Seismic Hazard Analysis: Guidance on the Uncertainty and Use of Experts.* NUREG/CR-6372. Two volumes. Washington, D.C.: U.S. Nuclear Regulatory Commission. TIC: 235076; 235074.

Carr, W.J. 1990. "Styles of Extension in the Nevada Test Site Region, Southern Walker Lane Belt; An Integration of Volcano-Tectonic and Detachment Fault Models." Chapter 13 of *Basin and Range Extensional Tectonics Near the Latitude of Las Vegas, Nevada.* Wernicke, B.P., ed. Memoir 176. Boulder, Colorado: Geological Society of America. TIC: 222540.

Chun, R.; Witte, M.; and Schwartz, M. 1987. *Dynamic Impact Effects on Spent Fuel Assemblies.* UCID-21246. Livermore, California: Lawrence Livermore National Laboratory. ACC: HQX.19881020.0031.

CRWMS M&O (Civilian Radioactive Waste Management System Management and Operating Contractor) 1998. *Probabilistic Seismic Hazard Analyses for Fault Displacement and Vibratory Ground Motion at Yucca Mountain, Nevada.* Milestone SP32IM3, September 23, 1998. Three volumes. Las Vegas, Nevada: CRWMS M&O. ACC: MOL.19981207.0393.

CRWMS M&O 2000. *Characterize Framework for Seismicity and Structural Deformation at Yucca Mountain, Nevada.* ANL-CRW-GS-000003 REV 00. Las Vegas, Nevada: CRWMS M&O. ACC: MOL.20000510.0175.

Day, W.C.; Dickerson, R.P.; Potter, C.J.; Sweetkind, D.S.; San Juan, C.A.; Drake, R.M., II; and Fridrich, C.J. 1998. *Bedrock Geologic Map of the Yucca Mountain Area, Nye County, Nevada.* Geologic Investigations Series I-2627. Denver, Colorado: U.S. Geological Survey. ACC: MOL.19981014.0301.

dePolo, C.M. 1994. "Estimating Fault Slip Rates in the Great Basin, USA." *Proceedings of the Workshop on Paleoseismology, 18-22 September, 1994, Marshall, California.* Prentice, C.S.; Schwartz, D.P.; and Yeats, R.S., eds. Open-File Report 94-568. Pages 48–49. Menlo Park, California: U.S. Geological Survey. TIC: 234812.

Dixon, T.H.; Robaudo, S.; Lee, J.; and Reheis, M.C. 1995. "Constraints on Present-Day Basin and Range Deformation from Space Geodesy." *Tectonics, 14,* (4), 755–772. Washington, D.C.: American Geophysical Union. TIC: 234271.

DOE (U.S. Department of Energy) 2002. *Yucca Mountain Science and Engineering Report.* DOE/RW-0539, Rev. 1. Washington, D.C.: U.S. Department of Energy, Office of Civilian Radioactive Waste Management. ACC: MOL.20020404.0042.

EPRI (Electric Power Research Institute) 1986. "Methodology." Volume 1 of *Seismic Hazard Methodology for the Central and Eastern United States.* EPRI NP-4726. Palo Alto, California: Electric Power Research Institute. TIC: 222575.

EPRI 1993. *Appendices for Ground Motion Estimation.* Volume 2 of *Guidelines for Determining Design Basis Ground Motions.* EPRI TR-102293. Palo Alto, California: Electric Power Research Institute. TIC: 226496.

Gomberg, J. 1991a. "Seismicity and Detection/Location Threshold in the Southern Great Basin Seismic Network." *Journal of Geophysical Research, 96,* (B10), 16401–16414. Washington, D.C.: American Geophysical Union. TIC: 212627.

Gomberg, J. 1991b. "Seismicity and Shear Strain in the Southern Great Basin of Nevada and California." *Journal of Geophysical Research, 96,* 16383–16399. Washington, D.C.: American Geophysical Union. TIC: 225033.

Harbert, W. and Cox, A. 1989. "Late Neogene Motion of the Pacific Plate." *Journal of Geophysical Research, 94,* (B3), 3052–3064. Washington, D.C.: American Geophysical Union. TIC: 240848.

Harmsen, S.C. and Bufe, C.G. 1992. *Seismicity and Focal Mechanisms for the Southern Great Basin of Nevada and California: 1987 through 1989.* Open-File Report 91-572. Denver, Colorado: U.S. Geological Survey. ACC: NNA.19920408.0001.

Herrera, M.L. 2004. *Evaluation of the Potential Impact of Seismic Induced Deformation on the Stress Corrosion Cracking of the YMP Waste Packages.* SIR-04-015, Rev. 1. San Jose, California: Structural Integrity Associates. ACC: MOL.20040311.0149.

Kotra, J.P.; Lee, M.P.; Eisenberg, N.A.; and DeWispelare, A.R. 1996. *Branch Technical Position on the Use of Expert Elicitation in the High-Level Radioactive Waste Program.* NUREG-1563. Washington, D.C.: U.S. Nuclear Regulatory Commission. TIC: 226832.

LSTC (Livermore Software Technology Corporation) 2001. *LS-DYNA, Theoretical Manual.* Livermore, California: Livermore Software Technology Corporation. TIC: 252119.

Majer, E.L.; Feighner, M.; Johnson, L.; Daley, T.; Karageorgi, E.; Lee, K.H.; Williams, K.; and McEvilly, T. 1996. *Surface Geophysics.* Volume I of *Synthesis of Borehole and Surface Geophysical Studies at Yucca Mountain, Nevada and Vicinity.* Milestone OB05M. Berkeley, California: Lawrence Berkeley National Laboratory. ACC: MOL.19970610.0150.

Martinez, L.J.; Meertens, C.M.; and Smith, R.B. 1998. "Rapid Deformation Rates Along the Wasatch Fault Zone, Utah, From First GPS Measurements with Implications for Earthquake Hazard." *Geophysical Research Letters, 25,* (4), 567–570. Washington, D.C.: American Geophysical Union. TIC: 246585.

McCalpin, J.P. 1995. "Frequency Distribution of Geologically Determined Slip Rates for Normal Faults in the Western United States." *Bulletin of the Seismological Society of America, 85,* (6), 1867–1872. El Cerrito, California: Seismological Society of America. TIC: 236669.

McGarr, A. 1984. "Some Applications of Seismic Source Mechanism Studies to Assessing Underground Hazard." *Proceedings of the 1st International Congress on Rockbursts and Seismicity in Mines, Johannesburg, 1982.* Gay, N.C. and Wainwright, E.H., eds. Pages 199–208. Johannesburg, South Africa: South African Institute of Mining and Metallurgy. TIC: 254652.

McGuire, R.K.; Silva, W.J.; and Costantino, C.J. 2001. *Technical Basis for Revision of Regulatory Guidance on Design Ground Motions: Hazard- and Risk-Consistent Ground Motion Spectra Guidelines.* NUREG/CR-6728. Washington, D.C.: U.S. Nuclear Regulatory Commission. TIC: 251294.

Menges, C.M., and Whitney, J.W. 1996. "Summary of Quaternary Faulting on the Paintbrush Canyon, Stagecoach Road, and Bow Ridge Faults." Chapter 4.4 of *Seismotectonic Framework and Characterization of Faulting at Yucca Mountain, Nevada.* Whitney, J.W., ed. Milestone 3GH100M. Denver, Colorado. U.S. Geological Survey. TIC: 237980. ACC: MOL.19970129.0041.

Mongano, G.S.; Singleton, W.L.; Moyer, T.C.; Beason, S.C.; Eatman, G.L.W.; Albin, A.L.; and Lung, R.C. 1999. *Geology of the ECRB Cross Drift - Exploratory Studies Facility, Yucca Mountain Project, Yucca Mountain, Nevada.* Deliverable SPG42GM3. Denver, Colorado: U.S. Geological Survey. ACC: MOL.20000324.0614.

NRC (U.S. Nuclear Regulatory Commission) 1989. "Seismic System Analysis." Revision 2 of Section 3.7.2 of *Standard Review Plan for the Review of Safety Analysis Reports for Nuclear Power Plants, LWR Edition, July 1987.* NUREG-0800. Washington, D.C.: U.S. Nuclear Regulatory Commission. ACC: MOL.20030910.0151.

Oliver, H.W.; Ponce, D.A.; and Hunter, W.C., eds. 1995. *Major Results of Geophysical Investigations at Yucca Mountain and Vicinity, Southern Nevada.* Open-File Report 95-74. Menlo Park, California: U.S. Geological Survey. ACC: MOL.19980305.0122.

Pezzopane, S.K.; Bufe, C.G.; Dawson, T.E.; Wong, I.G.; and Bott, J.D.J. 1996. "Historical Seismicity in the Yucca Mountain Region." Chapter 7 of *Seismotectonic Framework and Characterization of Faulting at Yucca Mountain, Nevada.* Whitney, J.W., ed. Milestone 3GSH100M. Denver, Colorado: U.S. Geological Survey. TIC: 237980. ACC: MOL.19970129.0041.

Pezzopane, S.K.; Whitney, J.W.; and Dawson, T.E. 1996. "Models of Earthquake Recurrence and Preliminary Paleoearthquake Magnitudes at Yucca Mountain." Chapter 5 of *Seismotectonic Framework and Characterization of Faulting at Yucca Mountain, Nevada.* Whitney, J.W., ed. Milestone 3GH100M. Denver, Colorado. U.S. Geological Survey. TIC: 237980. ACC: MOL.19970129.0041.

Ponce, D.A. 1996. *Interpretive Geophysical Fault Map Across the Central Block of Yucca Mountain, Nevada.* Open-File Report 96-285. Denver, Colorado: U.S. Geological Survey. ACC: MOL.19980302.0026.

Ponce, D.A. and Langenheim, V.E. 1994. *Preliminary Gravity and Magnetic Models Across Midway Valley and Yucca Wash, Yucca Mountain, Nevada.* Open-File Report 94-572. Menlo Park, California: U.S. Geological Survey. ACC: MOL.19990406.0399.

Potter, C.J.; Dickerson, R.P.; Sweetkind, D.S.; Drake, R.M., II.; Taylor, E.M.; Fridrich, C.J.; San Juan, C.A.; and Day, W.C. 2002. *Geologic Map of the Yucca Mountain Region, Nye County, Nevada.* Geologic Investigations Series I-2755. Denver, Colorado: U.S. Geological Survey. TIC: 253945.

Rogers, A.M.; Harmsen, S.C.; and Meremonte, M.E. 1987. *Evaluation of the Seismicity of the Southern Great Basin and Its Relationship to the Tectonic Framework of the Region.* Open-File Report 87-408. Denver, Colorado: U.S. Geological Survey. ACC: HQX.19880315.0004.

Rossman, A.J.; Short, T.H.; and Parks, M.T. 1998. "Bayes Estimators for the Continuous Uniform Distribution." *Journal of Statistic Education.* Alexandria, Virginia: American Statistical Association. Accessed April 7, 2003. TIC: 254033. http://www.amstat.org/publications/jse/v6n3/rossman.html

Sadigh, K.; Chang, C.-Y.; Abrahamson, N.A.; Chiou, S.J.; and Power, M.S. 1993. "Specification of Long-Period Ground Motions: Updated Attenuation Relationships for Rock Site Conditions and Adjustment Factors for Near-Fault Effects." *Proceedings of ATC 17-1 Seminar on Seismic Isolation, Passive Energy Dissipation, and Active Control, San Francisco, California, March 11-12, 1993. 1,* 59-70. Redwood City, California: Applied Technology Council. TIC: 238494.

Sanders, T.L.; Seager, K.D.; Rashid, Y.R.; Barrett, P.R.; Malinauskas, A.P.; Einziger, R.E.; Jordan, H.; Duffey, T.A.; Sutherland, S.H.; and Reardon, P.C. 1992. *A Method for Determining the Spent-Fuel Contribution to Transport Cask Containment Requirements.* SAND90-2406. Albuquerque, New Mexico: Sandia National Laboratories. ACC: MOV.19960802.0116.

Sauber, J. 1989. *Geodetic Measurement of Deformation in California.* NASA Technical Memoir 100732. Washington, D.C.: National Aeronautics and Space Administration. TIC: 242343.

Savage, J.C.; Lisowski, M.; Svarc, J.L.; and Gross, W.K. 1995. "Strain Accumulation Across the Central Nevada Seismic Zone, 1973-1994." *Journal of Geophysical Research, 100,* (B10), 20257–20269. Washington, D.C.: American Geophysical Union. TIC: 236811.

Schneider, J.F.; Abrahamson, N.A.; and Hanks, T.C. 1996. *Ground Motion Modeling of Scenario Earthquakes at Yucca Mountain, Final Report for Activity 8.3.1.17.3.3.* Volume 1. Denver, Colorado: U.S. Geological Survey. ACC: MOL.19980617.0477.

Silva, W. 1997. "Characteristics of Vertical Strong Ground Motions for Applications to Engineering Design." *Proceedings of the FHWA/NCEER Workshop on the National Representation of Seismic Ground Motion for New and Existing Highway Facilities held at the Park Plaza Hotel, Burlingame, California, May 29-30, 1997.* Friedland, I.M.; Power, M.S.; and Mayes, R.L., eds. Technical Report NCEER-97-0010. Pages 205–219. Buffalo, New York: National Center for Earthquake Engineering Research. TIC: 254525.

Silva, W.J.; Abrahamson, N.; Toro, G.; and Costantino, C. 1996. *Description and Validation of the Stochastic Ground Motion Model.* PE&A 94PJ20. El Cerrito, California: Pacific Engineering and Analysis. TIC: 245288.

Silva, W.J.; Stark, C.; Chiou, S.J.; Green, R.; Stepp, J.C.; Schneider, J.; and Anderson, D. 1990. "Non-linear Soil Models Based Upon Observations of Strong Ground Motions." *Seismological Research Letters, 61,* (1), 13. Abstract 11B-4. El Cerrito, California: Seismological Society of America, Eastern Section. TIC: 254667.

Simmons, A.M. 2004. *Yucca Mountain Site Description.* TDR-CRW-GS-000001 REV 02. Two volumes. Las Vegas, Nevada: Bechtel SAIC Company. ACC: DOC.20040120.0004.

Simonds, F.W.; Whitney, J.W.; Fox, K.F.; Ramelli, A.R.; Yount, J.C.; Carr, M.D.; Menges, C.M.; Dickerson, R.P.; and Scott, R.B. 1995. *Map Showing Fault Activity in the Yucca Mountain Area, Nye County, Nevada.* Miscellaneous Investigations Series Map I-2520. Denver, Colorado: U.S. Geological Survey. TIC: 232483.

Snow, J.K. and Wernicke, B.P. 2000. "Cenozoic Tectonism in the Central Basin and Range: Magnitude, Rate, and Distribution of Upper Crustal Strain." *American Journal of Science, 300,* (9), 659–719. New Haven, Connecticut: Yale University, Kline Geology Laboratory. TIC: 253039.

Spudich, P.; Fletcher, J.B.; Hellweg, M.; Boatwright, J.; Sullivan, C.; Joyner, W.B.; Hanks, T.C.; Boore, D.M.; McGarr, A.; Baker, L.M.; and Lindh, A.G. 1996. *Earthquake Ground Motions in Extensional Tectonic Regimes.* Open-File Report 96-292. Menlo Park, California: U.S. Geological Survey. TIC: 245279.

Spudich, P.; Fletcher, J.B.; Hellweg, M.; Boatwright, J.; Sullivan, C.; Joyner, W.B.; Hanks, T.C.; Boore, D.M.; McGarr, A.; Baker, L.M.; and Lindh, A.G. 1997. "SEA96–A New Predictive Relation for Earthquake Ground Motions in Extensional Tectonic Regimes." *Seismological Research Letters, 68,* (1), 190–198. El Cerrito, California: Seismological Society of America. TIC: 234935.

Spudich, P.; Joyner, W.B.; Lindh, A.G.; Boore, D.M.; Margaris, B.M.; and Fletcher, J.B. 1999. "SEA99: A Revised Ground Motion Prediction Relation for Use in Extensional Tectonic Regimes." *Bulletin of the Seismological Society of America, 89,* (5), 1156–1170. El Cerrito, California: Seismological Society of America. TIC: 253393.

Stewart, J.H. 1988. "Tectonics of the Walker Lane Belt, Western Great Basin: Mesozoic and Cenozoic Deformation in a Zone of Shear." *Metamorphism and Crustal Evolution of the Western United States.* Ernst, W.G., ed. Rubey Volume 7. Pages 683–713. Englewood Cliffs, New Jersey: Prentice-Hall. TIC: 218183.

Su, F.; Anderson, J.G.; Brune, J.N.; and Zeng, Y. 1996. "A Comparison of Direct S-Wave and Coda-Wave Site Amplification Determined from Aftershocks of the Little Skull Mountain Earthquake." *Bulletin of the Seismological Society of America, 86,* (4), 1006–1018. El Cerrito, California: Seismological Society of America. TIC: 236585.

Thatcher, W.; Foulger, G.R.; Julian, B.R.; Svarc, J.; Quilty, E.; and Bawden, G.W. 1999. "Present-Day Deformation Across the Basin and Range Province, Western United States." *Science, 283,* (5408), 1714–1718. Washington, D.C.: American Association for the Advancement of Science. TIC: 246227.

von Seggern, D.H. and Smith, K.D. 1997. *Seismicity in the Vicinity of Yucca Mountain, Nevada, for the Period October 1, 1995, to September 30, 1996.* Milestone Report SPT38AM4. Reno, Nevada: University of Nevada, Reno, Seismological Laboratory. ACC: MOL.19981124.0334.

Waiting, D.J.; Stamatakos, J.A.; Ferrill, D.A.; Sims, D.W.; Morris, A.P.; Justus, P.S.; and Ibrahim, A.K. 2003. "Methodologies for the Evaluation of Faulting at Yucca Mountain, Nevada." *Proceedings of the 10th International High-Level Radioactive Waste Management Conference (IHLRWM), March 30-April 2, 2003, Las Vegas, Nevada.* Pages 377–387. La Grange Park, Illinois: American Nuclear Society. TIC: 254559.

Whitney, J.W., ed. 1996. *Seismotectonic Framework and Characterization of Faulting at Yucca Mountain, Nevada.* Milestone 3GSH100M. Denver, Colorado: U.S. Geological Survey. ACC: MOL.19970129.0041 through MOL.19970129.0062.

Whitney, J.W. and Taylor, E.M., eds. 1996. "Quaternary Paleoseismology and Stratigraphy of the Yucca Mountain Site Area." Chapter 4 of *Seismotectonic Framework and Characterization of Faulting at Yucca Mountain, Nevada.* Whitney, J.W., ed. Milestone 3GSH100M. Denver, Colorado: U.S. Geological Survey. TIC: 237980. ACC: MOL.19970129.0041.

Williams, N.H. 2003. "Contract No. DE-AC28-01RW12101 - Key Technical Issue (KTI) Agreement: Preclosure Safety (PRE) 7.02." Letter from N.H. Williams (BSC) to J.D. Ziegler (DOE/ORD), November 24, 2003, PN/YM:mm - 1119039546, with enclosures. ACC: MOL.20040107.0077.

Wong, I.G. and Silva, W. 2003. *Development of Seismic Design Ground Motion Inputs.* Scientific Notebook SN-M&O-SCI-037-V3. ACC: MOL.20031027.0158; MOL.20031027.0159; MOL.20031027.0160.

YMP (Yucca Mountain Site Characterization Project) 1997. *Methodology to Assess Fault Displacement and Vibratory Ground Motion Hazards at Yucca Mountain.* Topical Report YMP/TR-002-NP, Rev. 1. Las Vegas, Nevada: Yucca Mountain Site Characterization Office. ACC: MOL.19971016.0777.

8.2 CODES, STANDARDS, REGULATIONS, AND PROCEDURES

10 CFR Part 63. Energy: Disposal of High-Level Radioactive Wastes in a Geologic Repository at Yucca Mountain, Nevada. Readily available.

8.3 DATA, LISTED BY DATA TRACKING NUMBER

LL040310323122.044. Input and Output Files of the MSTHM Micro-Abstractions for the Collapsed-Drift Cases for the TSPA-LA Low-Probability Seismic Scenario. Submittal date: 03/26/2004.

MO0206UNHAZ106.001. Uniform Hazard, Reference Event and Deaggregation Event Spectra at 10-6 Annual Exceedance Frequency Based on the Results of the Probabilistic Seismic Hazard Analyses for Yucca Mountain. Submittal date: 06/03/2002.

MO0301TMHIS106.001. Acceleration, Velocity, and Displacement Time Histories for the Repository Level at 10-6 Annual Exceedance Frequency. Submittal date: 01/28/2003.

MO0301TMHSB107.000. Time Histories Spectrally Conditioned to Point B for the Repository Level at 10-7 Annual Exceedance Frequency. Submittal date: 01/20/2004.

MO03061E9PSHA1.000. Spectral Acceleration and Velocity Hazard Curves Extended to 1E-9 Based on the Results of the PSHA for Yucca Mountain. Submittal date: 06/09/2003.

MO0401MWDRPSHA.000. Results of the Yucca Mountain Probabilistic Seismic Hazard Analysis (PSHA). Submittal date: 01/21/2004.

MO0402AVDTM105.001. Acceleration, Velocity, and Displacement Time Histories for the Repository Level at 10-5 Annual Exceedance Frequency. Submittal date: 02/09/2004.

MO0402SDSTMHIS.004. Seismic Design Spectra and Time Histories for the Surface Facilities Area (Point D/E) at 5E-4 Annual Exceedance Frequency. Submittal date: 02/09/2004.

MO0403AVDSC106.001. Acceleration, Velocity, and Displacement Time Histories for the Repository Level at 10-6 Annual Exceedance Frequency. Submittal date: 03/09/2004.

MO0403AVTMH107.003. Acceleration, Velocity, and Displacement Time Histories for the Repository Level at 10-7 Annual Exceedance Frequency. Submittal date: 03/22/2004.

MO0403SPASCRKD.000. Seismic Crack Density Model Outputs for LA. Submittal date: 03/09/2004.

APPENDIX A

ROCKFALL AND VIBRATORY LOADING EFFECTS ON THE MECHANICAL FAILURE OF CLADDING AND METHODOLOGY USED TO IMPLEMENT THE EFFECTS OF SEISMIC EFFECTS ON CLADDING (RESPONSE TO CLST 3.10 AND TSPAI 3.06)

Note Regarding the Status of Supporting Technical Information

This document was prepared using the most current information available at the time of its development. This Technical Basis Document and its appendices providing Key Technical Issue Agreement responses that were prepared using preliminary or draft information reflect the status of the Yucca Mountain Project's scientific and design bases at the time of submittal. In some cases this involved the use of draft Analysis and Model Reports (AMRs) and other draft references whose contents may change with time. Information that evolves through subsequent revisions of the AMRs and other references will be reflected in the License Application (LA) as the approved analyses of record at the time of LA submittal. Consequently, the Project will not routinely update either this Technical Basis Document or its Key Technical Issue Agreement appendices to reflect changes in the supporting references prior to submittal of the LA.

APPENDIX A

ROCKFALL AND VIBRATORY LOADING EFFECTS ON THE MECHANICAL FAILURE OF CLADDING AND METHODOLOGY USED TO IMPLEMENT THE EFFECTS OF SEISMIC EFFECTS ON CLADDING (RESPONSE TO CLST 3.10 AND TSPAI 3.06)

This appendix provides a response for Key Technical Issue (KTI) agreements Container Life and Source Term (CLST) 3.10 and for Total System Performance Assessment and Integration (TSPAI) 3.06. Agreement CLST 3.10 relates to the technical basis for the mechanical failure of cladding in response to the seismic effects of vibratory ground motion and of rockfall induced by vibratory ground motion. Agreement TSPAI 3.06 relates to the technical basis for representation of seismic effects on cladding in the total system performance assessment (TSPA).

A.1 KEY TECHNICAL ISSUE AGREEMENTS

A.1.1 CLST 3.10 and TSPAI 3.06

Agreement CLST 3.10 was reached during the U.S. Nuclear Regulatory Commission (NRC)/U.S. Department of Energy (DOE) Technical Exchange and Management Meeting on Container Life and Source Term held September 12 and 13, 2000, in Las Vegas, Nevada (Schlueter 2000). CLST KTI subissues 1, 2, 3, 4, and 6 were discussed at the meeting.

Agreement TSPAI 3.06 was reached during the NRC/DOE Technical Exchange and Management Meeting on Total System Performance Assessment and Integration held August 6 through 10, 2001, in Las Vegas, Nevada (Reamer 2001). TSPAI KTI subissues 1, 2, 3, and 4 were discussed at the meeting.

The wording of these agreements is as follows:

CLST 3.10

> Provide analysis of the rockfall and vibratory loading effects on the mechanical failure of cladding, as appropriate. DOE stated that the vibratory effects are documented in Sanders et al. 1992 SAND90-2406, A Method For Determining The Spent-Fuel Contribution To Transport Cask Containment Requirements. This will be discussed in the SDS KTI meeting. The analysis of the rockfall effects on the mechanical failure of cladding will be addressed if the agreed to updated rockfall analysis in Subissue #2, Item 8 and Subissue #1, Item 14 demonstrate that the rock will penetrate the drip shield and damage the waste package.

TSPAI 3.06[1]

> Provide the technical basis for the methodology used to implement the effects of seismic effects on cladding in revised documentation. DOE will demonstrate that the methodology used to represent the seismic effects of cladding does not result in an underestimation of risk in the regulatory timeframe (ENG2.1.1). DOE will provide the technical basis for the methodology used to implement the effects of seismic effects on cladding in revised documentation. DOE will demonstrate that the methodology used to represent the seismic effects of cladding does not result in an underestimation of risk in the regulatory timeframe in TSPA-LA. The documentation is expected to be available to NRC in FY 2003.

The NRC status for CLST 3.10 is identified as partly received, based on prior submission of a letter report (Brocoum 2001) in response to KTI agreements Structural Deformation and Seismicity (SDS) 1.02 and 2.03. The previously submitted letter report (i.e., Brocoum 2001) outlines the DOE strategy for postclosure seismic analysis for the license application. The DOE strategy responds to the NRC concern about the use of median fault displacement and ground-motion hazard curves as the basis for screening seismic features, events, and processes for the TSPA for site recommendation. The DOE has adopted mean seismic hazard curves for screening features, events, and processes for TSPA for license application and for developing the seismic consequence abstractions for TSPA for license application.

A.1.2 Related Key Technical Issue Agreements

Agreement CLST 3.10 is related to the rockfall analyses in agreement CLST 1.14 (see Appendix C of *Technical Basis Document No. 6: Waste Package and Drip Shield Corrosion*) and to the rockfall analyses for agreement CLST 2.08. CLST 1.14 is concerned with the effects of rockfall and the dead load from drift collapse on stress-corrosion cracking of the waste package and drip shield (Schlueter 2000, p. 4 of attachment). CLST 2.08 is concerned with rockfall calculations that address (1) the potential embrittlement of the waste package closure weld, (2) the thinning of the drip shield from corrosion and hydrogen embrittlement, and (3) the static load of fallen rock on the drip shield (Schlueter 2000, p. 7 of attachment).

The DOE analysis for CLST 1.14 concludes that the drip shield prevents rock blocks from impinging on or damaging the waste package. In effect, the drip shield functions as a mechanical barrier, preventing contact between the waste package, the rock block, and drip shield. The analysis also concludes that only small areas on the sides of the drip shield, limited to the region of connection between the bulkheads and the top plate, are vulnerable to stress-corrosion cracking induced by the static load from a collapsed drift. The location of these areas and the potential for any cracks to plug from evaporation-induced scale formation is such that the drip shield will continue to function as a flow barrier for drift seepage.

The analyses for CLST 1.14 include the effects of long-term degradation of the drip shield. First, the thickness of the drip-shield plates is reduced first by 2 mm and then by 3 mm to represent the potential effects of corrosion over the 10,000-year regulatory period. Second,

[1] ENG2.1.1 in this agreement refers to NRC integrated subissue ENG 2 (NRC 2002, Table 1.1-2).

material properties are evaluated at both ambient temperature and at 150°C to capture the impact of elevated temperature on structural response. The thinning of the plates and the use of material properties at elevated temperatures are simultaneously incorporated into all the structural response calculations for the drip shield response under seismic loads.

While the related KTI agreements address rockfall, the resolution of KTI agreements CLST 3.10 and TSPAI 3.06 is independent of that for CLST 1.14 and 2.08. The focus of this appendix is on damage to cladding induced by seismic effects, while seismic effects are not the subject of CLST 1.14 and 2.08. In addition, KTI agreements CLST 3.10 and TSPAI 3.06 do not directly consider stress corrosion cracking and long-term degradation of the drip shield or waste package, which are the primary concerns of CLST 1.14 and 2.08. The two sets of KTI agreements will be resolved and addressed separately. The DOE analysis of CLST 2.08 will be provided separately.

A.2 RELEVANCE TO REPOSITORY PERFORMANCE

The cladding around spent nuclear fuel can delay the release of radionuclides in the event that a waste package becomes breached. The cladding can be perforated or damaged by the seismic effects of vibratory ground motion and by rockfall induced by vibratory ground motion. An understanding of the mechanical response of cladding to seismic effects is important for the representation of cladding performance in the seismic scenario class for TSPA.

The discussion in this appendix is specifically for the cladding around spent nuclear fuel from commercial pressurized water reactors and commercial boiling water reactors. This appendix does not address the performance of naval spent nuclear fuel during seismic events. A planned classified Naval Nuclear Propulsion Program addendum to the license application will provide the seismic analysis for naval spent nuclear fuel.

A.3 RESPONSE

Two cladding failure modes have been considered in developing the cladding failure abstraction for TSPA. In the first failure mode, cladding may be perforated or sheared from acceleration of fuel-rod assemblies during waste package impacts induced by vibratory ground motions. This failure mode is similar to cladding failures that may result from dropping a transportation cask on an unyielding surface. In the second failure mode, vibratory ground motion may shake rock blocks loose from the drift walls. Large rock blocks could impact the drip shield, potentially collapsing the drip shield onto the waste package. If the waste package is crimped by this load, the cladding inside the waste package could be perforated or sheared by the impact.

The cladding damage abstraction for TSPA is based on the first failure mode. As discussed in Sections A.1.2 and 5.3.3 of this technical basis document, the drip shield prevents rock blocks from impinging on or damaging the waste package. More specifically, the deformation of the drip shield for even the largest rock blocks is less than the minimum clearance between the drip shield and waste package. The drip shield functions as a mechanical barrier, preventing contact between the waste package and the rock block and drip shield.

A damage abstraction for mechanical failure of cladding under vibratory ground motion is included in the seismic scenario class for TSPA (BSC 2003a, Section 6.7). This damage

abstraction is based on waste package structural response calculations for vibratory ground motions at the 10^{-5} per year, the 10^{-6} per year, and the 10^{-7} per year ground-motion hazard levels (BSC 2003b). These vibratory ground motions can generate end-to-end impacts between adjacent waste packages, resulting in high accelerations on the fuel assemblies and on the fuel rods inside the assemblies (BSC 2003c). The predicted fuel rod accelerations are large enough to perforate 100% of the fuel rod cladding for the 10^{-6} per year and the 10^{-7} per year ground-motion hazard levels (BSC 2003a, Section 6.7). The predicted accelerations for the 10^{-5} per year ground-motion level are large enough to perforate the fuel rod cladding for one of the three ground-motion cases evaluated. Given the approximations involved in generating the ground motions for these three cases, the cladding damage abstraction for TSPA conservatively assumes that 100% of the cladding will also be perforated for the 10^{-5} per year ground-motion level (BSC 2003a, Section 6.7).

Mechanical failure of cladding from rockfall induced by vibratory ground motion is not included in the seismic scenario class. Viewed as a mechanical barrier, the key failure modes of the drip shield are collapse, buckling, or separation. The drip shield is considered to collapse or buckle if its final configuration results in mechanical contact between the underside of the drip shield and the top of the waste package. Separation of drip shields results from the axial displacement of one drip shield relative to its neighbor, resulting in a direct path for seepage from the crown of the drift to fall directly on the waste package. Large rock blocks do not cause collapse or buckling of the drip shield. That is, the resulting deformation of the drip shield is less than the minimum clearance between drip shield and any waste package. Similarly, the static or dead loads from drift collapse do not cause collapse or buckling of the drip shield. The drip shields do not separate for the 10^{-6} per year ground-motion level and, by inference, for higher frequency ground motions. (A higher frequency ground motion has a smaller amplitude measured in terms of peak ground velocity or peak ground acceleration.) The drip shield, therefore, remains effective as a mechanical barrier for the 10^{-6} per year ground-motion level and for more frequent ground motions.

At the 10^{-7} per year ground-motion level, the drip shields are predicted to separate, potentially exposing the waste package to rockfall. However, this separation has no effect on the cladding damage abstraction because 100% of the cladding is already perforated for ground-motion hazards with an annual exceedance frequency less than or equal to 10^{-5} per year.

The methodology for abstracting the response of cladding to seismic effects and the computational algorithm for including the cladding damage abstraction in the TSPA is documented in *Seismic Consequence Abstraction* (BSC 2003a, Sections 6.7 and 6.10).

The information in this report is responsive to agreements CLST 3.10 and TSPAI 3.06 made between the DOE and NRC. The report contains the information that DOE considers necessary for NRC review for closure of these agreements.

A.4 BASIS FOR THE RESPONSE

The technical basis for the cladding damage abstraction in TSPA is explained in this section. The following information is presented here:

- The damage to the cladding from vibratory ground motion is analyzed in Section A.4.1. The cladding is modeled as 100% perforated (i.e., damaged) in TSPA for ground-motion hazards with an annual exceedance frequency less than or equal to 10^{-5} per year.

- The potential damage to cladding from rockfall induced by vibratory ground motion is analyzed in Section A.4.2.1 for the nonlithophysal zones and in Section A.4.2.2 for the lithophysal zones of the repository. In the nonlithophysal zones, even the largest rock blocks do not cause drip shield deformations that result in physical contact between the drip shield and waste package. In the lithophysal zones, the static load from a collapsed drift cannot fail or buckle the drip shield. It follows that the drip shield does not collapse or buckle under rockfall, providing a mechanical barrier against rockfall damage to the waste package and cladding.

- The potential damage to cladding from drip shield separation induced by vibratory ground motion is analyzed in Section A.4.2.3. Drip shield separation is not specifically represented in the cladding damage abstraction for TSPA because separation only occurs for ground motions with an annual exceedance frequency of less than 10^{-6} per year. At these ground-motion hazard levels, 100% failure of the cladding is already modeled as a result of mechanical interaction, and it is not necessary to represent drip shield separation in the cladding damage abstraction for TSPA.

A.4.1 Cladding Damage from Vibratory Ground Motion

The mechanical response of the waste package to vibratory ground motions can produce dynamic impacts between adjacent waste packages, between the waste package and its emplacement pallet, between the waste package and the drip shield, between the waste package and invert, and between the fuel assemblies and the internals of the waste package. During these impacts, the waste package may experience high acceleration in the axial and lateral directions. These accelerations can be transmitted to the fuel assemblies and to the cladding within the assemblies. The assemblies may impact the lid of a waste package due to the end-on (axial) impact of adjacent waste packages or the fuel rods may be pushed sideways, toward the sidewall of the waste package, during impact with the emplacement pallet or drip shield. Either of these impacts has the potential to cause the cladding to fail.

The end-on impact between two adjacent waste packages accounts for the majority of the mean damage to the waste package at the 10^{-6} per year and the 10^{-7} per year ground-motion levels (BSC 2003a, Tables 6 and 7). These results imply that the end-on impact of adjacent waste packages produces more severe forces and accelerations than the side-on impact between a waste package and the emplacement pallet or drip shield. These results are consistent with the conservative approach to the end-on impact calculations, which are based on a waste package impacting an unyielding plane of symmetry located midway between two adjacent waste packages (BSC 2003b). The maximum waste package velocities from end-on impacts at the 10^{-6} per year level range between 1.4 and 4.5 m/s (BSC 2003b, Tables 6.1.2-1 through 6.1.2-15; BSC 2003d, Tables 28 through 42). All realizations for the 10^{-6} per year ground motions have an impact velocity of at least 1.4 m/s. Similarly, the maximum waste package velocities for end-on impacts at the 10^{-7} per year level range between 1.3 and 6.5 m/s (BSC 2003b, Tables 6.2.2-1 through 6.2.2-15; BSC 2003d, Tables 43, 44, and 45; BSC 2003e, Tables 46 through 57). All

realizations for the 10^{-7} per year ground motions have an impact velocity of at least 1.3 m/s. (The minimum value for the 10^{-7} per year ground motions is less than that for the 10^{-6} per year ground motions because of the stochastic variability in the set of ground motions.)

The resulting fuel assembly accelerations due to this range of impact velocities have been analyzed using a finite-element representation of the fuel assemblies. The maximum peak acceleration and the average peak acceleration for the assemblies in a waste package are reported in *Maximum Accelerations on the Fuel Assemblies of a 21-PWR Waste Package During End Impacts* (BSC 2003c, Tables 4 and 5; BSC 2003f, Tables 14 and 15). The peak and average accelerations among the 21 fuel assemblies of the 21-PWR waste package were evaluated for cutoff frequencies of 450, 600, and 1,000 Hz. The accelerations for a cutoff frequency of 450 Hz are listed in Table A-1.

Table A-1. Fuel Assembly Accelerations from Waste Package–to–Waste Package Impacts for a 450 Hz Cutoff Frequency

Parameter	Initial Impact Velocity (m/s)				
	0.5	1	2	4	6
Maximum Peak Acceleration (g)	75	144	263	323	506
Average Peak Acceleration (g)	35	72	115	155	194

Source: BSC 2003c, Tables 4 and 5.

A cutoff frequency is required because the finite-element calculations for the fuel assembly accelerations do not include any damping. In this situation, the output is typically filtered through a low-pass, Butterworth filter to determine a more realistic acceleration time history. The cutoff frequency for the filter is a compromise between damping the extraneous numerical noise while leaving the fundamental modes of the structural response intact. Filtering the output below 400 Hz dampens the fundamental structural modes of the fuel assemblies, potentially leading to erroneous results. Filtering the output at greater than 1,000 Hz preserves numerical noise and can also lead to misleading results. A cutoff frequency of 450 Hz dampens the numerical noise but has minimal impact on the fundamental modes of the structural response of the fuel assemblies (BSC 2003c, Attachment VIII).

Interpolating on the results listed in Table A-1 for impact velocities of 1 and 2 m/s, the maximum peak acceleration is 180 g at 1.3 m/s and the average peak acceleration is 85 g at 1.3 m/s, both for the 450 Hz cutoff frequency. With a cutoff frequency of 600 Hz, the average peak accelerations for 1 and 2 m/s are 99 and 147 g, respectively (BSC 2003c, Table 4). The interpolated value for the average peak acceleration at 1.3 m/s is then 113 g for the 600 Hz cutoff. A comparison of the average peak accelerations for a 1.3 m/s impact with 450 Hz or 600 Hz cutoffs, 85 g and 113 g, respectively, indicates the relative insensitivity of average peak acceleration to the choice of cutoff frequency. These accelerations are for the minimum impact velocity. Table A-1 also shows that fuel assembly accelerations will be much greater for impact velocities between 1.3 and 6.5 m/s, which is the range for the 10^{-7} per year ground-motion level.

The integrity of fuel assembly cladding during cask drop or tipover incidents has been studied for Zircaloy-clad light water reactor spent nuclear fuel assemblies (Chun et al. 1987; Sanders et al. 1992). The work by Chun et al. (1987) is more useful here because it explicitly calculates

g-loads for axial buckling and for yielding due to side drops. The range of g-loads for failure due to axial buckling varies between 82 and 252 g for various fuel assemblies (Chun et al. 1987, Table 4). The range of g-loads for yielding due to side drops varies between 63 and 211 g for various fuel assemblies (Chun et al. 1987, Table 4). The actual g-loads for failure may be lower because the weight of the fuel pellets is not transferred to the cladding (Chun et al. 1987, p. 2), and the potential effects of cladding defects or existing failures are not included in the analysis by Chun et al. These effects increase the inertial mass or weaken the clad, potentially causing failures at lower g-loads than predicted by Chun et al. (1987).

Based on the velocities listed in Table A-1, end-on impacts of adjacent waste packages result in average fuel assembly accelerations of 85 g at the lowest impact velocity (1.3 m/s) and often much greater values for higher impact velocities. The use of a 600 Hz cutoff filter increases this minimum value to 113 g. Simple fuel rod failure criteria indicate that clad failure occurs between 82 and 252 g, depending on the type of fuel rod (Chun et al. 1987, Table 4). In this situation, 100% perforation (i.e., failure) of the cladding is reasonable whenever a ground-motion hazard occurs with an annual exceedance frequency less than or equal to 10^{-6} per year.

Three structural response calculations are also available for the 10^{-5} per year ground-motion hazard level. These three calculations use approximate ground-motion time histories, based on scaling[2] time histories for the 10^{-6} per year hazard level down to match the peak horizontal ground velocity for the 10^{-5} per year hazard. The results from the structural response calculations show that two calculations have no end-to-end waste package impacts and, hence, no failure of the cladding because the accelerations from the side-on impacts are small. The third calculation has a single impact at 1.3 m/s, resulting in 100% perforation (i.e., failure) of the cladding, as discussed above. Because of the limited number of calculations and the approximations in developing time histories for the 10^{-5} per year hazard, the cladding damage for the 10^{-5} per year ground-motion hazard has also been conservatively set to 100% perforation for TSPA.

Calculations are available for the structural response of the waste package to a single ground motion with annual exceedance frequencies of 5×10^{-4} per year and 10^{-4} per year (BSC 2003b, Sections 6.3 and 6.4). There is no damage to the cladding for this ground motion because there is no appreciable motion of the waste package and no impact between adjacent waste packages.

A.4.2 Cladding Damage from Rockfall Induced by Vibratory Ground Motion

Mechanical failure of cladding due to rockfall is not represented in TSPA because 100% of the cladding is perforated from direct vibratory ground motion for ground-motion hazards with an annual exceedance frequency less than or equal to 10^{-5} per year and because the drip shield provides a mechanical barrier that prevents rockfall from contacting the waste package for ground-motion hazards with an annual exceedance frequency of greater than or equal to 10^{-6} per year. The cladding is 100% perforated for high amplitude, low annual frequency ground motions, while the drip shield protects the cladding from rockfall for the smaller amplitude ground motions. In this situation, any additional damage to cladding from rockfall induced by

[2] The scaling factor, 0.4066, is derived in *Seismic Consequence Abstraction* (BSC 2003a, Equation I.3) as the peak ground velocity for the 10^{-5} per year ground motion divided by the peak ground velocity for the 10^{-6} per year ground motion.

vibratory ground motion is no longer relevant because the cladding is already 100% perforated, as shown by the last two lines in Table A-2. Table A-2 lists the cladding damage as a function of the ground-motion hazard.

Table A-2. Cladding Damage as a Function of Ground-Motion Exceedance Frequency

Ground-Motion Exceedance Frequency (per year)	Drip Shield Response to Rockfall Induced by Ground Motion	Cladding Response to Ground Motion
10^{-4}	Drip shield remains mechanically intact, protecting the waste package and cladding from rockfall.	Cladding is intact.
10^{-5}	Drip shield remains mechanically intact, protecting the waste package and cladding from rockfall.	Cladding is 100% perforated from ground motion alone (no rockfall).
10^{-6}	Drip shield remains mechanically intact, protecting the waste package and cladding from rockfall.	Cladding is 100% perforated from ground motion alone (no rockfall).
10^{-7}	Drip shield may separate.	Cladding is 100% perforated from ground motion alone (no rockfall).
10^{-8}	Drip shield may separate.	Cladding is 100% perforated from ground motion alone (no rockfall).

NOTE: Ground-motion amplitude increases as the exceedance frequency decreases.

This position is based on (1) drip shield structural response calculations for individual rock blocks impacting the drip shield in the nonlithophysal zones, (2) potential damage to the drip shield from drift collapse in the lithophysal zones of the repository, and (3) structural response calculations for the drip shield under vibratory ground motions. These damage mechanisms are further discussed in the following sections.

A.4.2.1 Drip Shield Damage from Rockfall in Nonlithophysal Zones

In the nonlithophysal zones, rock blocks can be shaken loose from the drift walls under vibratory ground motion. The potential damage to the drip shield from individual rock blocks is based on structural response calculations for a set of six representative rock blocks. These representative blocks span the full range of block mass and block kinetic energy predicted for the nonlithophysal zones of the repository (BSC 2003g, Attachment XI). The six representative rock sizes impact the drip shield from three different angles: vertically downward onto the top of the drip shield, at a 60° angle (with the horizontal) onto the transition region between the top and side of the drip shield, and horizontally into the side wall. The rocks impact the drip shield edge on, which conservatively bounds the damage from the impact process.

Table A-3 lists the damage to the drip shield for the rock blocks that span the response to the 10^{-6} and 10^{-7} per year ground-motion hazards (BSC 2003h, Section 5.5.1). The failed areas listed in Table A-3 are relevant to hydrologic flow through a small area of the drip shield and do not indicate mechanical failure or collapse of the overall structure. Each failed area is defined as the surface area of the finite elements wherein the residual stress from rock-block impact exceeds the tensile failure threshold for Titanium Grade 7 (UNS R52400) (50% of its yield strength, per *Seismic Consequence Abstraction* (BSC 2003a, Section 6.3.2)). The high residual stress in the failed areas will result in accelerated growth of a network of through-wall stress corrosion cracks. On the drip shield, these cracks are expected to plug from evaporation-induced

precipitation of calcite and other minerals in the seepage, preventing any significant advective flux through the drip shield.

Although the drip shield may be deformed from individual block impacts, it remains intact, preventing rock blocks from impacting the waste package and internals and preventing any seepage from contacting the waste package. More specifically, the drip shield does not collapse or buckle from any of the rock-block impacts, and the drip shield does not make contact with the waste package during or after the block impact. The maximum vertical displacement in the drip shield components occurs in the longitudinal stiffener for the rock block in Table A-3 with the maximum kinetic energy. This rock block corresponds to the block with maximum kinetic energy for the 10^{-7} per year ground-motion level and results in a permanent deflection of 25.4 cm (BSC 2003h, Section 6). For comparison, the clearance between the underside of the drip shield and the top of the waste package ranges between 367.1 and 1,132.1 mm (BSC 2004a, Figure 1). It follows that the drip shield prevents any mechanical damage to the waste package and cladding from large rock blocks that are shaken loose in the nonlithophysal zones due to vibratory ground motion.

Table A-3. Damaged Area from Individual Rock Blocks Impacting the Drip Shield

Rock Mass and Kinetic Energy (MT and J)	Failed Area (m^2) and Failed Area as a Percent of Total Drip Shield Surface Area		
	Vertical Rockfall (90° from horizontal)	Rockfall onto Drip Shield Corner (60° from horizontal)	Rockfall onto Drip Shield Sidewall (40° from horizontal)
11.5 MT Rock[a] (348,174 J)	4.304 (11.25%)	2.835 (7.41%)	1.126 (2.94%)
14.5 MT Rock (163,083 J)	3.508 (9.17%)	0.612 (1.60%)	0.079 (0.21%)
3.3 MT Rock (24,712 J)	0.548 (1.43%)	0.416 (1.09%)	0.0 (0.00%)
0.15 MT Rock (902 J)	0.0015 (0.00%)	0.0091 (0.02%)	0.0 (0.00%)
0.11 MT Rock (42 J)	0.0 (0.00%)	0.0 (0.00%)	0.0 (0.00%)
0.25 MT Rock (~0 J)	0.0 (0.00%)	0.0 (0.00%)	0.0 (0.00%)

Source: BSC 2003i, Tables 2 and 3.

NOTE: [a]The rock block with the maximum kinetic energy has greater velocity but less mass than the rock with the second greatest kinetic energy in the table.

A.4.2.2 Drip Shield Damage from Rockfall in Lithophysal Zones

In the lithophysal zones, the emplacement drifts are predicted to collapse from vibratory ground motions at the 10^{-6} per year hazard level and for lower frequency (higher amplitude) ground-motion hazards. The static loads from a collapsed drift using continuum or discontinuum representations of the host rock are not expected to collapse the drip shield from the mean value of the rock mass pressure predicted for the drip shield.

In the lithophysal zones, the rock mass is permeated with void spaces of varying size. Average joint spacing is less than 1 m, and, at certain locations, this spacing is much smaller, on the order

of 0.1 m (BSC 2003g, Section 6.1.4.1). This weak rock mass is expected to collapse into small fragments under the load imposed by a large vibratory ground motion. Rockfall calculations demonstrate that drifts in the lithophysal zones would collapse under the 10^{-6} per year vibratory ground motions (BSC 2003g, Section 6.4.1.1) and for lower frequency ground motions.

Small fragments from lithophysal failure have little capability to damage the drip shield because of the small mass and small kinetic energy of the individual fragments. A cubic fragment that is 0.1 m on a side has a volume of 0.001 m^3 and a mass of approximately 2.3 kg for a tuff density of 2,300 kg/m^3. The velocity of this fragment is 7.7 m/s for a 3-m drop under gravitational acceleration, and the associated kinetic energy is 68 J. Table A-3 shows that a 0.11 MT (110 kg) rock with 42 J of kinetic energy does not produce a failed area on the surface of the drip shield. A comparison of the mass and kinetic energy of the 0.1-m fragment with the heavier block in Table A-3 indicates that there should be essentially no damage from the impact of this fragment on the drip shield.

A cubic fragment that is 0.3 m on a side has a mass of 62 kg and a kinetic energy of 1,800 J. This fragment is approximately equivalent to the 0.15 MT (150 kg) rock with 902 J of kinetic energy in Table A-3. This rock produces no damage for the top and side impacts, and very small damage (0.02%) for the corner impact. Again, the damage for impact of a cubic fragment 0.3 m on a side should be negligible probabilistically because this large fragment is considered an extreme case for the lithophysal zone. In summary, the drip shield will not be significantly damaged by direct impact of small rock fragments in the lithophysal zone.

Seismically induced drift collapse in the lithophysal zones can also impose a static load on the drip shield from the weight of the natural backfill in the drifts as a result of the collapse. The structural response of the drip shield to the static load from a hypothetical engineered backfill and fallen host rock generated by tunnel collapse has been evaluated with dynamic structural response calculations. The layer of engineered backfill in these calculations is taken to be 0.9 m thick or 1.1 m thick. The fallen host rock is 5.5 m thick. The applied pressure from these materials is 143 kPa if the hypothetical engineered backfill is 0.9 m thick and 146 kPa if the engineered backfill is 1.1 m thick (BSC 2003j, Table 5.2-1 and Section 5.2). The thickness of the drip shield components was reduced first by 1 mm and then by 1.5 mm on all sides of each component to represent degradation of the drip shield from general corrosion (BSC 2003j, Section 5.3).

Dynamic structural response calculations were performed for the drip shield under this static load (BSC 2003j). The maximum stress component in the drip shield is less than the yield strength for this combined load (BSC 2003j, Section 6 and Table 6.2). At ambient temperature, the highest stress in the drip shield plates is 43% of the yield strength for Titanium Grade 7. At 150°C, the highest stress in the drip shield plates is 68% of the yield strength for Titanium Grade 7. In addition, the dynamic calculations can predict buckling if the stress conditions necessary for buckling are established. However, the average stress in the large support beams (the peripheral bulkheads) of the drip shield is far enough below the yield strength of Titanium Grade 24 (UNS R56405) to alleviate any concern of buckling. (The drip shield plates are fabricated from Titanium Grade 7, while the supporting structure is fabricated from Titanium Grade 24. Titanium Grade 24 is used for the supporting structure because its elastic yield strength and ultimate tensile strength are significantly greater than for Titanium Grade 7.)

A drip shield temperature of 150°C is appropriate and reasonable for evaluation of material properties at the time of the seismic event. This value (150°C) is conservative for evaluation of material properties during 98.5% of the first 10,000 years after repository closure. The thermal analysis is for an unfilled drift and considers three infiltration cases and five host-rock units (BSC 2004b, Figures 6.3-7 to 6.3-11). The thermal results are presented for the waste package, which provides an upper bound for the drip shield temperature. The peak waste package temperature ranges from 149.2°C to 177.8°C (BSC 2004b, Table 6.3-8). The waste package temperature time histories demonstrate that drip shield temperature exceeds 150°C for, at most, the first 150 years after ventilation ceases. In some cases, the duration of this high-temperature period may be 0 years, depending on the infiltration level and host rock unit. A maximum drip shield temperature of 177.8°C occurs at the peak of the thermal pulse, approximately 50 years after ventilation ceases (BSC 2004b, Table 6.3-8). The yield strength of Titanium Grade 7 decreases from 176 MPa at 150°C (BSC 2003j, Section 5.1) to 156 MPa at 350°F (176.7°C) (ASME 2001). On the other hand, this peak temperature occurs at a time (50 years) when there will be minimal degradation of the drip shield components, so the thickness reduction of 1 or 1.5 mm is not appropriate for the maximum temperature analysis. On balance, it is anticipated that these two competing effects (lower yield strength versus thicker drip shield components) will not cause the drip shield to buckle or fail.

Drip shield temperatures may also increase after the seismic event if the drift collapses and fills with rubble from the lithophysal rock. The rubble can provide a thermal blanket that may increase the drip shield temperature above its value for an unfilled drift. However, this long-term thermal effect is not expected to significantly damage the cladding for three reasons. First, drift collapse is predicted to occur for high amplitude, low probability seismic events at the 10^{-6} per year and lower frequency ground-motion levels (BSC 2003g, Section 6.4.1.1). However, the cladding is 100% perforated for TSPA purposes at these ground-motion levels, as summarized in Table A-2. Since the cladding is modeled as failed from these ground motions, the late-time thermal response of the drip shield is not incorporated into TSPA. Second, the change in drip shield temperature is not expected to be significant for seismic events after the thermal pulse. As an example, the drip shield temperature is approximately 100°C at 1,000 years (BSC 2004b, Table 6.3-8), so a temperature increase in excess of 50°C is required to exceed the 150°C temperature used to evaluate material properties. Third, the temperature excursion will be greatest for seismic events near the peak of the thermal pulse at 50 years, but the drip shield will not be significantly degraded by general corrosion at these early times and, therefore, will be less likely to fail.

These analyses and static loading calculations demonstrate that rockfall in the lithophysal zones also does not damage the waste package and cladding. The waste package and cladding are not damaged because the drip shield remains intact from rockfall during a seismic event, deflecting any rockfall away from the waste package.

A.4.2.3 Drip Shield Damage under Vibratory Ground Motion

The results from structural response calculations for the drip shield under vibratory ground motions at the 5×10^{-4} per year and 10^{-6} per year hazard levels are summarized as follows (BSC 2003k):

- One simulation performed at the 5×10^{-4} per year ground-motion level indicates that there is no damage to the drip shield (BSC 2003i, Calculation Results I).

- Fourteen simulations were performed at the 10^{-6} per year ground-motion level. The mean percent failed area is 0.70% and the maximum percent failed area is 2.13% (BSC 2003i, Table 4). These failed areas correspond to the areas of the drip shield where the local residual stress exceeds the tensile threshold for accelerated stress corrosion cracking in Titanium Grade 7. These deformed areas do not indicate buckling or collapse of the overall structure. The drifts are unfilled with rubble or natural backfill for these calculations.

Although the drip shield has permanent deformation from the 10^{-6} per year ground-motion hazard, it remains intact as a mechanical barrier because it does not collapse and adjacent drip shields do not separate from these vibratory ground motions. The response of the drip shield to the 10^{-7} per year ground-motion hazard is not discussed here because the cladding is assumed to be 100% perforated for ground motions equal to or greater than those at the 10^{-6} per year hazard level.

A.4.2.4 Summary for Rockfall Damage to Cladding

The analyses in this section demonstrate that the drip shield is predicted to remain intact as a mechanical barrier for rockfall for seismic hazards with annual exceedance frequencies of greater than 10^{-6} per year, as summarized in Table A-2. This position is based on (1) drip shield structural response calculations for individual rock blocks impacting the drip shield in the nonlithophysal zones; (2) potential damage to the drip shield from drift collapse in the lithophysal zones of the repository; and (3) structural response calculations for the drip shield under vibratory ground motions. In each of these cases, the drip shield remains intact as a mechanical barrier for rockfall because it does not collapse or separate from adjacent shields under vibratory ground motion and under rockfall induced by vibratory ground motion with annual exceedance frequencies of greater than 10^{-6} per year.

A.4.3 Cladding Damage Abstraction for Total System Performance Assessment

The damage abstraction for cladding under vibratory ground motion is set to 100% perforation of cladding for ground motions with annual exceedance frequencies of less than 10^{-5} per year. The technical basis for this damage abstraction is explained in Sections A.4.1 and A.4.2.

This damage abstraction does not underestimate risk because there are several inherent conservatisms in the analysis:

- The calculated accelerations from end-to-end impacts are based on an unyielding barrier between adjacent waste packages. This approach would be conservative even if

two adjacent waste packages of the same mass could move with equal but opposite velocities.

- Fuel assemblies with thicker cladding, such as Combustion Engineering fuel rods, are predicted to remain intact under 200 g loads and will, therefore, remain intact at the minimum impact velocity of 1.3 m/s for the waste packages. It follows that some packages will have a probability of cladding failure of less than 1, based on the ground-motion amplitude and on the expected numbers and types of fuel rods in the waste packages. This probability has been conservatively set to 1 in the TSPA algorithm to simplify the damage abstraction for the cladding.

The cladding damage is zero at the 5×10^{-5} per year ground-motion level. This approach is consistent with the results for structural response of the waste package to ground motion with annual exceedance frequencies of 5×10^{-4} per year and 10^{-4} per year (BSC 2003b, Sections 6.3 and 6.4). There is no damage to the cladding for this ground motion because there is no appreciable motion of the waste package and no impact between adjacent waste packages. This approach is also consistent with *Seismic Consequence Abstraction* (BSC 2003a, Assumption 5.1) whereby damage from vibratory ground motion first begins between the 10^{-4} and 10^{-5} per year ground-motion levels.

In terms of peak ground velocity, the abstraction for damage to the cladding is a simple lookup table with a linear interpolation between the four points in Table A-4. The mean annual exceedance frequencies of 5×10^{-5} per year and 10^{-5} per year have been replaced with the corresponding peak ground velocity values in the emplacement drifts, 0.55 and 1.067 m/s, respectively, based on the scaled hazard curve for the emplacement level (BSC 2003a, Table 5). The peak ground velocity values of 0 and 20 m/s are extreme values to avoid extrapolation beyond the bounds of the table during TSPA.

Table A-4. Abstraction for Damage to the Cladding from Vibratory Ground Motion

Annual Exceedance Frequency (1/yr)	Peak Ground Velocity (m/s)	Percent of Cladding Perforated (%)
> 1	0.0	0
5×10^{-5}	0.55	0
10^{-5}	1.067	100
$< 10^{-8}$	20	100

Source: BSC 2003a, Table 18.

There is no uncertainty in this abstraction because the abstraction represents a conservative, bounding estimate for cladding response as a function of peak ground velocity. The percent of cladding perforated is applied uniformly to the commercial spent nuclear fuel waste packages in the repository at the time of occurrence of the ground motion.

A.5 REFERENCES

ASME (American Society of Mechanical Engineers) 2001. *2001 ASME Boiler and Pressure Vessel Code (includes 2002 addenda).* New York, New York: American Society of Mechanical Engineers. TIC: 251425.

Brocoum, S. 2001. "Transmittal of Report Addressing Key Technical Issues (KTI) Structural Deformation and Seismicity (SDS)." Letter from S. Brocoum (DOE/YMSCO) to C.W. Reamer (NRC), October 25, 2001, OL&RC:TCG-0140, with enclosure. ACC: MOL.20020304.0297; MOL.20030714.0094.

BSC (Bechtel SAIC Company) 2003a. *Seismic Consequence Abstraction.* MDL-WIS-PA-000003 REV 00. Las Vegas, Nevada: Bechtel SAIC Company. ACC: DOC.20030818.0006.

BSC 2003b. *Structural Calculations of Waste Package Exposed to Vibratory Ground Motion.* 000-00C-EBS0-00300-000-00B. Las Vegas, Nevada: Bechtel SAIC Company. ACC: ENG.20030520.0003.

BSC 2003c. *Maximum Accelerations on the Fuel Assemblies of a 21-PWR Waste Package During End Impacts.* 000-00C-DSU0-01100-000-00A. Las Vegas, Nevada: Bechtel SAIC Company. ACC: ENG.20030327.0002.

BSC 2003d. *Repository Design Project, RPD/PA IED Typical Waste Package Components Assembly (7).* 800-IED-WIS0-00207-000-00A. Las Vegas, Nevada: Bechtel SAIC Company. ACC: ENG.20030707.0003.

BSC 2003e. *Repository Design Project, RDP/PA IED Typical Waste Package Components Assembly (8).* 800-IED-WIS0-00208-000-00A. Las Vegas, Nevada: Bechtel SAIC Company. ACC: ENG.20030707.0004.

BSC 2003f. *Repository Design Project, RDP/PA IED Typical Waste Package Components Assembly (4).* 800-IED-WIS0-00204-000-00A. Las Vegas, Nevada: Bechtel SAIC Company. ACC: ENG.20030702.0004.

BSC 2003g. *Drift Degradation Analysis.* ANL-EBS-MD-000027 REV 02. Las Vegas, Nevada: Bechtel SAIC Company. ACC: DOC.20030709.0003.

BSC 2003h. *Drip Shield Structural Response to Rock Fall.* 000-00C-TED0-00500-000-00A. Las Vegas, Nevada: Bechtel SAIC Company. ACC: ENG.20030327.0001.

BSC 2003i. *Design and Engineering, D&E / PA/C IED Interlocking Drip Shield and Emplacement Pallet.* 800-IED-WIS0-00401-000-00B. Las Vegas, Nevada: Bechtel SAIC Company. ACC: ENG.20030929.0008.

BSC 2003j. *Drip Shield Statically Loaded by Backfill and Loose Rock Mass.* 000-00C-TED0-00300-000-00A. Las Vegas, Nevada: Bechtel SAIC Company. ACC: ENG.20030224.0004.

BSC 2003k. *Structural Calculations of Drip Shield Exposed to Vibratory Ground Motion.* 000-00C-PEC0-00100-000-00A. Las Vegas, Nevada: Bechtel SAIC Company. ACC: ENG.20030618.0009.

BSC 2004a. *D&E / PA/C IED Emplacement Drift Configuration and Environment.* 800-IED-MGR0-00201-000-00B. Las Vegas, Nevada: Bechtel SAIC Company. ACC: ENG.20040326.0001.

BSC 2004b. *Multiscale Thermohydrologic Model.* ANL-EBS-MD-000049 REV 01. Las Vegas, Nevada: Bechtel SAIC Company. ACC: DOC.20040301.0004.

Chun, R.; Witte, M.; and Schwartz, M. 1987. *Dynamic Impact Effects on Spent Fuel Assemblies.* UCID-21246. Livermore, California: Lawrence Livermore National Laboratory. ACC: HQX.19881020.0031.

NRC (U.S. Nuclear Regulatory Commission) 2002. *Integrated Issue Resolution Status Report.* NUREG-1762. Washington, D.C.: U.S. Nuclear Regulatory Commission, Office of Nuclear Material Safety and Safeguards. TIC: 253064.

Reamer, C.W. 2001. "U.S. Nuclear Regulatory Commission/U.S. Department of Energy Technical Exchange and Management Meeting on Total System Performance Assessment and Integration (August 6 through 10, 2001)." Letter from C.W. Reamer (NRC) to S. Brocoum (DOE/YMSCO), August 23, 2001, with enclosure. ACC: MOL.20011029.0281.

Sanders, T.L.; Seager, K.D.; Rashid, Y.R.; Barrett, P.R.; Malinauskas, A.P.; Einziger, R.E.; Jordan, H.; Duffey, T.A.; Sutherland, S.H.; and Reardon, P.C. 1992. *A Method for Determining the Spent-Fuel Contribution to Transport Cask Containment Requirements.* SAND90-2406. Albuquerque, New Mexico: Sandia National Laboratories. ACC: MOV.19960802.0116.

Schlueter, J. 2000. "U.S. Nuclear Regulatory Commission/U.S. Department of Energy Technical Exchange and Management Meeting on Container Life and Source Term (September 12-13, 2000)." Letter from J. Schlueter (NRC) to S. Brocoum (DOE/YMSCO), October 4, 2000, with enclosure. ACC: MOL.20010731.0161.

INTENTIONALLY LEFT BLANK

APPENDIX B

SEISMIC INPUTS FOR PRECLOSURE DESIGN AND ANALYSES: METHODOLOGY AND AN EXAMPLE (RESPONSE TO RDTME 2.01, RDTME 2.02, RDTME 3.03, AND SDS 2.02)

Note Regarding the Status of Supporting Technical Information

This document was prepared using the most current information available at the time of its development. This Technical Basis Document and its appendices providing Key Technical Issue Agreement responses that were prepared using preliminary or draft information reflect the status of the Yucca Mountain Project's scientific and design bases at the time of submittal. In some cases this involved the use of draft Analysis and Model Reports (AMRs) and other draft references whose contents may change with time. Information that evolves through subsequent revisions of the AMRs and other references will be reflected in the License Application (LA) as the approved analyses of record at the time of LA submittal. Consequently, the Project will not routinely update either this Technical Basis Document or its Key Technical Issue Agreement appendices to reflect changes in the supporting references prior to submittal of the LA.

APPENDIX B

SEISMIC INPUTS FOR PRECLOSURE DESIGN AND ANALYSES: METHODOLOGY AND AN EXAMPLE (RESPONSE TO RDTME 2.01, RDTME 2.02, RDTME 3.03, AND SDS 2.02)

This appendix provides a response for Key Technical Issue (KTI) agreements Repository Design and Thermal-Mechanical Effects (RDTME) 2.01, RDTME 2.02, RDTME 3.03, and Structural Deformation and Seismicity (SDS) 2.02. These KTI agreements commit to providing reports and information to the U.S. Nuclear Regulatory Commission (NRC) that describe the methodology for developing preclosure seismic design inputs and also provide an example of implementing the methodology. The subject reports also give an overview of how seismic inputs are developed for use in analyses supporting the postclosure performance assessment.

B.1 KEY TECHNICAL ISSUE AGREEMENTS

KTI agreements RDTME 2.01, RDTME 2.02, RDTME 3.03, and SDS 2.02 are closely related and thus are addressed together for this response. The agreements refer to (1) a seismic design inputs analysis and model report, (2) Seismic Topical Report 3, and (3) an Appendix 7 meeting to present to the NRC draft seismic design inputs before the reports are completed and approved. This section lists the agreements and provides background information.

B.1.1 RDTME 2.01, RDTME 2.02, RDTME 3.03, and SDS 2.02

Agreements RDTME 2.01, RDTME 2.02, and RDTME 3.03 were reached during the NRC/U.S. Department of Energy (DOE) Technical Exchange and Management Meeting on Repository Design and Thermal-Mechanical Effects held February 6 to 8, 2001, in Las Vegas, Nevada. RDTME KTI subissues 1, 2, 3, and 4 were discussed at that meeting (Reamer and Williams 2001).

The wording of the RDTME agreements is as follows:

RDTME 2.01

> Provide Topical Report 3, Preclosure Seismic Design Inputs for a Geologic Repository at Yucca Mountain. Consistent with SDS Subissue 2, Agreement 2, the DOE will provide Seismic Topical Report 3, Preclosure Seismic Design Inputs for a Geologic Repository at Yucca Mountain, expected to be available to the NRC in January 2002.

RDTME 2.02

> Provide the substantive technical content of Topical Report 3. The DOE will provide the preliminary seismic design input data sets used in Site Recommendation design analyses to the NRC by April 2001. The DOE will provide the draft final seismic design inputs for license application via an Appendix 7 meeting after calculations are complete prior to delivery of Seismic Topical Report 3.

RDTME 3.03

> Provide the Seismic Design Inputs AMR and the Preclosure Seismic Design Inputs for a Geologic Repository at Yucca Mountain, Seismic Topical Report 3. Consistent with SDS Subissue 2, Agreement 2, the DOE will provide the Seismic Design Inputs analysis and model report and Preclosure Seismic Design Inputs for a Geologic Repository at Yucca Mountain, Seismic Topical Report 3. These documents are expected to be available to NRC in January 2002.

An annotated outline for the third seismic topical report was provided to the NRC in October 2000 (Brocoum 2000). In response, the NRC indicated its review resulted in no major comments (Reamer 2000).

In partial fulfillment of agreement RDTME 2.02, preliminary seismic design input data sets used in site recommendation design analyses were provided to the NRC (Brocoum 2001). The NRC reviewed those data and informed the DOE that they did not need any additional information pertaining to them (Reamer 2002). The NRC listed the status of the agreement as "Partly Received."

An Appendix 7 meeting was held August 6 to 8, 2002, that provided to the NRC draft information intended to be documented in the "Seismic Design Inputs AMR" and "Seismic Topical Report 3." Topics included results of geotechnical investigations that support development of seismic design inputs and an overview of the approach to be used. The geotechnical investigations discussed at that meeting are described in *Geotechnical Data for a Potential Waste Handling Building and for Ground Motion Analyses for the Yucca Mountain Site Characterization Project* (BSC 2002).

Agreement SDS 2.02 was reached during the NRC/DOE Technical Exchange and Management Meeting on Structural Deformation and Seismicity held October 11 to 12, 2000, in Las Vegas, Nevada. SDS KTI subissues 1, 2, 3, and 4 were discussed at that meeting (Schlueter 2000).

The wording of the SDS agreement is as follows:

SDS 2.02

> Provide the updated FEPs: Disruptive Events AMR, the Seismic Design Input Report, and the update to the Seismic Topical Report. DOE will provide the updated FEPs AMR to the NRC. Expected availability is January 2001. DOE will provide STR 3 to the NRC for their review. Expected availability is January 2002. The Seismic Design Inputs Report is expected to be available to the NRC by September 2001.

Features, Events, and Processes: Disruptive Events (CRWMS M&O 2000a) was provided to the NRC in 2001, and comments were transmitted to DOE (Reamer 2002). The NRC stated that this portion of the agreement was complete.

B.1.2 Related Key Technical Issues

None.

B.2 RELEVANCE TO REPOSITORY PERFORMANCE

For the preclosure phase of repository operation, seismic inputs are used to support design of systems, structures, and components that are important to safety. The seismic inputs are developed to be consistent with target levels of seismic hazard defined by mean annual probabilities of exceedance. In combination with the conservatism built into design procedures, acceptance criteria, codes, and standards, the preclosure seismic design inputs provide reasonable assurance that preclosure performance objectives will be met. Ultimately, evaluations as part of the preclosure safety analysis will demonstrate compliance to the dose standards.

For the postclosure period, seismic inputs are used in analyses supporting the seismic scenario class of the total system performance assessment. Seismic inputs with mean annual probabilities of exceedance greater than 10^{-8} are used to evaluate effects of vibratory ground motion, seismic-induced rockfall, and fault displacement on the engineered barrier system.

B.3 RESPONSE

For vibratory ground motion, the approach and examples of implementation are documented in *Development of Earthquake Ground Motion Input for Preclosure Seismic Design and Postclosure Performance Assessment of a Geologic Repository at Yucca Mountain, NV* (BSC 2004). (This report is the "Seismic Design Input Report" referred to in agreement SDS 2.02.) The seismic design input report and this technical basis document provide the information on development of preclosure seismic design inputs that the DOE agreed to provide to the NRC. Preparation of the topical report, *Preclosure Seismic Design Inputs for a Geologic Repository at Yucca Mountain* (i.e., Seismic Topical Report 3), is no longer planned. Rather, the DOE now intends to provide this information to the NRC through this technical basis document, supported by more detailed discussion in *Development of Earthquake Ground Motion Input for Preclosure Seismic Design and Postclosure Performance Assessment of a Geologic Repository at Yucca Mountain, NV* (BSC 2004), currently being updated, and *Characterize Framework for Seismicity and Structural Deformation at Yucca Mountain, Nevada* (CRWMS M&O 2000b). The ongoing update of *Development of Earthquake Ground Motion Input for Preclosure Seismic Design and Postclosure Performance Assessment of a Geologic Repository at Yucca Mountain, NV* (BSC 2004) will include ground-motion inputs for additional target annual probabilities of exceedance and reflect the current design concepts for the surface facilities. Completion of the update is expected in September 2004.

The approach for developing seismic inputs is based upon the mean seismic hazard curves developed by a probabilistic seismic hazard analysis (PSHA) for Yucca Mountain. The PSHA employed expert elicitation to characterize uncertainties about seismic sources, fault displacement potential, and ground-motion estimation models for the Yucca Mountain region. The expert elicitation process was carried out in accordance with guidance provided by Kotra et al. (1996), except that documentation of interim interpretations by the experts was not required to mitigate the possibility of anchoring. Uncertainties due to data limitations, scientific

uncertainties about applicable processes and models, and randomness due to seismic processes of ground-motion generation and the effects of variations in earth structure, as well as uncertainties in modeling fault displacement potential and variability, were explicitly incorporated into the analysis.

To develop seismic inputs for design and performance analyses, ground-motion results of the PSHA are modified to reflect site-specific effects of the upper approximately 300 m of material at Yucca Mountain. The effects of this material on ground motion were not considered in the PSHA, but need to be included in seismic inputs for analyses supporting design and performance assessment. A one-dimensional, random-vibration-theory-based, equivalent-linear site-response method is employed to model these effects. Seismic inputs are developed for appropriate hazard levels (mean annual probabilities of exceedance) depending on how the inputs will be used. For a given target hazard level, implementation of the site-response method takes into account the range of earthquake magnitudes contributing to the hazard, the uncertainty in the site seismic wave velocities, and the uncertainties about the dynamic properties of the site materials. Using this method, the developed seismic inputs maintain hazard consistency with the target hazard level at the control location corresponding to the PSHA results.

Output from the site-response calculation consists of site-specific response spectra and peak ground velocities that are hazard-consistent with the input target hazard level motions. Sites for which seismic inputs are developed are the waste emplacement level in the subsurface (for preclosure and postclosure purposes) and the area at the surface where repository operational facilities will be located (for preclosure purposes only). For the surface facilities area, strain-compatible soil properties are also an output of the site-response calculations. In addition, for hazard levels supporting preclosure design, values of strain, curvature, and peak ground motion are developed as a function of depth.

Seismic design ground-motion time histories are developed as part of the location-specific seismic inputs. Time histories for preclosure design analyses are developed by taking strong motion accelerograms from past earthquakes and modifying their response spectra to acceptably match the target response spectrum derived for any specific location; for example, the waste emplacement level or the surface facilities area. This analysis, called "spectral matching," generally follows the guidance provided by McGuire et al. (2001, Section 5). Exceptions to the guidance are described in *Development of Earthquake Ground Motion Input for Preclosure Seismic Design and Postclosure Performance Assessment of a Geologic Repository at Yucca Mountain, NV* (BSC 2004, Section 6.3.2.1.1). The strong motion accelerograms are selected so that the magnitudes and distances of the earthquakes that produced them are similar to the dominant magnitude and distance of earthquakes contributing to the Yucca Mountain site seismic hazard at the target hazard level. The spectral matching is carried out to develop an appropriate set of three-component time histories (two orthogonal horizontal components and the vertical component of motion) for preclosure seismic design analyses.

Time histories for postclosure seismic performance analyses also start with actual strong motion recordings from past earthquakes. For the derivation of these time histories, the recordings are scaled to the location-specific value of peak ground velocity corresponding to the analysis target hazard level. For some cases, the strong motion recordings are conditioned prior to scaling so that their response spectra are more representative of the Yucca Mountain site. Several

approaches are available to implement this conditioning and scaling. For conditioning, three approaches have been used: (1) no conditioning, (2) conditioning to the target response spectra associated with the reference rock outcrop (the control location) defined for the PSHA, and (3) conditioning to the target response spectra for the waste emplacement level. For scaling, in one case each component of ground motion was scaled to the appropriate site-specific peak ground velocity. For the other cases, one horizontal component was scaled to the target horizontal peak ground velocity and the second horizontal and vertical components were scaled to preserve the intercomponent variability of the original strong motion recordings.

The fault displacement PSHA results indicate that fault displacements for a range of existing faulting conditions will not exceed 0.1 cm for hazard levels appropriate for preclosure design analyses. Thus, the fault displacements are below engineering concern for preclosure design. Fault displacements are, however, included in evaluating postclosure performance.

The information in this report is responsive to agreements RDTME 2.01, RDTME 2.02, RDTME 3.03, and SDS 2.02 made between the DOE and NRC. The report contains the information that DOE considers necessary for NRC review for closure of these agreements.

B.4 BASIS FOR THE RESPONSE

In 1994 the DOE presented the NRC with an overview of its seismic hazard assessment and seismic design processes that discussed the preparation of three seismic topical reports (Milner 1994). The topical reports were to address, respectively, the methodology for carrying out a PSHA, the seismic design methodology, and development of seismic design inputs for a repository at Yucca Mountain. Topical reports addressing the first two topics were completed and submitted to the NRC (YMP 1997a; YMP 1997b). The second topical report is currently being revised to reflect the risk-informed philosophy embodied in 10 CFR Part 63. The third topical report, which is no longer planned, is the subject of the KTI agreements addressed by this appendix.

The DOE now intends to provide information on the development of seismic inputs for design and analyses, which was to be provided to the NRC in the third topical report, through this technical basis document, supported by more detailed discussion in *Development of Earthquake Ground Motion Input for Preclosure Seismic Design and Postclosure Performance Assessment of a Geologic Repository at Yucca Mountain, NV* (BSC 2004) and *Characterize Framework for Seismicity and Structural Deformation at Yucca Mountain, Nevada* (CRWMS M&O 2000b). The report *Development of Earthquake Ground Motion Input for Preclosure Seismic Design and Postclosure Performance Assessment of a Geologic Repository at Yucca Mountain, NV* (BSC 2004) is currently being updated to include results for additional target annual probabilities of exceedance and to reflect the current design concepts for the surface facilities. The DOE continues to plan on meeting with the NRC to discuss the methodology to develop seismic inputs and its implementation prior to submittal of a license application. Final seismic inputs for license application design will be presented in the license application and supporting calculations.

Acceptable seismic safety for the preclosure performance period is ensured through a combination of two important design components: (1) the design basis ground motion (DBGM)

or design basis fault displacement (DBFD) level, and (2) the design procedures, acceptance criteria, codes, and standards. The use of appropriate levels of DBGMs/DBFDs, adoption of nuclear-power-plant seismic design criteria and procedures, and demonstration of adequate seismic margins beyond the DBGMs/DBFDs are all part of the defense-in-depth seismic design strategy.

The seismic design strategy identifies two DBGM levels, DBGM-1 and DBGM-2, with mean annual probabilities of exceedance of 10^{-3} and 5×10^{-4}, respectively. In addition, the strategy includes evaluation of systems, structures, and components that are important to safety for ground motions with a mean annual probability of exceedance of 10^{-4} to demonstrate adequate seismic margin. For fault displacement, the primary strategy is to avoid faults for which seismic design would be required. In cases for which avoidance is not practical, appropriate mean annual probabilities of exceedance for design are identified as 10^{-4} and 5×10^{-5} (DBFD-1 and DBFD-2). Based on results from the PSHA, fault displacement hazard values at these levels are less than 0.1 cm for repository faulting conditions.

B.4.1 Overall Approach to Developing Seismic Design Inputs

Development of seismic design inputs is the last step in a process that began with collection of data to support the PSHA (see Section 2 of this technical basis document), continued with the implementation of the PSHA itself (see Section 3), and concludes with use of the PSHA results coupled with site-response analyses to derive location-specific motions for seismic design and analyses (Figure B-1). The results of the PSHA were obtained for a reference rock outcrop with generic rock properties appropriate for the entire repository area. These control motions do not account for the effect on ground motion of the upper approximately 300 m of materials at the site. The reference rock outcrop was used because site-specific data on the velocities and dynamic properties of the upper 300 m of rock and soil were limited at the time of the PSHA. Thus, site-response analyses are carried out to derive seismic design and seismic analysis input motions for specific locations (see Section 4). The approach to carry out this last step and examples of its implementation are described in *Development of Earthquake Ground Motion Input for Preclosure Seismic Design and Postclosure Performance Assessment of a Geologic Repository at Yucca Mountain, NV* (BSC 2004).

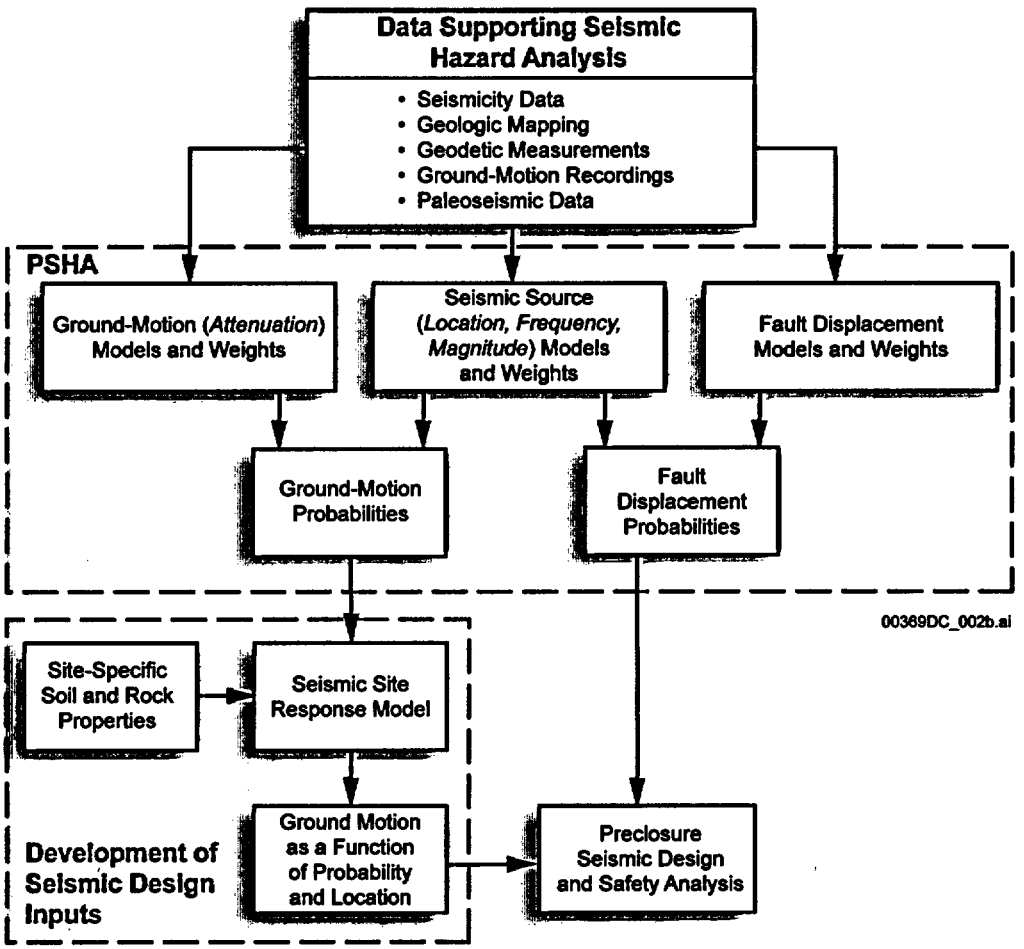

Figure B-1. Components of the Assessment of Preclosure Seismic System Performance

The approach to developing ground-motion inputs for any location follows guidance by McGuire et al. (2001, Section 6, Approach 2B) and conforms to the guidance from Regulatory Guide 1.165, *Identification and Characterization of Seismic Sources and Determination of Safe Shutdown Earthquake Ground Motion* (1997, Appendix C). This approach results in location-specific ground motions that are hazard-consistent with PSHA results for the Yucca Mountain site. Results of the PSHA form the basis for deriving control motions that are transferred to specific locations of repository facilities by means of location-specific site-response analyses. The approach preserves the hazard level of the control motions while incorporating location-specific uncertainty and randomness in dynamic material properties and addressing earthquake magnitude–related effects on the degree of nonlinearity in location-specific response. The input motions for seismic design or analysis at any location are hazard-consistent with the Yucca Mountain site control motions. This outcome is particularly important because the motions derived for any location properly incorporate uncertainties about basic processes and models that are input to the PSHA for the Yucca Mountain site, forming a continuous link between the seismic design and analysis inputs and basic scientific understanding of geologic processes in the site region.

The starting point for the approach is the output of the PSHA for Yucca Mountain expressed as hazard curves for various measures of ground motion (CRWMS M&O 2000b, Section 6.5.3) (Figure B-2, PSHA Results). Results are provided for spectral acceleration at structural response frequencies of 0.3, 0.5, 1, 2, 5, 10, 20, and 100 Hz (peak ground acceleration). Results for peak ground velocity are also determined. These results are for a hypothetical rock outcrop with material properties of tuff at the waste emplacement level (see Figure 3-2). This hypothetical rock outcrop is referred to as the PSHA reference rock outcrop.

For a given mean annual probability of exceedance, the ground-motion hazard results can be used to derive a response spectrum with a uniform probability of being exceeded, the uniform hazard spectrum (Uniform Hazard Spectra in Figure B-2). Comparison of the vertical and horizontal uniform hazard spectra for Yucca Mountain reveals characteristics of the vertical spectra that are inconsistent with ground-motion observations from large earthquakes recorded at close distances. Following a recommended approach by McGuire et al. (2001, Section 4.7) a revised vertical uniform hazard spectrum was developed (Revised Vertical Uniform Hazard Spectrum in Figure B-2). The horizontal uniform hazard spectrum and revised vertical uniform hazard spectrum are used in subsequent analyses to determine location-specific ground-motion inputs.

The uniform hazard spectrum is a broadband spectrum that reflects the contributions to hazard at the Yucca Mountain site from earthquakes with a range of magnitudes and distances. Use of such a spectrum as input to the location-specific site-response analysis could produce inappropriate results because use of broadband spectra can induce higher strains than any single earthquake scaled to the same peak acceleration level and result in ground motions that are not conservative. Thus, while the uniform hazard spectrum forms the basis for the ground motions used in the location-specific response analysis, it is not used directly. Rather, as described below, the uniform hazard spectrum is deaggregated to identify the distribution of earthquake magnitudes and distances that contribute to the spectrum for a given hazard level. Then, ground motions for appropriate magnitudes and distances representing the distribution of earthquakes are used for the calculation of location-specific response transfer functions.

To develop reference earthquakes, the guidance provided by Regulatory Guide 1.165 (1997, Appendix C) is generally followed. Exceptions are described in *Development of Earthquake Ground Motion Input for Preclosure Seismic Design and Postclosure Performance Assessment of a Geologic Repository at Yucca Mountain, NV* (BSC 2004, Section 6.2.2.4). The PSHA results for a given annual probability of exceedance are deaggregated to identify controlling earthquakes. Controlling earthquakes are determined from the deaggregated hazard for structural frequency ranges of 1 to 2 Hz and at 5 to 10 Hz (Reference Earthquakes in Figure B-2). Response spectra for the controlling earthquakes are then scaled to match the uniform hazard spectrum in the appropriate frequency range to retain hazard consistency with the site uniform hazard spectrum. These scaled spectra form the reference earthquake response spectra (Scaled Reference Earthquake Response Spectra in Figure B-2).

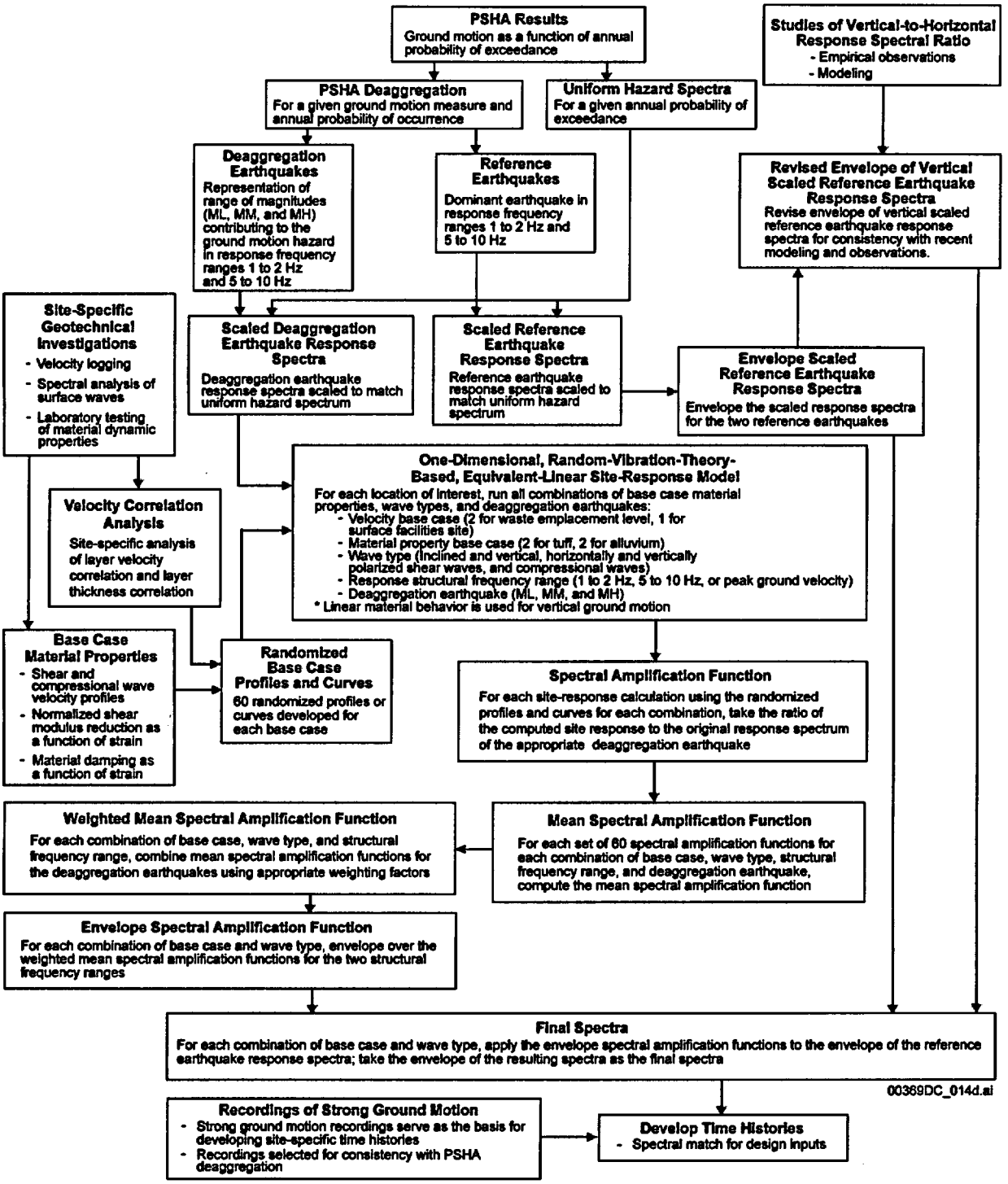

Figure B-2. Development of Location-Specific Ground Motions for Preclosure Design and Analyses

Site response is sensitive to the response spectrum of the input ground motion, which is related to earthquake magnitude. This effect would not be captured if the reference earthquake response spectra were used as the control motions for location-specific site-response calculations. To incorporate this effect, for both the 1 to 2 Hz and 5 to 10 Hz structural frequency ranges, three deaggregation earthquakes are identified to represent the range of magnitudes contributing to the

hazard (McGuire et al. 2001, Section 6.1, Approach 2B) (Deaggregation Earthquakes in Figure B-2). These earthquakes nominally represent the 5th, mean, and 95th fractile magnitudes and associated distances determined from the hazard deaggregation. As was done for the reference earthquakes, response spectra for the deaggregation earthquakes are scaled to match the uniform hazard spectrum in the appropriate structural frequency range (Scaled Deaggregation Earthquake Response Spectra in Figure B-2). The deaggregation earthquake response spectra then form the control motions for calculating location-specific transfer functions that are used to obtain hazard-consistent ground motions at specific locations for seismic design and analysis.

Location-specific inputs required to compute transfer functions include seismic velocity profiles and dynamic material properties. Results of geotechnical investigations are used as the basis for deriving these inputs (Site-Specific Geotechnical Investigations in Figure B-2). Uncertainties in the mean velocity profile and dynamic material properties are incorporated into the analysis. For the material above the waste emplacement level, two base case velocity profiles are used to represent uncertainty in the mean profile. For the surface facilities area, where uncertainty in the mean profile is less, a single base case profile is used. For the dynamic properties of site materials, multiple base case curves are also developed to represent uncertainty in mean values. Two sets of base case curves are developed each for the tuff and alluvial materials (Base Case Material Properties in Figure B-2). The site response is calculated for the range of combinations of velocity and dynamic material properties, and results are enveloped.

Random variability in location-specific velocity and dynamic material properties at the site are incorporated into the site-response computations. Location-specific velocity data are analyzed to determine the layer-to-layer correlation of seismic velocities and layer thickness (Velocity and Layer Thickness Correlation Analysis in Figure B-2). This information is used along with the location-specific base case velocity and material property curves to generate suites of randomized profiles and curves (Randomized Base Case Profiles and Curves in Figure B-2). The site response is calculated for combinations of the randomized velocity profiles and dynamic material properties curves and then normalized by the control motion to produce a suite of spectral amplification functions (Spectral Amplification Function in Figure B-2). This process is carried out for each control motion, an appropriate range of control motion incidence angle, and wave types. The multiple spectral amplification functions resulting from the randomization of profiles and curves span the uncertainty in site response and are averaged (Mean Spectral Amplification Function in Figure B-2). Next, for each combination, a weighted average is taken of the results for the three deaggregation earthquakes (Weighted Mean Spectral Amplification Function in Figure B-2) with the weights related to the fractile from the magnitude deaggregation that each deaggregation earthquake represents. Final transfer functions are then determined by enveloping, for each combination of inputs, over the results for the two structural frequency ranges (1 to 2 Hz and 5 to 10 Hz) (Envelope Spectral Amplification Function in Figure B-2).

For each location, the final transfer functions are applied to the envelope of the reference earthquake response spectra to obtain the final input response spectrum (Final Spectra in Figure B-2). Time histories for dynamic analyses are developed such that their response spectra properly match the final input response spectrum (Develop Time Histories in Figure B-2).

In the following sections, the steps in this analysis are described in more detail. First, the site-response model is discussed (Section B.4.2). Second, the development of inputs to the

site-response computation is presented (Sections B.4.3 and B.4.4). Then, the analyses to determine location-specific response spectra and strain-compatible soil properties are described (Section B.4.5). Finally, development of time histories that properly match the location-specific input response spectra is discussed (Section B.4.6). An example of implementing the analysis approach is given in Section B.4.7. A brief discussion of development and use of seismic inputs for analyses supporting postclosure performance assessment is also provided (Section B.4.8).

B.4.2 Site-Response Model

A site-response model for Yucca Mountain needs to treat seismic wave propagation through the site materials and take into account dynamic behavior of those materials. Inputs to the model consist of ground motion derived from the PSHA results (control motions) and material dynamic properties (density, velocity, shear modulus reduction, material damping) developed from location-specific geotechnical data, technical information, and scientific judgment. The computational method that is used incorporates nonlinear behavior using an equivalent-linear formulation. The equivalent-linear formulation approximates a second-order nonlinear equation, over a limited range of its variables, by a linear equation. Based on the effective strains computed for the ground motion using a linear analysis, the material dynamic properties are adjusted to be consistent with the effective strains. This process is iterated until changes in the parameters are below an established tolerance level.

The site materials are modeled as a one-dimensional layered system for the purpose of site response computations. A series of homogeneous horizontal layers, each of which is characterized by a velocity, density, and set of dynamic material properties, approximate the site materials. For the equivalent-linear formulation, dynamic material properties consist of curves describing how the shear modulus (normalized to its value at low strain) and material damping vary as a function of shearing strain level. Inclined and vertically propagating seismic waves are included in the computation.

The one-dimensional approximation is considered adequate. Two- and three-dimensional effects are included in the database of recorded ground motions that underlies ground-motion attenuation curves used at Yucca Mountain. Thus, those effects are included in the control motions that are input to the one-dimensional site-response model.

A consequence of the equivalent-linear formulation is the preservation of the superposition principle. For linear systems, this principle permits spectral decomposition and frequency-domain solutions. Thus, efficient frequency-domain solutions of the wave equation can be obtained using the propagator matrix solution scheme (Haskell 1960; Schnabel et al. 1972; Silva 1976). Following solution in the frequency-domain, the wavefields can be spectrally recomposed (summed over frequencies) through an inverse Fourier or Laplace transform.

Site-response computations for Yucca Mountain implement the equivalent-linear formulation of Seed and Idriss (1969). The ground motion that is input to the site model is derived from the results of the PSHA. The ground motion is characterized by its power spectral density and propagated through the site layers using the propagator matrix formulation of Silva (1976). For each layer, random vibration theory is used to determine peak time-domain values of shear strain based on the shear-strain power spectrum. Effective shear strains for the duration of the ground

motion are then estimated on the basis of the peak shear strain. The effective strains are used along with the dynamic property curves, which indicate how the shear modulus and material damping vary as a function of shear strain, to determine new iterated values of shear modulus and damping for each layer. The process is repeated until a strain-compatible linear solution is obtained. Because of the use of random vibration theory to determine peak shear strains in the time domain, the site-response model for Yucca Mountain is referred to as a random-vibration-theory-based equivalent-linear site-response model.

Implementation of this computational method is done with the software codes RASCALS V5.4 (Pacific Engineering and Analysis 2002a) and RASCALP V2.02 (Pacific Engineering and Analysis 2002b). For horizontal motion, RASCALS V5.4 treats horizontally polarized shear waves that are propagating vertically and at inclined angles and vertically polarized shear waves propagating at inclined angles. For vertical motion, RASCALP V2.02 treats vertically polarized shear waves propagating at inclined angles and compressional waves propagating vertically and at inclined angles. To determine angles of incidence, the earthquakes controlling the ground-motion hazard at a given mean annual probability of exceedance are determined and ray-tracing is used to compute the incident angles.

Because a one-dimensional model is used for Yucca Mountain, it does not explicitly incorporate two- and three-dimensional wave propagation effects (e.g., effects of topography, dipping layers). However, probabilistic ground-motion results for Yucca Mountain, from which input motions are derived, already include two- and three-dimensional wave propagation effects because these effects are included in the ground-motion database used to assess ground motion as part of the PSHA. While it is known that two- and three-dimensional wave propagation effects are present at all sites to some extent, validations have demonstrated that simple one-dimensional models accommodate the significant and stable features of site response (Silva, Abrahamson et al. 1996; Silva, Stark et al. 1990). Also, although lithostratigraphic units at Yucca Mountain generally dip to the east, velocity data gathered to date do not show a strong and systematic correlation with the dipping strata (e.g., BSC 2002, Section 6.4.3.2).

One-dimensional site-response analysis using an equivalent-linear formulation has proved successful when applied elsewhere. In a validation study (EPRI 1993, Appendix 6B), the random-vibration-theory-based equivalent-linear model was compared to three nonlinear models for three test cases. For each test case, ground motion was recorded at a soil site and a nearby rock site. The recorded rock motions were taken as the input to the site-response models, and the computed results were compared to the recorded soil site motions. Each of the sites was reasonably well characterized in terms of its velocities and dynamic material properties. Results of this validation study show little difference between equivalent-linear and fully nonlinear formulations for the ground-motion levels examined (peak ground accelerations between about 0.05 to 0.5 g). Both equivalent-linear and nonlinear formulations also compared favorably to the recorded motions. While this validation does not directly address the specific site materials and the entire range of ground-motion input levels for Yucca Mountain, it provides an acceptable degree of confidence that the modeling approach adequately captures nonlinear dynamic behavior.

Observations of seismic ground motion show evidence of nonlinear behavior for the horizontal component of motion. Vertical ground motion, however, generally shows linear behavior. In

computing site response at Yucca Mountain, nonlinear effects are included for horizontal motion, but vertical motion is treated in a linear fashion.

The model is discussed in more detail in *Development of Earthquake Ground Motion Input for Preclosure Seismic Design and Postclosure Performance Assessment of a Geologic Repository at Yucca Mountain, NV* (BSC 2004, Section 6.1) and references cited therein.

B.4.3 Development of Control Motion

The ground motion that serves as input to the site-response analysis is referred to as the control motion. For Yucca Mountain, the control motion is derived from the PSHA results. For a given mean annual probability of exceedance, first the hazard results are used to develop uniform hazard spectra. Then, low frequency (1 to 2 Hz) and high frequency (5 to 10 Hz) reference earthquakes are identified by deaggregating the uniform hazard spectrum. Next, the deaggregated distribution of earthquakes contributing to the hazard for a particular probability of exceedance is represented by the 5th, mean, and 95th percentile magnitudes and distances in the distribution (deaggregation earthquakes) for the purpose of computing site-response transfer functions. The results of the site-response analysis are spectral amplification (or transfer) functions that characterize the effects of the site on the input ground motion as a function of structural frequency. The spectral amplification functions are then applied to the envelope of the low and high frequency reference earthquake response spectra to derive the final location-specific input response spectra for preclosure seismic design (BSC 2004, Section 6.3.1).

Uniform Hazard Spectra–Uniform hazard spectra represent response spectral acceleration values, as a function of structural frequency, that have a uniform annual probability of being exceeded. During the PSHA, seismic hazard was determined for response spectral structural frequencies ranging from 0.3 to 100 Hz. For a given annual probability of being exceeded, a mean uniform hazard spectrum is constructed by taking the mean PSHA spectral acceleration value at each structural frequency that was analyzed (BSC 2004, Section 6.2.2.3).

Comparison of the vertical and horizontal uniform hazard spectra obtained from the PSHA results reveals characteristics in the vertical spectra that are not in accord with earthquake observations and ground-motion modeling results. Observations from earthquakes with magnitudes and distances comparable to those dominating the ground-motion hazard at Yucca Mountain at low mean annual probabilities of exceedance indicate that vertical component motion exceeds horizontal component motion at frequencies greater than about 10 Hz. Observations and numerical modeling also indicate that vertical response spectra for these earthquakes peak at higher frequencies than the corresponding horizontal response spectra. The relation between the horizontal and vertical uniform hazard spectra from the PSHA does not exhibit these features. Thus, a revised vertical uniform hazard spectrum is developed.

The revised vertical uniform hazard spectrum is developed following guidance by McGuire et al. (2001, Section 4.7). First, a vertical-to-horizontal response spectral ratio is determined for Yucca Mountain site conditions based on earthquake observations and results of numerical modeling. This site-specific ratio is then applied to the horizontal uniform hazard spectrum from the PSHA for given hazard levels to obtain the revised vertical uniform hazard spectrum (BSC 2004, Section 6.2.2.6). For vertical motion, this revised uniform hazard spectrum is used

in subsequent steps of the site-response analysis to derive location-specific seismic inputs for preclosure design and analyses.

Given the nature of a PSHA, the uniform hazard spectrum does not represent the response spectrum of a single earthquake but rather the integrated contributions of the range of earthquakes that contribute to the hazard at the Yucca Mountain site as expressed in the PSHA seismic-source interpretations. The uniform hazard spectrum is thus a broadband representation of the ground motion for a given annual probability of being exceeded.

The use of such a broadband motion, which reflects contributions from earthquakes of varying magnitudes and distances, would be inappropriate for site-response analysis. When the amplitudes of control motions cause significant nonlinear response of the site materials, broadband spectra can induce higher strains than any single earthquake scaled to the same peak acceleration level and thus perturb the calculated site response. Accordingly, reference earthquakes and deaggregation earthquakes were developed to represent the uniform hazard spectrum in the site-response analysis.

Reference Earthquakes–Development of low and high frequency reference earthquakes to represent the uniform hazard spectrum conforms with guidance by Regulatory Guide 1.165 (1997, Appendix C). PSHA results are deaggregated to identify which earthquakes (i.e., magnitude and distance combinations) contribute most to a given mean annual probability of exceedance. Deaggregation is carried out for both a high (5 to 10 Hz) and low (1 to 2 Hz) structural frequency range. Definition of the low structural frequency range differs slightly (1 to 2 Hz instead of 1 to 2.5 Hz) from the guidance in Regulatory Guide 1.165 (1997, Appendix C).

Based on the deaggregation results, a reference earthquake is identified for each structural frequency range by taking the mode magnitude and distance (BSC 2004, Section 6.2.2.4). The mode magnitude and distance was used, rather than the mean magnitude and distance as recommended in Regulatory Guide 1.165 (1997, Appendix C), because the mode values better represent the earthquakes that dominate the hazard for a given annual exceedance frequency (McGuire 1995, p. 1281). However, a moderate difference between the mode and mean has only a small effect on the reference earthquake spectral shape. Also, because the reference earthquake spectra are scaled to the uniform hazard spectrum in the appropriate structural frequency range, use of the mode instead of the mean has a negligible effect on the amplitude of the reference earthquake spectra at the structural frequencies at which they are scaled.

The response spectral shapes for the reference earthquakes are determined from the ground-motion relations that were input to the Yucca Mountain PSHA. The reference earthquake spectra are then scaled to match the uniform hazard spectrum (or revised uniform hazard spectrum for vertical motions) in the low and high structural frequency ranges (see Figure 4-3). The scaled reference earthquake response spectra are compared to the uniform hazard spectrum to ensure that, considered together, they adequately represent it. If significant gaps exist, the spectra are adjusted.

Reference earthquakes are identified for both the horizontal and vertical component of ground motion. For consistency, reference earthquakes for vertical motions were taken to be the same as those for horizontal motion. Once the location-specific response transfer function is determined

for a location of interest, it is applied to the envelope of the scaled response spectra for the reference earthquakes to obtain the input motion for that location.

Deaggregation Earthquakes–Response of site materials, which determines the ground-motion site response, depends on earthquake magnitude, as well as ground-motion amplitude. As magnitude increases, the response spectral shape of the ground-motion changes, and the duration and amplitude of strong ground-shaking typically increases. To obtain location-specific ground motions that are consistent in probability with the control location hazard, these effects are captured in the site-response analysis.

Deaggregation earthquakes are developed for the purpose of computing site-response transfer functions by deaggregating the ground-motion hazard for a given annual exceedance probability and structural frequency range (5 to 10 Hz or 1 to 2 Hz) (BSC 2004, Section 6.2.2.5). To represent the range of magnitudes contributing to the hazard for a given mean annual probability of exceedance, three earthquakes are identified corresponding nominally to the mean, 5th (low magnitude deaggregation earthquake), and 95th (high magnitude deaggregation earthquake) percentile of the magnitude distribution. In some cases, different percentiles were used to appropriately capture the magnitude distribution resulting from the deaggregation. Response spectra for the deaggregation earthquakes, determined using the PSHA ground-motion relations, are scaled to the uniform hazard spectrum in the appropriate structural frequency range (see Figure 4-4). The deaggregation earthquakes form the control motion for the site-response analysis. With three deaggregation earthquakes for each of two response structural frequency ranges (5 to 10 Hz and 1 to 2 Hz) and two components of ground motion (horizontal and vertical), 12 control motions are involved in determining the ground-motion site-response transfer functions.

B.4.4 Characterization of Site-Specific Material Properties

In addition to control motions, input to the site-response analysis consists of parameters that characterize the dynamic properties of the site materials. Key parameters are:

- Seismic velocity as a function of depth
- Shear modulus, normalized to its small-strain value, as a function of shearing strain
- Material damping, as a function of shearing strain.

Shear modulus reduction and variation in material damping as a function of shear strain are parameters that characterize the response of site materials to dynamic strains due to seismic wave propagation through them in the site-response analysis.

As a basis for determining values for these parameters, geotechnical investigations were carried out at Yucca Mountain. Because of uncertainty in the geotechnical parameters and the spatial extent of the locations where seismic input motions are required, both epistemic uncertainties and random variations in the parameter values need to be included. To determine location-specific ground motions that are consistent with the hazard for the Yucca Mountain site control location, these uncertainties and random variability must be incorporated into the site-response analysis, just as uncertainties and random variability were explicitly incorporated in the PSHA.

Geotechnical Investigations–Geotechnical investigations have been carried out to collect information on the material properties of the site (BSC 2002; BSC 2004, Sections 6.2.3 and 6.2.4). The studies focused on the two primary sites of interest: the surface facilities area and the area above the waste emplacement footprint. Studies consisted of drilling and logging boreholes, velocity surveys, and laboratory testing of rock and soil samples to determine the dynamic response properties of the materials (i.e., the shear modulus and damping behavior as a function of imposed dynamic strain level).

For the surface facilities area, 16 boreholes were drilled, ranging in depth from 99.8 to 667.8 ft (see Figure 4-5). Interpretations of geologic logs of the boreholes, along with previous information, provided adequate understanding of the geologic strata underlying the site. A soil layer overlies volcanic deposits that are faulted and dip to the east (see Figure 4-6). The thickness of the soil layer ranges from 0 ft at the edge of Exile Hill to more than 100 ft at the eastern edge of the characterized area.

To characterize the velocity of the soil and rock underlying the surface facilities site, velocity measurements were collected in the boreholes. Two techniques were employed: downhole and suspension logging. In addition, a surface-based method of characterizing velocity—spectral analysis of surface waves—was also applied. While the borehole velocity measurements provide information as a function of depth at a point, the spectral analysis of surface waves technique provides information along its survey line, filling in data between the boreholes. By combining the information from these two approaches, an adequate velocity characterization of the site was developed. Shear-wave velocity data from these studies are summarized in Figure 4-7. A discussion of the investigations and resulting data is found in *Geotechnical Data for a Potential Waste Handling Building and for Ground Motion Analyses for the Yucca Mountain Site Characterization Project* (BSC 2002).

For the repository block (i.e., the block of rock containing the waste emplacement area at a depth of about 300 m below the ground surface), velocity data were obtained from existing boreholes and spectral analysis of surface waves surveys (see Figure 4-8). In part because of logistical considerations and the locations of existing boreholes, coverage of the repository block is limited. Some data from boreholes near but not within the repository block therefore are used in assessing its velocity. Data from these boreholes extend to depths ranging from about 1,000 to almost 2,600 ft. Boreholes within the repository block are shallow, and data surveys reached depths ranging from about 25 to 180 ft. Results from spectral analysis of surface waves surveys range from near surface to 750 ft.

In addition to the spectral analysis of surface waves surveys carried out at the surface of the repository block, the spectral analysis of surface waves technique was applied within the main drift of the Exploratory Studies Facility. These measurements provide information on the velocity of the repository block at depths (980 to 1,150 ft) greater than those sampled using the spectral analysis of surface waves technique at the surface. Shear-wave velocity data from these studies are summarized in Figure 4-9. A discussion of the investigations and resulting data is found in *Geotechnical Data for a Potential Waste Handling Building and for Ground Motion Analyses for the Yucca Mountain Site Characterization Project* (BSC 2002).

To characterize the normalized shear modulus reduction and damping properties of the site materials, laboratory testing was carried out on rock and soil samples (BSC 2002, Section 6.2.10 and 6.3.3). Resonant column and torsional shear tests were performed to examine the nonlinear behavior of the materials as a function of shearing strain. Tested samples were from the Tiva Canyon Tuff and soil obtained from the surface facilities area. Testing was limited to small samples that may not fully represent in situ properties. Due to the nature of the materials, intact soil samples could not be obtained. Consequently, the samples were reconstituted in the laboratory prior to testing. Testing results are summarized in Figures 4-10 and 4-11. For tuff, systematic differences in nonlinear properties as a function of lithostratigraphic unit, degree of welding, and dry unit weight were not observed. Also, for tuff, only limited nonlinear behavior was observed at the strains obtained during testing (up to about 0.1% or less).

Velocity–Results of the geotechnical investigations form the basis for developing base case velocity profiles (compressional-wave and shear-wave) for the repository block and the surface facilities area. For the repository block, results of velocity surveys in deeper boreholes located near but outside the waste emplacement area, results from shallower boreholes, and results from spectral analysis of surface waves surveys indicate considerable uncertainty in the base case velocity profile. In addition, some portions of the block containing the waste emplacement area have not been well sampled. To represent this uncertainty, two base case profiles were developed (Figure B-3) and carried through the site-response analysis. Spectral analysis of surface waves results from the Exploratory Studies Facility provide the basis for the repository block velocity at a depth of about 300 m. For the surface facilities area, in addition to a base case profile for tuff, a base case profile for soil was developed. For each material, available data support development of a single base case profile at this location (Figure B-4). The velocity profile developed for the surface facilities area is representative of the portion of the area that lies southeast of the Exile Hill Fault splay. Details of development of the base case velocity profiles are documented in *Development of Earthquake Ground Motion Input for Preclosure Seismic Design and Postclosure Performance Assessment of a Geologic Repository at Yucca Mountain, NV* (BSC 2004, Section 6.2.3).

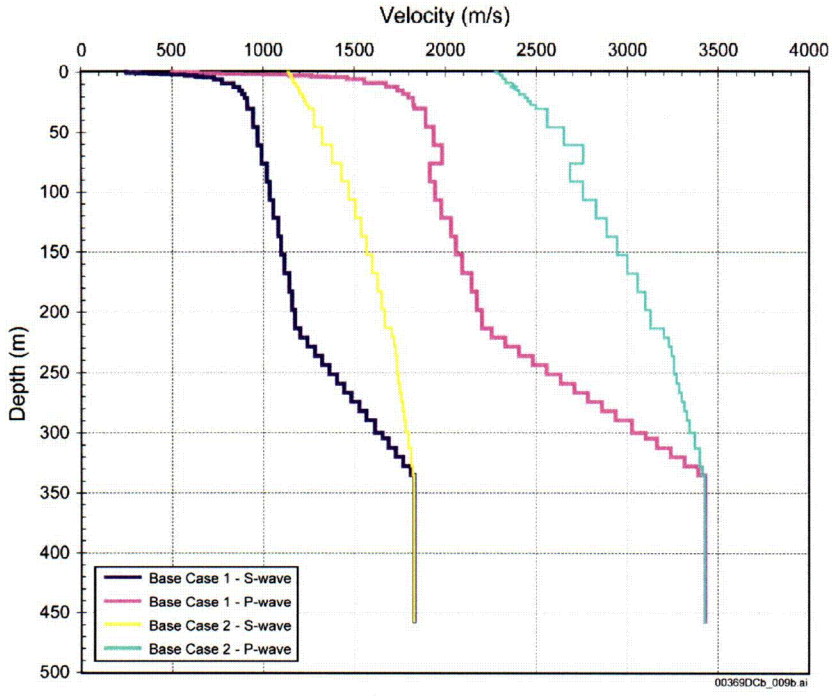

Source: BSC 2004, Figure 6.2-82.

Figure B-3. Repository Block Base Case Velocity Profiles

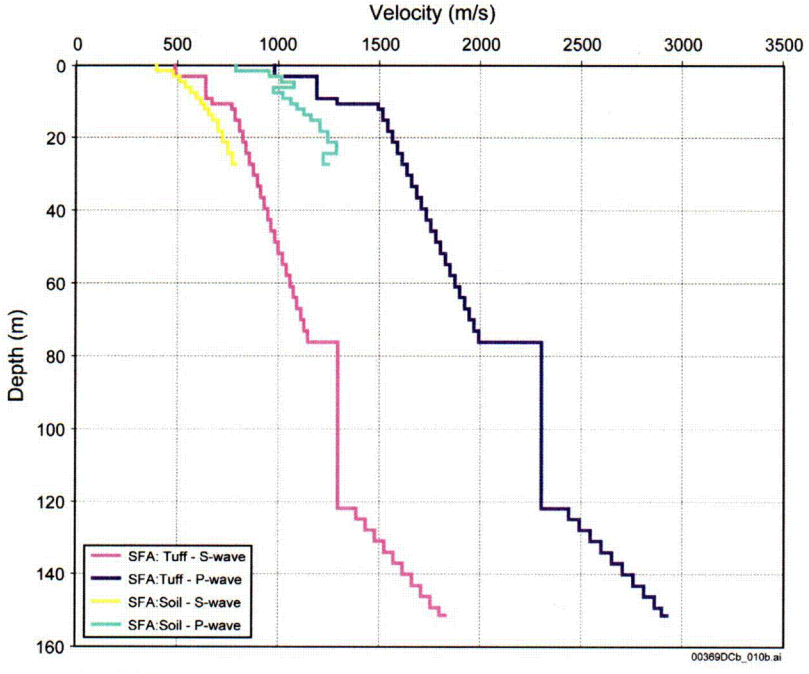

Source: BSC 2004, Figures 6.2-83 through 6.2-86.

NOTE: SFA = surface facilities area.

Figure B-4. Surface Facilities Area Base Case Velocity Profiles for Tuff and Soil

C38

In addition to uncertainty in the base case velocity profile, which is addressed by developing two profiles for repository block tuff, random variability in velocities across the site is also accommodated in the site-response analysis. To accomplish this, each base case profile is used as the basis to randomly generate a suite of 60 profiles that serve as input to the site-response model (see Figure 4-14). Correlation between layer velocities and thicknesses is based on an analysis of the available velocity data and, thus, is site-specific (BSC 2004, Section 6.2.3.6). For each of the randomly generated profiles, the depth of the profile is also varied using a uniform distribution from about 200 to 450 m for the repository block and about 120 to 180 m for the surface facilities site. This variation accounts for the range in overburden thickness above the waste emplacement area and in the depth at which the velocity reaches the value for the hypothetical reference rock outcrop from the PSHA.

Shear-Modulus Reduction and Material Damping–As ground motion increases and produces larger shear strains in the site materials, nonlinear behavior can take place. In the site-response computations, this nonlinear behavior is accounted for through changes in shear modulus and material damping. Laboratory testing provides significant information on such behavior for Yucca Mountain site materials but, because of the scale of samples tested, there is uncertainty in how these results relate to in situ properties. For tuff, the small samples tested may not reflect the effects of fractures and voids in the in situ rock and, thus, the tested samples may behave more linearly than the in situ rock. On the other hand, the process of collecting the samples may disturb them and cause them to behave more nonlinearly than in situ unfractured rock. For soil, the samples were disturbed and were reconstituted for testing. Thus, soil cementation that exists in situ is not reflected in the test results. Also, the size of the soil samples precludes inclusion of some of the larger soil components (e.g., gravel, cobbles, boulders). Thus, there is considerable uncertainty in how the soil testing results relate to in situ properties.

To accommodate uncertainty in mean normalized shear modulus reduction and material damping curves for tuff, two sets of base case curves were developed (Figure B-5). A generic, cohesionless soil curve (EPRI 1993, Appendix 7) is used, along with the laboratory testing data and professional judgment to develop the base-case curves. One set of curves represents the case in which in situ conditions consist of unfractured rock. The second set was developed to represent in situ conditions that reflect fracturing and heterogeneity, the effects of which are not captured in laboratory testing. For soil, two sets of curves are also developed to represent the uncertainty in mean dynamic properties (Figure B-6). One set of curves (base case #1) accommodates the possibility of little to no cementation in the field, as well as the lack of experience with this type of material in the geotechnical literature. The second set of curves (base case #2) represents the case in which in situ cementation breaks under strains produced by ground motion. The site-response model was run for each of these base case sets of dynamic property curves. For the surface facilities area, four cases were run reflecting the four combinations of tuff and soil base case curves. A more detailed discussion of the development of the base case curves is provided in *Development of Earthquake Ground Motion Input for Preclosure Seismic Design and Postclosure Performance Assessment of a Geologic Repository at Yucca Mountain, NV* (BSC 2004, Section 6.2.4.2 and 6.2.4.3).

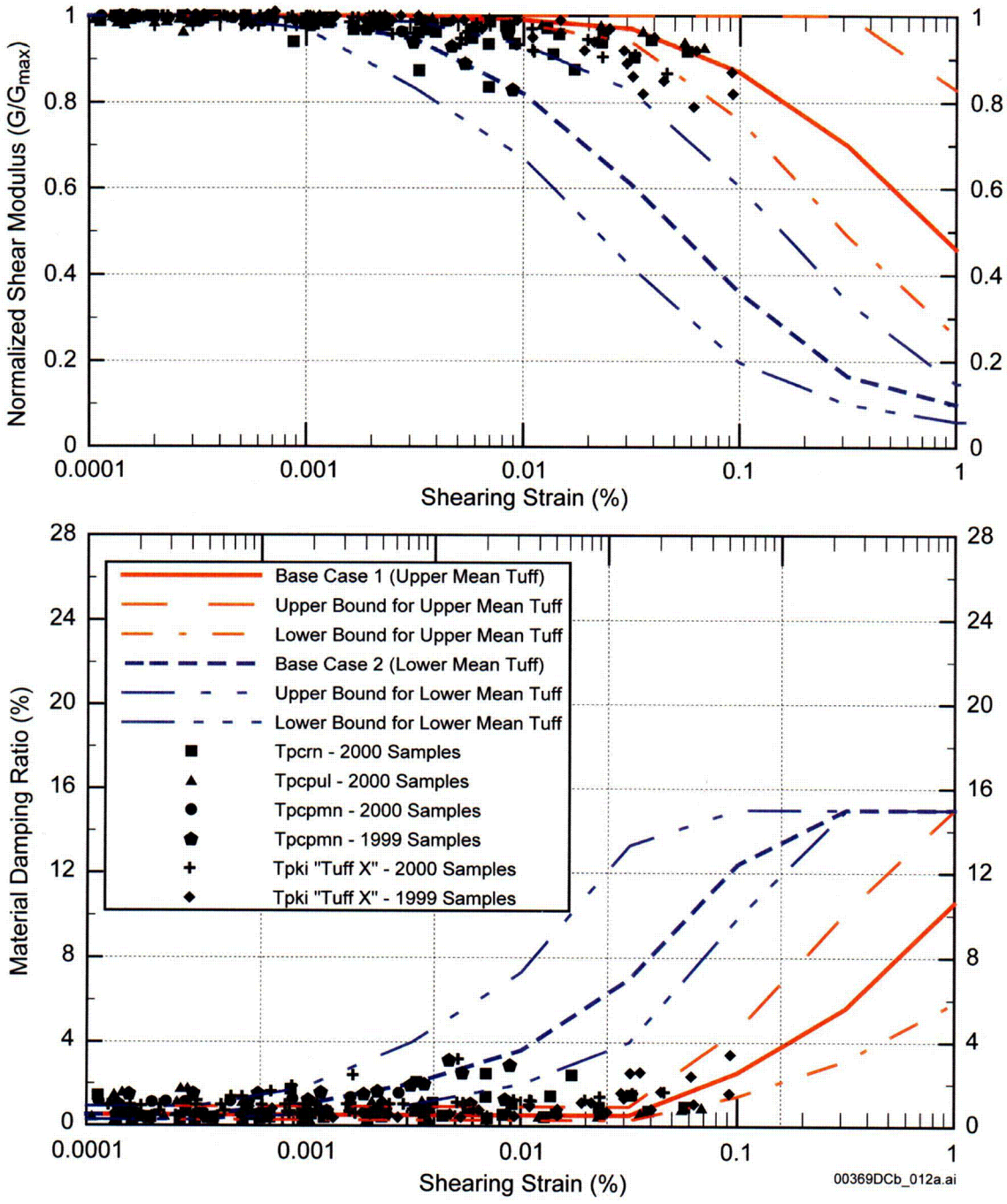

Source: BSC 2004, Figure 6.2-103.

Figure B-5. Base Case Tuff Normalized Shear Modulus and Material Damping Ratio

C39

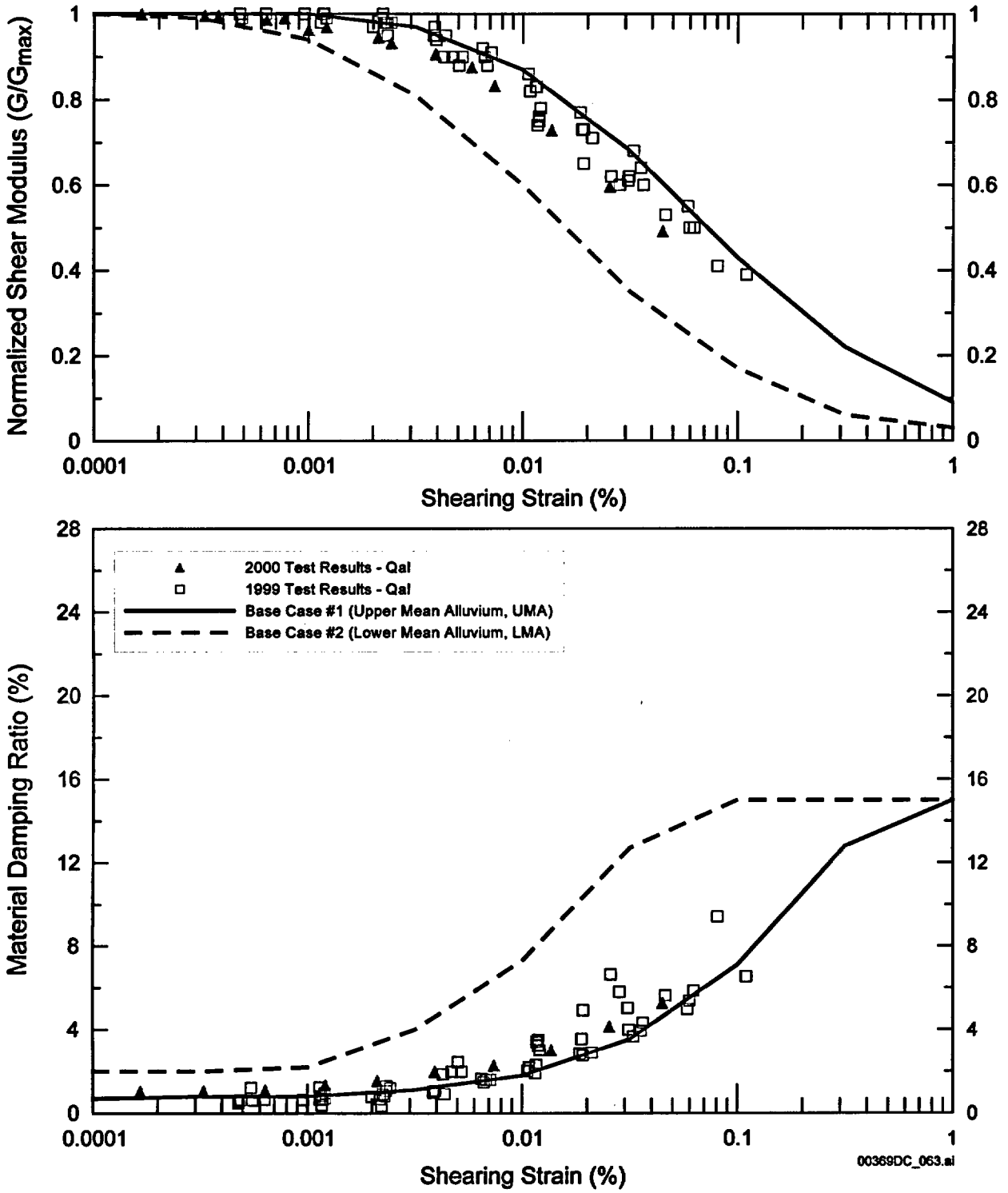

Source: BSC 2004; Wong and Silva 2003, p. 87.

NOTE: Qal = Quaternary alluvium.

Figure B-6. Base Case Soil Normalized Shear Modulus and Material Damping Ratio

In addition to uncertainty in the mean dynamic property curves, random variability about the mean curves is also accommodated in the site-response analysis. As for the velocity profiles, the variability is taken into account by randomly generating 60 sets of dynamic property curves for each base case curve and using those random curves in the analysis. The curves are allowed to vary between lower and upper bounds at ±2 standard deviations, assuming a normal distribution.

B.4.5 Transfer Functions

Site response can be thought of as a transfer function that transposes ground motion from the PSHA reference rock outcrop (the control location) to ground motion at a specific location where input ground motions are required. For earthquake response spectra, the transfer function describes the amplification or reduction of the control motion response spectrum as a function of frequency and is referred to as a spectral amplification function. The following section describes the approach for determining response spectra transfer functions for Yucca Mountain that result in location-specific ground motions that are hazard-consistent with the seismic hazard results for the control location. A discussion can be found in *Development of Earthquake Ground Motion Input for Preclosure Seismic Design and Postclosure Performance Assessment of a Geologic Repository at Yucca Mountain, NV* (BSC 2004, Section 6.3.1.1.2).

To determine the response spectrum transfer function, the six control motion earthquakes for horizontal and vertical component motion—three deaggregation earthquakes (low, mean, and high magnitude) for two structural frequency ranges (5 to 10 Hz and 1 to 2 Hz)—are used for the site-response calculation. For each deaggregation earthquake (control motion), the site-response calculation is carried out for 60 randomized velocity profiles and dynamic property curves. For locations where multiple base case profiles or curves were developed to represent uncertainty, the process is carried out for each base case. In addition, the process is carried out for the different seismic wave types that are considered. For horizontal motion, these consist of inclined and vertically incident horizontally polarized shear waves and vertically polarized shear waves. For vertical motion, the wave types are inclined and vertically incident compression waves and inclined shear waves.

The result of each calculation is a response spectrum that reflects how the input motion response spectrum is modified by the site materials. For each deaggregation earthquake and combination of base case velocity profile, dynamic material property curves, and wave type, the mean of the resulting response spectra for the 60 randomized profiles and curves is taken. This mean computed spectrum for each deaggregation earthquake is then divided by the corresponding input deaggregation earthquake spectrum to produce a spectral amplification function. The spectral amplification function shows how the control motion response spectrum was modified by the site response as a function of structural frequency. It includes the effects of random variability in site material properties.

Then, for each combination of base case velocity profile, dynamic material property curves, and wave type, a weighted mean is computed of the spectral amplification functions for the three deaggregation earthquakes. Most weight is given to the mean deaggregation earthquake, with lower weight given to the low- and high-magnitude deaggregation earthquakes, which correspond to the 5th and 95th percentiles of the deaggregation magnitude distribution. The result of this step is a set of transfer functions for each of the two structural frequency ranges and

ground-motion components corresponding to each combination of base case velocity profile, dynamic property curves, and wave types. These weighted mean transfer functions include any earthquake magnitude- and amplitude-dependent effects on the dynamic response of site materials.

Next, for each combination of ground-motion component, velocity profile, dynamic material property curves, and wave type, the weighted mean transfer functions for the high and low structural frequency range are enveloped. The resulting transfer functions are applied to the envelope of the response spectra for the high and low structural frequency reference earthquakes. Alternatively, the transfer functions could be applied to the horizontal uniform hazard spectrum. By applying them to the envelope of the reference earthquake response spectra, the resulting ground motions are somewhat larger. This step results in a suite of response spectra that reflect the associated site response for each combination of base case velocity profile, dynamic material property curves, and wave type. The final site-response spectrum for each component of ground motion is then obtained by enveloping the combinations of base case velocity profile, dynamic material property curves, and wave type. The final location-specific response spectra thus reflect uncertainty in the base case velocity profile and dynamic material properties at the site. This process is illustrated in Figure 4-17 of the technical basis document.

In addition to seismic design response spectra, the site-response model is also used to develop strain-compatible soil properties for use in soil-structure interaction analyses. Properties were developed as a function of depth reflecting effects of the strains produced by the ground motion. Properties addressed were compressional-wave and shear-wave velocities, compressional-wave and shear-wave damping, and Poisson's ratio. Following guidance provided in "Seismic System Analysis" (NRC 1989a, Section 3.7.2), best-estimate and upper- and lower-bound soil columns were determined that are consistent with the site-response ground motions. These soil columns were determined on the basis of the multiple site-response computations that accommodate the uncertainty and random variability in site geotechnical properties. The best-estimate soil column is taken as the mean of the results and the lower- and upper-bound columns at the plus or minus1 standard deviation levels.

B.4.6 Seismic Design Time Histories

The final step in producing location-specific ground motions was the development of seismic design time histories based on the location-specific seismic input spectra. To develop time histories that will be used in design analyses, a spectral-matching approach was used. Each set of time histories consists of two horizontal component records and one vertical component record. Acceleration, velocity, and displacement records were produced. For a given mean annual exceedance probability and location of interest, one or more sets of time histories may be developed.

The time histories are based on actual recordings of strong ground motion from earthquakes in the western United States and around the world (McGuire et al. 2001, Appendix B). The original recordings are modified to reflect the results of the site-response analyses for a location of interest. Recordings for use are selected to represent those earthquakes (magnitudes and distances) that dominate the seismic hazard at a given annual probability of exceedance. By basing the time histories on actual earthquake recordings and choosing records consistent with

the seismic hazard, the resulting time histories will exhibit realistic phase characteristics and durations.

The spectral-matching approach involves developing time histories whose response spectra closely match target response spectra determined through site-response analyses (see Figure 4-18). Matching can be done either for individual records or, if multiple sets of time histories are involved, done so that the mean of the response spectra matches the target spectrum, but individual spectra do not. Matching is carried out in general accordance with the recommendations of McGuire et al. (2001, Section 5). However, recommendations to compare time domain characteristics (e.g., duration, the ratio of peak ground velocity to peak ground acceleration) of developed time histories to observed cataloged values for western U.S. conditions are inappropriate for Yucca Mountain because the Yucca Mountain site conditions differ from those for the cataloged events. Also, for the waste emplacement level, the motions are not expected to be similar to the free-field motions documented by McGuire et al. (2001).

The recommendations of McGuire et al (2001, Section 5) suggest modifications to the guidance for nuclear power plants (NRC 1989b). *Standard Review Plan for the Review of Safety Analysis Reports for Nuclear Power Plants, LWR Edition, July 1987* (NRC 1989b) incorporates specific guidance to consider the minimum power spectral density of ground-motion records input to building, component, and soil models. This guidance prevents the development of time histories with response spectra that envelope the design spectra across a given frequency range, even though the power spectral density (or, equivalently, the Fourier amplitude spectrum) of the input ground motion could possess low levels (gaps) within the same frequency range. For such a case, the computed system response may be underpredicted if, for example, the soil-structure interaction frequencies fall within those gaps. Because of the ambiguities in the definition of a power spectral density, as well as the effort involved in developing a minimum power spectral density requirement for an arbitrary target response spectrum, the recommended revised criteria of McGuire et al. (2001, Section 5) eliminate the need for a separate power spectral density check. They impose, instead, a minimum and maximum matching criteria for the target 5%–damped response spectrum. The intent of the more stringent matching guidance is to ensure that the developed ground motion does not have any significant gaps in frequency content. These revised criteria satisfy the general intent of the guidance in *Standard Review Plan for the Review of Safety Analysis Reports for Nuclear Power Plants, LWR Edition, July 1987* (NRC 1989b), which is currently defined in detail only for the spectral shape embodied by the Regulatory Guide 1.60, *Design Response Spectra for Seismic Design of Nuclear Power Plants* (1973) spectrum.

More detail on the approach to developing seismic design time histories is provided in *Development of Earthquake Ground Motion Input for Preclosure Seismic Design and Postclosure Performance Assessment of a Geologic Repository at Yucca Mountain, NV* (BSC 2004, Section 6.3.2).

B.4.7 Implementation of the Approach to Develop Seismic Design Input

This section presents an example of implementing the overall approach to developing ground-motion design inputs, including use of the random-vibration-theory-based equivalent-linear site-response model. The results include uncertainty and random variability in

the reference (control) location ground-motion hazard results, as well as in the site response. Results are presented for a mean annual probability of exceedance of 5×10^{-4} at the waste emplacement level and for the surface facilities area.

Waste Emplacement Level–Site-specific design response spectra with a 5×10^{-4} mean annual probability of exceedance for the waste emplacement level are shown in Figure B-7. The peak ground acceleration for the horizontal component is 0.19 g and for the vertical component 0.16 g. More detail on effects of the different base case velocity profiles and dynamic material property curves can be found in *Development of Earthquake Ground Motion Input for Preclosure Seismic Design and Postclosure Performance Assessment of a Geologic Repository at Yucca Mountain, NV* (BSC 2004, Section 6.3.1.2).

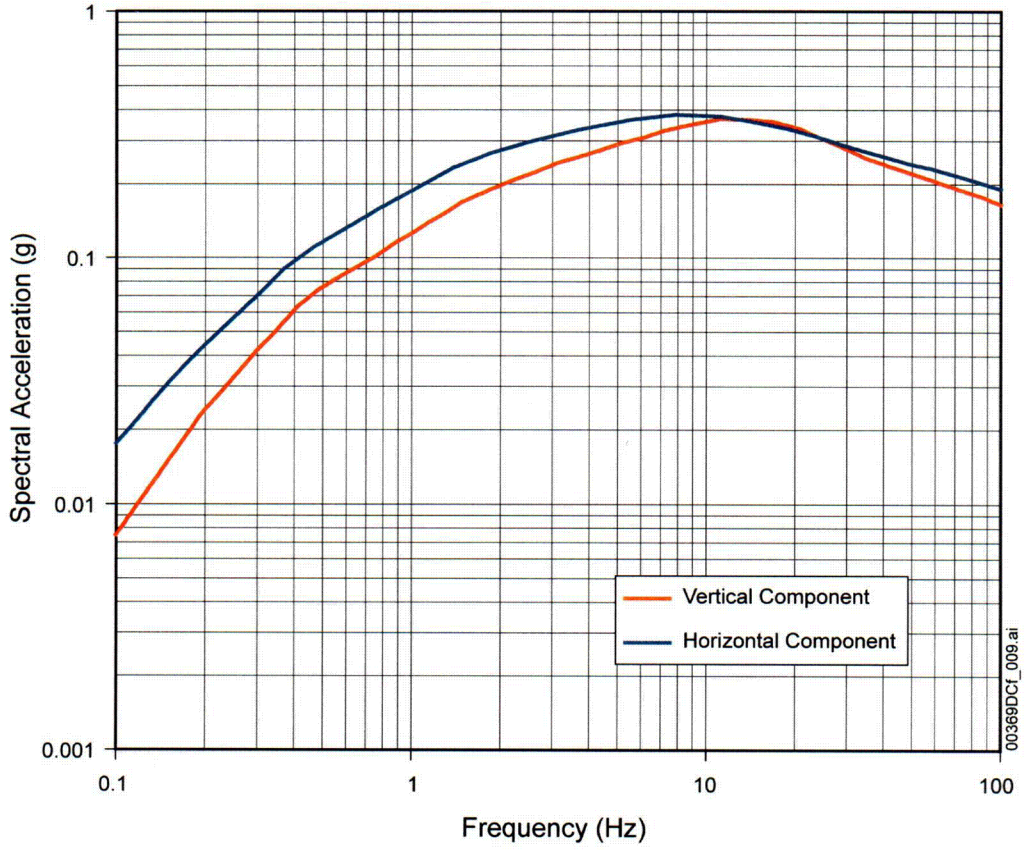

Source: BSC 2004, Figures 6.3-5 and 6.3-6.

Figure B-7. Seismic Design Response Spectra with a Mean Annual Probability of Exceedance of 5×10^{-4} for the Waste Emplacement Level

C40

Time histories for the waste emplacement level with a mean annual probability of exceedance of 5×10^{-4} were developed using the spectral-matching approach. One three-component set of time histories was developed (Figure B-8). The input strong ground-motion records were from the 1994 Northridge earthquake (magnitude 6.7), Duarte-Mel Canyon Rd. Station (McGuire et al. 2001, Appendix B). These records were recorded at a rock site about 52 km from the earthquake. They were selected based on the deaggregation of the control location ground-motion hazard. For this exceedance level, the hazard is dominated by a magnitude 7.0 earthquake at 51 km for the 1 to 2 Hz structural frequency range and by a magnitude 6.3 earthquake at 5 km for the 5 to 10 Hz range. Following guidance by McGuire et al. (2001, Section 5), the input records were chosen to more closely match the dominant earthquake for the low-frequency range to obtain time histories with longer duration.

Surface Facilities Area–Site-specific design response spectra (5% damping) with a 5×10^{-4} mean annual probability of exceedance for the surface facilities area are shown in Figure B-9. The peak ground acceleration for the horizontal component is 0.58 g and for the vertical component is 0.52 g. Velocity profiles used in developing these seismic inputs relied on data from boreholes and spectral analysis of surface waves surveys located southwest of the Exile Hill Fault (BSC 2004, Section 6.2.3.4).

Time histories for the surface facilities area with an annual probability of exceedance of 5×10^{-4} were developed using the spectral-matching approach. Five three-component sets of time histories were developed; an example is shown in Figure B-10. Associated strain-compatible soil columns were also developed from the site-response analysis for the surface facilities area. Strain-compatible soil properties generated include V_S and damping, V_P and damping, and Poisson's ratio. For each of these properties, the median and $\pm 1\sigma$ (16th and 84th percentile) iterated values are determined. These columns are to be used to define the range of site properties that need to be considered in soil-structure interaction analyses. Results are documented in DTN: MO0403SPWHB5E4.005.

Further description of the development of the seismic input data for the surface facilities area is found in *Development of Earthquake Ground Motion Input for Preclosure Seismic Design and Postclosure Performance Assessment of a Geologic Repository at Yucca Mountain, NV* (BSC 2004, Section 6.3.2.3.1). That report provides more detail on implementation of the approach but addresses an earlier case including 15 ft of engineered fill at the top of the soil column. The report is currently being updated to address the current case for the surface facilities area, which does not include use of engineered fill. While the details of the soil column will be updated in the revised report, the approach described has not changed.

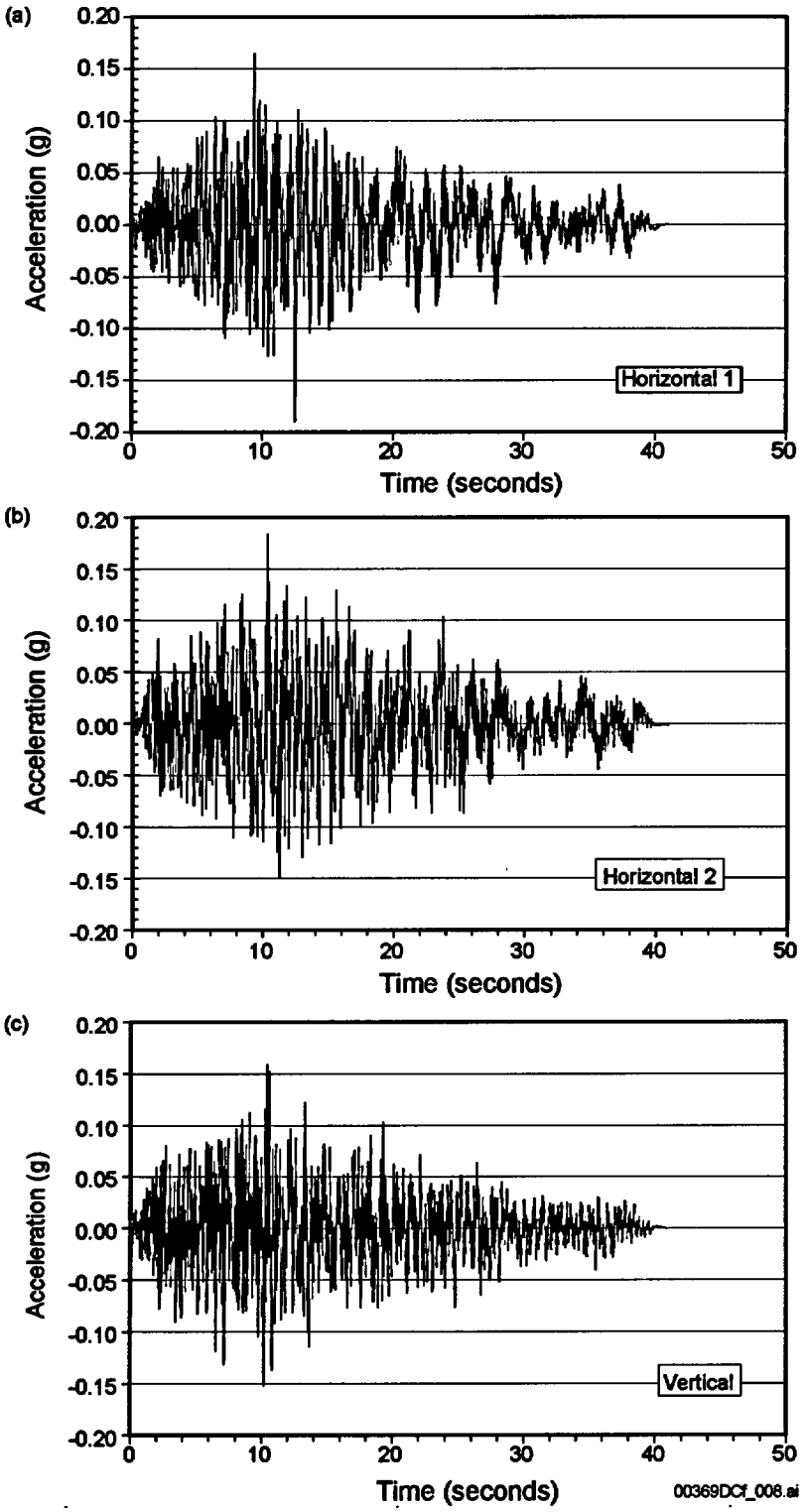

Source: BSC 2004, Figures III-1 through III-3.

Figure B-8. Time Histories with a Mean Annual Probability of Exceedance of 5×10^{-4} for the Waste Emplacement Level

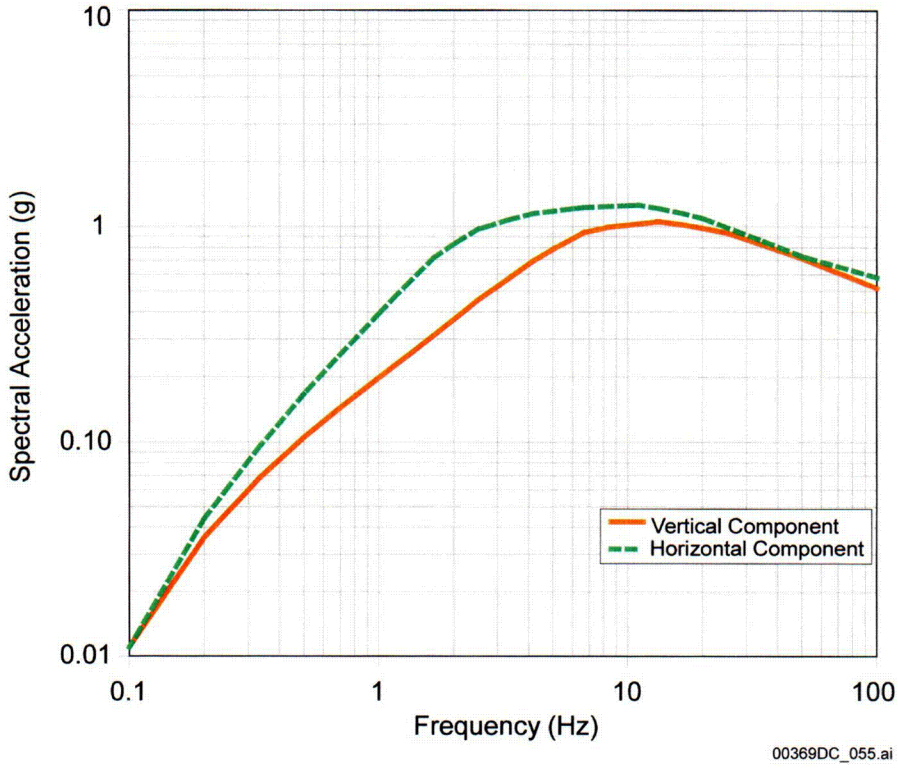

Source: DTN: MO0402SDSTMHIS.004.

Figure B-9. Seismic Design Response Spectra with a Mean Annual Probability of Exceedance of 5×10^{-4} for the Surface Facility Area

C41

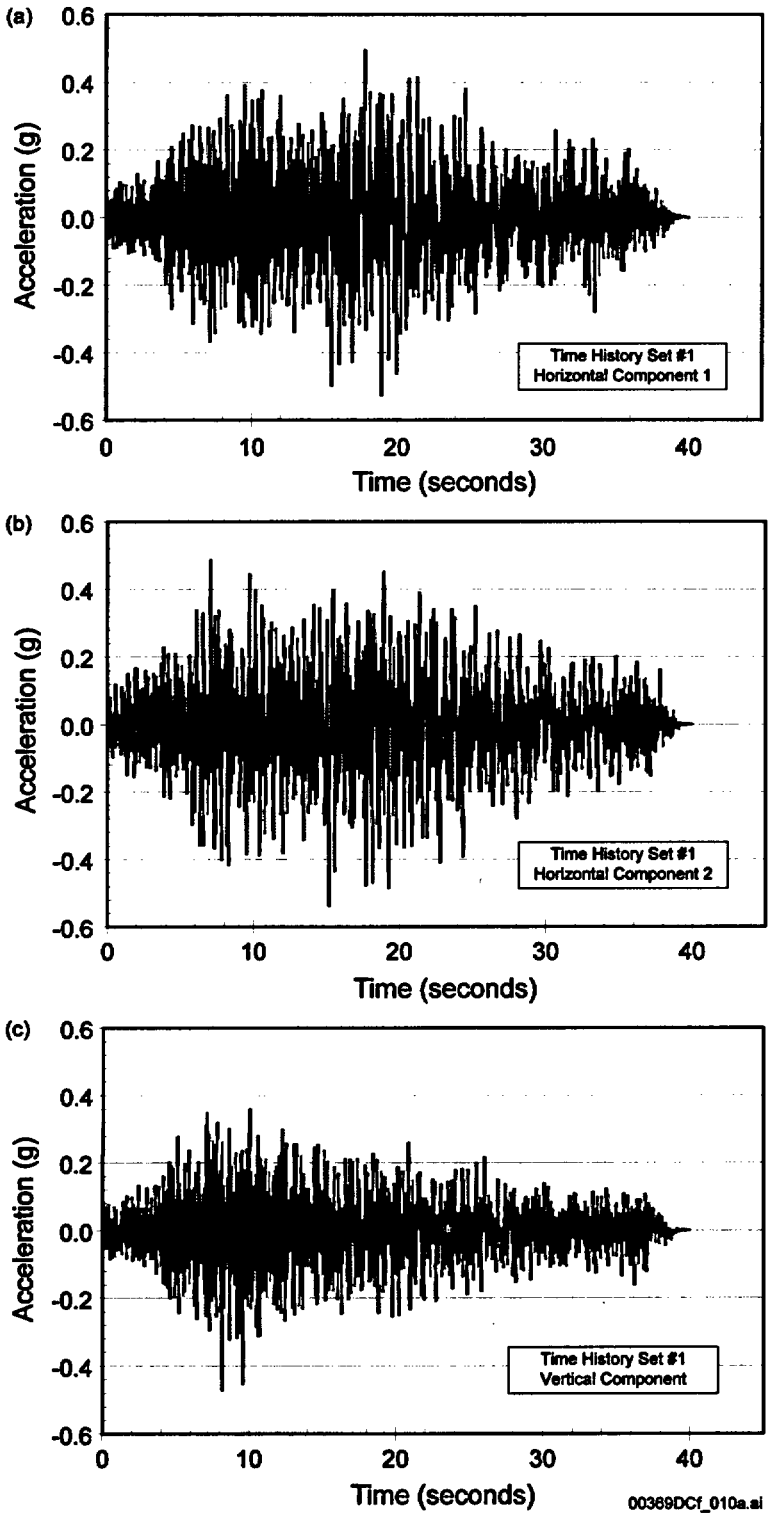

Source: DTN: MO0402SDSTMHIS.004.

Figure B-10. Time Histories with a Mean Annual Probability of Exceedance of 5×10^{-4} for the Surface Facilities Area

B.4.8 Overview of Seismic Inputs for Postclosure Analyses

The overall approach to developing seismic inputs for postclosure analyses is similar to that used to develop inputs for preclosure design analyses. The main difference is that, rather than develop time histories that are spectrally matched to target response spectra, the time histories developed for postclosure analyses are scaled to peak ground velocity. This approach is taken because damage to underground structures has been correlated with peak ground velocity (e.g., McGarr 1984, pp. 204 to 207). Thus, for postclosure purposes, the site-response analyses are used to determine location-specific peak ground velocity in addition to response spectra (Figure B-11).

In implementing the site-response approach for peak ground velocity, the method for incorporating uncertainty and randomness in site material properties remains the same. The site-response analysis is used to determine location-specific peak ground velocity for the range of combinations of velocity profiles and dynamic material property curves. However, rather than determining just a spectral amplification function from each computation, a peak ground velocity scaling factor is also determined. The peak ground velocity scaling factor is obtained by normalizing the location-specific peak ground velocity to the peak ground velocity from the PSHA for the given mean annual probability of exceedance (i.e., to the peak ground velocity for the control location). The peak ground velocity scaling factors are averaged and enveloped over in a similar fashion to that used for the transfer functions (Figure B-11).

To develop time histories in the peak-ground-velocity scaling approach, the strong motion recordings from past earthquakes are scaled so that their peak ground velocity matches the peak ground velocity determined in the site-response analysis for the waste emplacement level. The records may be scaled so that both horizontal components match the target horizontal peak ground velocity, and the vertical component matches the target vertical peak ground velocity. Alternatively, one horizontal component may be scaled to the target horizontal peak ground velocity and the scaling of the other components done in a manner to maintain the intercomponent variability of the original recordings. Both of these methods have been used at Yucca Mountain.

For postclosure analyses using time history inputs, the goal is not to ensure that design acceptance criteria are met but rather to determine how the designed structures, systems, and components that will remain after the repository is closed perform under earthquake loads that are significantly beyond their design basis. In addition to determining the consequences of these low-probability ground motions, another goal is to evaluate the variability in the consequences. Because much of the variability in consequences will be driven by random variability in the ground motion, the time histories for postclosure analyses are developed to capture and represent that random variability. For each annual exceedance probability of interest, 17 sets of time histories are developed. The recordings used as a basis for the time histories are selected to have a range of magnitudes and distances that corresponds to the magnitudes and distances of earthquakes contributing to the seismic hazard at the given annual exceedance probability. This ensures the ensuing analyses will take into account an appropriate range of response spectral shapes, amplitudes, and durations.

In analyses supporting evaluation of postclosure performance, typically 15 time histories are used. Seventeen sets of time histories are developed to provide two extra sets that can be used if

one of the first 15 sets is found to be inappropriate. For example, in one case, time history set 15 exhibits an anomalous low vertical response spectrum at high frequencies, and thus, it is replaced by set 16.

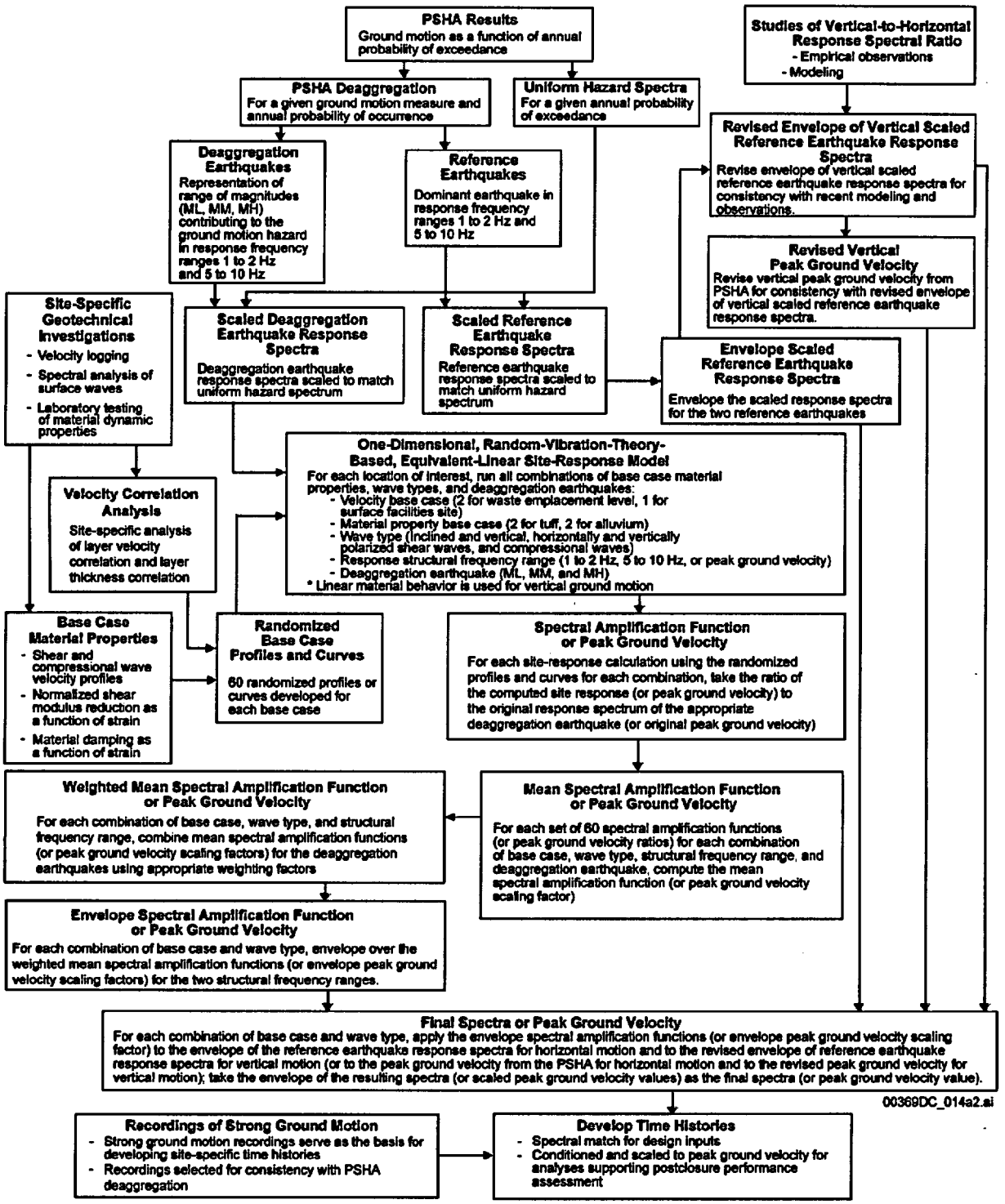

Figure B-11. Development of Location-Specific Seismic Inputs for Preclosure Design and Postclosure Performance Assessment Analyses

A variation of the peak-ground-velocity scaling approach is to spectrally condition the original strong ground-motion records before using them to develop time histories. Spectral conditioning modifies the original strong motion records so that their response spectra reflect, to a greater degree, the site conditions at Yucca Mountain. Conditioning can be done with respect to the PSHA reference rock outcrop conditions (the control location conditions) or to the waste emplacement level conditions that include the site response. Conditioning is accomplished using a weak spectral match. A strong spectral match is not desired in this case because it would tend to reduce the random variability of the original recordings.

Time histories to support postclosure analyses have been developed for mean annual probabilities of exceedance of 10^{-5}, 10^{-6}, and 10^{-7}. In addition, time histories developed for a mean annual probability of exceedance of 5×10^{-4} (for preclosure analyses) have also been used to support the evaluation of potential postclosure seismic effects. These time histories are used to evaluate the consequences of seismic ground motions having a greater than 1 in 10,000 chance of occurring during the 10,000-year postclosure regulatory period (BSC 2003a). Example time histories for postclosure analyses are presented in Section 4.2 of the technical basis document. A more detailed description of time histories with mean annual probabilities of exceedance of 10^{-6} and 10^{-7} can be found in *Development of Earthquake Ground Motion Input for Preclosure Seismic Design and Postclosure Performance Assessment of a Geologic Repository at Yucca Mountain, NV* (BSC 2004, Section 6.3.2).

Use of time histories to evaluate the potential consequences during the postclosure period of seismic events with an annual probability of occurrence greater than 10^{-8} is described in *Drift Degradation Analysis* (BSC 2003b), *Structural Calculations of Waste Package Exposed to Vibratory Ground Motion* (BSC 2003c), *Structural Calculations of Drip Shield Exposed to Vibratory Ground Motion* (BSC 2003d), and *Seismic Consequence Abstraction* (BSC 2003a). *Seismic Consequence Abstraction* (BSC 2003a) also addresses the effects of fault displacement during the postclosure period.

B.5 REFERENCES

B.5.1 Documents Cited

Brocoum, S. 2000. "Annotated Outline for Topical Report, 'Preclosure Seismic Design Inputs for a Geologic Repository at Yucca Mountain.'" Letter from S. Brocoum (DOE/YMSCO) to C.W. Reamer (NRC), October 5, 2000, OLRC:JTS-0013, with enclosure. ACC: MOL.20001101.0194.

Brocoum, S. 2001. Transmittal of Report Addressing Key Technical Issues (KTI) Structural Deformation and Seismicity (SDS). Letter from S. Brocoum (DOE/YMSCO) to C.W. Reamer (NRC), April 25, 2001, OL&RC:TCG-1098, with enclosures. ACC: MOL.20010619.0345.

BSC (Bechtel SAIC Company) 2002. *Geotechnical Data for a Potential Waste Handling Building and for Ground Motion Analyses for the Yucca Mountain Site Characterization Project.* ANL-MGR-GE-000003 REV 00. Las Vegas, Nevada: Bechtel SAIC Company. ACC: MOL.20021004.0078.

BSC 2003a. *Seismic Consequence Abstraction.* MDL-WIS-PA-000003 REV 00. Las Vegas, Nevada: Bechtel SAIC Company. ACC: DOC.20030818.0006.

BSC 2003b. *Drift Degradation Analysis.* ANL-EBS-MD-000027 REV 02. Las Vegas, Nevada: Bechtel SAIC Company. ACC: DOC.20030709.0003.

BSC 2003c. *Structural Calculations of Waste Package Exposed to Vibratory Ground Motion.* 000-00C-EBS0-00300-000-00B. Las Vegas, Nevada: Bechtel SAIC Company. ACC: ENG.20030520.0003.

BSC 2003d. *Structural Calculations of Drip Shield Exposed to Vibratory Ground Motion.* 000-00C-PEC0-00100-000-00A. Las Vegas, Nevada: Bechtel SAIC Company. ACC: ENG.20030618.0009.

BSC 2004. *Development of Earthquake Ground Motion Input for Preclosure Seismic Design and Postclosure Performance Assessment of a Geologic Repository at Yucca Mountain, NV.* MDL-MGR-GS-000003 REV 00, with errata. Las Vegas, Nevada: Bechtel SAIC Company. ACC: DOC.20031201.0001, DOC.20040401.0004.

CRWMS M&O (Civilian Radioactive Waste Management System Management and Operating Contractor) 2000a. *Features, Events, and Processes: Disruptive Events.* ANL-WIS-MD-000005 REV 00 ICN 1. Las Vegas, Nevada: CRWMS M&O. ACC: MOL.20001218.0007.

CRWMS M&O 2000b. *Characterize Framework for Seismicity and Structural Deformation at Yucca Mountain, Nevada.* ANL-CRW-GS-000003 REV 00. Las Vegas, Nevada: CRWMS M&O. ACC: MOL.20000510.0175.

EPRI (Electric Power Research Institute) 1993. *Appendices for Ground Motion Estimation.* Volume 2 of *Guidelines for Determining Design Basis Ground Motions.* EPRI TR-102293. Palo Alto, California: Electric Power Research Institute. TIC: 226496.

Haskell, N.A. 1960. "Crustal Reflection of Plane SH Waves." *Journal of Geophysical Research, 65,* (12), 4147–4150. Washington, D.C.: American Geophysical Union. TIC: 222421.

Kotra, J.P.; Lee, M.P.; Eisenberg, N.A.; and DeWispelare, A.R. 1996. *Branch Technical Position on the Use of Expert Elicitation in the High-Level Radioactive Waste Program.* NUREG-1563. Washington, D.C.: U.S. Nuclear Regulatory Commission. TIC: 226832.

McGarr, A. 1984. "Some Applications of Seismic Source Mechanism Studies to Assessing Underground Hazard." *Proceedings of the 1st International Congress on Rockbursts and Seismicity in Mines, Johannesburg, 1982.* Gay, N.C. and Wainwright, E.H., eds. Pages 199–208. Johannesburg, South Africa: South African Institute of Mining and Metallurgy. TIC: 254652.

McGuire, R.K. 1995. "Probabilistic Seismic Hazard Analysis and Design Earthquakes: Closing the Loop." *Bulletin of the Seismological Society of America, 85,* (5), 1275–1284. El Cerrito, California: Seismological Society of America. TIC: 232947.

McGuire, R.K.; Silva, W.J.; and Costantino, C.J. 2001. *Technical Basis for Revision of Regulatory Guidance on Design Ground Motions: Hazard- and Risk-Consistent Ground Motion Spectra Guidelines.* NUREG/CR-6728. Washington, D.C.: U.S. Nuclear Regulatory Commission. TIC: 251294.

Milner, R. 1994. Transmittal of Annotated Outline for DOE Topical Report, "Seismic Design Methodology for a Geologic Repository at Yucca Mountain." Letter from R.A. Milner (DOE) to J.J. Holonich (NRC), August 22, 1994. ACC: HQO.19940823.0017.

NRC (U.S. Nuclear Regulatory Commission) 1989a. "Seismic System Analysis." Revision 2 of Section 3.7.2 of *Standard Review Plan for the Review of Safety Analysis Reports for Nuclear Power Plants, LWR Edition, July 1987.* NUREG-0800. Washington, D.C.: U.S. Nuclear Regulatory Commission. ACC: MOL.20030910.0151.

NRC 1989b. "Seismic Design Parameters." Revision 2 of Section 3.7.1 of *Standard Review Plan for the Review of Safety Analysis Reports for Nuclear Power Plants, LWR Edition, July 1987.* NUREG-0800. Washington, D.C.: U.S. Nuclear Regulatory Commission. ACC: MOL.20030910.0150.

Pacific Engineering and Analysis 2002a. *Software Code: RASCALS.* V5.4. PC, DOS 6.22. 10389-5.4-00.

Pacific Engineering and Analysis 2002b. *Software Code: RASCALP.* V2.02. PC, DOS 6.22. 10388-2.02-00.

Reamer, C.W. 2000. "Annotated Outline for Topical Report, 'Preclosure Seismic Design Inputs for a Geologic Repository at Yucca Mountain.'" Letter from C.W. Reamer (NRC) to S.J. Brocoum (DOE/YMSCO), December 15, 2000. ACC: HQO.20010508.0025.

Reamer, C.W. 2002. "Review of Documents Pertaining to Key Technical Issue Agreements." Letter from C.W. Reamer (NRC) to S. Brocoum (DOE/YMSCO), February 8, 2002, 0222021603, with enclosure. ACC: MOL.20020607.0089.

Reamer, C.W. and Williams, D.R. 2001. Summary Highlights of NRC/DOE Technical Exchange and Management Meeting on Repository Design and Thermal-Mechanical Effects. Meeting held February 6-8, 2001, Las Vegas, Nevada. Washington, D.C.: U.S. Nuclear Regulatory Commission. ACC: MOL.20010307.0511 through MOL.20010307.0521.

Schlueter, J. 2000. "U.S. Nuclear Regulatory Commission/U.S. Department of Energy Technical Exchange and Management Meeting on Structural Deformation and Seismicity (October 11-12, 2000)." Letter from J. Schlueter (NRC) to S. Brocoum (DOE/YMSCO), October 27, 2000, with enclosure. ACC: MOL.20010730.0232.

Schnabel, P.D.; Lysmer, J.; and Seed, H.B. 1972. *SHAKE: A Computer Program for Earthquake Response.* EERC 72-12. Berkeley, California: Earthquake Engineering Research Center, University of California. TIC: 241102.

Seed, H.B. and Idriss, I.M. 1969. "Influence of Soil Conditions on Ground Motions during Earthquakes." *Journal of the Soil Mechanics and Foundations Division, 95,* (SM1), 99–137. New York, New York: American Society of Civil Engineers. TIC: 254823.

Silva, W.J. 1976. "Body Waves in a Layered Anelastic Solid." *Bulletin of the Seismological Society of America, 66,* (5), 1539–1554. El Cerrito, California: Seismological Society of America. TIC: 241277.

Silva, W.J.; Abrahamson, N.; Toro, G.; and Costantino, C. 1996. *Description and Validation of the Stochastic Ground Motion Model.* PE&A 94PJ20. El Cerrito, California: Pacific Engineering and Analysis. TIC: 245288.

Silva, W.; Stark, C.; Chiou, S.J.; Green, R.; Stepp, J.C.; Schneider, J.; and Anderson, D. 1990. "Non-linear Soil Models Based Upon Observations of Strong Ground Motions." *Seismological Research Letters, 61,* (1), 13. Abstract 11B-4. El Cerrito, California: Seismological Society of America, Eastern Section. TIC: 254667.

Wong, I.G. and Silva, W. 2003. *Development of Seismic Design Ground Motion Inputs.* Scientific Notebook SN-M&O-SCI-037-V3. ACC: MOL.20031027.0158; MOL.20031027.0159; MOL.20031027.0160.

YMP (Yucca Mountain Site Characterization Project) 1997a. *Methodology to Assess Fault Displacement and Vibratory Ground Motion Hazards at Yucca Mountain.* Topical Report YMP/TR-002-NP, Rev. 1. Las Vegas, Nevada: Yucca Mountain Site Characterization Office. ACC: MOL.19971016.0777.

YMP 1997b. *Preclosure Seismic Design Methodology for a Geologic Repository at Yucca Mountain.* Topical Report YMP/TR-003-NP, Rev. 2. Las Vegas, Nevada: Yucca Mountain Site Characterization Office. ACC: MOL.19971009.0412.

B.5.2 Codes, Standards, and Regulations

10 CFR Part 63. Energy: Disposal of High-Level Radioactive Wastes in a Geologic Repository at Yucca Mountain, Nevada. Readily available.

Regulatory Guide 1.60, Rev. 1. 1973. *Design Response Spectra for Seismic Design of Nuclear Power Plants.* Washington, D.C.: U.S. Atomic Energy Commission. TIC: 232770.

Regulatory Guide 1.165. 1997. *Identification and Characterization of Seismic Sources and Determination of Safe Shutdown Earthquake Ground Motion.* Washington, D.C.: U.S. Nuclear Regulatory Commission. Readily available.

B.5.3 Data, Listed by Data Tracking Number

MO0402SDSTMHIS.004. Seismic Design Spectra and Time Histories for the Surface Facilities Area (Point D/E) at 5E-4 Annual Exceedance Frequency. Submittal date: 02/09/04.

MO0403SPWHB5E4.005. Strain Compatible Soil Properties for the Surface Facilities Area (Point #) at 5E-4 Annual Exceedance Frequency. Submittal date: 03/15/04.

APPENDIX C

EXPERT ELICITATION OF GROUND-MOTION INTERPRETATIONS FOR THE YUCCA MOUNTAIN PROBABILISTIC SEISMIC HAZARD ANALYSIS: TREATMENT OF UNCERTAINTY AND FEEDBACK (RESPONSE TO SDS 2.01 AIN-1)

Note Regarding the Status of Supporting Technical Information

This document was prepared using the most current information available at the time of its development. This Technical Basis Document and its appendices providing Key Technical Issue Agreement responses that were prepared using preliminary or draft information reflect the status of the Yucca Mountain Project's scientific and design bases at the time of submittal. In some cases this involved the use of draft Analysis and Model Reports (AMRs) and other draft references whose contents may change with time. Information that evolves through subsequent revisions of the AMRs and other references will be reflected in the License Application (LA) as the approved analyses of record at the time of LA submittal. Consequently, the Project will not routinely update either this Technical Basis Document or its Key Technical Issue Agreement appendices to reflect changes in the supporting references prior to submittal of the LA.

APPENDIX C

EXPERT ELICITATION OF GROUND-MOTION INTERPRETATIONS FOR THE YUCCA MOUNTAIN PROBABILISTIC SEISMIC HAZARD ANALYSIS: TREATMENT OF UNCERTAINTY AND FEEDBACK (RESPONSE TO SDS 2.01 AIN-1)

This appendix provides a response for Key Technical Issue (KTI) agreement Structural Deformation and Seismicity (SDS) 2.01 additional information need (AIN)-1. This KTI agreement provides for additional documentation of the ground-motion expert elicitation process that was implemented in developing ground-motion inputs for the Yucca Mountain probabilistic seismic hazards analysis (PSHA).

C.1 KEY TECHNICAL ISSUE AGREEMENT

C.1.1 SDS 2.01 AIN-1

Agreement SDS 2.01 was reached during the U.S. Nuclear Regulatory Commission (NRC)/U.S. Department of Energy (DOE) Technical Exchange and Management Meeting on SDS held October 11 to 12, 2000, in Las Vegas, Nevada. SDS KTI subissues 1, 2, 3, and 4 were discussed at the meeting (Schlueter 2000).

The wording of the agreement is as follows:

SDS 2.01

> Regarding ground motion, provide documentation, or point the NRC to the documentation on the expert elicitation process, regarding the feedback to the subject matter experts following the elicitation of their respective judgements. DOE will provide documentation demonstrating the adequacy of the elicitation feedback process by December 2000.

After the technical exchange, DOE provided additional information to the NRC from two seismic workshops (Whitney 1997a, 1997b) as enclosures to a letter from Brocoum (2000). The NRC reviewed this information and considered the information as not sufficient for a potential licensing review and identified an AIN (Reamer 2001):

SDS 2.01 AIN-1

> DOE needs to provide clear documentation of the expert elicitation process and its implementation, specifically with regard to the feedback process associated with the experts' interpretation, evaluation, and validation of their ground motion models. Documentation of the experts' reasoning is as important as the elicitation process. Therefore, the documentation should include: the experts' rationale for their interpretations, evaluations and validations based on feedback; rationale for the experts' understanding and acknowledgment of how their results would be used by DOE to develop seismic design input values for pre-closure and post-closure analyses.

Documentation should be consistent with the guidelines in NUREG-1563 (e.g., section on post-elicitation feedback, p. 28).

In light of this AIN and as a follow-up to the NRC review, an onsite representative meeting was held on August 27 and 28, 2002, to examine file material which fully documents the ground-motion elicitation process that was implemented.

C.1.2 Related Key Technical Issues

Agreement SDS 2.01 AIN-1 is related to comment J-27 (NRC 2002, p. B-4) of TSPAI 2.02. Comment J-27 expressed the NRC concern that, for the total system performance assessment for the site recommendation (TSPA-SR), the screening evaluation for the feature, event, and process (FEP) 1.2.03.01.00 (Seismic Activity) depended on results of the PSHA for Yucca Mountain. Providing the additional documentation to resolve the concern about the PSHA ground-motion expert elicitation expressed in agreement SDS 2.01 AIN-1 will also address comment J-27 of TSPAI 2.02.

C.2 RELEVANCE TO REPOSITORY PERFORMANCE

Results of the PSHA, which used the Senior Seismic Hazard Analysis Committee Level-4 formal expert elicitation process, form the basis for development of seismic inputs supporting seismic design and performance assessment for the seismic scenario.

For the preclosure phase of repository operation, seismic inputs are used to support design and analyses of systems, structures, and components that are important to safety. The seismic inputs are developed to be consistent with target levels of seismic hazard defined by mean annual probabilities of exceedance. In combination with the conservatism inherent in the design procedures, acceptance criteria, codes, and standards, the preclosure seismic design inputs provide reasonable assurance that preclosure performance objectives will be met. Ultimately, evaluations as part of the preclosure safety analysis will demonstrate compliance to the dose standards.

For the postclosure period, seismic inputs are used in analyses supporting the seismic scenario class of the total system performance assessment. Seismic inputs with mean annual probabilities of exceedance greater than 10^{-8} are used to evaluate seismic effects on the engineered barrier system. Effects of vibratory ground motion, seismic-induced rockfall, and fault displacement are evaluated.

C.3 RESPONSE

The expert elicitation process, including treatment of uncertainty and feedback, was properly implemented following the Senior Seismic Hazard Analysis Committee Level-4 expert elicitation guidance (Budnitz et al. 1997) as part of the ground-motion assessment component of the PSHA for Yucca Mountain. The elicitation also generally followed guidance in NUREG-1563 (Kotra et al. 1996), except that interim interpretations were not required to be documented by the experts to mitigate the possibility of anchoring. Implementation was carried out in accordance with the Yucca Mountain Project–U.S. Geological Survey quality management procedure YMP-USGS-QMP-3.16, *Scientific Expert Elicitation*. Experts were trained in how to

properly assess uncertainties prior to the start of the process. Methods for properly assessing uncertainties were also reviewed, as necessary, during elicitation interviews, workshops, and working meetings.

As part of the elicitation process, experts were provided appropriate feedback on their interpretations through a workshop, in elicitation meetings, and through exchanges with the Ground Motion Facilitation Team, which provided the technical leadership to facilitate interactions and elicit interpretations by the experts. The experts were provided documentation of their own ground-motion assessments and those of the other experts for comparison and verification that assessments were as they intended. Feedback included information on median values, uncertainties, and variability. Initial feedback also included example seismic hazard results based on the preliminary seismic source and ground-motion interpretations. Three formal feedback cycles were implemented. Experts were allowed to make revisions as they considered appropriate to express their assessments of ground-motion estimation uncertainty until their interpretations were finalized.

Experts participating in the PSHA for Yucca Mountain were required to document the rationale for their final interpretations resulting from the elicitation process. To avoid the likelihood that experts would anchor themselves to their preliminary interpretations, documentation of the rationale for preliminary interpretations and for changes as a result of the feedback process were not required. Instead, ground-motion data packages (Abrahamson and Becker 1997a to 1997v) document the changes made during the elicitation process. These data packages fully document the elicitation and assessment process. The final interpretations are documented in *Probabilistic Seismic Hazard Analyses for Fault Displacement and Vibratory Ground Motion at Yucca Mountain, Nevada* (CRWMS M&O 1998, Appendix F).

The information in this report is responsive to agreement SDS 2.01 made between DOE and NRC and the associated AIN (AIN-1). It is also responsive to agreement TSPAI 2.02, comment J-27. The report contains the information that DOE considers necessary for NRC review for closure of this agreement.

C.4 BASIS FOR THE RESPONSE

Agreement item SDS 2.01 and an associated AIN raise issues about the ground-motion expert elicitation component of the PSHA for Yucca Mountain. The issues pertain to the feedback process, the large range of interpreted ground motions and uncertainties, and documentation of the elicitation process. This section supplements documentation found in *Probabilistic Seismic Hazard Analyses for Fault Displacement and Vibratory Ground Motion at Yucca Mountain, Nevada* (CRWMS M&O 1998), *Characterize Framework for Seismicity and Structural Deformation at Yucca Mountain, Nevada* (CRWMS M&O 2000), workshop summaries (Hayes 1995; Whitney 1997a, 1997b; Parks 1998), and ground-motion data packages (Abrahamson and Becker 1997a to 1997y). It provides documentation that the experts were adequately prepared and that they received adequate feedback to their interpretations consistent with state-of-knowledge guidance, which seeks to document the unbiased uncertainty of the informed scientific community about ground-motion estimation. Documentation of the feedback process is described. Differences in the epistemic uncertainties of any given expert's interpretations

relative to those of the other ground-motion experts are the result of appropriate implementation of the expert elicitation process.

The PSHA for Yucca Mountain followed guidance provided by Budnitz et al. (1997) for a study level 4 PSHA. The Yucca Mountain PSHA is also generally in accord with the guidance given by Kotra et al. (1996), except that interim interpretations were not required to be documented by the experts to mitigate the possibility of anchoring. Implementation of the PSHA followed procedure YMP-USGS-QMP-3.16. The overall elicitation process consists of the following steps:

1. The experts' identification of processes, models, and parameters that require evaluation and the scope of data needed to perform the evaluations and assessments of uncertainty
2. An exchange among the experts of their evaluations of processes, alternative models, and model parameters and their preliminary interpretations
3. Elicitation and documentation of the experts' individual assessments
4. Working meetings in which the experts and the Facilitation Team together reviewed the experts' assessments and clarified elicitation issues
5. Feedback, including a formal feedback workshop to provide preliminary hazard results and demonstrate how the experts' assessments contribute to the hazard results
6. The experts' final documentation of their assessments
7. Calculation of hazard results using the experts' final assessments.

These steps were accomplished through a process that included three structured workshops, individual expert elicitation interviews, and two working meetings held to address topics identified at the workshops that required additional discussion and feedback. During the expert elicitation process, the experts revised their characterizations of the ground motion and its estimated uncertainty several times. These revisions are documented in a series of Yucca Mountain ground-motion data packages (Abrahamson and Becker 1997a to 1997v). A meeting held at the completion of the elicitation process closed the feedback process by providing the final hazard results and summarizing how they would be used in design and performance assessment analyses. Table C-1 summarizes the ground-motion expert elicitation activities.

Table C-1. Timeline of Ground-Motion Elicitation Activities

Date	Activity	Product Provided to Ground-Motion Experts
April 20–21, 1995	Data Needs Workshop	Workshop presentations and handouts (Hayes 1995). Data needs list (CRWMS M&O 1998, Table D-1)
January 9–10, 1997	Methods, Models, and Preliminary Interpretations Workshop	Workshop presentations and handouts (Whitney 1997a). Data Vol. 1 (2/97 with periodic updates): Data (Abrahamson and Becker 1997w)
February 11, 1997	Working Meeting 1	None
March 17–20, 1997	Expert Interviews	None
April 16–18, 1997	Feedback Workshop	Workshop presentations and handouts (Whitney 1997b).
May 7, 1997	Working Meeting 2	Data Vol. 2 (May 18, 1997): Proponent Models by Case, Spectra Plots (Abrahamson and Becker 1997y)
Mid-May to early June 1997	Revision 1 Input from Experts	Data Vol. 3 (June 5, 1997): Expert Point Estimates, Horizontal Component, Rev. 1 (Abrahamson and Becker 1997a)
		Data Vol. 4 (May 12, 1997): Expert Point Estimates, Vertical Component, Rev. 1 (Abrahamson and Becker 1997b)
		Data Vol. 5 (May 15, 1997): Expert Estimates by Case, Spectra Plots, Rev. 1 (Abrahamson and Becker 1997c)
		Data Vol. 6 (May 21 to May 29, 1997): Regression Models, Rev. 1: Vol. 6A: Anderson, Boore, Campbell (Abrahamson and Becker 1997d); Vol. 6B: McGarr, Silva, Somerville, Walck (Abrahamson and Becker 1997e)
		Data Vol. 1B (June 1997): Data (Abrahamson and Becker 1997x)
Late May to mid-June 1997	Revision 2 Input from Experts	Data Vol. 7 (June 10, 1997): Expert Point Estimates and Proponent Models, Horizontal, Rev. 2 (Abrahamson and Becker 1997f)
		Data Vol. 8 (June 7, 1997): Expert Point Estimates and Proponent Models, Vertical, Rev. 2 (Abrahamson and Becker 1997g)
		Data Vol. 9 (June 4, 1997): Expert Estimates by Case, Spectra Plots, Rev. 2 (Abrahamson and Becker 1997h)
		Data Vol. 10 (May 31, 1997 to June 11, 1997): Regression Models: Anderson (Vol. 10A) (Abrahamson and Becker 1997i) Boore (Vol. 10B) (Abrahamson and Becker 1997j) Campbell (Did not develop Rev. 2 inputs) McGarr (Vol. 10D) (Abrahamson and Becker 1997k) Silva (Vol. 10E) (Abrahamson and Becker 1997l) Somerville (Vol. 10F) (Abrahamson and Becker 1997m) Walck (Vol. 10G) (Abrahamson and Becker 1997n)

Table C-1. Timeline of Ground-Motion Elicitation Activities (Continued)

Date	Activity	Product Provided to Ground-Motion Experts
July 1997	Revision 3 (Final) Input from Experts	Regression Models, Rev. 3: Anderson (Vol. 11A) (Abrahamson and Becker 1997o) Boore (Vol. 11B) (Abrahamson and Becker 1997p) Campbell (Vol. 11C) (Abrahamson and Becker 1997q) McGarr (Vol. 11D) (Abrahamson and Becker 1997r) Silva (Vol. 11E) (Abrahamson and Becker 1997s) Somerville (Vol. 11F) (Abrahamson and Becker 1997t) Walck (Vol. 11G) (Abrahamson and Becker 1997u)
		Data Vol. 12 (July 1997): Expert Estimates by Case, Spectra Plots, Rev. 3 (Abrahamson and Becker 1997v)
April 6, 1998	Final Results Meeting–Summary of Probabilistic Seismic Hazard Analysis	Meeting presentations and handouts (Parks 1998).

The expert's ground-motion characterizations consisted of a suite of point estimates for the spectral acceleration and peak velocity of the horizontal and vertical components of motion for specified earthquake magnitudes and source-site geometries (distances). These estimates included the familiar median ground motion, μ, and aleatory variability, σ. The associated epistemic uncertainties of these quantities (σ_μ, σ_σ) were also estimated by the experts. The experts' point estimates were the basis for developing attenuation relations. The regression analyses were performed by the Ground Motion Facilitation Team and reviewed by the experts to ensure that their assessments were properly captured.

To address the concern expressed by the NRC about the "large range of differences among experts' interpretations of ground motion effects" (Reamer 2001), Sections C.4.1 and C.4.2 summarize activities carried out as part of the expert elicitation process that deal with characterizing ground-motion uncertainty and with the feedback component of the process. Section C.4.3 addresses documentation of the process.

C.4.1 Characterizing Ground-Motion Uncertainty

As part of the ground-motion expert elicitation process, the experts were provided appropriate training and information to develop their interpretations of ground motion and uncertainty. To ensure that the experts were knowledgeable about the requirements and processes for assessing aleatory variability and epistemic uncertainty, these requirements and processes were emphasized in the three workshops, the working meetings, and each expert elicitation interview. This section summarizes the discussions and activities supporting the interpretations of ground-motion uncertainties.

In the Methods, Models, and Preliminary Interpretations Workshop (held in conjunction with the Seismic Source Characterization Preliminary Interpretations Workshop), Peter Morris, normative expert on elicitation, provided elicitation training (Whitney 1997c). This training included an introduction to quantifying uncertainty using probabilities, as well as a discussion of known cognitive biases to avoid, such as the tendency of experts to underestimate uncertainties and to become anchored in an initial assessment. The concepts of epistemic uncertainty and aleatory variability and the concepts of parametric and modeling uncertainty were first presented in the

Data Needs Workshop by Gabriel Toro, leader of the PSHA calculations team (Hayes 1995). He restated this presentation and expanded on it at the Methods, Models, and Preliminary Interpretations Workshop (Whitney 1997a). Uncertainty partitioning was presented in a matrix format (Table C-2). The Methods, Models, and Preliminary Interpretations Workshop occurred as the experts were beginning to develop their ground-motion estimates. At that meeting, Gabriel Toro explained uncertainty partitioning into epistemic and aleatory components and gave an example that was particularly relevant to the ground-motion experts' work. He related epistemic uncertainty on the median (μ) to the question of confidence in the estimate of μ and listed several values of σ_μ related to levels of confidence. Summaries of the workshops (Hayes 1995; Whitney 1997a) describe his presentations. The experts were provided with copies of the presentation materials, including transparencies sketched during the workshops, and with the workshop report. The presentation stimulated extensive discussion among the experts and between the experts and the Facilitation Team that clarified the experts' understanding of the required assessments and of the processes that would be implemented to facilitate their assessments.

Table C-2. Uncertainty Partitioning for Ground Motion

		Seismic-Hazard Analyst	
		Uncertainty	Randomness
Ground-Motion Analyst	Modeling	Uncertainty about the true model bias (i.e., to what extent model has a tendency to overpredict or underpredict observations)	Unexplained scatter due to physical processes not included in the model (e.g., slip distribution, crustal heterogeneity)
	Parametric	Uncertainty about median stress drop for Basin and Range, depth distribution, etc.	Event-to-event variation in stress drop or focal depth, etc.

Source: Hayes 1995.

Additionally, at the Methods, Models, and Preliminary Interpretations Workshop and the Feedback Workshop, Norman Abrahamson, the Ground Motion Facilitation Team leader, discussed the partitioning, referring numerous times to Gabriel Toro's matrix (Table C-2). His focus in the Methods, Models, and Preliminary Interpretations Workshop was parametric versus modeling partitioning because this is an issue that arises with ground-motion estimation based on numerical simulation procedures. The aleatory and epistemic partitioning had been emphasized earlier in the workshop.

The expert elicitation interviews occurred between the Methods, Models, and Preliminary Interpretations Workshop and the Feedback Workshop. Each expert was elicited separately (Table C-3). During the elicitation interviews, the experts described their initial ground-motion models to the Ground Motion Facilitation Team. In each case, the Ground Motion Facilitation Team identified inconsistencies in the partitioning of uncertainty into the four elements of the uncertainty matrix. The uncertainty matrix was again explained to each expert to ensure the expert's complete understanding of the requirements and the process. The inconsistencies in the uncertainty partitioning were discussed with the experts during the elicitation interview. The experts then discussed approaches to correcting these inconsistencies in their models. This feedback to their initial models gave the experts a clear understanding of the uncertainties in the context of their own models.

Table C-3. Ground-Motion Elicitation Interview Schedule

Interview Date	Expert	Ground Motion Facilitation Team Personnel	Observers
March 17, midday	Silva	Abrahamson, Savy, Becker	Morris
March 18, a.m.	Campbell	Abrahamson, Savy, Becker	None
March 18, p.m.	Walck	Abrahamson, Savy, Becker	None
March 19, a.m.	Anderson	Abrahamson, Savy, Becker	Ibrahim
March 19, p.m.	McGarr	Abrahamson, Becker	Ibrahim
March 20, a.m.	Boore	Abrahamson, Becker	Ibrahim
March 20, p.m.	Somerville	Abrahamson, Savy, Becker	None

At the Feedback Workshop, Norman Abrahamson further discussed the uncertainty partitioning. He concentrated on the propagation of errors because this was a common issue for many of the experts' initial models. To demonstrate the concepts, he used the point source stochastic model (one of the proponent models) as an example (Whitney 1997b). In this example, he computed the uncertainties for each of the four boxes in the uncertainty matrix. This exercise provided a specific example demonstrating how to implement the requirements for uncertainty assessments.

The form of the probability distributions for σ_μ and σ_σ was discussed at the Methods, Models, and Preliminary Interpretations Workshop. The experts were told that the process should place no constraints on their interpretations and that they could, for example, specify asymmetric or symmetric distributions; however, none of the experts elected to use asymmetric distributions. All of the experts assumed a lognormal distribution for the epistemic uncertainty in the median (σ_μ) and a normal distribution for the epistemic uncertainty in the aleatory variability (σ_σ). The reason for using symmetric distributions was that the experts did not have a technical basis for assuming a more complicated distribution (e.g., asymmetric).

In summary, interactions between the Ground Motion Facilitation Team and the ground-motion experts, and among the experts themselves, clarified and resolved issues related to assessing ground-motion uncertainty. Interaction took place in the workshops, in elicitation interviews, and in working meetings. Appropriate training and feedback by the Ground Motion Facilitation Team clarified each expert's understanding in the context of their own models so that their final models appropriately reflected their individual assessments.

C.4.2 Feedback

The experts were required to develop point estimates for a total of 51 magnitude-distance-faulting scenarios. At the time of the Feedback Workshop, the experts had addressed a subset of 16 cases for discussion. The balance of their work took place following the Feedback Workshop but with the insights gained during that workshop. Additional feedback was provided to the experts as they developed their final models. The complete feedback process is described below.

The experts evaluated alternative proponent models as part of the development of their individual assessments. The proponent models were summarized in a data package of two volumes of information supplied to each expert (Abrahamson and Becker 1997w, 1997x).

Following the Feedback Workshop, the data package format was used to display the experts' point estimates and track revisions. Table C-4 describes the content of each volume.

Table C-4. Summary of Ground-Motion Data Packages Used in Feedback Process

Volume	Description and Date	Reference
1 and 1b	Yucca Mountain Ground-Motion Data, 2/97: proponent models	Abrahamson and Becker 1997w, 1997x
2	Proponent Models by Case, Spectra Plots, 5/97	Abrahamson and Becker 1997y
3	Expert Point Estimates, Horizontal Component, Rev. 1, 5/97	Abrahamson and Becker 1997a
4	Expert Point Estimates, Vertical Component, Rev. 1, 5/97	Abrahamson and Becker 1997b
5	Expert Estimates by Case, Spectra Plots, Rev. 1, 5/97	Abrahamson and Becker 1997c
6 (A and B)	Regression Models, Rev 1, 5/97 (Vol. 6A for Anderson, Boore, Campbell; Vol. 6B for McGarr, Silva, Somerville, Walck)	Abrahamson and Becker 1997d, 1997e
7	Expert Point Estimates and Proponent Models, Horizontal, Rev. 2, 6/97	Abrahamson and Becker 1997f
8	Expert Point Estimates and Proponent Models, Vertical, Rev. 2, 6/97	Abrahamson and Becker 1997g
9	Expert Estimates by Case, Spectra Plots, Rev. 2, 6/97	Abrahamson and Becker 1997h
10 (A, B, D, E, F, G)	Regression Models, Rev. 2, 6/97 10A-Anderson 10B-Boore 10D-McGarr 10E-Silva 10F-Somerville 10G-Walck (Campbell did not provide Rev. 2 models)	Abrahamson and Becker 1997i to 1997n
11 (A, B, C, D, E, F, G)	Regression Models, Rev. 3, 7/97 11A-Anderson 11B-Boore 11C-Campbell 11D-McGarr 11E-Silva 11F-Somerville 11G-Walck	Abrahamson and Becker 1997o to 1997u
12	Expert Estimates by Case, Spectra Plots, Rev. 3, 7/97	Abrahamson and Becker 1997v

For each of the 51 point estimates, the experts developed weights for the alternative proponent models combined with various conversion factors (data package Vol. 1 and 1b (Abrahamson and Becker 1997w, 1997x)). The proponent models were sorted into four classes: empirical models, finite-fault numerical simulations, stochastic point-source numerical simulations, and blast-based models. The conversion factors were used to model Yucca Mountain–specific conditions.

The experts supplied the first complete set of weights for the 51 cases in May 1997. Using their weights and conversion factors, the Ground Motion Facilitation Team then computed the median and standard deviation of μ (median ground motion) and σ (aleatory variability). The Ground Motion Facilitation Team also developed simplified parametric equations to describe the point estimates for use in the PSHA calculations. These results were provided to each expert.

Comparisons between the estimates from the different experts were also provided so that each expert was made aware of the interpretations of the other experts (data package Vol. 5, 9, and 12 (Abrahamson and Becker 1997c, 1997h, 1997v)). With this feedback, the experts reevaluated their point estimates, made revisions, and informed the Ground Motion Facilitation Team of their changes. The first revision was followed with a second in June 1997, and in July 1997 the final revision was completed. Not all experts chose to provide three revisions–some provided more changes and some fewer–but complete sets of figures showing the comparisons were supplied for the three revisions. The experts also reviewed the parameterization of their point estimates to ensure that the parameters adequately represented their models.

Final feedback was provided to the experts at a Final Results Meeting in April 1998 (Parks 1998). At that meeting, the results of the PSHA were summarized for the seismic source and fault displacement characterization expert teams and the ground-motion characterization experts. In addition to the PSHA results, presentations were made describing how the results would be used in design and performance assessment.

The evolution of the experts' assessments of ground motion and uncertainty can be seen by considering one of the 51 cases: horizontal ground motions at a distance of 1 km from a magnitude 6.5 strike-slip faulting earthquake. Estimates of median motion μ were stable through all revisions (Figure C-1). The tight clustering indicates the experts generally agreed on these values. Similar plots of the aleatory variability σ (Figure C-2) show an increasing spread between the values; two experts generally decreased their estimates and one increased it. With the exception of one expert, estimates of σ_μ evolved in an opposite trend as the spread generally tightened (Figure C-3). Because estimates of σ_σ differed little in the three revisions, only regression models were produced (data package Vol. 6, 10, and 11 (Abrahamson and Becker 1997d, 1997e, 1997i to 1997u)). Comparisons of the σ_σ regression models show little significant change over the three revisions.

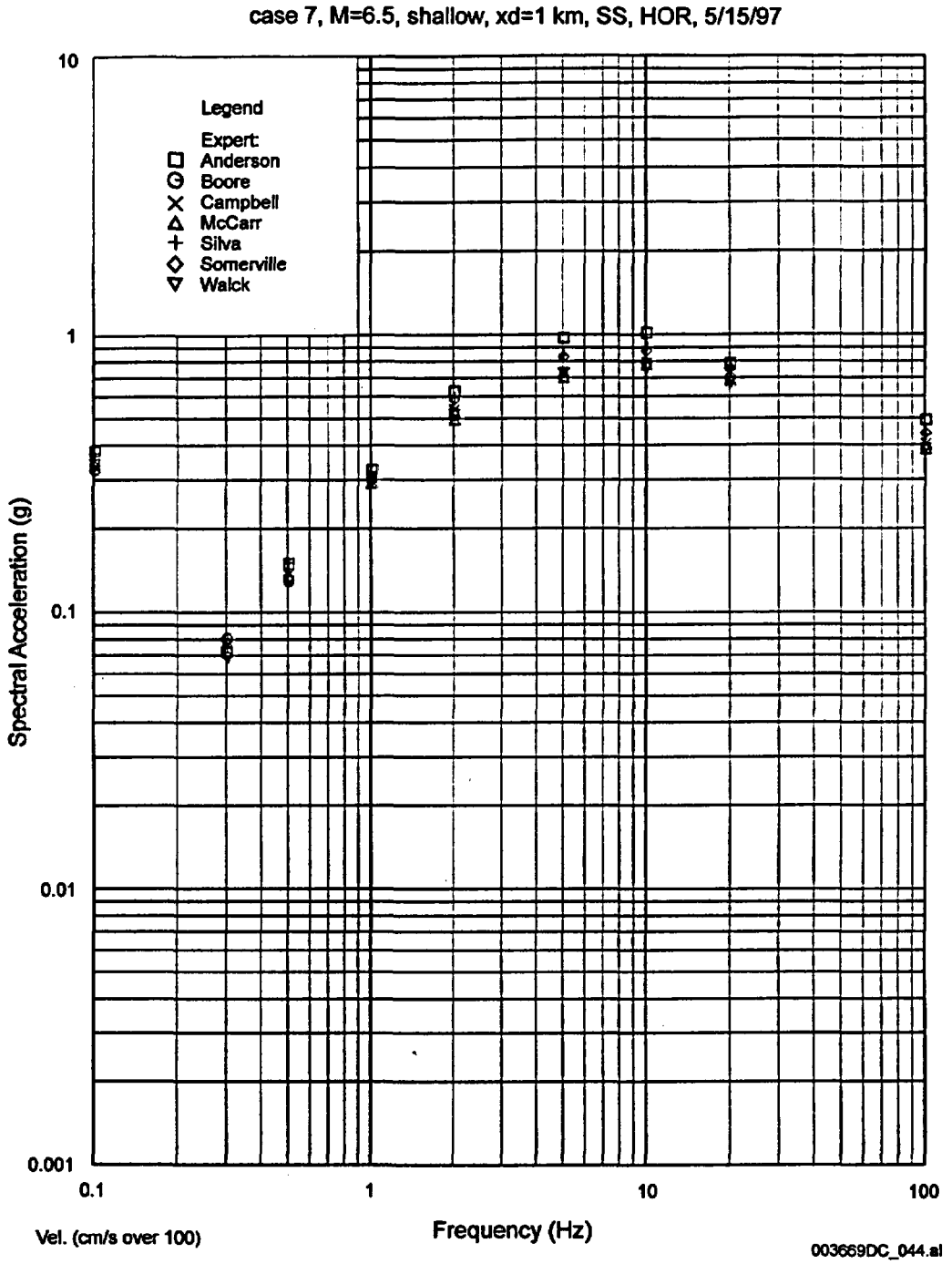

Source: Abrahamson and Becker 1997c.

NOTE: Estimates are for horizontal ground motion from a magnitude 6.5 strike-slip faulting earthquake at a distance of 1 km. For convenience, estimates for peak ground velocity are shown on this figure along with those for spectral acceleration. They are plotted on the left side of the figure (at a frequency of 0.1 Hz) in units of centimeters per second (cm/s) divided by 100 so that the values lie in the same range as the spectral acceleration values that are plotted. Peak ground velocity values are between 30 and 40 cm/s.

Figure C-1a. Example Median Ground-Motion Point Estimates for Rev. 1

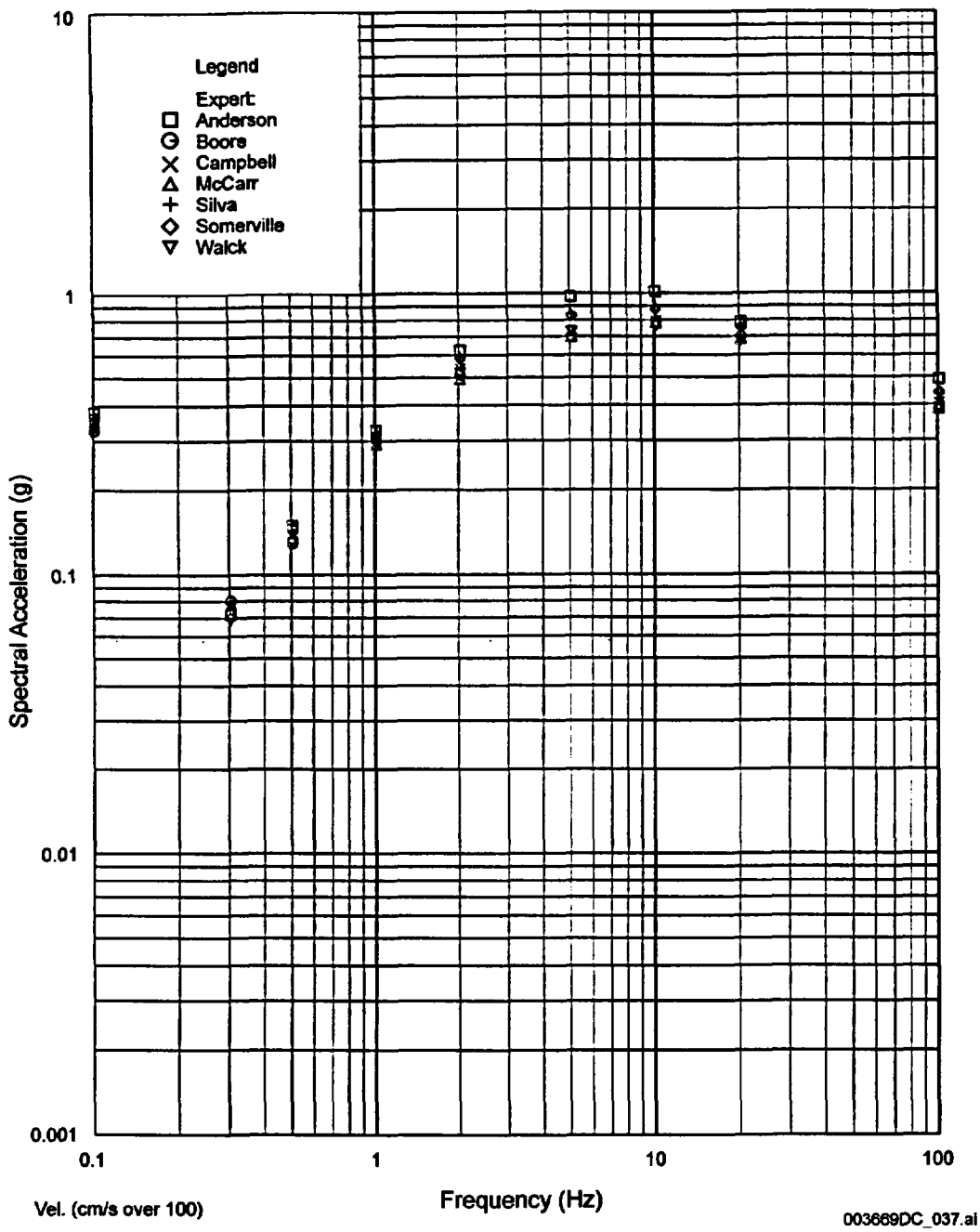

Source: Abrahamson and Becker 1997h.

NOTE: Estimates are for horizontal ground motion from a magnitude 6.5 strike-slip faulting earthquake at a distance of 1 km. For convenience, estimates for peak ground velocity are shown on this figure along with those for spectral acceleration. They are plotted on the left side of the figure (at a frequency of 0.1 Hz) in units of centimeters per second (cm/s) divided by 100 so that the values lie in the same range as the spectral acceleration values that are plotted. Peak ground velocity values are between 30 and 40 cm/s.

Figure C-1b. Example Median Ground-Motion Point Estimates for Rev. 2

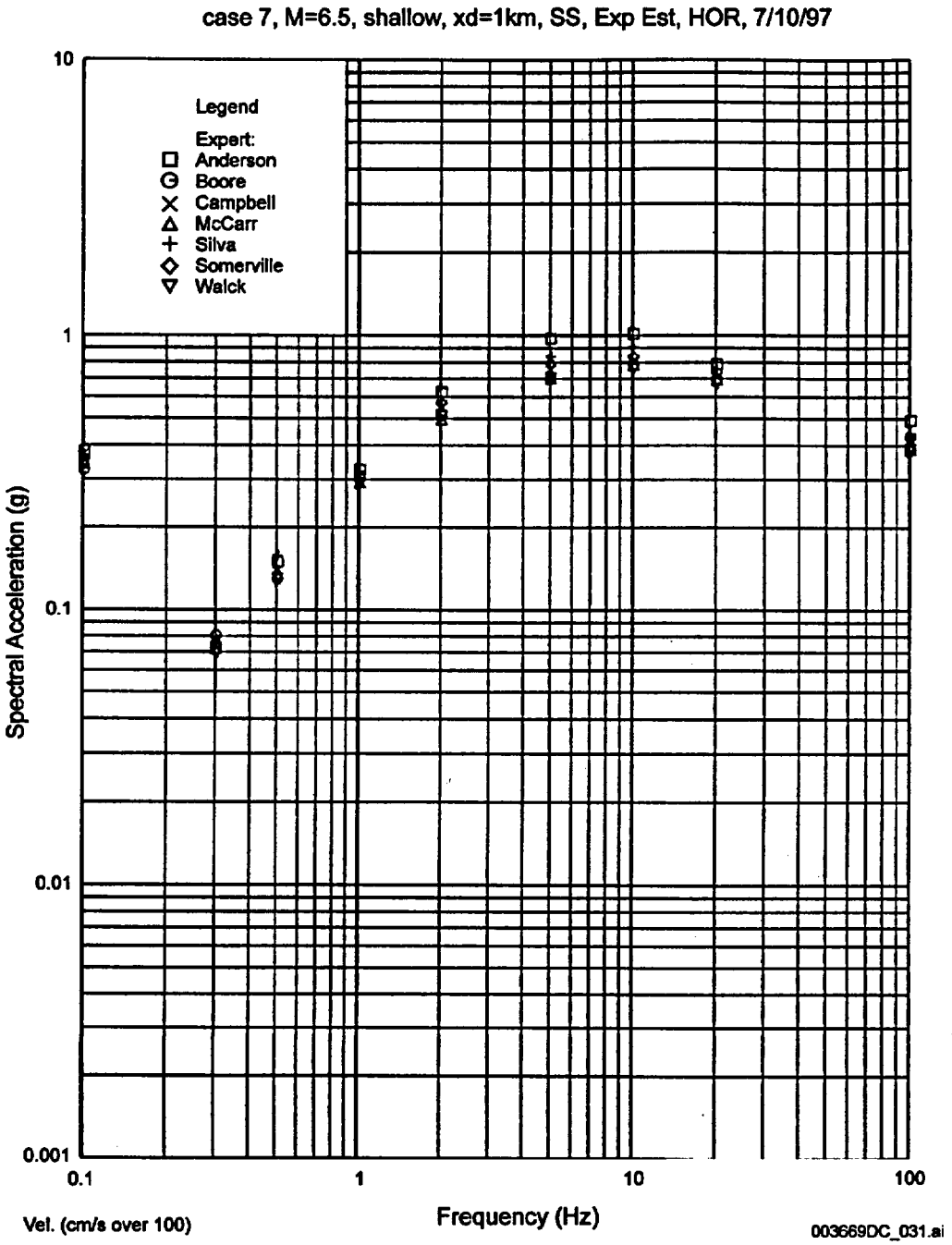

Source: Abrahamson and Becker 1997v.

NOTE: Estimates are for horizontal ground motion from a magnitude 6.5 strike-slip faulting earthquake at a distance of 1 km. For convenience, estimates for peak ground velocity are shown on this figure along with those for spectral acceleration. They are plotted on the left side of the figure (at a frequency of 0.1 Hz) in units of centimeters per second (cm/s) divided by 100 so that the values lie in the same range as the spectral acceleration values that are plotted. Peak ground velocity values are between 30 and 40 cm/s.

Figure C-1c. Example Median Ground-Motion Point Estimates for Rev. 3

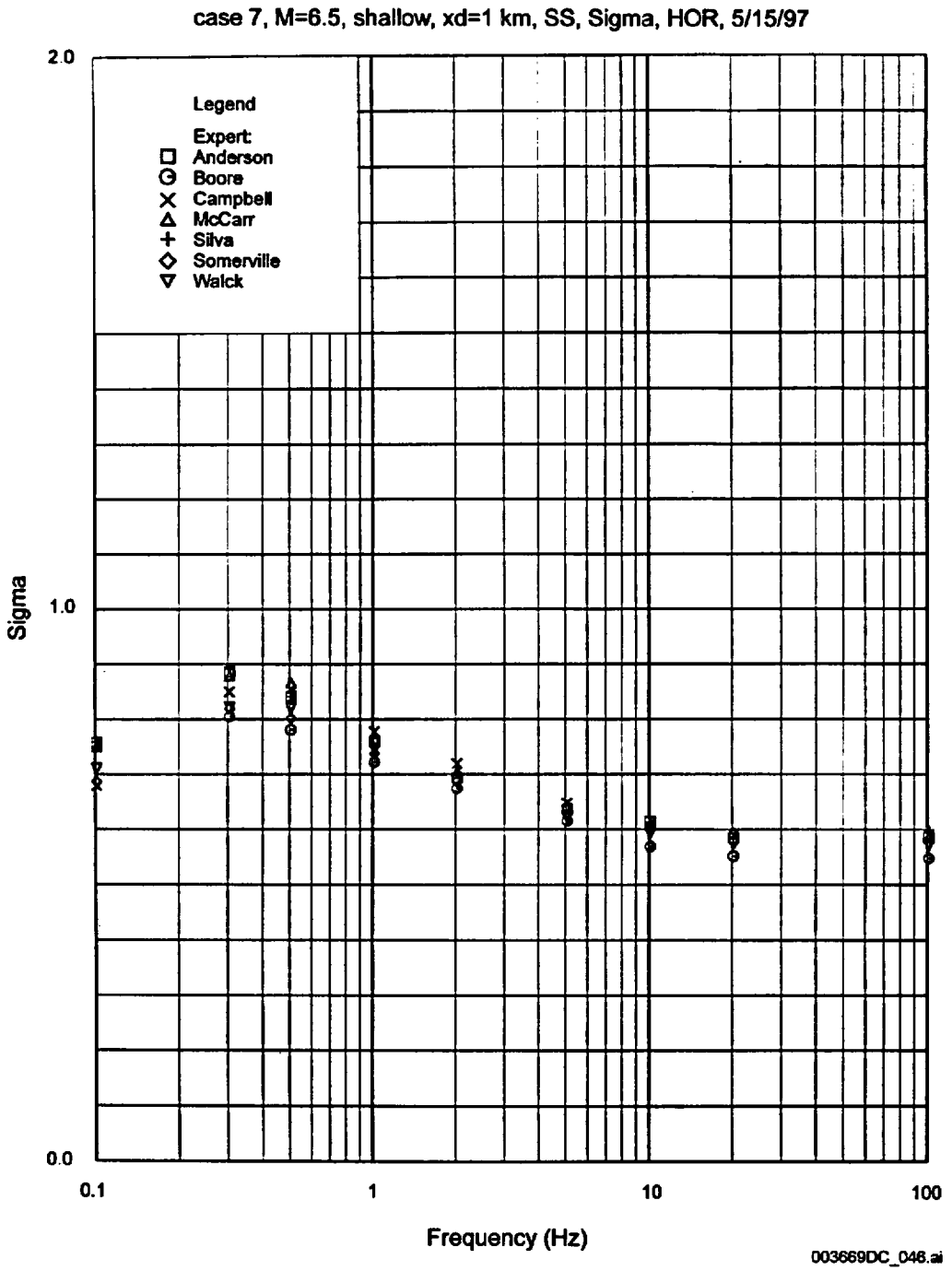

Source: Abrahamson and Becker 1997c.

NOTE: Estimates are for horizontal ground motion from a magnitude 6.5 strike-slip faulting earthquake at a distance of 1 km. For convenience, estimates for peak ground velocity are shown on this figure along with those for spectral acceleration. They are plotted on the left side of the figure (at a frequency of 0.1 Hz).

Figure C-2a. Example Median Aleatory Variability Estimates for Rev. 1

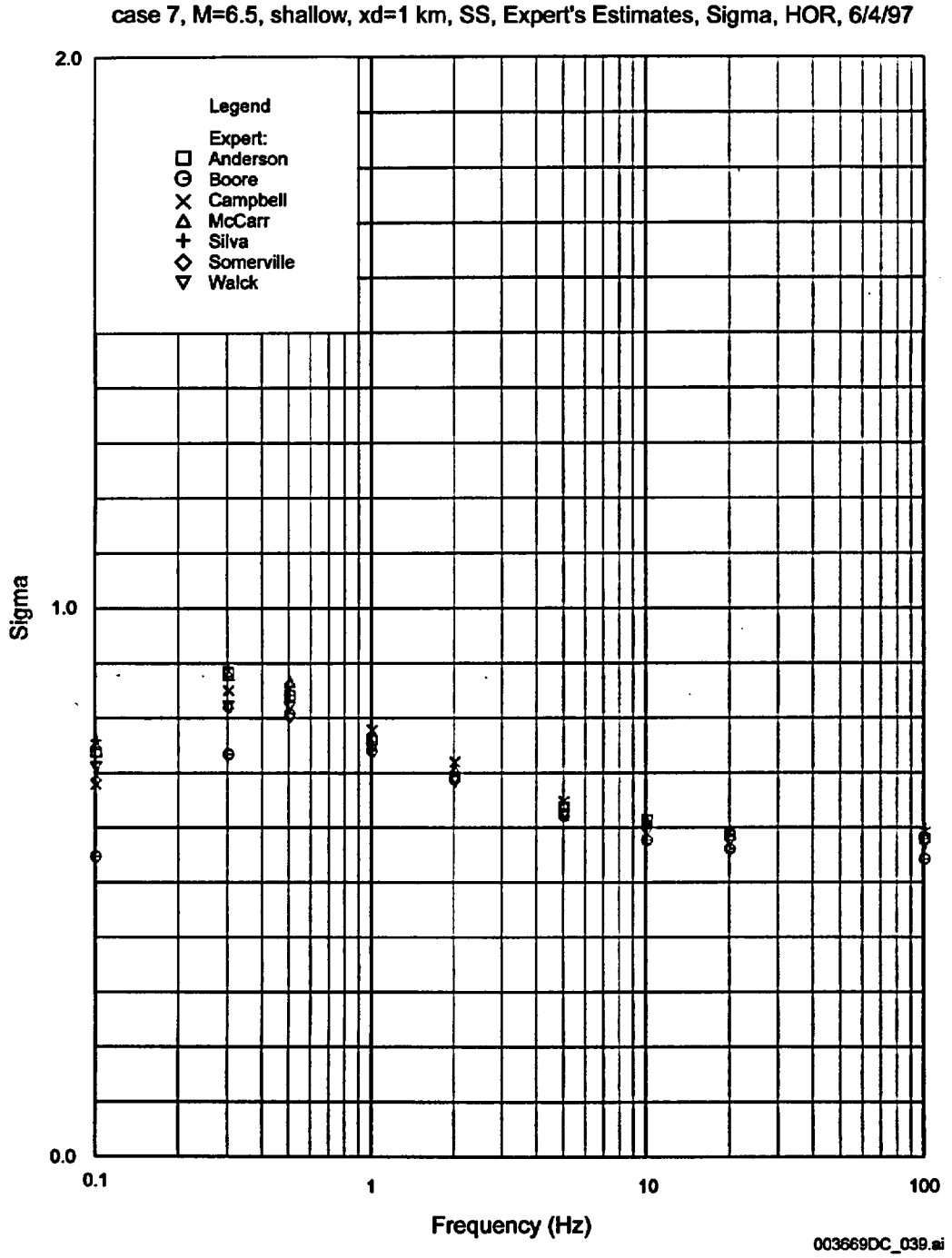

Source: Abrahamson and Becker 1997h.

NOTE: Estimates are for horizontal ground motion from a magnitude 6.5 strike-slip faulting earthquake at a distance of 1 km. For convenience, estimates for peak ground velocity are shown on this figure along with those for spectral acceleration. They are plotted on the left side of the figure (at a frequency of 0.1 Hz).

Figure C-2b. Example Median Aleatory Variability Estimates for Rev. 2

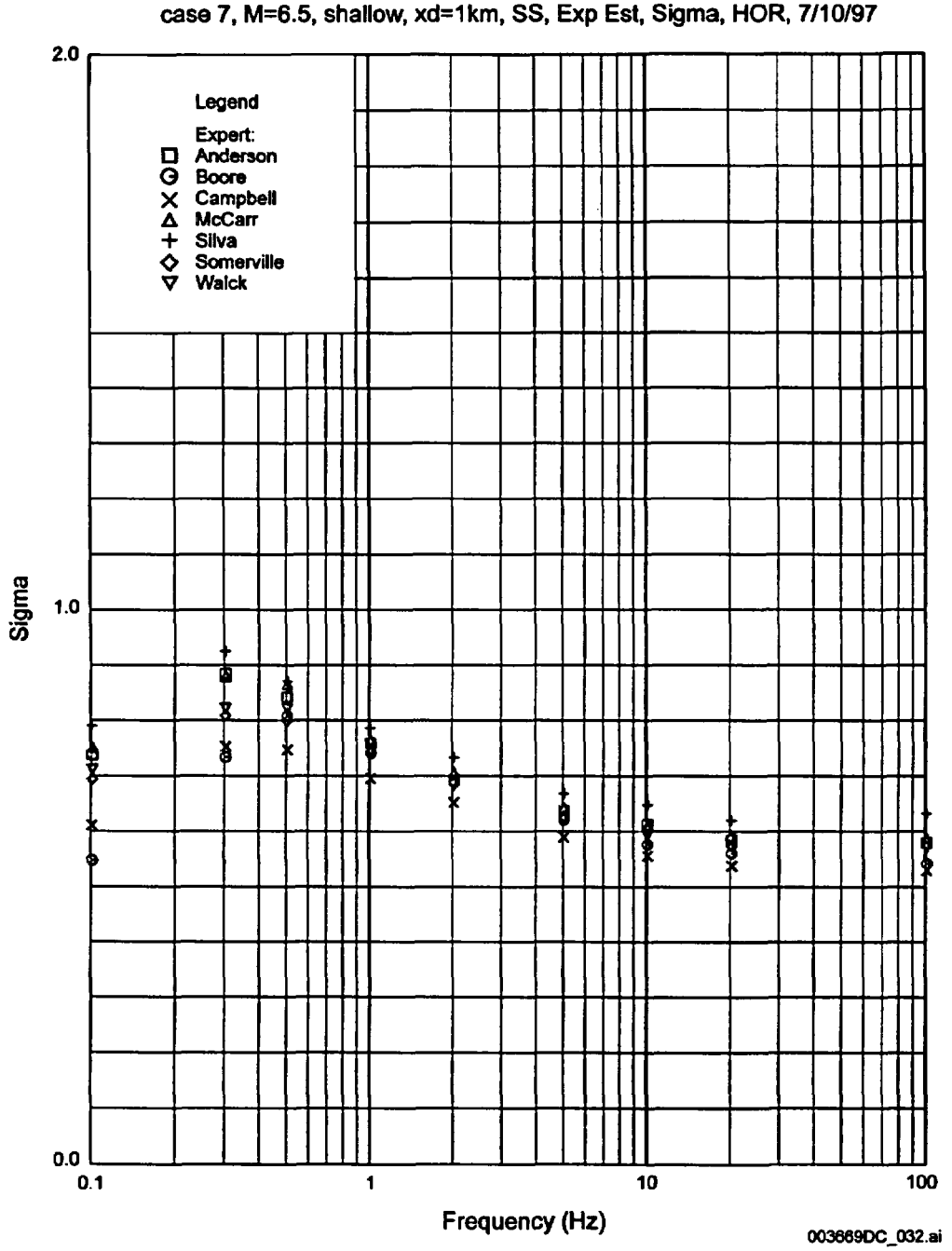

Source: Abrahamson and Becker 1997v.

NOTE: Estimates are for horizontal ground motion from a magnitude 6.5 strike-slip faulting earthquake at a distance of 1 km. For convenience, estimates for peak ground velocity are shown on this figure along with those for spectral acceleration. They are plotted on the left side of the figure (at a frequency of 0.1 Hz).

Figure C-2c. Example Median Aleatory Variability Estimates for Rev. 3

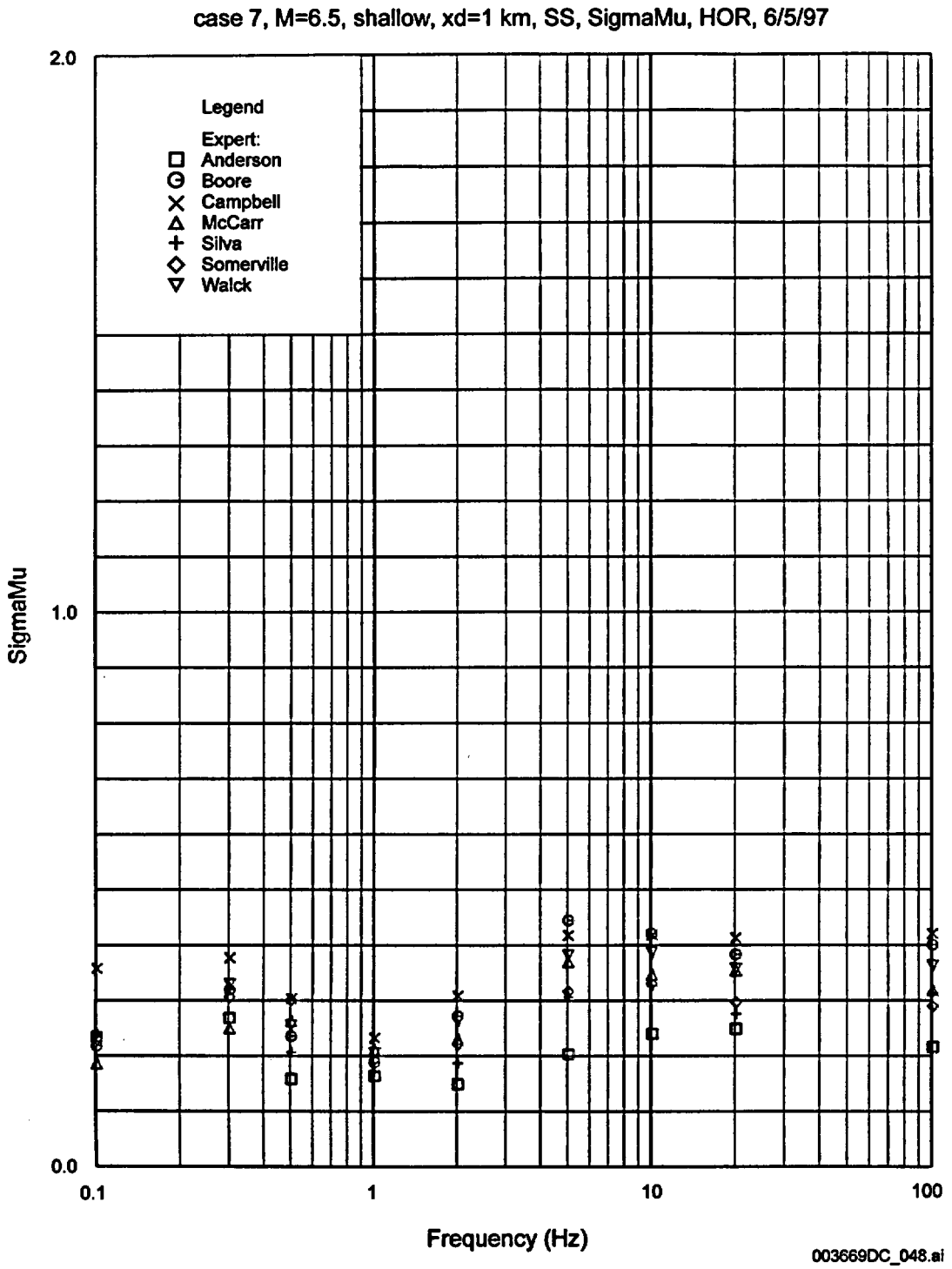

Source: Abrahamson and Becker 1997c.

NOTE: Estimates are for horizontal ground motion from a magnitude 6.5 strike-slip faulting earthquake at a distance of 1 km. For convenience, estimates for peak ground velocity are shown on this figure along with those for spectral acceleration. They are plotted on the left side of the figure (at a frequency of 0.1 Hz).

Figure C-3a. Example Epistemic Uncertainty on Median Ground-Motion Estimates for Rev. 1

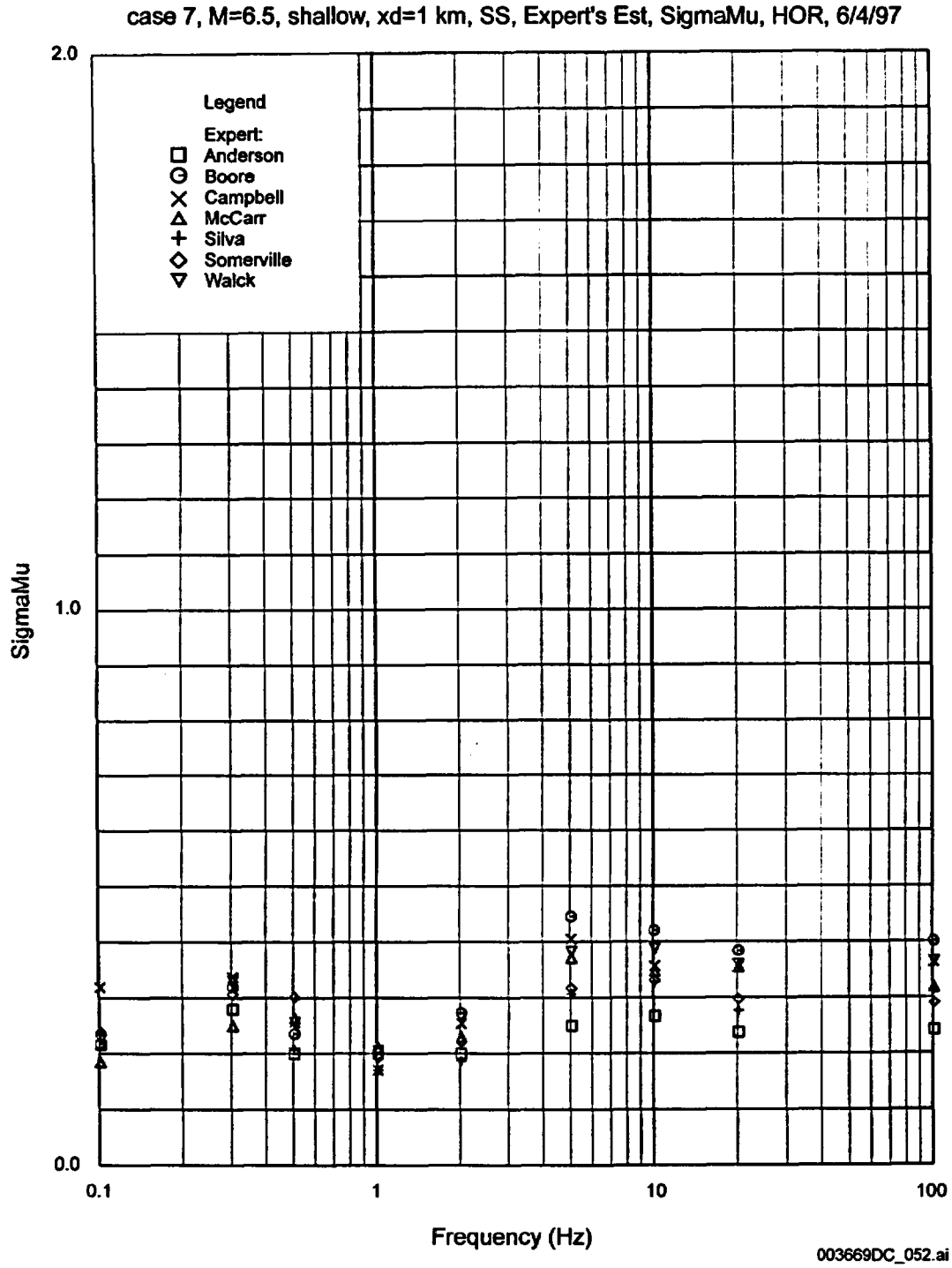

Source: Abrahamson and Becker 1997h.

NOTE: Estimates are for horizontal ground motion from a magnitude 6.5 strike-slip faulting earthquake at a distance of 1 km. For convenience, estimates for peak ground velocity are shown on this figure along with those for spectral acceleration. They are plotted on the left side of the figure (at a frequency of 0.1 Hz).

Figure C-3b. Example Epistemic Uncertainty on Median Ground-Motion Estimates for Rev. 2

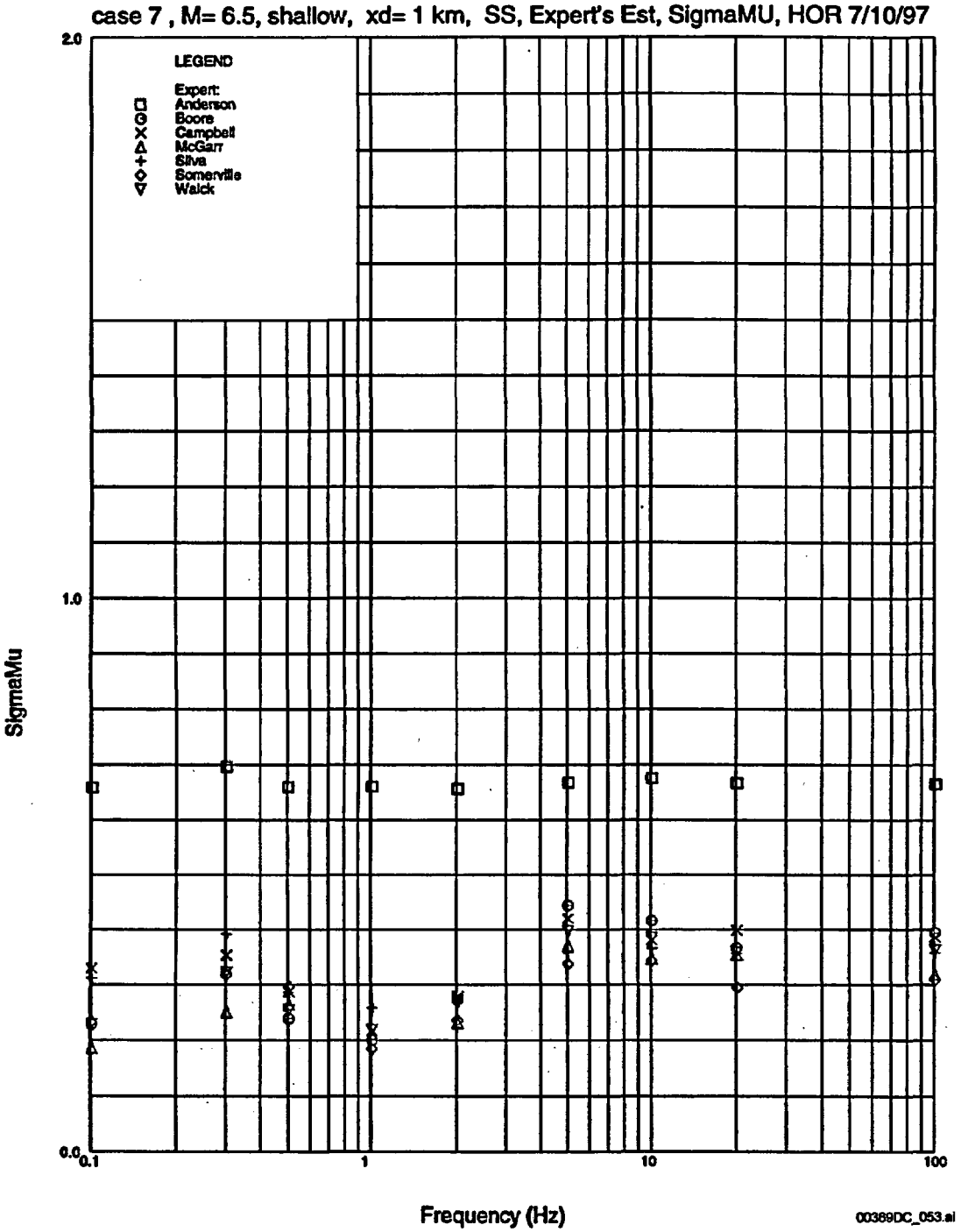

Source: Abrahamson and Becker 1997v.

NOTE: Estimates are for horizontal ground motion from a magnitude 6.5 strike-slip faulting earthquake at a distance of 1 km. For convenience, estimates for peak ground velocity are shown on this figure along with those for spectral acceleration. They are plotted on the left side of the figure (at a frequency of 0.1 Hz).

Figure C-3c. Example Epistemic Uncertainty on Median Ground-Motion Estimates for Rev. 3

In making revisions, the experts considered factors such as the tendency of experts to underestimate uncertainty, epistemic uncertainty in the parameters for numerical simulations, and geologic information (e.g., the existence of precariously balanced rocks at Yucca Mountain).

C.4.3 Documentation

Documentation of the ground-motion expert elicitation component of the PSHA for Yucca Mountain is consistent with guidance by Budnitz et al. (1997). It is also in general accord with guidance by Kotra et al. (1996), except that the rationale for preliminary assessments was not documented to avoid having the experts become anchored to them.

The documentation of each expert's final assessment is contained in his or her elicitation summary (CRWMS M&O 1998, Appendix F). These summaries describe and provide the basis for the final assessments of ground motion and uncertainty that resulted from the elicitation process. Preliminary assessments are documented in the ground-motion data package volumes (Table C-4) (Abrahamson and Becker 1997a to 1997y).

Documentation of the feedback process consists of the Feedback Workshop summary (Whitney 1997b), the ground-motion data packages that were provided to the experts (Abrahamson and Becker 1997a to 1997y), and the summary of the final results meeting (Parks 1998). After each revision cycle, the experts were provided with ground-motion data packages (Table C-4) that allowed them to assess the implications of their assessments relative to those of the other experts. The data packages provided information on median ground motion (μ), the aleatory variability (σ), and the associated epistemic uncertainties of these quantities (σ_μ, σ_σ).

The overall elicitation process is described in *Probabilistic Seismic Hazard Analyses for Fault Displacement and Vibratory Ground Motion at Yucca Mountain, Nevada* (CRWMS M&O 1998); *Characterize Framework for Seismicity and Structural Deformation at Yucca Mountain, Nevada* (CRWMS M&O 2000); and in workshop and meeting summaries (Hayes 1995; Whitney 1997a, 1997b; Parks 1998). These reports describe and document the steps that were carried out to appropriately implement the expert elicitation process.

C.5 REFERENCES

C.5.1 Documents Cited

Abrahamson, N.A. and Becker A.M. 1997a. *Ground Motion Characterization at Yucca Mountain, Nevada.* Milestone SPG28EM4. Volume 3: Expert Point Estimates Horizontal Component Revision 1. Denver, Colorado: U.S. Geological Survey. ACC: MOL.20030205.0122.

Abrahamson, N.A. and Becker A.M. 1997b. *Ground Motion Characterization at Yucca Mountain, Nevada.* Milestone SPG28EM4. Volume 4: Expert Point Estimates Vertical Component Revision 1. Denver, Colorado: U.S. Geological Survey. ACC: MOL.20030205.0123.

Abrahamson, N.A. and Becker A.M. 1997c. *Ground Motion Characterization at Yucca Mountain, Nevada.* Milestone SPG28EM4. Volume 5: Expert Estimates by Case Spectra Plots, Rev. 1. Denver, Colorado: U.S. Geological Survey. ACC: MOL.20030205.0124.

Abrahamson, N.A. and Becker A.M. 1997d. *Ground Motion Characterization at Yucca Mountain, Nevada.* Milestone SPG28EM4. Volume 6A: Regression Models, Rev. 1, Experts: Anderson, Boore, and Campbell. Denver, Colorado: U.S. Geological Survey. ACC: MOL.20030205.0125.

Abrahamson, N.A. and Becker A.M. 1997e. *Ground Motion Characterization at Yucca Mountain, Nevada.* Milestone SPG28EM4. Volume 6B: Regression Models, Rev. 1 Experts: McGarr, Somerville, and Walck. Denver, Colorado: U.S. Geological Survey. ACC: MOL.20030205.0126.

Abrahamson, N.A. and Becker A.M. 1997f. *Ground Motion Characterization at Yucca Mountain, Nevada.* Milestone SPG28EM4. Volume 7: Expert Point Estimates and Proponent Models, Horizontal, Rev. 2. Denver, Colorado: U.S. Geological Survey. ACC: MOL.20030205.0127.

Abrahamson, N.A. and Becker A.M. 1997g. *Ground Motion Characterization at Yucca Mountain, Nevada.* Milestone SPG28EM4. Volume 8: Expert Point Estimates and Proponent Models, Vertical, Rev. 2. Denver, Colorado: U.S. Geological Survey. ACC: MOL.20030205.0128.

Abrahamson, N.A. and Becker A.M. 1997h. *Ground Motion Characterization at Yucca Mountain, Nevada.* Milestone SPG28EM4. Volume 9: Expert Estimates by Case Spectra Plots, Rev. 2. Denver, Colorado: U.S. Geological Survey. ACC: MOL.20030205.0129.

Abrahamson, N.A. and Becker A.M. 1997i. *Ground Motion Characterization at Yucca Mountain, Nevada.* Milestone SPG28EM4. Volume 10A: Regression Models, Rev. 2, Expert: Anderson. Denver, Colorado: U.S. Geological Survey. ACC: MOL.20030205.0130.

Abrahamson, N.A. and Becker A.M. 1997j. *Ground Motion Characterization at Yucca Mountain, Nevada.* Milestone SPG28EM4. Volume 10B: Regression Models, Rev. 2, Expert: Boore. Denver, Colorado: U.S. Geological Survey. ACC: MOL.20030205.0131.

Abrahamson, N.A. and Becker A.M. 1997k. *Ground Motion Characterization at Yucca Mountain, Nevada.* Milestone SPG28EM4. Volume 10D: Regression Models, Rev. 2, Expert: McGarr. Denver, Colorado: U.S. Geological Survey. ACC: MOL.20030205.0132.

Abrahamson, N.A. and Becker A.M. 1997l. *Ground Motion Characterization at Yucca Mountain, Nevada.* Milestone SPG28EM4. Volume 10E: Regression Models, Rev. 2, Expert: Silva. Denver, Colorado: U.S. Geological Survey. ACC: MOL.20030205.0133.

Abrahamson, N.A. and Becker A.M. 1997m. *Ground Motion Characterization at Yucca Mountain, Nevada.* Milestone SPG28EM4. Volume 10F: Regression Models, Rev. 2, Expert: Somerville. Denver, Colorado: U.S. Geological Survey. ACC: MOL.20030205.0134.

Abrahamson, N.A. and Becker A.M. 1997n. *Ground Motion Characterization at Yucca Mountain, Nevada.* Milestone SPG28EM4. Volume 10G: Regression Models, Rev. 2, Expert: Walck. Denver, Colorado: U.S. Geological Survey. ACC: MOL.20030205.0135.

Abrahamson, N.A. and Becker A.M. 1997o. *Ground Motion Characterization at Yucca Mountain, Nevada.* Milestone SPG28EM4. Volume 11A: Regression Models, Rev. 3, Expert: Anderson. Denver, Colorado: U.S. Geological Survey. ACC: MOL.20030205.0136.

Abrahamson, N.A. and Becker A.M. 1997p. *Ground Motion Characterization at Yucca Mountain, Nevada.* Milestone SPG28EM4. Volume 11B: Regression Models, Rev. 3, Expert: Boore. Denver, Colorado: U.S. Geological Survey. ACC: MOL.20030205.0137.

Abrahamson, N.A. and Becker A.M. 1997q. *Ground Motion Characterization at Yucca Mountain, Nevada.* Milestone SPG28EM4. Volume 11C: Regression Models, Rev. 3, Expert: Campbell. Denver, Colorado: U.S. Geological Survey. ACC: MOL.20030205.0138.

Abrahamson, N.A. and Becker A.M. 1997r. *Ground Motion Characterization at Yucca Mountain, Nevada.* Milestone SPG28EM4. Volume 11D: Regression Models, Rev. 3, Expert: McGarr. Denver, Colorado: U.S. Geological Survey. ACC: MOL.20030205.0139.

Abrahamson, N.A. and Becker A.M. 1997s. *Ground Motion Characterization at Yucca Mountain, Nevada.* Milestone SPG28EM4. Volume 11E: Regression Models, Rev. 3, Expert: Silva. Denver, Colorado: U.S. Geological Survey. ACC: MOL.20030205.0140.

Abrahamson, N.A. and Becker A.M. 1997t. *Ground Motion Characterization at Yucca Mountain, Nevada.* Milestone SPG28EM4. Volume 11F: Regression Models, Rev. 3, Expert: Somerville. Denver, Colorado: U.S. Geological Survey. ACC: MOL.20030205.0141.

Abrahamson, N.A. and Becker A.M. 1997u. *Ground Motion Characterization at Yucca Mountain, Nevada.* Milestone SPG28EM4. Volume 11G: Regression Models, Rev. 3, Expert: Walck. Denver Colorado: U.S. Geological Survey. ACC: MOL.20030205.0142.

Abrahamson, N.A. and Becker, A.M. 1997v. *Ground Motion Characterization at Yucca Mountain, Nevada.* Milestone SPG28EM4. Volume 12: Expert Estimates by Case Spectra Plots, Rev. 3. Denver, Colorado: U.S. Geological Survey. ACC: MOL.20030205.0143.

Abrahamson, N.A. and Becker, A.M. 1997w. *Ground Motion Characterization at Yucca Mountain, Nevada.* Milestone SPG28EM4. Volume 1: Reference Material for Proponent Models. Denver, Colorado: U.S. Geological Survey. ACC: MOL.20030205.0119.

Abrahamson, N.A. and Becker, A.M. 1997x. *Ground Motion Characterization at Yucca Mountain, Nevada.* Milestone SPG28EM4. Volume 1b: Additional Reference Material for Proponent Models. Denver, Colorado: U.S. Geological Survey. ACC: MOL.20030205.0120.

Abrahamson, N.A. and Becker A.M. 1997y. *Ground Motion Characterization at Yucca Mountain, Nevada.* Milestone SPG28EM4. Volume 2: Proponent Models by Case Spectra Plots. Denver, Colorado: U.S. Geological Survey. ACC: MOL.20030205.0121.

Brocoum, S. 2000. "U.S. Department of Energy Workshops on Ground Motion at Yucca Mountain, Nevada," Letter from S. Brocoum (DOE/YMSCO) to M.J. Bell (NRC), December 21, 2000, with enclosures. ACC: MOL.20010301.0311.

Budnitz, R.J.; Apostolakis, G.; Boore, D.M.; Cluff, L.S.; Coppersmith, K.J.; Cornell, C.A.; and Morris, P.A. 1997. *Recommendations for Probabilistic Seismic Hazard Analysis: Guidance on the Uncertainty and Use of Experts.* NUREG/CR-6372. Two volumes. Washington, D.C.: U.S. Nuclear Regulatory Commission. TIC: 235076; 235074.

CRWMS M&O (Civilian Radioactive Waste Management System Management and Operating Contractor) 1998. *Probabilistic Seismic Hazard Analyses for Fault Displacement and Vibratory Ground Motion at Yucca Mountain, Nevada.* Milestone SP32IM3, September 23, 1998. Three volumes. Las Vegas, Nevada: CRWMS M&O. ACC: MOL.19981207.0393.

CRWMS M&O 2000. *Characterize Framework for Seismicity and Structural Deformation at Yucca Mountain, Nevada.* ANL-CRW-GS-000003 REV 00. Las Vegas, Nevada: CRWMS M&O. ACC: MOL.20000510.0175.

Hayes, L.R. 1995. "Transmittal of Deliverable 3GSH502M - Prov Results: Summary Data Assessment Workshop, WBS 1.2.3.2.8.3.6." Letter from L.R. Hayes (USGS) to S. Jones (DOE/YMSCO), May 31, 1995, with enclosure. ACC: MOL.19960124.0011; MOL.19960124.0012.

Kotra, J.P.; Lee, M.P.; Eisenberg, N.A.; and DeWispelare, A.R. 1996. *Branch Technical Position on the Use of Expert Elicitation in the High-Level Radioactive Waste Program.* NUREG-1563. Washington, D.C.: U.S. Nuclear Regulatory Commission. TIC: 226832.

NRC (U.S. Nuclear Regulatory Commission) 2002. *Integrated Issue Resolution Status Report.* NUREG-1762. Washington, D.C.: U.S. Nuclear Regulatory Commission, Office of Nuclear Material Safety and Safeguards. TIC: 253064.

Parks, B. 1998. "Completion of Level 4 Milestone SPG28RM4, Final Workshop Summary Due April 27, 1998." Memorandum from B. Parks (USGS) to R. Craig (USGS), April 27, 1998, with enclosure. ACC: MOL.19981028.0349; MOL.20030812.0118.

Reamer, C.W. 2001. "Structural Deformation and Seismicity Key Technical Issue Agreements: Additional Information Needed." Letter from W. Reamer (NRC) to S. Brocoum (DOE/YMSCO), August 3, 2001, with enclosure. ACC: MOL.20011001.0306.

Schlueter, J. 2000. "U.S. Nuclear Regulatory Commission/U.S. Department of Energy Technical Exchange and Management Meeting on Structural Deformation and Seismicity (October 11-12, 2000)." Letter from J. Schlueter (NRC) to S. Brocoum (DOE/YMSCO), October 27, 2000, with enclosure. ACC: MOL.20010730.0232.

Whitney, J. 1997a. "Completion of Level 4 Milestone SPG28BM4, Summary of Ground Motion Characterization Workshop #2: Methods and Models, Preliminary Interpretations." Memorandum from J. Whitney (USGS) to R. Craig (USGS), February 5, 1997, with enclosure. ACC: MOL.19990504.0060; MOL.19990504.0061.

Whitney, J. 1997b. "Completion of Level 4 Milestone SPG28DM4, Summary of Ground Motion Characterization Feedback Workshop #3, Due 5/13/97." Memorandum from J. Whitney (USGS) to R. Craig (USGS), May 13, 1997, with enclosure. ACC: MOL.19990504.0057; MOL.19990504.0058.

Whitney, J. 1997c. "Completion of Level 4 Milestone SPG28KM4, Summary of Seismic Source Characterization Preliminary Interpretations Workshop #4." Memorandum from J. Whitney (USGS) to R. Craig (USGS), February 3, 1997, with enclosure. ACC: MOL.19980223.0191; MOL.19980223.0192.

C.5.2 Codes, Standards, Regulations, and Procedures

YMP-USGS-QMP-3.16, R0. *Chapter 3 - Scientific Investigation and Design Control, Section 16 - Scientific Expert Elicitation.* Denver, Colorado: U.S. Geological Survey. ACC: MOL.19970127.0096.

APPENDIX D

DOCUMENTATION OF SEISMIC FRAGILITY CURVES AND SEISMIC RISK ANALYSIS (RESPONSE TO SDS 2.04 AIN-1)

Note Regarding the Status of Supporting Technical Information

This document was prepared using the most current information available at the time of its development. This Technical Basis Document and its appendices providing Key Technical Issue Agreement responses that were prepared using preliminary or draft information reflect the status of the Yucca Mountain Project's scientific and design bases at the time of submittal. In some cases this involved the use of draft Analysis and Model Reports (AMRs) and other draft references whose contents may change with time. Information that evolves through subsequent revisions of the AMRs and other references will be reflected in the License Application (LA) as the approved analyses of record at the time of LA submittal. Consequently, the Project will not routinely update either this Technical Basis Document or its Key Technical Issue Agreement appendices to reflect changes in the supporting references prior to submittal of the LA.

APPENDIX D

DOCUMENTATION OF SEISMIC FRAGILITY CURVES AND SEISMIC RISK ANALYSIS (RESPONSE TO SDS 2.04 AIN-1)

This appendix provides a response for Key Technical Issue (KTI) agreement Structural Deformation and Seismicity (SDS) 2.04 additional information need (AIN)-1. This AIN relates to the development and documentation of seismic fragility curves and seismic risk analysis for the total system performance assessment (TSPA).

D.1 KEY TECHNICAL ISSUE AGREEMENT

D.1.1 SDS 2.04 AIN-1

Agreement SDS 2.04 was reached during the U.S. Nuclear Regulatory Commission (NRC)/U.S. Department of Energy (DOE) Technical Exchange on Structural Deformation and Seismicity KTI held October 11 and 12, 2000, in Las Vegas, Nevada (Schlueter 2000a).

The wording of SDS 2.04 (Schlueter 2000a, p. 2 of enclosure) is as follows:

SDS 2.04

> The approach to evaluate seismic risk, including the assessment of seismic fragility and evaluation of event sequences is not clear to the NRC, provide additional information. DOE believes the approach contained in the FEPs AMR will be sufficient to support the Site Recommendation. The updated FEPs AMR is expected to be available in January 2001.

Based on NRC review of the updated analysis model report *Features, Events, and Processes: Disruptive Events* (CRWMS M&O 2000), provided to implement the SDS 2.04 agreement, the NRC determined that additional information is needed to support a licensing review (Reamer 2001a, pp. 3 and 4 of enclosure).

The wording of the AIN is as follows:

SDS 2.04 AIN-1

> DOE needs to provide documentation of methodology, technical bases and data for:
>
> (1) the development of seismic fragility curves for structures, systems and components used in performance assessments, including assurance that the necessary data will be available for the time period of interest (TPI), when needed. Moreover, this documentation should address: the range of failure modes that can occur for individual components, component interactions, etc.; consideration of component deterioration and its effect on the seismic

capacity; the use of a step function to define conditional probability of cladding failure;

(2) conducting a seismic risk analysis for the repository, including the assessment of the effect of cladding failure on design bases, barrier or system performance, or performance confirmation. This documentation should describe the identification, modeling and evaluation of the range of accident scenarios that could occur in the repository as a result of a seismic event during the TPI; and

(3) any additional points discussed in NRC's review, above.[1]

D.1.2 Related Key Technical Issue Agreements

This AIN is related to CLST 3.10, which defines the mechanical failure of cladding from seismic effects, and to TSPAI 3.06, which explains the methodology for including cladding damage induced by seismic events into TSPA. Further details on CLST 3.10 and TSPAI 3.06 can be found in Appendix A.

This AIN is also related to CLST 2.09, which asks the DOE to demonstrate that "the drip shield and waste package mechanical analysis addressing seismic excitation is consistent with the design basis earthquake covered in the SDS KTI" (Schlueter 2000b, p. 8 of enclosure). This technical basis document is focused on low-probability seismic events and postclosure repository performance, but it also includes discussion of the less severe, higher probability (i.e., more frequent) ground motion that is considered in preclosure seismic design and safety analyses. This technical basis document and appendix do not, however, describe preclosure seismic strategy or preclosure seismic design analyses. These aspects of preclosure design are described in *Development of Earthquake Ground Motion Input for Preclosure Seismic Design and Postclosure Performance Assessment of a Geologic Repository at Yucca Mountain, NV* (BSC 2003a) and in *Preliminary Seismic Analysis for Preclosure Safety Analysis* (BSC 2003b). The DOE response to CLST 2.09 will be provided separately.

D.2 RELEVANCE TO REPOSITORY PERFORMANCE

The seismic scenario class is based on (1) abstractions for the response of engineered barrier system (EBS) components to seismic effects at the repository, and on (2) a methodology for incorporating these abstractions in a seismic scenario class for TSPA. The seismic effects addressed are vibratory ground motion, fault displacement, and rockfall induced by ground motion. The EBS components are the drip shield, the waste package, the fuel cladding, and the invert. The response to seismically induced accident scenarios is defined by the continuous fraction (0 to 1) of surface areas on the waste package, drip shield, or cladding that are damaged by ground motion, by fault displacement, and by rockfall induced by ground motion. In the context of the seismic scenario, damaged states for the waste package and drip shield are based on a residual tensile stress threshold that can lead to accelerated stress corrosion cracking, resulting in the potential failure of the component as a barrier to flow and transport.

[1] "Above" refers to the NRC review comments under item (3) SDS 2.04 in "Structural Deformation and Seismicity Key Technical Issue Agreements: Additional Information Needed" (Reamer 2001b).

Seismic effects on the host rock are directly considered in determining the potential for rockfall to damage the drip shield in the lithophysal and nonlithophysal zones of the repository. Seismic effects on the emplacement pallet are included in the structural response calculations but not carried over into performance assessment because the presence of the pallet is conservatively ignored for transport calculations. Seismic effects on the invert are also not included in performance assessment because the structural response calculations transfer the ground motion in the host rock directly to the surface of the invert. Seismically induced changes in drift seepage are included in performance assessment for emplacement drifts in lithophysal rock zones because the drifts are predicted to collapse for large amplitude ground motion; changes in drift seepage are not included for drifts in the nonlithophysal rock.

D.3 RESPONSE

The seismic scenario class for TSPA is based on damage abstractions for EBS components in response to the seismic effects of vibratory ground motion, fault displacement, and rockfall induced by vibratory ground motion. These damage abstractions have a role in TSPA that is equivalent to the role of fragility curves in a probabilistic risk assessment for a nuclear power plant. That is, abstractions and fragility curves represent the probability of failure as a function of the amplitude of the ground motion or fault displacement. The damage abstractions are based on the failure mechanism of accelerated stress corrosion cracking in response to high residual tensile stress from mechanical deformation during a seismic event. The abstractions define the probability of seismically induced damaged area being less than a given fraction (0 to 1) as a function of the amplitude of the ground motion or fault displacement. These damage abstractions are the generalization of the fragility curve concept to a continuous measure of the damage state. The damage abstractions include consideration of interactions between EBS components and the interaction between the host rock and EBS components due to seismic effects. The damage abstractions include consideration of the potential degradation of EBS components over a 20,000-year time period to demonstrate the robustness of the system beyond the 10,000-year regulatory period.

The seismic scenario class for TSPA is based on Monte Carlo simulation, rather than on the fault tree analysis that is commonly used for probabilistic risk assessment of nuclear power plants. Monte Carlo simulation is reasonable for the repository because the accident sequences for the repository are simple in comparison to a nuclear power plant, and the emphasis in TSPA is on predicting a continuous range of reasonable component behaviors, rather than the probability of failure or no failure for a reactor component. Further details on the Monte Carlo approach are provided in Section D.4.1.

The damage abstractions and computational methodology are defined in *Seismic Consequence Abstraction* (BSC 2003c), which provides a description of the technical bases and input data for the seismic risk analysis for TSPA. The completion of *Seismic Consequence Abstraction* (BSC 2003c) in August 2003 completes the DOE response to SDS 2.04.

The information in this report is responsive to agreement SDS 2.04 and the associated AIN (AIN-1) made between the DOE and NRC. The report contains the information that DOE considers necessary for NRC review for closure of this agreement.

D.4 BASIS FOR THE RESPONSE

This section is organized to be directly responsive to the information needs identified by the NRC for SDS 2.04 AIN-1. This section and Appendix A of this technical basis document define the methodology and technical bases for the development of seismic damage abstractions for the EBS components, the range of failure modes for these components, the dynamic interactions among the components, consideration of component degradation, conduct of a seismic risk analysis, and effect of cladding failure on system performance (Table D-1).

Table D-1. Crosswalk of Information Needs for SDS 2.04 AIN-1 to this Appendix

Information Need in SDS 2.04 AIN-1	DOE Response
Development of seismic fragility curves for performance assessment	Section D.4.1 presents the rationale for using damage abstractions in the seismic scenario class for TSPA, rather than fragility curves.
Range of failure modes that can occur	Section D.4.2 describes the range of failure modes for the EBS components under vibratory ground motion and fault displacement.
Component interactions	Section D.4.3 describes the interactions among EBS components during vibratory ground motion and fault displacement. This section also provides references to the data that form the basis for the damage abstractions.
Step function for conditional probability of cladding failure	Section D.4.1 provides the rationale for using continuous damage abstractions, rather than step functions for damage, in TSPA.
Consideration of component deterioration	Section D.4.3 defines the representation of deterioration in the finite-element calculations for the waste package, drip shield, and cladding.
Conducting a seismic risk analysis for the repository	Section D.4.4 explains the computational methodology for the seismic scenario class for TSPA
Effect of cladding failure	Appendix A of this technical basis document explains the damage abstraction for cladding failure and its representation in TSPA.

The primary references for the technical bases and sources of data for the seismic damage abstractions are summarized in Table D-2.

Table D-2. Major References for Technical Bases and Data Used in the Seismic Abstractions

Damage Process	Reference
Uncertainty in input parameters for rockfall and structural response calculations	*Sampling of Stochastic Input Parameters for Rockfall and Structural Response Calculations Under Vibratory Ground Motion* (BSC 2003d)
Damage to the waste package from vibratory ground motion	*Structural Calculations of Waste Package Exposed to Vibratory Ground Motion* (BSC 2003e)
Damage to the drip shield from vibratory ground motion	*Structural Calculations of Drip Shield Exposed to Vibratory Ground Motion* (BSC 2003f)
Damage to the drip shield from rockfall	*Drift Degradation Analysis* (BSC 2003g) and *Drip Shield Structural Response to Rock Fall* (BSC 2003h)
Acceleration of the fuel assemblies and cladding due to end-to-end waste package impacts	*Maximum Accelerations on the Fuel Assemblies of a 21-PWR Waste Package During End Impacts* (BSC 2003i) and *Structural Calculations of Waste Package Exposed to Vibratory Ground Motion* (BSC 2003e)
Fault displacement and ground-motion hazard curves for determining the amplitude of seismic events	*Probabilistic Seismic Hazard Analyses for Fault Displacement and Vibratory Ground Motion at Yucca Mountain, Nevada* (CRWMS M&O 1998)
Damage abstractions and computational algorithm for seismic scenario class	*Seismic Consequence Abstraction* (BSC 2003c)

D.4.1 Role of Damage Abstractions in Total System Performance Assessment

The TSPA for the repository is based on a Monte Carlo approach. A Monte Carlo approach represents potential future histories of the repository in a probabilistic framework that propagates uncertainty through the sampling of uncertain parameters, uncertain models, and time-dependent processes. The Monte Carlo approach is a reasonable choice for risk analysis of a geologic repository because the engineered barriers are relatively simple structures, the response of the geologic barriers may vary over orders of magnitude, and opportunity for human intervention is limited after repository closure. The choice of a Monte Carlo approach also has a precedent. The compliance certification application for the Waste Isolation Pilot Plant (DOE 1996) is based, in part, on a performance assessment that incorporates a Monte Carlo approach. This performance assessment methodology was approved by the U.S. Environmental Protection Agency in its certification decision (40 CFR 194 Part III).

Probabilistic risk assessments for a nuclear power plant are often based on a fault tree analysis that is supported in the seismic case by fragility curves for the plant's important structures, systems, and components. In contrast to a geologic repository, a nuclear power plant is an extremely complex engineered structure with accident sequences that are strongly influenced by component and subsystem interactions and by human intervention, including operator error. The geology of the reactor site plays a role in defining seismic hazard curves but the local geology is not a primary containment barrier for the plant.

Seismic fragility curves are an integral part of the seismic probabilistic risk assessment. A seismic fragility curve defines the probability of failure of a structure, system, or component in response to an initiating event, as a function of the intensity of that event, such as the peak ground acceleration. A seismic fragility curve is often parameterized by the median peak ground acceleration required to fail a component and the logarithmic standard deviation that represents

the composite uncertainty about this median value (Kennedy and Ravindra 1984, Section 3.2). A fragility curve is ideal for defining the probability of component failure for a given seismic initiating event. This probability can be directly input into the branch of the fault tree that incorporates failure or no failure of a specific component, system, or structure for a wide variety of event sequences. Note that the fragility curve does not allow for the component state to have a continuous range, only to fail completely or to remain fully functional.

Performance assessment for the repository is based on a Monte Carlo approach to predicting future states of the repository. The engineered barriers of the repository are relatively simple engineered structures when compared to a nuclear power plant. This relative simplicity results in relatively simple accident sequences, without the potential for human intervention after repository closure. The geology of the site is a barrier for the repository. Since the geology is spatially variable and its response over 10,000 years is uncertain, the emphasis in performance assessment is on predicting a range of reasonable geologic behaviors, rather than the probability of failure versus no failure of a reactor component. The Monte Carlo approach provides an ideal technique for sampling a wide range of geologic behaviors in a probabilistic framework.

The Monte Carlo approach adopted for the seismic scenario in TSPA does not require the probability of component failure. Rather, each realization of the Monte Carlo method needs to determine the level of damage to EBS components for a given amplitude of the seismic initiating event. This amplitude is random, governed by the probabilistic seismic hazard curve, just as it is in a risk analysis for a nuclear plant. This amplitude is defined in terms of peak ground velocity for the repository, rather than peak ground acceleration for a power plant, because the former is more relevant to the response of the host rock and to structural response with sliding and impact. For a given level of the ground-motion amplitude, the level of damage in the EBS components has uncertainty, just as the component state (failure or functional) in a nuclear power plant does. So just as the power plant component is represented by a failure probability (given the peak ground acceleration), the damage to an EBS component is represented in the Monte Carlo method by a distribution (at a given value of peak ground velocity). The parameters of the distribution (i.e., central value, spread, upper bound, etc.) are a function of the amplitude of the seismic event, just as the simpler component failure probabilities are for a power plant probabilistic risk assessment. Formally, the abstraction and fragility curves are both known as conditional probability distributions because they are conditional on the amplitude of the seismic initiating event.

This damage distribution is referred to as a damage abstraction for the seismic scenario in TSPA. Damage abstractions have been developed for the waste package, drip shield, and cladding under vibratory ground motion. A damage abstraction has not been developed for the drip shield under rockfall induced by vibratory ground motion because any resulting cracks in the drip shield are expected to plug from evaporation-induced precipitation of calcite and other minerals in the groundwater (BSC 2003j, Section 6.3.7). The last case is an example of treating interaction among components, where the drift itself is recognized as a component of the EBS. The data that support these damage abstractions are based on structural response calculations that also include interactions among the engineered components (see Table D-2 for a list of references).

As a specific example, damage to the waste package from vibratory ground motion is represented as a uniform distribution whose lower bound is zero and whose upper bound is a

linear function of the peak ground velocity of the seismic event. This distribution form and the parameters of the linear function are based on analysis of the results from dynamic structural response calculations for the waste package under a carefully selected statistical sample of friction coefficients and of recorded earthquake ground motion adjusted to have precisely one of several peak ground velocity amplitudes. Each TSPA realization in the seismic scenario first samples the amplitude (i.e., the value of the peak ground velocity) and the timing of the seismic event. The upper bound of the corresponding uniform distribution for damage to the waste package can then be calculated, and this distribution is then sampled (once per realization) to determine the percent of failed area on the surface of the waste package. The Monte Carlo approach does not need the probability of complete failure of the waste package, as might be represented by a fragility curve. Rather, it needs the degree of damage to each EBS component as this relates to radionuclide release from the EBS and ultimately to dose to the reasonably maximally exposed individual. Nevertheless, the damage abstractions for TSPA play the same role in the Monte Carlo analysis scheme as the fragility curves do for a fault tree analysis in a probabilistic risk assessment.

An independent technical review of several model abstractions has been performed, and an alternate analysis of the damage information for the waste package and drip shield has been presented (BSC 2003c, Sections 6.5.3 and 6.6.3.1). These alternative analyses are structured around a conventional fragility approach, rather than a damage abstraction. Following this approach, a lognormally distributed approximation of the damage surface is fit by trial and error. A comparison of the lognormal distribution with the distributions for the damage abstractions identifies regions where the damage abstraction is nonconservative with respect to the lognormal distribution. When significant nonconservatisms were identified, the damage abstractions for TSPA were modified to remain conservative with respect to the lognormal distributions.

D.4.2 Range of Failure Modes

Mechanical processes that occur during an extreme seismic event can result in permanent structural deformation and residual tensile stress in EBS components. These mechanical processes include impacts between adjacent waste packages and between the waste package and its emplacement pallet, the surrounding drip shield, and the invert. Impacts will also occur between the drip shield and the emplacement pallet, the invert, and even the drift wall. These mechanical processes may also include other loads, such as static load from rockfall or thermal load, in addition to the seismic load; however, these static and thermal loads are small relative to seismic loads for the extreme ground motion that occurs only with low probability during the 10,000-year regulatory period.

Permanent structural deformation during these mechanical processes has the potential to result in immediate tensile failures from puncture or tearing. Puncture or tearing can only occur when a material reaches its ultimate tensile strain in a local region. Since Alloy 22 and Titanium Grade 7 are ductile metals, the ultimate tensile strain is much greater than the strain corresponding to the yield strength at the elastic–plastic transition. The waste package and drip shield will, therefore, begin to yield and deform from impact forces long before reaching the ultimate tensile strain point. In fact, the robustness of the waste package and drip shield makes it unlikely that immediate failure from puncture or tearing will occur even for the most intense, very low probability ground motion.

While immediate failure is unlikely, the presence of sufficiently high residual tensile stress may nonetheless result in enhanced local degradation from stress corrosion cracking or localized corrosion (pitting or crevice corrosion). Since the residual stress threshold to initiate accelerated corrosion is often near the yield strength, as opposed to the ultimate tensile strength, this combined mechanical-chemical failure mechanism is expected to be the most likely cause of failure of the waste package and drip shield as barriers to flow and transport should there be a very low probability seismic event.

Application of a residual tensile stress threshold for seismic failures is nonmechanistic in the sense that detailed calculations with accelerated corrosion rates or stress corrosion crack propagation are not used to determine the actual time to failure after a seismic event. Rather, a barrier is conservatively assumed to fail immediately once the residual tensile stress threshold is exceeded, resulting in the formation of a network of stress corrosion cracks (Herrera 2004) through the areas exceeding the residual stress threshold. The residual tensile stress threshold is simply referred to as the residual stress threshold or the stress threshold in this appendix, with the understanding that the principal residual stress must always be tensile to initiate an accelerated corrosion process.

The values of residual stress thresholds for seismic response are similar to the criteria for initiation of stress corrosion cracking on smooth surfaces of Alloy 22 and Titanium Grade 7 (BSC 2003j, Section 6.2.1). The use of a stress-corrosion-cracking initiation criterion is appropriate for seismic analysis because regions where the residual stress from mechanical damage exceeds the tensile failure criterion are expected to be severely cold-worked and, hence, potentially subject to enhanced stress corrosion cracking. "Cold-worked" refers to the process of working or deforming a metal at a temperature below that at which it crystallizes. In the present context, the deformation occurs during the impact process, whereby metal is strained from an elastic state to a plastic state, and possibly back again, at relatively low temperatures. The cold-worked regions are also potentially subject to enhanced general and localized corrosion.

A residual stress threshold is a conservative failure criterion because actual stress corrosion cracking will have a propagation time until failure. The current approach is appropriate because it is consistent with other tensile failure criteria (BSC 2003j, Section 6.2.1), because the residual stress failure criterion is transparent, and because it is easily applied to the output from structural response calculations.

Permanent deformation could also result in immediate puncture or tearing of an EBS component if the localized strain exceeds the ultimate tensile strain. The nonlinear stress–strain relationships for the structural response calculations includes the potential for immediate breach of EBS components through tensile and shear failure, although the computational meshes are generally too coarse to realistically simulate a localized puncture. Supporting calculations for waste package drops on the emplacement pallet indicate that the maximum stress intensity for the impact velocities observed in the vibratory ground-motion calculations is significantly below the ultimate tensile strength (BSC 2003k). In this situation, a localized puncture or tearing of the waste package will not occur, and the seismic damage abstractions for the waste package and drip shield are based on a residual tensile stress threshold as a failure criterion. In a similar fashion, the drip shield is not expected to buckle from the static load of a large rockfall (BSC 2003c, Section 6.6.2).

D.4.2.1 Morphology of the Stress Corrosion Crack

Seismically induced deformation can lead to crack initiation and crack propagation on the waste package. Accelerated stress corrosion cracking can occur when the conditions on waste package concurrently provide (1) high residual tensile stress, (2) a material that has been cold-worked during the seismic event, and (3) a range of aqueous brine environments that support corrosion. Once initiated, the strain fields (residual stresses) produced by the seismically induced impacts can drive crack growth. Depending on the stress distribution, cracking may propagate through-wall if the stress intensity factor remains positive. If multiple cracks are initiated in the same general area, the theoretical potential exists for multiple cracks to intersect or coalesce, creating a continuous crack around the deformed region. If this continuous crack is smooth, straight, and through-wall, a section of material could potentially separate from the cold-worked region, providing a potential advective pathway through the outer corrosion barrier.

It is very unlikely that a residual stress profile would be created that would allow an initiated stress corrosion crack to propagate both through-wall and circumscribing a dent or deformed area from a localized load. Any through-wall residual stress fields resulting from seismic impact loads would be a secondary-type stress (displacement-controlled). There is no significant stress from other sources, such as stress induced by internal pressure. In addition, stresses and strains are generally of higher magnitude at the outer surface and tend to decrease through the thickness for the deformation-induced damage from a seismic event. In this situation, any crack that initiates and propagates may arrest before penetrating the full thickness of the outer barrier and is highly unlikely to have a sufficiently positive stress intensity factor to result in both through-wall and 360° cracking around the entire dent.

Even postulating that a through-wall crack occurs and circumscribes the dented area, the nature of stress corrosion cracking will preclude the dented area from falling out. Cracks in Alloy 22 are transgranular, but whether transgranular or intergranular, the crack path has complex local branches with a roughness and tortuosity, as illustrated in Figure 5-3 (Herrera 2004, Figure 2-1), that make it essentially impossible for an inner "plug" to disengage from the vessel in the absence of a superimposed primary load (i.e. significant internal pressure).

This analysis is consistent with many years of experience with stress corrosion cracks in light water reactor components and other internally pressurized systems. A number of incidents of stress corrosion cracking have been observed in light water reactors involving both austenitic stainless steels and nickel-based alloys (Herrera 2004, Appendix A). The observed stress corrosion cracking has been extensive in many of these incidents, sometimes becoming fully circumferential in response to weld-induced residual tensile stress and pressure-induced primary stresses. But even under these conditions, which are more severe than anticipated in the postseismic environment, there has never been a documented case where a section of material dropped out as a result of the observed cracking (Herrera 2004, Appendix A).

D.4.2.2 Effective Area for Flow and Transport through the Waste Package

Since the most likely failure mechanism from a seismic event is accelerated stress corrosion cracking (Herrera 2004) and since the deformed or failed areas that exceed the residual stress failure for Alloy 22 are expected to remain physically intact, it is reasonable to represent these

areas as a dense network of stress corrosion cracks rather than as a plug of material that separates from the outer barrier. Note that the effective area for flow and transport through a barrier will be substantially less than the failed area because the cross-sectional area of the stress corrosion cracks is much less than the surface area that exceeds the residual stress threshold.

The effective area for flow and transport through the crack network is based on a range of crack densities and crack widths for four geometries of closely spaced networks (Herrera 2004, Section 6.2). In this conservative approach, centers of through-wall cracks are located in a densely packed hexagonal array and are separated by at least a wall thickness. The wall thickness is anticipated to be the minimum possible separation because stress relief from propagation of adjacent cracks relieves the local stress intensity factor, preventing tighter spacing between through-wall cracks. The width of each crack is estimated by assuming an elliptical opening with constant through-wall stress given by the elastic yield strength. This is a conservative approach because the crack tips tend to narrow at the inner surface and because stress relief from adjacent cracks will again tend to reduce the local stress levels at a crack.

The ratio of the effective area for flow and transport through the waste package to the failed area that exceeds the residual stress threshold is given by the product of the crack density per unit surface area and the gap area per crack. This area ratio ranges from 0.00328 to 0.0131 (Herrera 2004, Table 6-1) for the four crack networks. Stated differently, the effective area through the crack network is a factor of 76 to 305 less than the failed surface area that exceeds the residual stress threshold. For TSPA, there are two options for flow and transport through the crack network on the waste package: (1) advective flow and transport and diffusive transport, and (2) diffusive transport only.

D.4.2.3 Plugging of Cracks on the Drip Shield

The Titanium Grade 7 plates of the drip shield are also subject to stress corrosion cracking induced by residual stresses from seismic ground motion and from rockfall induced by seismic ground motion. However, the presence of a crack network in the drip shield is not represented in the seismic scenario class for TSPA because the drip shield cracks are predicted to plug within a few hundred years after a seismic event, preventing a significant flux of liquid seepage from falling on the waste package. The cracks will plug from mineral precipitation resulting from evaporation of seepage and from in-filling of the crack gap with corrosion products. Once the cracks are plugged, the quantity of liquid that can pass through the drip shield and impinge on the waste package will be reduced to a negligible level. The presence of the crack network in the drip shield is therefore not included in TSPA.

As with Alloy 22, the most likely failure mechanism for Titanium Grade 7 after a seismic event is accelerated stress corrosion cracking, rather than immediate puncture or tearing of the drip shield. The deformed or dented region is expected to remain physically intact because individual cracks are complex, branching structures with high surface roughness and tortuosity. In this situation, it is reasonable to represent the areas that exceed the residual stress failure criterion for Titanium Grade 7 as a network of stress corrosion cracks, rather than as an intact material that separates from the outer barrier.

The small heat flux across the drip shield will result in evaporation of slowly flowing seepage, causing a scale deposit to form around the mouth of the crack and also within the crack. A detailed calculation of the expected rate of crack plugging due to evaporation-induced precipitation of calcite has been performed for a pore water of typical composition dripping onto a drip shield (BSC 2001a). Cracks are sealed within a few hundred years when water is allowed to flow through the cracks at the expected (very low) rate for thin film flow (BSC 2001a, Section 6.3). Before the crack is sealed, the lack of a significant gradient to drive liquid through the crack, the potential for strong capillary forces if a droplet bridges the crack gap, and the observed high tortuosity and roughness of the crack geometry (Herrera 2004) will minimize any advective flux through the cracks. Once a crack is plugged with precipitates, the magnitude of the liquid flux through the crack will become insignificant because of the expected high density of calcite deposits (BSC 2001a, Section 2, Figures 2-1 and 2-2).

For example, the formation of scale deposits, primarily calcium carbonate (calcite), is well documented in flow systems in seawater environments and in heat exchangers with natural brines, such as in desalination plants (carrying approximately 6% NaCl solutions) and in potash plants (carrying greater than 12% mixtures of NaCl/KCl). Mineral deposits form rapidly at elevated temperatures and must be regularly removed to avoid loss of heat exchanger efficiency. In the case of seepage based on the J-13 groundwater from Yucca Mountain, calcite precipitation is the first stage of the concentration process (BSC 2001b, Section 6.7.1). Other minerals will also precipitate from J-13 groundwater, such as amorphous silica.

The sealing process may take thousands of years when a liquid droplet bridges a crack. However, the associated capillary forces when a liquid droplet is present prevent any advective flux from passing through the crack in this situation.

This analysis has not been extended to stress corrosion cracks in the waste package for the seismic scenario class. Rapid plugging of cracks requires evaporation of groundwater and precipitation of minerals. The initial precipitation of minerals will occur on the drip shield, which is directly exposed to the seepage of groundwater into the emplacement drifts. Secondary precipitation may occur on the waste package. However, the mineral concentrations on the waste package would be reduced by the initial precipitation on the drip shield and diluted by the presence of any condensate that falls onto the waste package from the underside of the drip shield. In this situation, TSPA allows for two options for flow and transport through the waste package: (1) advective and diffusive transport through the crack network, and (2) diffusive transport only.

D.4.3 Range of Component Interactions and Response

D.4.3.1 Structural Response of the Waste Package to Ground Motion

Structural response calculations have been performed to determine the damage from impacts between the waste package and emplacement pallet and from impacts between adjacent waste packages under vibratory ground motion (BSC 2003e). The potential for damage from impacts between the waste package and drip shield is included in the analysis but produces negligible damage because the drip shield is much less massive and unrestrained.

Damage to the waste package from vibratory ground motion is determined by structural response calculations using a commercially available version of the finite element program LS-DYNA V960 (LSTC 2001). A set of 15 calculations for the dynamic waste package response was performed for a set of 15 ground motions with a peak ground velocity of 2.44 m/s, corresponding to the 10^{-6} per year ground-motion level. (The peak ground velocity refers to the maximum amplitude of the first horizontal velocity component for each of the 15 sets of three component ground motions.) A similar set of calculations was also performed for a peak ground velocity of 5.35 m/s, corresponding to the 10^{-7} per year ground-motion level (BSC 2003e). The stochastic (uncertain) input parameters for the 15 simulations are the 15 sets of three-component ground-motion time histories, the metal-to-metal friction coefficient, and the metal-to-rock friction coefficient. A Monte Carlo sampling scheme defines the appropriate combinations of ground-motion time histories and friction coefficients (BSC 2003d, Section 6.4) for each peak ground velocity level.

These calculations incorporate the potential for general corrosion to degrade the waste package over the first 20,000 years after repository closure by reducing the thickness of the Alloy 22 outer barrier on the waste package by 2 mm. These calculations evaluate mechanical properties at 150°C to represent the potential degradation in mechanical strength if a seismic event occurs during the initial thermal pulse after repository closure. Thermal analyses for an unfilled drift predict that the waste package temperature will be less than or equal to 150°C for 98.5% of the first 10,000 years after repository closure. The thermal analysis considers three infiltration cases and five host rock units (BSC 2004, Figures 6.3-7 through 6.3-11). Since the drifts are expected to be largely unfilled at the onset of the seismic event, 150°C is a reasonable value for evaluation of material properties during the seismic event.

The adequacy of the finite-element mesh for the structural response calculations was confirmed by a mesh refinement study. Similarly, the effect of the use of rigid elements to reduce run times was evaluated through detailed mesh refinement studies that support the primary calculations (BSC 2003e, Attachments IX and VI). The results from these studies demonstrate that the numerical solution is reasonably independent of the number, type, and size of finite elements.

D.4.3.2 Structural Response of the Drip Shield to Ground Motion

Structural response calculations have been performed to determine the damage from impacts between the drip shield and the waste package, emplacement pallet, invert, and drift wall under vibratory ground motion (BSC 2003f). In addition to damage caused by impact, it is also possible that adjacent drip shields will be separated during high-amplitude ground motion. Separated drip shields allow seepage to fall directly on a waste package, independent of the response of stress corrosion cracks as flow pathways.

Damage to the drip shield from vibratory ground motion is determined by structural response calculations using a commercially available version of the finite element program LS-DYNA V960 (LSTC 2001). A set of 15 calculations for the dynamic drip shield response was performed for a set of 15 ground-motion results with a peak ground velocity of 2.44 m/s. A similar set of calculations was also performed for a peak ground velocity of 5.35 m/s (BSC 2003f). The stochastic (uncertain) input parameters for the 15 calculations are the 15 sets of three-component ground-motion time histories, the metal-to-metal friction coefficient, and the

metal-to-rock friction coefficient. A Monte Carlo sampling scheme defines the appropriate combinations of ground-motion time histories and friction coefficients (BSC 2003d, Section 6.4). The set of 15 ground-motion time histories for these analyses is identical with that for the analyses of waste package response to vibratory ground motion.

These calculations incorporate the potential for corrosion to degrade the drip shield over the first 20,000 years after repository closure by reducing the thickness of the drip shield plates by 2 mm. These calculations evaluate mechanical properties at 150°C to represent the potential degradation in mechanical strength if a seismic event occurs during the initial thermal pulse after repository closure. A drip shield temperature of 150°C is appropriate and reasonably conservative for evaluation of material properties at the time of the seismic event. This value (150°C) is conservative for evaluation of material properties during 98.5% of the first 10,000 years after repository closure; the thermal analysis is for an unfilled drift (BSC 2004, Figure 6.3-7 to 6.3-11).

The peak waste package temperature, which provides an upper bound for the peak drip shield temperature, varies between 149°C and 177°C for the three infiltration bins and five host rock units (BSC 2004, Table 6.3-8). The yield strength of Titanium Grade 7 decreases from 176 MPa at 150°C (BSC 2003l, Section 5.1) to 155 MPa[2] at 178°C. On the other hand, this peak temperature occurs at a time (50 years) when there will be minimal degradation of the drip shield components, so the thickness reduction of 2 mm is inappropriate for the maximum temperature analysis. On balance, it is anticipated that these two competing effects (lower yield strength versus thicker drip shield components) will not significantly change the mechanical response of the drip shield at 150°C.

The adequacy of the finite-element mesh was confirmed by a mesh refinement study to demonstrate that the numerical solution is reasonably independent of the number of finite elements and their size (BSC 2003f, Attachment III).

D.4.3.3 Structural Response of the Cladding to Ground Motion

The structural response of the cladding to ground motion is discussed in Appendix A.

D.4.3.4 Structural Response to Seismically Induced Rockfall

Although stress corrosion cracks on the drip shield are predicted to plug from evaporation-induced precipitation of mineral deposits, the drip shield may fail as a flow barrier due to buckling and collapse under loads from rockfall induced by ground motion. The rockfall calculations that define the potential loads from individual rock blocks in the nonlithophysal zones or from a collapsed drift in the lithophysal zones are described in this section.

[2] The yield strength at 178°C (352°F) is interpolated from known values at 300°F and 350°F, based on the data and formula in *Drip Shield Statically Loaded by Backfill and Loose Rock Mass* (BSC 2003l, Section 5.1): Yield strength at 178°C = 177 MPa + (156 MPa – 177 MPa)/(350°F – 300°F) * (352°F – 300°F) = 155 MPa.

D.4.3.4.1 Rockfall in the Nonlithophysal Zone

Geologic structure and rock strength define the failure mode in the nonlithophysal rock. The failure mode in these rocks results from stress-induced yield in the intact rock or along joint surfaces, followed by gravity-induced drop of discrete rock blocks. The analysis of the failure mechanism is complicated by the fact that the jointing in the nonlithophysal zones is usually of short continuous trace length and inherently discontinuous, thus forming few kinematically removable blocks. This type of discontinuous jointing results in an inherently stronger rock mass compared to typical jointed rock where the block structure is well defined by multiple, continuous joint sets (BSC 2003g, Executive Summary).

Analysis of rockfall in the nonlithophysal zone requires ground-motion time histories, fracture geometries, and fracture properties as input parameters or boundary conditions for the calculations. To ensure adequate representation of uncertainty and variability, the inputs for individual rockfall calculations are sampled from 15 ground-motion results at (horizontal) peak ground velocity levels of 2.44 m/s and 5.35 m/s (corresponding to the 10^{-6} and 10^{-7} per year ground-motion levels) and from 105 synthetic fracture patterns. These synthetic fracture patterns (BSC 2003g, Section 6.1.6) for the rockfall analysis are drawn from a random sampling of 105 centroid locations within a cube of rock that is 100 m on a side. A Monte Carlo sampling scheme provides the appropriate combinations of ground motion and synthetic fracture pattern for the rockfall analyses (BSC 2003d, Sections 6.1 and 6.2).

D.4.3.4.2 Rockfall in the Lithophysal Zone

The lithophysal rock mass is characterized by about 20% lithophysal cavities by volume. This rock type has numerous small-scale fractures between lithophysae that result in a weak rock mass relative to the nonlithophysal rock. Lithophysal failure is controlled by the transient ground-motion-induced stress concentrations that occur around the excavation. The mode of failure is primarily from tension generated during the rarefaction phase of vertically traveling compression waves (BSC 2003g, Executive Summary).

A lithophysal rockfall model was developed using the two-dimensional discontinuum code UDEC. In this model, the rock mass is represented as an assembly of polygonal, elastic blocks in which the bond strength of the blocks is calibrated so that the overall mechanical behavior of the mass is consistent with the material model developed for the lithophysal rock. The lithophysal rockfall model allows for the formation of fractures between blocks (i.e., the formation of internal fracturing), separation, and instability (under action of gravity) of the rock mass around the drift. The UDEC model is based on unsupported drift openings (BSC 2003g, Section 6.4).

To ensure adequate representation of uncertainty and variability, the rockfall calculations must represent the variability in mechanical properties of lithophysal rock. This was achieved through the use of five rock mass categories. Rock mass category 1 represents a weak rock with a lithophysal porosity of 25% to 30%. Rock mass category 5 represents strong lithophysal rock with a lithophysal porosity of less than 10%. Rock mass categories 2, 3, and 4 represent intermediate cases with lithophysal porosities of 20% to 25%, 15% to 20%, and 10% to 15%, respectively. The effective mechanical properties corresponding to these rock mass categories

vary with the porosity of the lithophysae (BSC 2003g, Tables 34 and 45). Each rockfall calculation with a given ground-motion time history was repeated three times, using rock mass categories 1, 3, and 5, to span the range of mechanical properties in the lithophysal zones.

D.4.3.4.3 Damage to the Drip Shield from Rockfall in the Nonlithophysal Zone

A set of six representative blocks and three representative impact locations was selected to span the range of blocks from the nonlithophysal rockfall calculations. The idea behind this approach is to perform a limited set of calculations that span the range of rock sizes, rock velocities, rock impact angles, and rock impact points on the drip shield. This limited set of calculations then provides the basis for determining the response of the drip shield (1) to the maximum rock blocks in the nonlithophysal zone and (2) to the smaller blocks that can be ejected during drift collapse in the lithophysal zone.

The selection of representative rocks is based on their kinetic energy because the impact energy of a rock block should provide a reasonable correlation with failed area (see Table 5-3). The impact energies associated with the selected rocks correspond to the minimum, the 5th percentile, the median (50th percentile), the 95th percentile, and the maximum of the sorted impact energies for the 2.44 m/s peak ground velocity time histories (BSC 2003g, Attachment XI). A sixth block has been added to capture the maximum rock block energy observed for the 5.35 m/s peak ground velocity ground motion.

Damage to the drip shield from impact of individual rock blocks is determined by structural response calculations using a commercially available version of the finite-element program LS-DYNA V960 (LSTC 2001). The objective of these calculations is to determine the areas on the drip shield where the residual first principal stress in the drip shield plates exceeds the failure criterion for Titanium Grade 7 and to determine the potential for buckling and collapse during impact from rock blocks with the greatest kinetic energy. The rationale for using the first principal stress as a measure of susceptibility to accelerated corrosion is documented in the response to RDTME 3.18, Appendix F of *Technical Basis Document No. 6: Waste Package and Drip Shield Corrosion.*

These calculations incorporate the potential for corrosion to degrade the drip shield over the first 20,000 years after repository closure by reducing the thickness of the drip shield plates by 2 mm. The 20,000-year period is selected to demonstrate that repository performance remains robust well after the 10,000-year regulatory period has ended. These calculations also evaluate mechanical properties at 150°C to represent the potential degradation in mechanical strength if a seismic hazard occurs during the initial thermal pulse after repository closure.

D.4.3.4.4 Damage to the Drip Shield from Rockfall in the Lithophysal Zone

Two potential sources of damage to the drip shield have been considered in the lithophysal zone: damage from the individual rock fragments that fall onto the drip shield and the static load on the drip shield from drift collapse. The individual rock fragments are too small to do significant damage to the drip shield, and the mean static loads from a collapsed drift are predicted not to collapse the drip shield. Damage to the drip shield from rockfall in the lithophysal zone is not included in the drip-shield damage abstraction for TSPA on this basis.

In the lithophysal zones, the rock mass is permeated with void spaces of varying size. Average joint spacing is less than 1 m, and, at certain locations, this spacing is much smaller, on the order of 0.1 m (BSC 2003g, Section 6.1.4.1). Drifts in the lithophysal zones are predicted to collapse into small fragments with particle sizes of centimeters to decimeters (BSC 2003g, Section 8.1) under the loads imposed by vibratory ground motion with a peak ground velocity of 2.44 m/s or greater.

The small fragments from drift collapse in the lithophysal zones will not damage the drip shield because the small mass and energy of the individual fragments cannot cause significant permanent deformation of the drip shield. The probability of large coherent (key) blocks being generated by the collapse process in the lithophysal zones is very low (BSC 2003g, Section 6.4.3).

Drift collapse in the lithophysal zones can impose a static load on the drip shield from the weight of the natural backfill that fills the drifts as a result of the collapse. The structural response of the drip shield to this dead load from debris on the drip shield has been evaluated with structural response calculations (BSC 2003l) using the LS-DYNA software. The static load for these calculations is represented as the equivalent pressure from a layer of sand backfill that is about 1 m thick and a layer of fragmented rock backfill that is 5.5 m thick. The calculations are performed using material properties at room temperature and at 150°C. Thermal analyses for an unfilled drift predict that the drip shield temperature will be less than or equal to 150°C for 98.5% of the first 10,000 years after repository closure (BSC 2004, Figures 6.3-7 to 6.3-11). In this situation, 150°C is a reasonable and conservative temperature value for evaluation of material properties during the seismic event. The calculations also consider a general thinning of the drip shield components by 1 mm on all sides or by 1.5 mm on all sides to represent the potential for structural degradation from long-term general corrosion.

The maximum stress in all components of the drip shield is always less than the yield strength for this combined load (BSC 2003l, Section 6 and Table 6.2). In addition, the average stress in the large support beams (the peripheral bulkheads) of the drip shield is far enough below the yield strength of Titanium Grade 24 to alleviate any concern of buckling. (The drip shield plates are fabricated from Titanium Grade 7, while the supporting framework is fabricated from Titanium Grade 24.)

The peak waste package temperature, and by inference the peak drip shield temperature, varies between 149.2°C and 177.8°C for the three infiltration bins and five host rock units (BSC 2004, Table 6.3-8). The yield strength of Titanium Grade 7 decreases from 176 MPa at 150°C (BSC 2003l, Section 5.1) to 155 MPa at 178°C (see footnote 2 in Section D.4.3.2). On the other hand, this peak temperature occurs at a time (50 years) when there will be minimal degradation of the drip shield components, so the thickness reduction of 2 mm is inappropriate for a maximum temperature analysis. On balance, it is anticipated that these two competing effects (lower yield strength versus thicker drip shield components) will not fail or buckle the drip shield.

Drip shield temperatures may also increase after the seismic event if the drift collapses and fills with rubble from the lithophysal rock. In effect, the rubble can provide a thermal blanket that may increase the drip shield temperature above its value for an unfilled drift. However, this long-term thermal effect is not expected to significantly impact the integrity of the drip shield.

First, the change in drip shield temperature is not expected to be significant for seismic events after the thermal pulse. As an example, the drip shield temperature is less than 110°C at 1,000 years (BSC 2004, Figures 6.3-7 to 6.3-11), so a very large temperature change is required to exceed the 150°C temperature used to evaluate material properties. Second, the temperature excursion will be greatest for seismic events near the peak of the thermal pulse at 50 years, but the drip shield will not be significantly degraded by general corrosion at these early times and, hence, will be less likely to fail. So the long-term thermal effect from rubble is not expected to significantly impact the integrity of the drip shield.

The equivalent pressure approach for these static load calculations does not consider stress risers due to the presence of angular rock fragments with sharp edges. Local deformation of the drip shield plates and the potential for load bridging the natural backfill should redistribute these stress risers into a more uniform external load on the drip shield.

It is important to differentiate between dynamic and static failure criteria for the drip shield. For dynamic loading of the drip shield due to rockfall, an area fails as a flow barrier when the residual stress exceeds 50% of the yield strength of Titanium Grade 7. This failure is a combined chemical-mechanical response of a cold-worked material to dynamic impacts. For static loading, the failure of the drip shield is determined by mechanical rupture or buckling of the drip shield. In the static situation, a local stress below 100% of the yield strength of Titanium Grade 7 and below any stress-related criterion for buckling implies no failure of the drip shield.

D.4.3.4.5 Damage to the Waste Package and Cladding from Rockfall

Damage to the waste package and cladding from rockfall has not been included in the damage abstractions for TSPA. The drip shield is predicted to remain effective as a mechanical barrier for the 10^{-6} per year ground-motion level and, by implication, for all higher frequency ground motion. (A higher frequency ground motion has smaller amplitude measured in terms of peak ground velocity or peak ground acceleration.) In effect, the drip shield does not collapse under the impact of even the largest rock blocks, preventing any contact between the waste package and cladding and the rock blocks and drip shield (BSC 2003h).

Drip shield separation only occurs at the 10^{-7} per year ground-motion level and, by inference, for all smaller-frequency, higher-amplitude ground motion (BSC 2003f). Drip shield separation potentially exposes the waste package and cladding to direct impact from rock blocks. However, drip-shield separation is not expected to damage waste packages in the lithophysal zones of the repository because the lithophysal rock is predicted to shatter into small fragments (see Section D.4.3.4.4) that have little potential to damage the waste package and cladding. Therefore, the waste package and cladding should not be damaged by rockfall in the lithophysal zones. Since 85% of the emplacement drifts are in lithophysal zones, only 15% of the waste packages are potentially exposed to rock blocks in the nonlithophysal zones of the repository.

The ground motion at the 10^{-7} per year level, when the drip shields are predicted to separate, are extremely intense. This ground motion not only causes the drip shields to separate, but crushes the rock blocks in the nonlithophysal zones. The 10^{-7} per year ground motion result in complete drift collapse for all 15 ground-motion sets in the nonlithophysal rock (BSC 2003m, Section 6.3.1.6.3). In other words, the large rock blocks fail under the seismic load, fragmenting

into smaller pieces. These smaller pieces are anticipated to have little potential to damage the waste package and cladding, similar to the situation in the lithophysal rock, as discussed in Section D.4.3.4.4.

In summary, the drip shield is predicted to remain effective as a mechanical barrier for the 10^{-6} per year ground-motion level and by implication for all higher-frequency, lower–amplitude ground motion. Once ground motion becomes intense enough to separate the drip shields, the drifts are predicted to collapse in both the lithophysal and nonlithophysal zones. Drift collapse will crush the host rock into small fragments that have little potential to damage the waste package and cladding. Damage to the waste package and cladding from rockfall has not been included in the seismic scenario for TSPA on this basis.

D.4.3.6 Damage from Fault Displacement

Seismic events can also result in fault displacements within the emplacement drifts. Fault displacement could impact key EBS components in two ways:

(1) Separation between adjacent drip shields could allow a pathway for seepage to contact the waste packages, thereby potentially accelerating corrosion-induced waste package failure.

(2) Fault displacement could cause mechanical damage to the waste packages directly.

For a fault displacement that occurs along an emplacement drift, a sudden discontinuity in the floor and roof of the tunnel may occur. This would result in one portion of the tunnel being displaced relative to the adjacent section. Such a discontinuity in the tunnel axis could cause separation of adjacent drip shields and, if severe enough, could cause shearing of a waste package at that location.

The actual response of the EBS components to a fault displacement scenario is complicated. As a conservative simplification, the fault displacement is analyzed considering:

- The fault is perpendicular to the tunnel axis with the displacement being purely vertical.
- The fault displacement occurs at a discrete point, creating a knife-edge discontinuity.

Vertical faulting is consistent with the faults investigated in the Cross-Drift tunnel that was excavated as part of the Enhanced Characterization of the Repository Block investigation (Mongano et al. 1999, pp. 51 to 59). Treating the faults as perpendicular to the tunnel axis is conservative, in the sense that no credit is taken for sideways movement of the waste packages that could lessen the degree to which fault displacement could cause damage.

A sudden discontinuity in the tunnel floor would tend to raise one end of a drip shield and waste package. However, the other EBS components, specifically the invert and emplacement pallet, would also be affected. A significant amount of the invert (ballast) from the elevated portion of the tunnel is expected to fall into the lower tunnel segment. In addition, the steel supports in the invert and the emplacement pallet may collapse at the plane of displacement, further degrading the integrity of the invert.

The exact details of these events are difficult to predict. As a simplification, the approximation is made that the emplacement pallet collapses into the invert on the elevated side of the fault. No credit is taken for any further shifting of the ballast in the invert. This is a conservative assumption because the unsupported ballast will fall into the lowest parts of the drift, providing additional clearance between the waste package and drip shield. Using this approximation, the clearance around the waste package ranges from 606 to 1,398 mm, based on the drip shield internal height and the diameter of the waste package type (BSC 2003c, Table 20).

A determination of waste package failure is made by comparing the available clearance between waste package type and drip shield with the fault displacement hazard for secondary and generic faults within the repository block. At mean annual exceedance frequencies between 10^{-7} and 10^{-8} per year, waste package failure may occur for any of the waste packages placed directly over the four known faults intersecting the emplacement drifts and over the small generic faults characterized by 2 m total offset. If the fault displacement hazard curve predicts a displacement that is greater than the clearance between waste package and drip shield, then the waste package is assumed to fail.

When a waste package fails by fault displacement, there are two consequences for TSPA: (1) the failed area on the waste package is determined by sampling a uniform distribution with a lower bound of zero and an upper bound equal to the area of the waste package lid and (2) the drip shield and 100% of the cladding associated with this waste package are also assumed to fail as barriers to flow and transport. Failure of naval fuel rod cladding is treated the same as commercial spent nuclear fuel for the purpose of damage from fault displacement.

The failed area on the waste package represents the extremes of response. The failed area can be 0% for a package that experiences very minor crimping without failure. The failed area can also be as large as the waste package lid, if the lid welds are broken from severe crimping of the waste package due to fault displacement. The failed area is represented as a uniform distribution between these bounds and sampled whenever a significant fault displacement occurs. The potential for crimping to generate a network of stress corrosion cracks is conservatively ignored in the damage abstraction for fault displacement.

A sheared drip shield will allow all seepage to pass through it. Similarly, cladding becomes 100% perforated in response to a fault displacement that can shear a waste package. The consequences for the drip shield and cladding represent conservative, bounding approximations.

This approach is reasonable because there is significant uncertainty in the expected magnitude of fault displacements at very low probabilities, and because the detailed response of EBS components is difficult to predict. Given this lack of precision, a highly detailed calculation of drip shield and waste package response to fault displacement is not warranted.

D.4.4 Methodology for Seismic Risk Analysis

The seismic scenario class is based on a single modeling case with a focus on seismic events with frequencies less than 10^{-4} per year because the associated ground motion and fault displacements have the potential to cause damage to the EBS components. The response of the drip shield, waste package, and cladding is represented through damage abstractions for the EBS

components under vibratory ground motion and fault displacement. The failed areas on the EBS components define pathways for release of radionuclides through the engineered barriers. Once radionuclides are released from the EBS, flow and transport in the unsaturated zone and the saturated zone are generally based on the same models and algorithms as for the nominal scenario class. Biosphere calculations and parameters for the seismic scenario class are also unchanged from those for the nominal scenario class. The methodology for the seismic risk analysis for TSPA is defined in *Seismic Consequence Abstraction* (BSC 2003c, Section 6.10).

The impact of seismic effects on repository performance is being represented in TSPA by a scenario that is separate from the nominal scenario class. The rationale for defining a separate scenario class is based on several key observations:

- Seismic events with annual frequencies down to 10^{-8} per year must be considered by TSPA (10 CFR 63.114).

- The nominal scenario class cannot determine the impact of low-probability seismic events in a computationally efficient manner. A separate scenario class for seismic effects is desirable.

  Accurate representation of events with annual probability of occurrence down to 10^{-8} per year would require millions of realizations in the nominal scenario class, which is not computationally feasible. The alternative is to define a separate scenario for seismic effects that determines dose in a probability-weighted manner.

- The mean dose time history is the main parameter for compliance determinations.

  Radionuclide release limits for the repository are expressed in terms of the mean of the distribution of projected doses to the reasonably maximally exposed individual, per 10 CFR 63.303 and 63.311. Calculation of releases from the seismic scenario class must generate mean dose for consistency with the nominal scenario class.

- Damage from seismic events is expressed as a failed area or as an effective cross-sectional area for flow and transport through the surfaces of the drip shield, the waste package, and the cladding.

  The damage from seismic events is based on the separation area for advective flow through the drip shield, on the effective cross-sectional area of a network of stress corrosion cracks for flow and transport through the waste package, and on the perforation of the cladding. These areas are a function of the amplitude of the seismic event, such as horizontal peak ground velocity. The individual damage abstractions for the waste package, the drip shield, and the cladding are based on the results from structural response calculations and rockfall calculations, as discussed in Section D.4.3.

- The damage to the waste package, cladding, and drip shield from vibratory ground motion is applied throughout the repository. Each waste package in the repository has the same effective cross-sectional area determined by the appropriate damage abstraction; similarly, the percent of drip shield separation and the percent of perforated

cladding is applied uniformly throughout the repository. This approach is reasonable because the performance criteria in 10 CFR 63.303 and 63.311 are expressed as the mean dose and because damage to the drip shield from rockfall is not included in TSPA, based on plugging of stress corrosion cracks from evaporation-induced precipitation of mineral deposits in the groundwater. Finally, the damage to the waste package, cladding, and drip shield from fault displacement is applied only to those EBS components that are directly located over the secondary faults and generic fractures in the repository.

The mean dose for the seismic scenario class is calculated using a two-step approach: (1) TSPA generates a set of R realizations that sample the levels of seismic effects with the potential to generate releases from the EBS, and (2) the mean or expected dose time history is calculated using a weighted sum and average of the dose time histories from the R realizations evaluated during the first step. Additional postprocessing can present results as cumulative distribution functions or as complementary cumulative distribution functions or can evaluate the variability of the dose time histories, if necessary.

D.5 REFERENCES

D.5.1 Documents Cited

BSC (Bechtel SAIC Company) 2001a. *Plugging of Stress Corrosion Cracks by Precipitates.* CAL-EBS-MD-000017 REV 00. Las Vegas, Nevada: Bechtel SAIC Company. ACC: MOL.20011010.0168.

BSC 2001b. *Environment on the Surfaces of the Drip Shield and Waste Package Outer Barrier.* ANL-EBS-MD-000001 REV 00 ICN 02. Las Vegas, Nevada: Bechtel SAIC Company. ACC: MOL.20010724.0082.

BSC 2003a. *Development of Earthquake Ground Motion Input for Preclosure Seismic Design and Postclosure Performance Assessment of a Geologic Repository at Yucca Mountain, NV.* MDL-MGR-GS-000003 REV 00D. Las Vegas, Nevada: Bechtel SAIC Company. ACC: MOL.20030929.0120.

BSC 2003b. *Preliminary Seismic Analysis for Preclosure Safety Analysis.* CAL-MGR-MD-000012 REV 00A. Las Vegas, Nevada: Bechtel SAIC Company. ACC: DOC.20030930.0001.

BSC 2003c. *Seismic Consequence Abstraction.* MDL-WIS-PA-000003 REV 00. Las Vegas, Nevada: Bechtel SAIC Company. ACC: DOC.20030818.0006.

BSC 2003d. *Sampling of Stochastic Input Parameters for Rockfall and Structural Response Calculations Under Vibratory Ground Motion.* ANL-EBS-PA-000009 REV 00. Las Vegas, Nevada: Bechtel SAIC Company. ACC: DOC.20030707.0003.

BSC 2003e. *Structural Calculations of Waste Package Exposed to Vibratory Ground Motion.* 000-00C-EBS0-00300-000-00B. Las Vegas, Nevada: Bechtel SAIC Company. ACC: ENG.20030520.0003.

BSC 2003f. *Structural Calculations of Drip Shield Exposed to Vibratory Ground Motion.* 000-00C-PEC0-00100-000-00A. Las Vegas, Nevada: Bechtel SAIC Company. ACC: ENG.20030618.0009.

BSC 2003g. *Drift Degradation Analysis.* ANL-EBS-MD-000027 REV 02. Las Vegas, Nevada: Bechtel SAIC Company. ACC: DOC.20030709.0003.

BSC 2003h. *Drip Shield Structural Response to Rock Fall.* 000-00C-TED0-00500-000-00A. Las Vegas, Nevada: Bechtel SAIC Company. ACC: ENG.20030327.0001.

BSC 2003i. *Maximum Accelerations on the Fuel Assemblies of a 21-PWR Waste Package During End Impacts.* 000-00C-DSU0-01100-000-00A. Las Vegas, Nevada: Bechtel SAIC Company. ACC: ENG.20030327.0002.

BSC 2003j. *Stress Corrosion Cracking of the Drip Shield, the Waste Package Outer Barrier, and the Stainless Steel Structural Material.* ANL-EBS-MD-000005 REV 01 ICN 00. Las Vegas, Nevada: Bechtel SAIC Company. ACC: DOC.20030717.0001.

BSC 2003k. *Drop of Waste Package on Emplacement Pallet—A Mesh Study.* 000-00C-DSU0-02200-000-00A. Las Vegas, Nevada: Bechtel SAIC Company. ACC: ENG.20030915.0001.

BSC 2003l. *Drip Shield Statically Loaded by Backfill and Loose Rock Mass.* 000-00C-TED0-00300-000-00A. Las Vegas, Nevada: Bechtel SAIC Company. ACC: ENG.20030224.0004.

BSC 2003m. *Drift Degradation Analysis.* ANL-EBS-MD-000027 REV 02 ICN 1E. Las Vegas, Nevada: Bechtel SAIC Company. ACC: MOL.20040120.0078.

BSC 2004. *Multiscale Thermohydrologic Model.* ANL-EBS-MD-000049 REV 01. Las Vegas, Nevada: Bechtel SAIC Company. ACC: MOL.20040301.0004.

CRWMS M&O (Civilian Radioactive Waste Management System Management and Operating Contractor) 1998. *Probabilistic Seismic Hazard Analyses for Fault Displacement and Vibratory Ground Motion at Yucca Mountain, Nevada.* Milestone SP32IM3, September 23, 1998. Three volumes. Las Vegas, Nevada: CRWMS M&O. ACC: MOL.19981207.0393.

CRWMS M&O 2000. *Features, Events, and Processes: Disruptive Events.* ANL-WIS-MD-000005 REV 00 ICN 1. Las Vegas, Nevada: CRWMS M&O. ACC: MOL.20001218.0007.

DOE (U.S. Department of Energy) 1996. *Title 40 CFR Part 191 Compliance Certification Application for the Waste Isolation Pilot Plant.* DOE/CAO-1996-2184. Twenty-one volumes. Carlsbad, New Mexico: U.S. Department of Energy, Carlsbad Area Office. TIC: 240511.

Herrera, M.L. 2004. *Evaluation of the Potential Impact of Seismic Induced Deformation on the Stress Corrosion Cracking of the YMP Waste Packages.* SIR-04-015, Rev. 1. San Jose, California: Structural Integrity Associates. ACC: MOL.20040311.0149.

Kennedy, R.P. and Ravindra, M.K. 1984. "Seismic Fragilities for Nuclear Power Plant Risk Studies." *Nuclear Engineering and Design, 79,* 47–68. Amsterdam, The Netherlands: Elsevier. TIC: 243985.

LSTC (Livermore Software Technology Corporation) 2001. *LS-DYNA Keyword User's Manual.* Version 960. Two volumes. Livermore, California: Livermore Software Technology Corporation. TIC: 252119.

Mongano, G.S.; Singleton, W.L.; Moyer, T.C.; Beason, S.C.; Eatman, G.L.W.; Albin, A.L.; and Lung, R.C. 1999. *Geology of the ECRB Cross Drift - Exploratory Studies Facility, Yucca Mountain Project, Yucca Mountain, Nevada.* Deliverable SPG42GM3. Denver, Colorado: U.S. Geological Survey. ACC: MOL.20000324.0614.

Reamer, C.W. 2001a. "Structural Deformation and Seismicity Key Technical Issue Agreements: Additional Information Needed." Letter from C.W. Reamer (NRC) to S.J. Brocoum (DOE/YMSCO), August 3, 2001, with enclosure. ACC: MOL.20011001.0306.

Reamer, C.W. 2001b. "U.S. Nuclear Regulatory Commission/U.S. Department of Energy Technical Exchange and Management Meeting on Total System Performance Assessment and Integration (August 6 through 10, 2001)." Letter from C.W. Reamer (NRC) to S. Brocoum (DOE/YMSCO), August 23, 2001, with enclosure. ACC: MOL.20011029.0281.

Schlueter, J. 2000a. "U.S. Nuclear Regulatory Commission/U.S. Department of Energy Technical Exchange and Management Meeting on Structural Deformation and Seismicity (October 11-12, 2000)." Letter from J. Schlueter (NRC) to S. Brocoum (DOE/YMSCO), October 27, 2000, with enclosure. ACC: MOL.20010730.0232.

Schlueter, J. 2000b. "U.S. Nuclear Regulatory Commission/U.S. Department of Energy Technical Exchange and Management Meeting on Container Life and Source Term (September 12-13, 2000)." Letter from J. Schlueter (NRC) to S. Brocoum (DOE/YMSCO), October 4, 2000, with enclosure. ACC: MOL.20010731.0161.

D.5.2 Codes, Standards, and Regulations

10 CFR Part 63. Energy: Disposal of High-Level Radioactive Wastes in a Geologic Repository at Yucca Mountain, Nevada. Readily available.

40 CFR Part 194. Protection of Environment: Criteria for the Certification and Recertification of the Waste Isolation Pilot Plant's Compliance with the Disposal Regulations: Certification Decision; Final Rule. Readily available.

INTENTIONALLY LEFT BLANK